Scuola di dottorato
Università degli studi di Milano-Bicocca

Department of Physics G. Occhialini
PhD program in Physics and Astronomy – XXXVII cycle

Methods for extracting spectral densities from Euclidean lattice correlators

Matteo Saccardi
Registration number 813395

Tutor: Prof. **Leonardo Giusti**
Supervisor: Prof. **Mattia Bruno**

Coordinator: Prof. Stefano Ragazzi

Academic year 2023/2024

List of Publications

For an updated list, see

- Orcid: https://orcid.org/0000-0002-3701-9085
- INSPIRE: https://inspirehep.net/authors/2784995

Articles

[1] L. Giusti and M. Saccardi, *Four-dimensional factorization of the fermion determinant in lattice QCD, Phys. Lett. B* **829** (2022) 137103

[2] M. Bruno, L. Giusti, and M. Saccardi, *Spectral densities from Euclidean lattice correlators via the Mellin transform*, arXiv:2407.04141

[3] M. Bruno, L. Giusti, and M. Saccardi, Publication in preparation

Proceedings

[4] M. Saccardi and L. Giusti, *Four-dimensional domain decomposition for the factorization of the fermion determinant, PoS* **LATTICE2022** (2023) 386

[5] M. Bruno, L. Giusti, and M. Saccardi, *On the prediction of spectral densities from lattice qcd, IL NUOVO CIMENTO* **47 C** (2024) 197

[6] M. Saccardi, M. Bruno, and L. Giusti, *Spectral densities from Euclidean-time lattice correlation functions*, Proceeding to the 41st International Symposium on Lattice Field Theory (**LATTICE2024**), in preparation

Contents

Introduction

Spectral densities and their smeared version with analytically known kernel functions encode dynamical information on a wide variety of phenomenologically interesting quantities, such as inclusive multiparticle hadronic scattering cross sections, semi-leptonic decay rates, and non-static properties of the quark-gluon plasma in thermal Quantum Chromodynamics (QCD), to name a few. Our long-term goal is their ab initio, non-perturbative extraction from the Euclidean time dependence of correlation functions.

Lattice QCD provides the only known framework to extract non-perturbative predictions of QCD from first principles. The theory is defined on a finite, discrete lattice, that regulates ultraviolet divergences, and in Euclidean time, enabling a Boltzmann interpretation of path integral averages. QCD is recovered in the continuum and infinite-volume limits of Lattice QCD, where theoretical predictions are obtained from path integral averages estimated from systematically improvable Monte Carlo methods.

With modern numerical techniques reaching unprecedented levels of precision, and given the remarkable recent progresses in High Performance Computing, in this Thesis we address two stumbling blocks that affect the computation of spectral densities on the lattice. First of all, it is hard to define an explicit, direct dependence of spectral densities on Euclidean correlation functions. More precisely, the problem can be phrased as that of computing an inverse Laplace transform from the knowledge of correlation functions only on the Euclidean time axis, a notoriously ill-posed *inverse problem* which is further complicated by the finite, discrete and intrinsically noisy nature of lattice data. Secondly, the majority of the hadronic correlators computed in Euclidean Quantum Field Theories is affected by an exponential degradation of their signal-to-noise (StN) ratios, worsening the quality of data at large temporal distances. This affects the extraction of many physically interesting quantities, notable examples being baryon masses and matrix elements, the Hadronic Vacuum Polarization and the Light-by-Light scattering contributions to the muon $g-2$, and the form factors of semileptonic decays.

As first pointed out by Parisi and Lepage, an exponential loss of statistical precision is observed in most of the hadronic correlation functions of theoretical and phenomenological interest at large Euclidean distances, when states contributing to the variance are lighter than those contributing to the central value. In standard Lattice QCD simulations, the number of configurations necessary to reach a given statistical precision would increase with the square of that exponential factor. This exponential loss of significance

is tackled by *multilevel algorithms*, where the locality of the theory is exploited in order to design new estimators with a reduced variance, achieving exponential improvements where the StN problem is worse. However, the non-local dependence of the fermion determinant on the gauge field limits our ability to simulate Lattice QCD with fermions through local updates. For this reason, the first original contribution of this Thesis, published in Refs. [1, 4], consists in the four-dimensional generalization of a recent proposal for a one-dimensional factorization of the gauge-field dependence of the fermion determinant. An overlapping domain decomposition in four-dimensions leads to a block-local action in the gauge and in the auxiliary bosonic fields, with a small remainder that can be included in the observable through a reweighting procedure. Besides paving the way to multilevel integration schemes, this factorization can be beneficial also in the context of simulations in large volumes, as well as in making the parallelization of Monte Carlo algorithms and codes more efficient.

To address the second problem, building on a wide mathematical literature, in this Thesis we introduce analytic, explicit relations to *solve the inverse problem* through a linear combination of the correlators with analytically known, real and computable coefficients. Our results, reported in Refs. [2, 3, 6], enable also a direct estimation of finite-volume and discretization effects on the estimated (smeared) spectral densities, which may be directly inferred from those analytically known for the correlators. Our techniques can also be directly applied to other fields of research and science where data is available under similar constraints and the target observable is related to a similar inversion with respect to what can be effectively measured.
Such formulae are first derived in the continuum and generalized to the case of spectral densities satisfying subtracted dispersion relations. The analytical control of the solution allows us to explicitly quantify systematic errors due to a finite temporal extent of the lattice. In the discrete case, instead, a trivial discretization of the continuum coefficients, whose zeros are geometrically distributed, would lead to large discretization errors on the resulting reconstruction. In order to accommodate the practical necessity of employing evenly-spaced data, we also derive an explicit, analytic formula to exactly perform such reconstruction. We additionally discuss the effects of statistical errors on the resulting reconstruction: the inherently noisy nature of lattice data might spoil the results, which hinge on delicate cancellations in the linear combination of correlation functions with wildly oscillating coefficients. Moreover, we present a few preliminary numerical results, extending our previous analysis published in Ref. [5] for the isovector vector spectral density, extracted from accurate multilevel data.

This Thesis is organized as follows. In Chapter 1, we provide a concise introduction to QCD, focusing on its non-perturbative path integral definition. Its formulation on a spacetime lattice is reviewed in Chapter 2, with a detailed discussion of the StN problem. Spectral densities and inverse problems are reviewed in Chapter 3, illustrating several examples within the context of QCD. Our original contributions are detailed in Chapters 4 and 5, where we present multilevel algorithms and address the analytic reconstruction of spectral densities from Euclidean correlation functions, respectively.

Chapter 1

Quantum Chromodynamics

Quantum Chromodynamics (QCD) is the renormalizable Quantum Field Theory (QFT) that describes strong interactions between colored quarks and gluons [7]. Its defining gauge symmetry group is the non-Abelian $SU(N_c)$ group, where $N_c = 3$ is the number of colors [8–11]. Non-perturbative approaches are essential to explain the hadron spectrum as well as describe low-energy phenomena such as spontaneous chiral symmetry breaking, the running of the coupling constant [12–14], and color confinement [15].

In this Chapter, we introduce such key aspects of QCD, with a strong emphasis on non-perturbative methods. In Section 1.1, we introduce the path integral formulation of QCD, describing its classical gluonic and fermionic actions. In Section 1.2, we complete the definition of QCD as a QFT by introducing its non-perturbative renormalization through hadronic renormalization schemes. The QCD spectrum is described in Section 1.3, while the classical and quantum symmetries of the theory are detailed in Section 1.4, with a more thorough discussion regarding the spontaneous breaking of chiral symmetry and the implications of the anomaly in axial singlet transformations. Unless states otherwise, we work in Euclidean spacetime for later convenience, where we set $\mu = 0$ as the temporal direction in our convention, and implicit summation over repeated indices is assumed throughout.

1.1 The QCD path integral

The path integral formalism allows to define QFTs non-perturbatively, and to derive theoretical predictions ab initio, i.e. from first principles. In this Section, we introduce the classical action and the continuum definition of the QCD path integral, while we defer to the next Section the discussion of the renormalization procedure, required to define a predictive theory. We note that finite expressions can only be obtained once spacetime is also discretized and defined on a finite volume, where they can be evaluated via numerical and computational methods, forming the core of Lattice QCD, which is the focus of Chapter 2.

1.1.1 The path integral and the Euclidean metric

Being a QFT, all the terms in the QCD action

$$S_{\rm QCD} = \int d^4x\, \mathcal{L}_{\rm QCD}\,, \tag{1.1.1}$$

where $\mathcal{L}_{\rm QCD}$ is the QCD Lagrangian density, are fixed by requiring that

1. the action is invariant under transformations of the $SU(3)$ gauge group;
2. fermions (quarks) are triplets in the fundamental representation of $SU(3)$;
3. the terms in $\mathcal{L}_{\rm QCD}$ have mass dimension ≤ 4 to ensure renormalizability.

From the knowledge of the QCD action, detailed in the next Subsection, the theory is quantized through its path integral definition. The Wick rotation from Minkowskian to Euclidean spacetime

$$x_0 \to i x_0^E\,, \quad x^i \to x_i^E\,, \quad \partial_0 \to i\partial_0^E\,, \quad \partial_i \to \partial_i^E\,, \quad x_\mu y^\mu \to -x_\mu^E y_\mu^E\,, \tag{1.1.2}$$

relates Minkowskian to Euclidean actions $S_M \to -iS_E \equiv -iS$ and allows us to estimate the partition function

$$Z = \int [dA]\,[d\overline{\psi}]\,[d\psi] e^{-S_{\rm QCD}[A_\mu,\overline{\psi},\psi]} \tag{1.1.3}$$

and expectation values

$$\langle \mathcal{O} \rangle = \frac{1}{Z} \int [dA]\,[d\overline{\psi}]\,[d\psi]\, e^{-S_{\rm QCD}[A,\overline{\psi},\psi]} \mathcal{O}[A,\overline{\psi},\psi]\,, \tag{1.1.4}$$

where the measure $[d\cdot]$ spans over all possible field configurations, with the field content specified later on in this Section. The exponentially decaying factor $e^{-S_{\rm QCD}}$ in Eq. (1.1.4) allows Euclidean correlation functions (operator expectation values) to be interpreted as stochastic thermal averages, enabling the application of well-known methods of statistical mechanics to study QFTs. If needed, our final predictions can thus be rotated back to physical Minkowskian time.

Moreover, Euclidean spacetime provides a rigorous framework for axiomatic QFTs. It is well known that any QFT may be formulated from first principles in terms of Feynman amplitudes in Euclidean spacetime [16], from which the corresponding Minkowskian amplitudes can be reconstructed, provided a set of physically plausible axioms is satisfied. The vice versa holds as well. This result is known as the Osterwalder-Schrader theorem [17], which mirrors the Wightman axioms for QFTs in Minkowski spacetime [18].

1.1.2 The QCD action

We now want to construct the QCD action following the properties detailed above. Specifically, we express $S_{\rm QCD} = S_{\rm G} + S_{\rm F}$, separating the gluonic $S_{\rm G}$ and fermionic $S_{\rm F}$ actions, which we study individually.

Yang-Mills theory: gluons

QCD is based on local gauge invariance under the $SU(3)$ group, with the corresponding quanta known as *gluons*. The gauge fields in QCD are represented by $A_\mu(x) = A^a_\mu(x)T^a$, where $\mu = 0,\dots,3$ is the Lorentz index, and $a = 1,\dots,8$ is the color index associated with the $SU(3)$ algebra $\mathfrak{su}(3)$, whose Hermitian generators are denoted as T^a and satisfy $\mathrm{Tr}\{T^aT^b\} = \delta^{ab}/2$. The non-Abelian field strength tensor is

$$F_{\mu\nu} = i[D_\mu, D_\nu] = F^a_{\mu\nu}T^a\,, \quad D_\mu = \partial_\mu - iA_\mu \tag{1.1.5}$$

where D_μ is the covariant derivative. The components of $F_{\mu\nu}$ can be written in terms of the structure constants f^{abc} of $\mathfrak{su}(3)$

$$F^a_{\mu\nu} = \partial_\mu A^a_\nu(x) - \partial_\nu A^a_\mu(x) + f^{abc}A^b_\mu(x)A^c_\nu(x)\,, \quad f^{abc} = -2i\,\mathrm{Tr}\{[T^a,T^b]T^c\} \tag{1.1.6}$$

where the third term in $F^a_{\mu\nu}$ is due to the non-Abelian nature of $SU(3)$ and it is responsible for gluon self-interactions. Under a local gauge transformation

$$G(x) = \exp\{i\theta(x)\} \in SU(3)\,, \quad \theta(x) = \theta^a(x)T^a \in \mathfrak{su}(3) \tag{1.1.7}$$

the gauge field and the strength tensor transform as

$$A_\mu(x) \to iG(x)D_\mu G(x)^\dagger\,, \quad F_{\mu\nu}(x) \to G(x)F_{\mu\nu}(x)G(x)^\dagger\,. \tag{1.1.8}$$

The gluonic action in QCD is then given by two gauge-invariant contributions with mass dimension ≤ 4, namely

$$S_{\mathrm{G}}[A_\mu] = \frac{1}{2g_0^2}\int d^4x\ \mathrm{Tr}\{F_{\mu\nu}(x)F_{\mu\nu}(x)\}\,, \tag{1.1.9}$$

which is invariant due to the trace over color indices, and

$$S_{\mathrm{Q}}[A_\mu] = -i\theta\int d^4\,q(x)\,, \quad q(x) = \frac{1}{32\pi^2}\epsilon_{\mu\nu\rho\sigma}\,\mathrm{Tr}\{F_{\mu\nu}(x)F_{\rho\sigma}(x)\}\,, \tag{1.1.10}$$

which explicitly violates parity, where $q(x)$ is the topological charge density. Note that CP violation has not been observed in strong interactions so far, with experiments constraining $|\theta| \leqslant 10^{-10}$, see Ref. [19]. Unless stated otherwise, we assume $\theta = 0$ and, noting that the operators appearing in S_{G} and S_{Q} do not mix under renormalization, we neglect S_{Q} in the rest of this Thesis.

Fermionic fields: quarks

In QCD, fermions represent the matter fields, and the quark fields ψ are Dirac spinors in the fundamental representation of $SU(3)_{\mathrm{c}}$. Under the local gauge transformation in Eq. (1.1.7), they transform as

$$\psi(x) \to G(x)\psi(x)\,, \quad D_\mu\psi(x) \to G(x)D_\mu\psi(x)\,, \quad \overline{\psi}(x) \to \overline{\psi}(x)G(x)^\dagger \tag{1.1.11}$$

where γ_μ are the usual Dirac gamma matrices satisfying Clifford algebra in Euclidean time, $\{\gamma_\mu, \gamma_\nu\} = 2\delta_{\mu\nu}$. The quark-gluon interaction is introduced via the covariant derivative defined above, and considering the only two gauge-invariant operators with mass dimension ≤ 4 we obtain the gauge-invariant Dirac action

$$S_{\mathrm{F}}[\overline{\psi}, \psi, A_\mu] = \int d^4x\, \overline{\psi}(x)\, (\gamma_\mu D_\mu + m)\, \psi(x)\,, \tag{1.1.12}$$

where m is the bare quark mass.

A theory with N_{f} quark flavors is described by simply considering multiple copies of the single-quark Lagrangian. The resulting full QCD Lagrangian density with N_{f} quark flavors is thus

$$\mathcal{L}_{\mathrm{QCD}} = \sum_{\mathrm{f}=1}^{N_{\mathrm{f}}} \overline{\psi}_{\mathrm{f}}(\gamma_\mu D_\mu + m_{\mathrm{f}})\psi_{\mathrm{f}} + \frac{1}{2g^2}\,\mathrm{Tr}\{F_{\mu\nu}F_{\mu\nu}\}\,, \tag{1.1.13}$$

where m_{f} is the bare mass of the quark field ψ_{f}.

1.2 Renormalization

A further step is required in order to extract physical predictions from the path integral formulation of QCD. This is achieved through a process known as *renormalization*, which entails two key steps: introducing a regularization and adopting a renormalization scheme. This is a necessary step in order to properly define any predictive QFT[1].

Regularization – The first step in the renormalization procedure is to rigorously define expectation values $\langle \mathcal{O} \rangle$ as in Eq. (1.1.4). The only known non-perturbative approach that allows to do so is the *lattice* regularization, consisting in defining the theory on a discrete spacetime lattice. The theory is automatically regulated in the ultraviolet region, with a hard momentum cutoff equal to π/a due to a non-zero lattice spacing a.

Renormalization Schemes – If we were to remove the regularization parameter a while keeping the bare parameters fixed – specifically, the values of the coupling constant and masses –, we would retrieve divergent results. A further step is required to complete the renormalization procedure, namely choosing a renormalization scheme. This involves defining the dependence of bare quantities on the regulating parameter by fixing a certain set of observables to their physical values. For a renormalizable theory as QCD, it is sufficient to introduce a finite set of renormalization conditions. In order to fix this dependence, different conditions i.e. different renormalization schemes can be employed.

1.2.1 Non-perturbative renormalization

We now focus on non-perturbative renormalization, anticipating that the results derived here from a non-perturbative definition of the regularization and the renormalization

[1]Without it, perturbative studies quickly reveal the presence of ultraviolet (UV) divergences in momentum integrals, which must be canceled order by order to define physically meaningful quantities.

scheme are fully non-perturbative themselves, including renormalization group equations.

The starting point of *hadronic renormalization schemes* is the definition of non-perturbative renormalization conditions in terms of physical observables, such as hadron masses, decay constants or matrix elements, which are required to assume prescribed values. Once this dimensionful scale, e.g. a mass, is fixed, other dimensionful quantities can be determined by calculating dimensionless ratios relative to this initial choice. Having in mind applications in Lattice QCD, where the regulating parameter is the lattice spacing a, we can fix the bare coupling constant g_0 dependence on a by requiring that, as a varies, the mass of a hadron $M_H(g_0, a)$ computed at chosen g_0 and a matches its physical value $(M_H^{\mathrm{PHYS}})^2$,i.e.

$$M_H^2(g_0, a) \equiv \left(M_H^{\mathrm{PHYS}}\right)^2 \quad \rightarrow \quad g_0 = \left(aM_H^{\mathrm{PHYS}}\right) \tag{1.2.1}$$

which can be defined in the limit of massless quarks, thus being independent of bare quark masses. Since QCD is renormalizable, this condition is sufficient to fix the dependence $g_0 = g_0(aM_H)$, ensuring that varying the coupling is equivalent to changing the lattice spacing while keeping the hadron mass constant. A possible choice is to set M_H equal to the mass of the proton, although other reference scales, such as the pion decay constant, can also be used.
Additional conditions are required to fix the dependence of other bare parameters. For instance, we can fix the mass of the light quarks $m_u = m_d \equiv m_l$ and of the strange quark m_s from the pion and kaon masses, i.e.

$$\begin{cases} m_\pi^2(a, g_0, m_l, m_s) = \left(m_\pi^{\mathrm{PHYS}}\right)^2 \\ M_K^2(a, g_0, m_l, m_s) = \left(M_K^{\mathrm{PHYS}}\right)^2 \end{cases} \rightarrow \begin{cases} m_l = m_l(aM_H^{\mathrm{PHYS}}, am_\pi^{\mathrm{PHYS}}, aM_K^{\mathrm{PHYS}}) \\ m_s = m_s(aM_H^{\mathrm{PHYS}}, am_\pi^{\mathrm{PHYS}}, aM_K^{\mathrm{PHYS}}) \end{cases} \tag{1.2.2}$$

where the additional dependence on aM_H^{PHYS} on the r.h.s. is dictated by Eq. (1.2.1). The same procedure can be applied to compute the normalization of local operators by fixing a certain matrix element of this operator to assume a prescribed value.

Matching to other schemes

Once the set of renormalization conditions has been defined, we can match a given hadronic scheme with any other renormalization scheme, such as the perturbative $\overline{MS}$ scheme of dimensional regularization, through the computation of the running of renormalized couplings and quark masses, as well as connecting operators and fields renormalization constants. This turns out to be useful to compare results for couplings or quark masses between non-perturbative and perturbative approaches. A possible scheme in Lattice QCD is the Schrödinger Functional (SF) scheme [20], with periodic spatial boundary conditions and Dirichlet boundary conditions in time, allowing to control the variation of the scale $\mu = 1/L$ through changes in the spatial extent of the system L. In this scheme, the coupling constant is defined by the response of the system to variations

in the boundary conditions, and recursive finite-size techniques allow matching lattices at different volumes, effectively constructing a non-perturbative renormalization group. Since Ward-Takashi Identities are non-perturbative by definition[2] , they can be used to define additional non-perturbative conditions. For instance, the light quark masses at a fixed μ can be defined using the PCAC relation, see Eqs. (1.4.16) and (1.4.18). The operators involved in this relation are defined within the non-perturbative SF scheme, with the spatial box size set to $L = 1/\mu$. We can define non-perturbatively renormalized couplings and masses

$$g^2_{\rm R}(\mu) \equiv g^2_{\rm SF}(\mu) = Z_g(g_0, a\mu) g_0^2\,, \quad m_{\rm R}(\mu) \equiv m_{\rm SF}(\mu) = Z_m(g_0, a\mu) m_0 \tag{1.2.3}$$

as well as renormalized fields

$$(A_R)_\mu = Z_3^{1/2}(g_0, a\mu) A_\mu\,, \quad \psi_R = Z_2(g_0, a\mu)\psi\,. \tag{1.2.4}$$

All the renormalization constants Z_i are also functions of $M_P^{\rm PHYS}, \ldots$, as they depend on the initial renormalization conditions imposed in the fully non-perturbative hadronic renormalization scheme. These renormalized quantities can then be computed in the perturbative SF scheme as well, and only at this point can they be matched to any other perturbative scheme.

Another approach to define a non-perturbative matching procedure is the Wilson flow [21–23], where the evolution of gauge fields in a fictitious flow-time variable effectively suppressess UV divergences and isolates the IR features of QCD, providing a physical scale at which precise non-perturbative renormalization conditions can be defined.

1.2.2 Renormalization group equations

The invariance of physical quantities under changes in the renormalization scale μ is expressed by the Callan-Symanzik renormalization group (RG) equations [24,25]. These equations dictate how renormalized couplings and masses evolve as a function of μ, ensuring that the physical content of the theory remains unchanged. As noted above, starting from a non-perturbative regularization and renormalization scheme, they are valid non-perturbatively. We can start from the definitions of renormalized coupling, mass and fields as in Eqs. (1.2.3) and (1.2.4), where we note that the renormalization constants can only depend on dimensionless parameters. Renormalized quantities are both scale and scheme dependent, but they can be defined non-perturbatively e.g. in Lattice QCD as detailed above, thus making the whole RG non-perturbative.
A generic scale dependent, amputated and connected bare correlation function $\Gamma_0^{(n_{\rm G}, n_{\rm F})}$ involving $n_{\rm G}$ gauge and $n_{\rm F}$ fermionic fields renormalizes as

$$\Gamma_R^{(n_{\rm G}, n_{\rm F})}(\{x_j\}; \mu, g_R, m_R) = \Gamma_0^{(n_{\rm G}, n_{\rm F})}(\{x_j\}; g_0, m_0) \left(Z_3^{1/2}\right)^{n_{\rm G}} \left(Z_2^{1/2}\right)^{2n_{\rm F}} \tag{1.2.5}$$

[2]These identities are derived through a change of variables in the path integral, and their functional form is independent of the realization of their generating symmetries, see Subsection 1.4.1.

where we emphasize the scale dependence of the renormalized correlator $\Gamma_R^{(n_G,n_F)}$, which is also a function of renormalized coupling and masses. The RG equation follows from the requirement that $\frac{d}{d\mu}\Gamma_0^{(n_G,n_F)} = 0$, which can be rewritten as

$$\left[\mu\frac{\partial}{\partial\mu} + \beta\frac{\partial}{\partial g_R} + \gamma_m m_R\frac{\partial}{\partial m_R} - n_G\gamma_3 - 2n_F\gamma_2\right]\Gamma_R^{(n_G,n_F)} = 0 \tag{1.2.6}$$

where we introduced

$$\beta(g_R) = \lim_{a\to 0}\left[\mu\left.\frac{\partial g_R}{\partial\mu}\right|_{g_0,m_0,a}\right], \quad \gamma_m(g_R) = \lim_{a\to 0}\left[\frac{\mu}{m_R}\left.\frac{\partial m_R}{\partial\mu}\right|_{g_0,m_0,a}\right] \tag{1.2.7}$$

and

$$\gamma_3(g_R) = \lim_{a\to 0}\left[\frac{1}{2}\mu\left.\frac{\partial \ln Z_3}{\partial\mu}\right|_{g_0,m_0,a}\right], \quad \gamma_2(g_R) = \lim_{a\to 0}\left[\frac{1}{2}\mu\left.\frac{\partial \ln Z_2}{\partial\mu}\right|_{g_0,m_0,a}\right]. \tag{1.2.8}$$

The β and γ_m functions exactly describe how the parameters of the theory behave at different energy scales. The β function can be expanded as $\beta(g_R) = -g_R^3\sum_{k=0}^{+\infty} b_k g_R^{2k}$ and the first coefficients can be computed perturbatively [26]. For QCD with N_f flavors and $N_c = 3$ colors we obtain

$$b_0 = \frac{1}{4\pi^2}\left(\frac{11}{3}N_c - \frac{2}{3}N_f\right) > 0\,, \quad b_1 = \frac{1}{4\pi^2}\left[\frac{34}{3}N_c^2 - \left(\frac{13}{3}N_c - \frac{1}{N_c}\right)N_f\right] > 0\,. \tag{1.2.9}$$

A similar expansion and computation can be done for

$$\gamma_m(g_R) = -g_R^2\sum_{k=0}^{\infty} d_k g_R^{2k}\,, \quad d_0 = \frac{1}{(4\pi)^2}\,3\,\frac{N_c^2-1}{N_c}\,. \tag{1.2.10}$$

Notice that b_0, b_1 and d_0 are universal coefficients, i.e. they are scheme independent, and their signs are crucial to understand the approximate behavior of QCD at high energies through approximate solutions of Eqs. (1.2.7). Considering only the first term in β we obtain

$$g_R^2 = \frac{1}{b_0\ln\frac{\mu^2}{\Lambda^2}} \xrightarrow{\mu\to\infty} 0 \tag{1.2.11}$$

which defines the property of *asymptotic freedom* [27–29]: quarks weakly interact at high energies (as long as strong interaction is concerned), allowing for a perturbative approach in this regime.

1.2.3 Renormalization group invariants: Λ_{QCD} and masses

In order to study the dependence of the coupling on the scale, we need to solve the differential equation in Eq. (1.2.7), finding the non-perturbative result

$$\mu_1\exp\left\{-\int_{\overline{g}}^{g(\mu_1)}\frac{dg}{\beta(g)}\right\} = \mu_2\exp\left\{-\int_{\overline{g}}^{g(\mu_2)}\frac{dg}{\beta(g)}\right\}, \tag{1.2.12}$$

where both the r.h.s. and the l.h.s. are independent of the choice of the scale, thus defining a RG invariant scale. We can also apply a subtraction to avoid divergences that would otherwise arise in setting the lower bound of the integral in Eq. (1.2.12) to zero, based on the perturbative knowledge of b_0, b_1, obtaining the RG invariant scale

$$\Lambda_{\rm QCD} = \mu \left(b_0 g^2\right)^{-b_1/(2b_0^2)} e^{-1/(2b_0 g^2)} \exp\left\{ - \int_0^g dx \left[\frac{1}{\beta(x)} + \frac{1}{b_0 x^3} - \frac{b_1}{b_0^2 x} \right] \right\} . \tag{1.2.13}$$

This definition is completely non-perturbative. Even though it is invariant under RG equations, i.e. it satisfies the massless RG equation

$$\left(\mu \frac{\partial}{\partial \mu} + \beta \frac{\partial}{\partial g} \right) \Lambda_{\rm QCD} = 0 \, , \tag{1.2.14}$$

the definition of $\Lambda_{\rm QCD}$ is still scheme dependent. Notice also the explicit breaking of classical scale invariance, since $\Lambda_{\rm QCD}$ is a dimensionful quantity in a classically scale invariant theory, a property called *dimensional transmutation*.

Similarly, a RG invariant mass can be defined from γ_m in Eq. (1.2.7), finding

$$m_R(\mu_1) \exp\left\{ - \int_{\overline{g}}^{g(\mu_1)} dg \, \frac{\gamma_m(g)}{\beta(g)} \right\} = m_R(\mu_2) \exp\left\{ - \int_{\overline{g}}^{g(\mu_2)} dg \, \frac{\gamma_m(g)}{\beta(g)} \right\} \tag{1.2.15}$$

from which the RG invariant, scheme-independent mass can be defined as

$$M \equiv m_R(\mu) \left(2 b_0 g^2\right)^{-d_0/(2b_0)} \exp\left\{ - \int_0^g dx \left[\frac{\gamma_m(x)}{\beta(x)} - \frac{d_0}{b_0} \frac{1}{x} \right] \right\} \tag{1.2.16}$$

which satisfies the massive RG equation

$$\left[\mu \frac{\partial}{\partial \mu} + \beta \frac{\partial}{\partial g} + \gamma_m m_R \frac{\partial}{\partial m_R} \right] M = 0 \, . \tag{1.2.17}$$

1.2.4 The running of the coupling constant

The physical hadron mass is the only free parameter we need to fix in the hadronic renormalization scheme as in Eq. (1.2.1) to address the running of the coupling constant. Since the latter is a dimensionless parameter, it can only depend on the the scale μ via the dimensionless ratios $\mu/\Lambda_{\rm QCD}$, μ/M_H.

The procedure we presented above to introduce non-perturbative renormalization schemes can be applied to explicitly compute the running of the coupling constant. For instance, in the Schrödinger Functional scheme [20], the running with the scale $\mu = 1/L$ can be studied using step-scaling functions σ, describing how the coupling changes as the spatial extent L is doubled through $\sigma(\alpha(L)) = \alpha(2L)$. These functions σ can be computed non-perturbatively on the lattice, to then trace the evolution of the coupling constant from perturbative high-energy to non-perturbative low-energy scales. The left plot in Fig. 1.1 shows the calculation of the running of the strong coupling constant

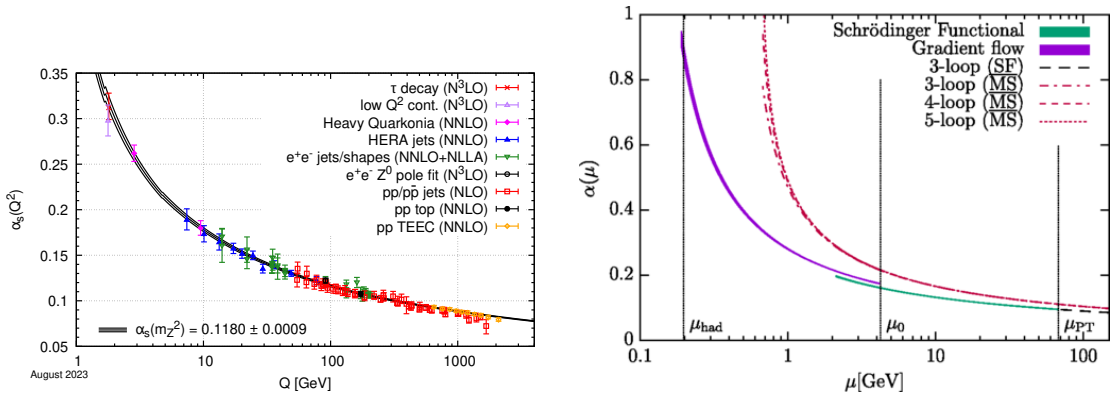

Figure 1.1: On the left: perturbative determination of the running of the strong coupling constant as a function of the energy scale Q, cf. Fig. 9.5 in Ref. [30]. On the right: non-perturbative determination of the running coupling of $N_\mathrm{f} = 3$ QCD from integrating the non-perturbative β functions in the Schrödinger Functional and Gradient Flow renormalization schemes in Lattice QCD, from Ref. [31].

$\alpha_s = g^2/(4\pi)$ at different orders in perturbation theory using various experimental inputs, leading to the perturbative result $\alpha_s(M_Z^2) = 0.1175(10)$ [30]. Progresses in Lattice QCD have recently enabled a non-perturbative determination of the QCD running coupling, shown in the right plot of Fig. 1.1, taken from Ref. [31]. The world average lattice determination is provided by the FLAG collaboration, including several contributions leading to the final estimate $\alpha_s(M_Z^2) = 0.1184(8)$ [32]. This shows an impressive agreement between non-perturbative predictions, based on the non-perturbative renormalization procedure described above, necessitating a few experimental inputs such as hadron masses or decay constants, and perturbative predictions at different orders, based on completely different experimental inputs. The current final world average is given by a combination of these two estimates, and it is equal to $\alpha_s(M_Z^2) = 0.1180(9)$ [30].

1.3 Hadron spectrum

The QCD spectrum consists of a tower of many states of composite particles, known as hadrons, which are bound states made of quarks ψ_f. An essential feature of QCD is *confinement*, namely that all hadrons must be colorless, i.e. singlets under $SU(3)_\mathrm{c}$ transformations. Confinement prevents color charges from being isolated, until a pair of quark and antiquark becomes energetically more convenient and is spontaneously produced. It can be explained by the presence of a constant term in the force between a pair of quarks (color charges) as a function of their separation, i.e. with a linear *string* term in the corresponding energy. The most common particles are *mesons*, bosonic particles built by combining a quark and an antiquark, such as the pion or the kaon, and *baryons*, fermionic particles formed by three quarks, such as the proton (uud) and neutron (udd).

To explore the QCD spectrum, we consider a simple but instructive example, restricting ourselves to the case of $N_f = 3$ light quark flavors: up, down and strange quarks. In the limit where these quarks are degenerate, the theory exhibits an $SU(3)$ flavor symmetry. The light meson spectrum can then be classified into representations based on flavor symmetry. Group theory tells us that combining a quark in the fundamental representation (3) of $SU(3)$ with an antiquark in the anti-fundamental representation ($\overline{3}$) yields $3 \otimes \overline{3} = 1 \oplus 8$, which correspond to a singlet and an octet of meson states represented in Fig. 1.2. As further motivated in Subsection 1.4.2, the singlet is a single pseudoscalar meson of the form $\eta_1 = (u\overline{u} + d\overline{d} + s\overline{s})/\sqrt{3}$, while the octet consists of the following light pseudoscalar mesons, which are spinless and antisymmetric under parity transformations:

- *pions* are formed by up and down quarks as $\pi^+ = u\overline{d}$, $\pi^- = d\overline{u}$, $\pi^0 = (u\overline{u} - d\overline{d})/\sqrt{2}$;
- *kaons* involve the strange quark as $K^+ = u\overline{s}$, $K^- = s\overline{u}$, $K^0 = d\overline{s}$, $\overline{K}^0 = s\overline{d}$;
- η_8 is a neutral meson, combining all three quarks as $\eta_8 = (u\overline{u} + d\overline{d} - 2s\overline{s})/\sqrt{6}$.

An interesting feature of QCD is that the η_1 and η_8 states do not correspond directly to the experimentally observed η and η' mesons. Only in the isosymmetric limit we can perform the assignment $\eta = \eta_8$ and $\eta' = \eta_0$, whereas in Nature we observe a breaking of the exact flavor symmetry, and an associated mixing

$$\begin{pmatrix} \eta \\ \eta' \end{pmatrix} = \begin{pmatrix} \cos\theta & -\sin\theta \\ \sin\theta & \cos\theta \end{pmatrix} \begin{pmatrix} \eta_8 \\ \eta_1 \end{pmatrix} \tag{1.3.1}$$

with the small mixing angle $\theta \in (-10°, -20°)$ [30]. We note that the large mass of the η' w.r.t. the η and the other light mesons is naturally explained by the Witten-Veneziano mechanism described in Subsection 1.4.3. A similar analysis applies to baryon states as well, allowing them to be classified according to their flavor content and spin configurations. For instance, in the case of $N_f = 3$, the combination of three quarks results in flavor multiplets such as the baryon octet and decuplet. These multiplets include well-known particles such as the proton, neutron, and Σ, Ξ, and Ω baryons.

Lattice QCD has been successful in predicting non-perturbatively from first principles the masses and other properties of many meson and baryon states, providing a quantitative comparison with experimental results, as illustrated in Fig. 1.3. This agreement highlights the power of Lattice QCD in capturing the essential features of the strong interaction and validating our understanding of the QCD spectrum.

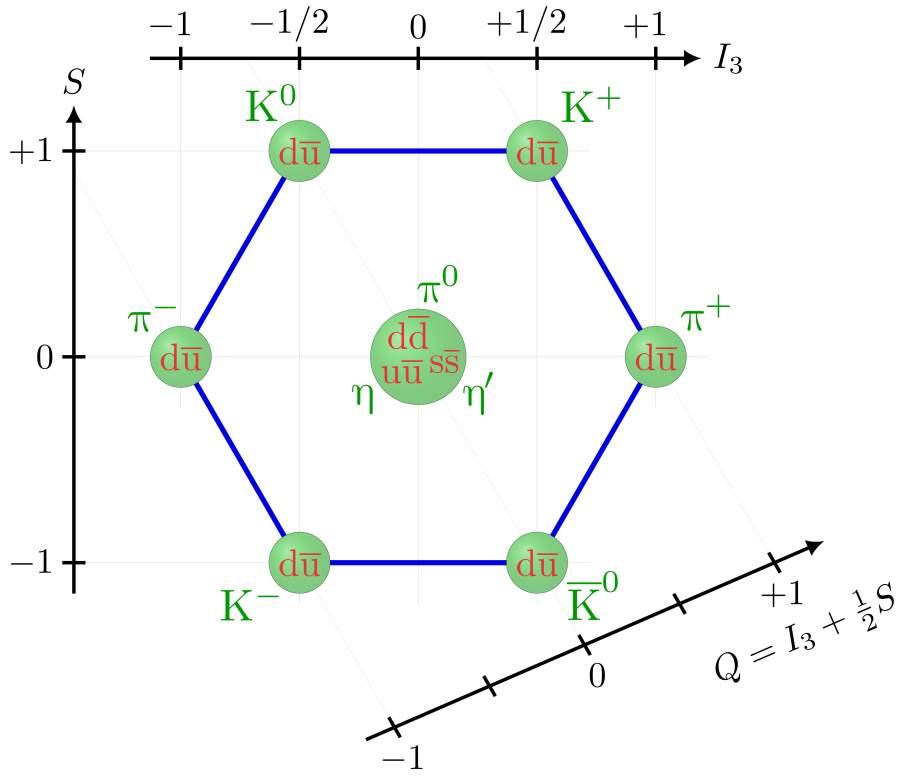

Figure 1.2: Light meson octet in QCD.

1.4 Chiral symmetry

Many low-energy properties of QCD can be derived from flavor and chiral symmetry. We can define chiral left and right flavor components of quarks as

$$\psi_{L,R} = P_{L,R}\,\psi\,, \quad P_L = \frac{1-\gamma_5}{2}\,, \quad P_R = \frac{1+\gamma_5}{2}\,, \quad \psi = \begin{pmatrix} \psi_1 \\ \psi_2 \\ \vdots \\ \psi_{N_\mathrm{f}} \end{pmatrix}, \tag{1.4.1}$$

where in Euclidean time we set $\gamma_5 = \gamma_0\gamma_1\gamma_2\gamma_3$. Noticing that the QCD action in Eq. (1.1.3) is diagonal in flavor space, we can rewrite its fermionic part as

$$S_\mathrm{F} = \int d^4x \left[\overline{\psi}_L\gamma_\mu D_\mu\psi_L + \overline{\psi}_R\gamma_\mu D_\mu\psi_R + \overline{\psi}_R M^\dagger\psi_L + \overline{\psi}_L M\psi_R\right](x) \tag{1.4.2}$$

where $M = M^\dagger = \mathrm{diag}(m_1, m_2, \ldots, m_{N_\mathrm{f}})$ is the diagonal mass matrix. The first two terms in the action are invariant under the gloabl chiral group $U(N_\mathrm{f})_L \otimes U(N_\mathrm{f})_R$ which independently rotates left and right components of each quark flavor, while the mass terms explicitly break the symmetry. It is useful to decompose the full chiral group as

$$U(N_\mathrm{f})_L \otimes U(N_\mathrm{f})_R = U(1)_L \otimes SU(N_\mathrm{f})_L \otimes U(1)_R \otimes SU(N_\mathrm{f})_R\,, \tag{1.4.3}$$

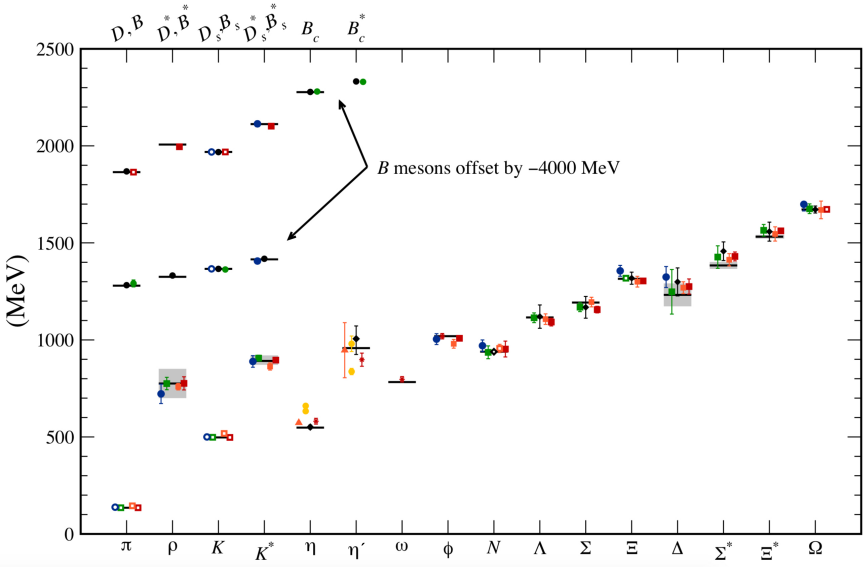

Figure 1.3: Hadron spectrum from Lattice QCD for different discretization choices. Horizontal bars (gray boxes) denote experimentally measured masses (widths). See Fig. 15.9 in Ref. [30] and references therein.

where the associated transformations act only on flavor indices as

$$\psi_{L,R} \to \psi'_{L,R} = V_{L,R}\psi_{L,R}\,, \quad V_{L,R} = \exp\left\{i\epsilon^0_{L,R} + i\epsilon^a_{L,R}T^a\right\}. \tag{1.4.4}$$

The corresponding infinitesimal transformations are

$$\psi_{L,R} \to \psi'_L = V_{L,R}\psi_{L,R} \simeq \left(1 + i\,\epsilon^0_{L,R} + i\,\epsilon^a_{L,R}\,T^a\right)\psi_L \tag{1.4.5}$$

under which

$$\begin{aligned}\psi = \psi_L + \psi_R &\to \left(1 + i\,\epsilon^0_L + i\,\epsilon^a_L\,T^a\right)\psi_L + \left(1 + i\,\epsilon^0_R + i\,\epsilon^a_R\,T^a\right)\psi_R \\ &= \left(1 + i\,\frac{\epsilon^0_L + \epsilon^0_R}{2} + i\,\frac{\epsilon^0_R - \epsilon^0_L}{2}\,\gamma_5 + i\,\frac{\epsilon^a_L + \epsilon^a_R}{2}\,T^a + i\,\frac{\epsilon^a_R - \epsilon^a_L}{2}\,T^a\,\gamma_5\right)\psi\,, \end{aligned} \tag{1.4.6}$$

$$\overline{\psi} \to \overline{\psi}\left(1 - i\,\frac{\epsilon^0_L + \epsilon^0_R}{2} + i\,\frac{\epsilon^0_R - \epsilon^0_L}{2}\,\gamma_5 - i\,\frac{\epsilon^a_L + \epsilon^a_R}{2}\,T^a + i\,\frac{\epsilon^a_R - \epsilon^a_L}{2}\,T^a\,\gamma_5\right). \tag{1.4.7}$$

It is now interesting to consider the following subgroups of the chiral group:

1. $U(1)_V$ vectorial singlet subgroup: $\epsilon^0_L = \epsilon^0_R$, $\epsilon^a_L = \epsilon^a_R = 0$;
2. $U(1)_A$ axial singlet subgroup: $\epsilon^0_L = -\epsilon^0_R$, $\epsilon^a_L = \epsilon^a_R = 0$;
3. $SU(N_\mathrm{f})_V$ non-Abelian vectorial subgroup: $\epsilon^0_L = \epsilon^0_R = 0$, $\epsilon^a_L = \epsilon^a_R$;
4. the remaining non-Abelian axial transformation, with $\epsilon^0_L = \epsilon^0_R = 0$ and $\epsilon^a_L = -\epsilon^a_R$, does not form a group.

1.4.1 Chiral symmetry of the quantum theory

In QFTs, a symmetry of the action does not always correspond to a symmetry of the quantum theory. For a classical symmetry to be extended to a symmetry of the corresponding QFT, a few conditions must be met, namely the path integral measure being invariant under symmetry transformations and the renormalization procedure preserving this symmetry. If these conditions are not met, the classical symmetry is said to be *anomalous*. A well-known example is the classical scale invariance being broken due to dimensional transmutation during the renormalization procedure, linked to the quantization spoiling the traceless property of the classical energy-momentum tensor.

In general, considering a transformation under which a field changes as $\mathcal{O} \to \mathcal{O} + \delta\mathcal{O}$ and the action transforms as $S \to S + \delta S$, a simple change of variables of the path integral leads to the general form of Ward-Takashi identities (WTIs)

$$\langle \delta\mathcal{O} \rangle = \langle \mathcal{O}\delta S \rangle + \langle \ln[\mathcal{J}]\mathcal{O} \rangle \,, \tag{1.4.8}$$

where $\mathcal{J}$ is the determinant of the Jacobian of the transformation of the path integral measure. For the subgroups of the chiral group mentioned above, it turns out that only $U(1)_A$ transformations cause a non-trivial Jacobian. Therefore, the axial $U(1)_A$ symmetry is anomalous, making QCD not invariant under the entire chiral group even in the massless limit.

Axial singlet $U(1)_A$ anomaly

The anomalous breaking of the axial $U(1)_A$ symmetry stems from the variation of the path integral measure under these transformations[3], since

$$d\overline{\psi}d\psi \to e^{-2i\epsilon_A^0 Q} d\overline{\psi}d\psi \tag{1.4.9}$$

where Q is the topological charge in Eq. (1.1.10).
The anomalous WTI can be derived[3] from Eq. (1.4.8) and it is given by

$$-i\epsilon_A^0 \partial_\mu^x \langle A_\mu^0(x)\mathcal{O}(y) \rangle = -2i\epsilon_A^0 N_{\mathrm{f}} \langle q(x)\mathcal{O}(y) \rangle + \langle \delta\mathcal{O}(y) \rangle \,. \tag{1.4.10}$$

By choosing $\mathcal{O}$ as the topological charge density q, defined in Eq. (1.1.10), the local axial WTI in the chiral limit $m \to 0$ becomes

$$\langle \partial_\mu A_\mu^0(x) q(0) \rangle = 2N_{\mathrm{f}} \langle q(x)q(0) \rangle \,, \quad m = 0 \,. \tag{1.4.11}$$

This relation is useful in the Witten-Veneziano mechanism, relating the $U(1)_A$ anomaly to the large mass of the η' meson, see Subsection 1.4.3.

[3] Here we only provide the formal derivation and results, which can be properly defined in the context of Lattice QCD, employing Ginsparg-Wilson discretization of fermions [33–35], see Subsection 2.3.3, which preserve a lattice version of chiral symmetry defined from Lüscher transformations [36].

Vector singlet $U(1)_V$ transformations

The $U(1)_V$ symmetry remains exact for any value of the masses, with the associated WTIs given by

$$-i\epsilon_V^0 \partial_\mu \langle V_\mu^0(x)\mathcal{O}\rangle = \langle \delta\mathcal{O}\rangle\,, \quad V_\mu^0 \equiv \overline{\psi}\gamma_\mu\psi\,. \tag{1.4.12}$$

Therefore, the charge $\overline{V}^0$ associated to this current is always conserved in QCD, i.e. for any invariant observable $\mathcal{O}$ under vector singlet transformations we have

$$\partial_{x_0}\langle \overline{V}^0(x_0)\mathcal{O}(y)\rangle = 0\ \forall x_0 \neq y_0\,, \quad \overline{V}^0 = \int d^3\mathbf{x}\, V^0(x)\,. \tag{1.4.13}$$

This conserved charge is identified as the baryonic number, which measures the difference between the number of quarks and antiquarks.

Vector non-singlet subgroup $SU(N_\mathrm{f})_V$

The general form of WTIs for the transformations of the non-Abelian vector subgroup, often called *isospin* for $N_\mathrm{f} = 2$ and *generalized isospin* for $N_\mathrm{f} = 3$, is

$$-i\epsilon_V^a \partial_\mu \langle V_\mu^a(x)\mathcal{O}\rangle = -i\epsilon_V^a \langle \overline{\psi}(x)[M,T^a]\psi(x)\mathcal{O}\rangle + \langle \delta\mathcal{O}\rangle\,, \quad V_\mu^a \equiv \overline{\psi}\gamma_\mu T^a\psi\,. \tag{1.4.14}$$

The corresponding charge $\overline{V}_0^a = \int d^3\mathbf{x}\, V_0^a(x)$ is conserved only when $[M,T^a] = 0$, i.e. with degenerate quark masses.

Axial non-singlet transformations

The general form of the WTIs associated with axial non-singlet transformations is

$$-i\epsilon_A^a \partial_\mu \langle A_\mu^a(x)\mathcal{O}\rangle = -i\epsilon_A^a \langle \overline{\psi}(x)\gamma_5\{T^a,M\}\psi(x)\mathcal{O}\rangle + \langle \delta\mathcal{O}\rangle\,, \quad A_\mu^a \equiv \overline{\psi}\gamma_5 T^a\psi\,. \tag{1.4.15}$$

The associated charge $\overline{A}_0^a(x_0) = \int d^3\mathbf{x}\, A_0^a(x)$ is conserved only if $M = 0$. By inserting a pseudoscalar current $P^b = \overline{\psi}T^b\gamma_5\psi$, we can derive the important WTI referred to as PCAC (Partially Conserved Axial Current) relation

$$\partial_\mu^x \langle A_\mu^a(x)P^b(y)\rangle = \langle \overline{\psi}(x)\gamma_5\{T^a,M\}\psi(x)P^b(y)\rangle - \delta(x-y)\langle \overline{\psi}(y)\left\{T^a,T^b\right\}\psi(y)\rangle\,. \tag{1.4.16}$$

This identity remains unchanged if renormalized quantities are inserted[4]. For this reason, the PCAC relation is commonly used to define quark masses, e.g. taking $M = m\mathbb{1}$ we have

$$m = \frac{\partial_\mu^x \langle A_\mu^a(x)P^b(y)\rangle}{2\langle P^a(x)P^b(y)\rangle}\,, \quad x \neq y \tag{1.4.17}$$

where the numerator and the denominator on the r.h.s. can be independently computed non-perturbatively, e.g. in Lattice QCD simulations. The PCAC equation is also useful for analyzing spontaneous chiral symmetry breaking in QCD, as we now discuss.

[4]This holds in the chiral limit, where $Z_S\langle S^0\rangle$ is finite, with Z_S being the renormalization constant associated to the scalar singlet density S^0 defined below Eq. (1.4.18). Beyond the chiral limit, the renormalized scalar singlet density S_R^0 mixes also with a term proportional to $(M + M^\dagger)$ (spurionic fields), making S_R^0 ambiguously defined.

1.4.2 Spontaneous chiral symmetry breaking

A rich spectrum of hadrons emerges at the fundamental QCD energy scale $\Lambda_{\rm QCD}$, as shown in Fig. 1.3. Pions are a notable exception, since their light masses have a deep reason which ultimately stems from the spontaneous symmetry breaking of chiral symmetry. Assuming for simplicity degenerate quark masses $M = m\mathbb{1}$, the PCAC relation in Eq. (1.4.16) simplifies to

$$\langle \partial_\mu A^a_\mu(x) P^b(0)\rangle = 2m\langle P^a(x)P^b(0)\rangle - \frac{1}{N_{\rm f}}\delta^4(x)\delta^{ab}\langle S^0\rangle\,, \tag{1.4.18}$$

where $S^0 = \overline{\psi}\psi = \overline{\psi}_L\psi_R + \overline{\psi}_R\psi_L$ is the scalar singlet density. The QCD action is left invariant under non-Abelian axial transformations, which are also anomaly-free. In this case, the vacuum expectation value $\langle S^0\rangle \neq 0$ indicates the *spontaneous breaking* of chiral symmetry.
This property has some interesting consequences. We can consider Eq. (1.4.18) in the chiral limit, make use of Lorentz invariance and integrate it over a four-dimensional sphere centered in the origin to obtain

$$\langle A^a_\mu(x) P^b(0)\rangle = -\delta^{ab}\frac{x_\mu}{(x^2)^2}\frac{\langle S^0\rangle}{2\pi^2 N_{\rm f}}\,. \tag{1.4.19}$$

When projected to zero-momentum, this relation implies

$$\langle \overline{A}^a_0(x_0) P^b(0)\rangle = -\frac{\delta^{ab}}{2N_{\rm f}}\langle S^0\rangle \quad \forall\, x_0 \neq 0 \tag{1.4.20}$$

where $\overline{A}^a_0(x_0) = \int d^3\mathbf{x}\, A^a_0(x)$. Note that the r.h.s. does not depend on x_0. The lightest states contributing to the l.h.s. of this expression are the pions π^a, sharing the same quantum numbers as the pseudoscalar singlet densities P^a. Introducing the matrix elements

$$\langle \pi^b(p)|P^a(x)|0\rangle = -i\,\delta^{ab}G_\pi e^{-\omega_\pi(\mathbf{p})x_0}e^{-i\,\mathbf{p}\cdot\mathbf{x}}\,, \tag{1.4.21}$$

$$\langle 0|A^a_\mu(x)|\pi^b(p)\rangle = i\,\delta^{ab}F_\pi\, p_\mu e^{-\omega_\pi(\mathbf{p})x_0}e^{i\,\mathbf{p}\cdot\mathbf{x}}\,, \tag{1.4.22}$$

where $\omega_\pi(\mathbf{p}) = \sqrt{m_\pi^2 + |\mathbf{p}|^2} = p^0$, we can write the completeness of states as

$$\begin{aligned} \mathbb{1} &= \sum_c \int \frac{d^3\mathbf{p}}{(2\pi)^3\, 2p^0}\,|\pi^c(p)\rangle\langle\pi^c(p)| + (\dots)\,, \\ \langle\pi^a(\mathbf{p})|\pi^b(\mathbf{p}')\rangle &= (2\pi)^3\, 2p^0\delta^{(3)}(\mathbf{p}-\mathbf{p}')\delta^{ab}\,, \end{aligned} \tag{1.4.23}$$

where $(\dots)$ stands for the contribution of higher energy states. Inserting the above identities in Eq. (1.4.20) and using the Heisenberg representation

$$\mathcal{O}(x) = e^{x_0\mathbb{H}}e^{-i\mathbb{p}\cdot\mathbf{x}}\mathcal{O}(0)e^{-x_0\mathbb{H}}e^{i\mathbb{p}\cdot\mathbf{x}}\,, \tag{1.4.24}$$

where $\mathbb{H}$ and $\mathbb{p}$ are the QCD Hamiltonian and spatial momentum operators, it follows that

$$\langle \overline{A}_0^a(x_0) P^b(0) \rangle = \delta^{ab} \frac{G_\pi F_\pi}{2} e^{-m_\pi x_0} + (...) \tag{1.4.25}$$

where $m_\pi = \omega_\pi(\mathbf{0})$. According to Eq. (1.4.20), the r.h.s. of Eq. (1.4.25) must be independent of x_0. For this expression to remain x_0-independent, QCD must possess $N_\mathrm{f}^2 - 1$ massless pions (pseudoscalar particles) when $\langle S^0 \rangle \neq 0$ in the chiral limit. This also leads to the relation

$$G_\pi F_\pi = -\frac{\langle S^0 \rangle}{N_\mathrm{f}}\bigg|_{m=0} . \tag{1.4.26}$$

However, in Nature quarks and pions are not massless: their masses are small but finite, with pions having a non-zero light mass of approximately $m_\pi \simeq 140\,\mathrm{MeV}$. To understand this, we re-evaluate the relations above for the case of non-zero but degenerate quark masses $m \neq 0$. Saturating Eq. (1.4.16) with pion states at $x_0 \neq 0$ yields

$$m_\pi^2 F_\pi = 2 m G_\pi \, . \tag{1.4.27}$$

Combining this with Eq. (1.4.26), we obtain the Gell-Mann-Oakes-Renner (GMOR) relation [37]

$$\lim_{m\to 0} \frac{m_\pi^2 F_\pi^2}{2m} = -\frac{\langle S^0 \rangle}{N_\mathrm{f}}\bigg|_{m=0} . \tag{1.4.28}$$

This relation is crucial to understand why pions are light in Nature: rather than having a large mass $m_\pi \propto \Lambda_\mathrm{QCD}$, the GMOR relation in Eq. (1.4.28) immediately implies that

$$m_\pi^2 \propto \Lambda_\mathrm{QCD} \times m \tag{1.4.29}$$

which explicitly shows that $m_\pi \ll \Lambda_\mathrm{QCD}$, since $m \ll \Lambda_\mathrm{QCD}$.

The GMOR relation has been extensively validated through various numerical studies. Its evidence from Lattice QCD simulations is illustrated in Fig. 1.4, taken from Ref. [38], see also Refs. [39, 40]. Essentially, the Banks-Casher formula [39, 41–43] relates the spectral density ρ of the Dirac operator with the order parameter of chiral SSB, as given by[3]

$$-\frac{\langle S^0 \rangle}{N_\mathrm{f}}\bigg|_{m=0} = \pi \rho(0) \, , \quad \rho(\lambda) = \frac{1}{V} \sum_i \langle \delta(\lambda - \lambda_i) \rangle \, , \tag{1.4.30}$$

where λ_i are the eigenvalues of the Dirac operator. This relation can be read in both directions: a non-zero spectral density $\rho(0)$ implies the presence of a non-vanishing chiral condensate $\langle S^0 \rangle$, breaking the symmetry. Conversely, a non-zero value of $\langle S^0 \rangle$ leads to condensation of eigenmodes near the origin of the spectrum. Numerical studies have confirmed the validity of this mechanism, showing that modes do indeed condense near the origin as predicted by the Banks-Casher relation [40, 44].

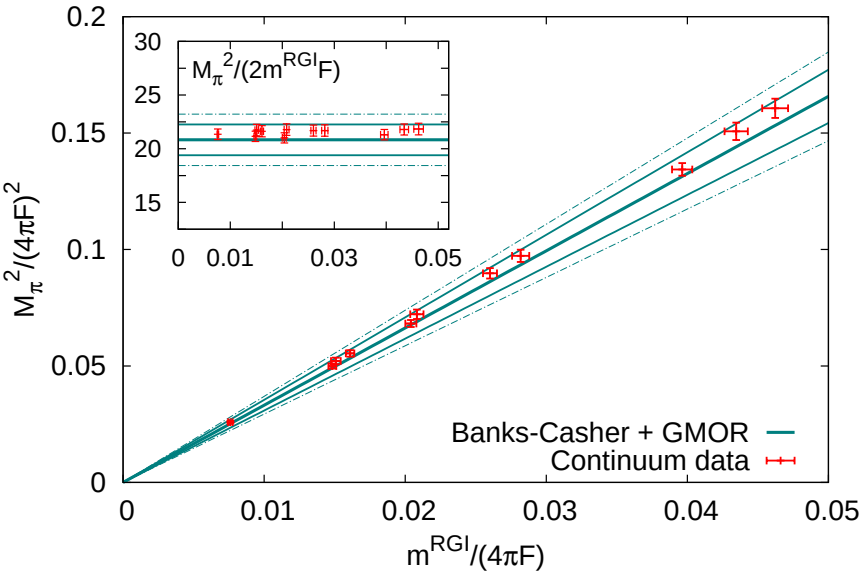

Figure 1.4: Numerical proof of the GMOR relation, cf. Eq. (1.4.28), from Ref. [38]. The blue line and its error are the GMOR contribution to m_π^2, derived from the computation of $\langle S^0 \rangle$ on the lattice. The red dots are instead obtained from direct calculation of m_π^2.

1.4.3 The Witten-Veneziano mechanism

The axial anomaly has profound implications for QCD phenomenology, one of which is the large mass of the η' meson compared to other light mesons. This is naturally explained by the Witten-Veneziano relation, a result linking the anomaly to the mass spectrum of QCD and ultimately providing a deeper understanding of the explicit breaking of classical $U(1)_A$ symmetry at the quantum level.

Starting from the anomalous WTI in the massless limit, shown in Eq. (1.4.11), we integrate it over $\int d^4x$. We obtain that the topological susceptibility

$$\chi \equiv \chi(0)\,, \quad \chi(p) = \int d^4x\, e^{ipx} \langle q(x) q(0) \rangle \tag{1.4.31}$$

satisfies the relation

$$\chi \xrightarrow{m \to 0} 0 \quad \forall\, \frac{N_\mathrm{f}}{N_\mathrm{c}} \quad \text{at } m = 0\,, \tag{1.4.32}$$

while the topological charge density q, introduced in Eq. (1.1.10), also satisfies $q = 0$ $\forall\, N_\mathrm{f}/N_\mathrm{c}$ in this limit, as long as no massless particle is present in this channel and a mass gap $\omega_\mathrm{thr} > 0$ exists. Applying subtractions from the Källén-Lehmann representation of $\chi(p)$, see Subsection 3.1.1, and noting the presence of the lightest η' meson state in the pseudoscalar flavor singlet channel, with mass $M_{\eta'}$ and the same quantum numbers

as $q(x)$, we obtain

$$\chi(p) = C_0\Lambda_{\rm QCD}^4 + C_1\Lambda_{\rm QCD}^2 p^2 + C_2\cdot(p^2)^2 - \frac{R^2}{p^2+m_{\eta'}^2} + (p^2)^3\int_{\omega_{\rm thr}^2}^{\infty} ds\,\frac{\rho(s)}{(s+p^2)s^3}\,. \quad (1.4.33)$$

The parameter R is defined from

$$R^2 = |\langle 0|q(0)|\eta'\rangle|^2 = \frac{F_{\eta'}^2 m_{\eta'}^4}{2N_{\rm f}}\,, \quad \langle 0|\overline{A}_0(x_0)|\eta'\rangle = i\sqrt{2N_{\rm f}}F_{\eta'}m_{\eta'}e^{-m_{\eta'}x_0} \quad (1.4.34)$$

where $F_{\eta'}$ is the decay constant of the η' meson. As $p\to 0$ and in the Yang-Mills limit $N_{\rm f}/N_{\rm c}\to 0$, Eq. (1.4.33) implies that the topological susceptibility of the pure Yang-Mills theory, $\chi_{\rm YM}$, satisfies

$$\chi_{\rm YM} = C_0\Lambda_{\rm QCD}^4\,. \quad (1.4.35)$$

On the other hand, we can consider Eq. (1.4.32) in the limit of massless quarks, obtaining

$$C_0\Lambda_{\rm QCD}^4 = \frac{R^2}{p^2+m_{\eta'}^2}\,. \quad (1.4.36)$$

The combination of Eqs. (1.4.35) and (1.4.36) leads to the celebrated Witten-Veneziano relation [45, 46]:

$$\lim_{N_{\rm f}/N_{\rm c}\to 0}\lim_{m\to 0}\frac{R^2}{m_{\eta'}^2} = \chi_{\rm YM}\,. \quad (1.4.37)$$

This relation reveals that the η' meson acquires a large mass due to the $U(1)_A$ anomaly, which is responsible for a non-zero topological susceptibility in pure gauge theory, even in the massless quark limit. The anomalous WTI in Eq. (1.4.32) implies that the topological susceptibility vanishes in the massless quark limit for any number of flavors. This can be explained by the presence of the η' meson, whose large mass is a direct consequence of the non-vanishing topological susceptibility in pure Yang-Mills theory, $\chi_{\rm YM}$. This quantity has been computed in Lattice QCD in Ref. [22], resulting in

$$\chi_{\rm YM} = (180.5(5)(43)\,{\rm MeV})^4\,, \quad (1.4.38)$$

where the first error is statistical and the second one is due to lattice systematics, and it is compatible with the chiral perturbation theory result [46]

$$\frac{F_\pi^2}{6}\left(m_\eta^2 + m_{\eta'}^2 - 2m_K^2\right)\Big|_{\rm exp} \simeq (180\,{\rm MeV})^2\,. \quad (1.4.39)$$

This concludes our presentation of QCD. The concepts presented in this Chapter set the stage for the subsequent one, which focuses on the formulation of QCD on a finite and discrete lattice.

Chapter 2

Lattice QCD

In this Chapter we describe the formulation of Lattice QCD, i.e. the only known framework at present to define and study QCD non-perturbatively from first principles. As described in Chapter 1, QCD manifests asymptotic freedom and confinement, and thus must be studied non-perturbatively at low energies. The non-perturbative definition of the theory is possible on a discrete lattice, that regulates UV divergences. Our presentation focuses on QCD with quarks, but it can be straightforwardly generalized to any (non-) interacting QFT, gauge group and representation. We refer to Refs. [47–49] for a general and comprehensive introduction to this topic.

2.1 Preliminaries

The theoretical framework for Lattice QCD calculations is the path integral formalism in Euclidean time, which allows to estimate expectation values of composite operators as in Eq. (1.1.4) once the action and a non-perturbative renormalization scheme have been chosen. In order to give a precise meaning to the path integrals for a gauge theory, we define it in a finite lattice with discretized space-time coordinates, with lattice spacing a and finite volume $T \times L^3$, where T, L indicate the lattice temporal and spatial lengths respectively. The resulting path integral expressions for correlation functions are well-defined, as only a finite number of degrees of freedom is involved. In our convention, $\mu = 0$ indicates the Euclidean temporal direction. We also need to set boundary conditions (BCs) to properly define the theory on a finite volume. In this way, the path integral reduces to an ordinary multidimensional integral, which can be evaluated numerically e.g. with Monte Carlo methods. This lattice structure will be eventually removed by taking the infinite volume and the zero lattice spacing (continuum) limits to retrieve physical results, allowing to extract systematically improvable theoretical predictions from first principles with 3-4 input parameters (e.g. hadron masses required in hadronic renormalization schemes). For the purposes of this discussion, if not explicitly stated otherwise, we only consider observables with exponentially suppressed finite-volume ef-

fects (FVEs)[1] which we neglect, since their effects of $O(e^{-m_\pi L})$ are around a few percent or less for typical Lattice QCD applications, where $m_\pi L \geq 4$.

The lattice acts as a UV regulator, as the lattice spacing induces a cutoff $\frac{\pi}{a}$ on momenta. Additionally, when the theory is confined to a finite volume, momenta become quantized, e.g. in a cubic box of size L with periodic boundary conditions we have $\mathbf{p} = \frac{2\pi}{L}\mathbf{n}$, $\mathbf{n} \in (\mathbb{N} \bmod \frac{L}{a})^3$. Usual UV divergences are recovered in the classical continuum limit, i.e. considering $a \to 0$ without imposing further constraints, and need to be removed through parameter and operator non-perturbative renormalization, as discussed in Section 1.2. In the non-perturbative hadronic renormalization scheme, detailed in Subsection 1.2.1, the renormalization conditions are set by requiring a few physically relevant quantities, such as hadron masses, to be fixed at their physical values. Bare parameters, such as the coupling constant and bare quark masses, then acquire a non-trivial dependence on the lattice spacing (cutoff), following the *lines of constant physics* as a varies.

In order to properly define the path integral, we need to discretize the QCD action, ideally preserving its defining local gauge invariance. The gauge-invariant gluonic and fermionic discrete actions are discussed respectively in Sections 2.2 and 2.3. In the continuum limit, discretization effects vanish and it is possible to boost the continuum convergence, for instance by making discretization errors of $O(a^2)$ rather than of $O(a)$, as detailed in Section 2.4. Computational strategies in Lattice QCD are described in Section 2.5, with one of the biggest obstacles which currently hinder improvements in numerical simulations, the so-called *signal-to-noise ratio* (StN) *problem*, being discussed in Section 2.6. A possible and very promising solution to such problem is the topic of Chapter 4.

2.2 Gluonic action on the lattice

The gluonic action in the continuum formulation takes the form in Eq. (1.1.9) and it is invariant under the gauge transformation in Eq. (1.1.7). In order to study its realization on the lattice, we could naïvely discretize the derivatives in the field strength $F_{\mu\nu}$ using either their forward or backward definitions

$$\partial_\mu \psi(x) = \frac{\psi(x + a\hat{\mu}) - \psi(x)}{a}, \quad \partial^*_\mu \psi(x) = \frac{\psi(x) - \psi(x - a\hat{\mu})}{a}, \tag{2.2.1}$$

where $\hat{\mu}$ is the lattice versor in the direction μ, or their symmetrized version

$$\frac{1}{2}\left(\partial_\mu + \partial^*_\mu\right)\psi(x) = \frac{1}{2a}\left[\psi(x + a\hat{\mu}) - \psi(x - a\hat{\mu})\right] \tag{2.2.2}$$

[1] Power-like FVEs might arise when considering kinematical regimes where virtual particles may potentially go on-shell. In Appendix B we discuss how these are not simply an unwanted lattice effects, but rather a powerful window into resonance physics, given a map of the finite-volume spectrum to S-matrix elements [50–54].

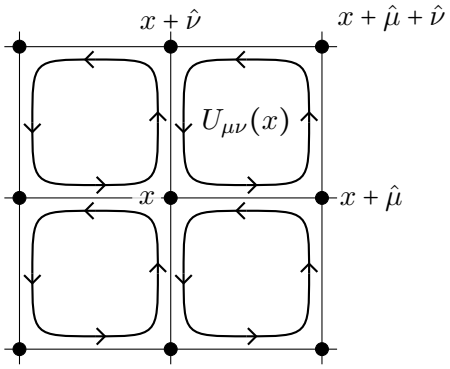

Figure 2.1: Representation [55] of the plaquette $U_{\mu\nu}(x)$ on the lattice, see Eq. (2.2.4).

with improved $O(a^2)$ discretization errors. The resulting action would be gauge-invariant only up to discretization errors. Yet, since the local gauge symmetry defines the theory, it would be much more preferable for it to be exactly preserved also on the lattice.

The original idea for describing an exactly gauge-invariant theory on the lattice was initially proposed by Wilson in his seminal work of 1974 [15] and consists in a complete shift of paradigm. The fundamental gauge fields at each lattice site x and for any Euclidean space-time direction $\mu = 0, \ldots, 3$, are the links (related to the links between different lattice sites)

$$U_\mu(x) \in SU(3)\,, \quad U^G_\mu(x) = G(x)U_\mu(x)G^\dagger(x+a\hat{\mu})\,. \tag{2.2.3}$$

They act as parallel transporters, as explicitly shown in Eq. (2.3.10). The shortest closed path on the lattice is shown in Fig. 2.1. It is known as the *plaquette*

$$U_{\mu\nu}(x) = U_\mu(x)U_\nu(x+a\hat{\mu})U^\dagger_\mu(x+a\hat{\nu})U^\dagger_\nu(x)\,, \quad U^G_{\mu\nu}(x) = G(x)U_{\mu\nu}(x)G^\dagger(x) \tag{2.2.4}$$

and it is useful to construct the exactly gauge-invariant Wilson action

$$S_{\rm G}[U] = \frac{\beta}{2}\sum_x\sum_{\mu,\nu}\left\{1-\frac{1}{2N_{\rm c}}\,{\rm Tr}\big\{U_{\mu\nu}(x)+U^\dagger_{\mu\nu}(x)\big\}\right\}\,, \quad \beta = \frac{2N_{\rm c}}{g_0^2} \tag{2.2.5}$$

with $N_{\rm c} = 3$ for our purposes. By defining $U_\mu(x) = e^{-ia\overline{A}_\mu(x)}$ as the discretization of the parallel transport between two neighboring sites, and considering the classical continuum limit of Eq. (2.2.5), it is easy to check that we correctly recover the continuum result in Eq. (1.1.9) written in terms of $\overline{A}_\mu$, up to $O(a^2)$ discretization effects. We emphasize that the fundamental gauge fields are now elements of the compact gauge group rather

than of its algebra[2]. Therefore, the Haar integral

$$Z = \int [dU]\, e^{-S_G[U]}, \quad [dU] = \prod_{x,\mu} [dU_\mu(x)] \tag{2.2.6}$$

is finite, where the Haar measure $[dU]$ is the correct gauge-invariant measure to integrate over the $SU(3)$ group manifold.

2.3 Fermionic action

We now want to define the lattice counterpart of the continuum fermionic action in Eq. (1.1.12). We consider the quark fields $\psi(x)$ to be located on the lattice sites x and carry N_c color, N_f flavor and 4 spinor indices.

2.3.1 The free case

For simplicity, we begin with the *non-interacting case*, $A_\mu = 0$. It might be tempting to naïvely discretize the derivatives in Eq. (1.1.12) using Eq. (2.2.1) or the symmetric Eq. (2.2.2). With the latter, the resulting discretized action

$$\begin{aligned} S_F &= a^4 \sum_x \left\{ \frac{1}{2a} \left[\overline{\psi}(x)\gamma_\mu \psi(x + a\hat{\mu}) - \overline{\psi}(x)\gamma_\mu \psi(x - a\hat{\mu}) \right] + m\overline{\psi}(x)\psi(x) \right\} \\ &= \int_{IBZ} \frac{d^4q}{(2\pi)^4} \overline{\psi}(q) \left(i\gamma_\mu \overline{q}_\mu + m \right) \psi(q), \quad \psi(x) = \int_{IBZ} \frac{d^4q}{(2\pi)^4} e^{iqx} \psi(q) \end{aligned} \tag{2.3.1}$$

can be rewritten in Fourier space within the first Brillouin zone (IBZ), where each momentum component lies in $\left[-\frac{\pi}{a}, \frac{\pi}{a}\right]$, and where $\overline{q}_\mu = \sin(q_\mu a)/a$. The resulting propagator

$$\langle \psi(x)\overline{\psi}(0) \rangle = \int_{IBZ} \frac{d^4q}{(2\pi)^4} \frac{-i\gamma_\mu \overline{q}_\mu + m}{\sum_\mu \overline{q}_\mu^2 + m^2} e^{iqx} \tag{2.3.2}$$

has 16 different poles even in the classical continuum limit, i.e. the naïve discretization of the fermionic action in Eq. (2.3.1) describes 16 different fermions. This problem is known as *fermion doubling* and it is a consequence of a more general

Theorem 2.3.1 (Nielsen-Ninomiya theorem [58])**.** *The following properties of the discretized Dirac operator $D(q)$ on the reciprocal lattice cannot all be satisfied at once:*

1. *$D(q)$ is a periodic smooth function of q_μ with period $\frac{2\pi}{a}$;*
2. *in the continuum limit, $D(q) \xrightarrow{a\to 0} [i\gamma_\mu q_\mu + O(aq)]$;*

[2]This allows to avoid any ambiguity in the integration over physically equivalent configurations of the gauge field $A_\mu \in \mathfrak{su}(3)$, known as Gribov copies [56] and related by a gauge transformation, usually treated to all orders in perturbation theory (but not non-perturbatively) by considering in the action additional fields known as ghosts [57]. Wilson's proposal is instead well-defined, and thus ghosts are introduced on the lattice only if one is interested in studying its perturbative formulation.

3. *$D(q)$ is invertible $\forall q \neq 0 \mod \frac{2\pi}{a}$ i.e. it only has one zero (pole in the correlator), corresponding to the particle that has to be discretized;*

4. *$D(q)$ is chirally invariant, i.e. $\{\gamma_5, D(q)\} = 0$.*

The first two properties are necessary to define a proper lattice discretization for $D(q)$. Since the massless naïve discrete action in Eq. (2.3.1) does not break chiral symmetry, similarly to the continuum, it could not possibly describe a single fermion, and in fact the third property has been found not to hold. In order to solve this problem, many proposals have been put forward.

2.3.2 Wilson fermions

Wilson's proposal [15] is to introduce in the naïve action new $O(a)$ terms, explicitly breaking chiral symmetry and vanishing in the classical continuum limit, with

$$S_{\mathrm{F}} = a^4 \sum_x \overline{\psi} \left(D_{\mathrm{W}} + m\right) \psi \,, \quad D_{\mathrm{W}} = \frac{1}{2} \left\{ \gamma_\mu \left(\partial_\mu + \partial_\mu^*\right) - a \partial_\mu^* \partial_\mu \right\} \tag{2.3.3}$$

which can be equivalently rewritten as

$$S_{\mathrm{F}} = \int_{\mathrm{IBZ}} \frac{d^4q}{(2\pi)^4} \overline{\psi}(q) K(q) \psi(q) \,, \quad K(q) = i\gamma_\mu \overline{q}_\mu + m + \frac{a}{2}\hat{q}^2 \,, \quad \hat{q}_\mu = \frac{2}{a} \sin \frac{q_\mu a}{2} \tag{2.3.4}$$

leading to

$$\langle \psi(x) \overline{\psi}(0) \rangle = \int_{\mathrm{IBZ}} \frac{d^4q}{(2\pi)^4} \frac{-i\gamma_\mu \overline{q}_\mu + m + \frac{a}{2}\hat{q}^2}{\sum_\mu \overline{q}_\mu^2 + \left(m + \frac{a}{2}\hat{q}^2\right)^2} e^{iqx} \,. \tag{2.3.5}$$

In the massless free case, apart from $q_\mu = 0$, the additional poles $q_\mu = \frac{\pi}{a}\hat{\mu}$ for some μ receive $\hat{q}_\mu = \frac{2}{a}\hat{\mu}$ contributions. Therefore, these modes become infinitely massive in the classical continuum limit, where they correctly decouple from the theory.

2.3.3 Overlap fermions

Chiral symmetry is crucial in physics, as motivated in Section 1.4. Besides the deep consequences of its spontaneous breaking, as the presence of (nearly) Goldstone bosons, in QCD it additionally imposes multiplicative quark mass renormalization. Following the much more exhaustive list of Refs. [33–36, 59, 60], here we define a new Dirac operator, satisfying a relation that plays the rôle of chiral symmetry on the lattice.

The mildest way to break chiral symmetry is by the Ginsparg-Wilson (GW) relation [33]

$$\gamma_5 D + D\gamma_5 = \overline{a} D \gamma_5 D \,, \quad \overline{a} = \frac{a}{1+s} \tag{2.3.6}$$

which can be rewritten as

$$\gamma_5 D + D\hat{\gamma}_5 = 0 \,, \quad \hat{\gamma}_5 = \gamma_5 (1 - \overline{a} D) \,, \quad \hat{\gamma}_5^2 = 1 \,. \tag{2.3.7}$$

In Ref. [34], Neuberger introduced the *overlap* Dirac operator satisfying GW relation

$$D_{\mathrm{O}} = \frac{1}{\overline{a}}\left(1 - \frac{A}{\sqrt{A^\dagger A}}\right) = \frac{1}{\overline{a}}\left[1 + \gamma_5 \frac{\gamma_5(\overline{a}D_{\mathrm{W}} - 1)}{\sqrt{A^\dagger A}}\right] \tag{2.3.8}$$

where[3] $A = 1 - \overline{a}D_{\mathrm{W}}$ and $\gamma_5 D_{\mathrm{W}}\gamma_5 = D_{\mathrm{W}}^\dagger$, where D_{W} is the Wilson term in Eq. (2.3.3)[4]. We refer to Ref. [35] for further details. We also note that domain-wall fermions [59] allow to recover the overlap operator in some limits [60][5].

The GW relation plays an important rôle in Lattice QCD, allowing to define the lattice counterpart of chiral symmetry, known as Lüscher symmetry, and of left and right chiral fermions [36]. In this framework, many properties of the continuum theory can be proved, such as the Witten-Veneziano formula, related to the $U(1)_A$ anomaly and the large mass of the η', see Subsection 1.4.3, and the Banks-Casher relation, associated to chiral spontaneous symmetry breaking, see Subsection 1.4.2 and Eq. (1.4.30). We also anticipate that $O(a)$ lattice artifacts are absent for this discretization.

2.3.4 The interacting case

Let us now generalize the above discussion to the case of an *interacting theory*. Interactions are included as is customary by requiring the action to be invariant under the local gauge group $SU(3)_{\mathrm{c}}$ transformations. The fermionic action thus cannot include contributions of the form $\overline{\psi}(x)\psi(y)$ with $x \neq y$ since they are not gauge-invariant, as they transform into $\overline{\psi}(x)G^\dagger(x)G(y)\psi(y)$. Therefore, a factor that depends on the gauge field A_μ must be included inside this term. We can introduce the covariant Schwinger line integral

$$U(x,y) = \exp\left\{ig_0 \int_x^y dz_\mu\, A_\mu(z)\right\} \quad \rightarrow \quad G(x)U(x,y)G^\dagger(y) \tag{2.3.9}$$

such that contributions of the form $\overline{\psi}(x)U(x,y)\psi(y)$ are gauge-invariant. This allows us to better understand Wilson's choice to adopt the infinitesimal version of the Schwinger line as the fundamental degree of freedom, rather than the gauge fields. In fact, we can consider $y = x + \epsilon$ for an arbitrarily small path ϵ, so that the Schwinger line integral can be approximated as $U(x, x+\epsilon) \approx e^{ig_0\epsilon_\mu A_\mu(x)}$, which resembles a link variable once we consider $\epsilon = a\hat{\mu}$, cf. Eq. (2.2.3). The discretized gauge-invariant fermionic action thus

[3] This operator is not ultra-local, a desirable property in order to satisfy cluster decomposition, making it expensive to simulate. Though, this operator is exponentially local, in the sense that $\|\frac{1}{\sqrt{A^\dagger A}}(x,y)\| \sim e^{-\frac{c}{a}|x-y|}$, as $a \to 0$, safely allowing any analysis based on power-counting (such as OPE).

[4] In the interacting case, it suffices to employ the definition of the interacting Wilson term in Eq. (2.3.11).

[5] Massless chiral fermions in four dimensions can be defined from 5-dimensional interacting massive fermions bound to a domain-wall mass defect, with doublers explicitly removed. The inverse of the overlap operator is retrieved from the low-energy effective action of the light fermion field of the domain-wall fermion.

requires a slight change of the definition of the discretized derivatives as

$$\nabla_\mu \psi(x) = \frac{1}{a}\left[U_\mu(x+a\hat{\mu})\psi(x+a\hat{\mu}) - \psi(x)\right] \,, \; \nabla^*_\mu \psi(x) = \frac{1}{a}\left[\psi(x) - U^\dagger_\mu(x-a\hat{\mu})\psi(x-a\hat{\mu})\right] \tag{2.3.10}$$

where the action of the gauge links as parallel transporters is explicit.

Interacting Wilson fermions

Wilson's proposal [15], already reviewed in Subsection 2.3.2 for the free case, is now generalized as

$$S_{\mathrm{F}}[U,\overline{\psi},\psi] = a^4 \sum_x \overline{\psi}\,(D_{\mathrm{W}} + m)\,\psi \,, \quad D_{\mathrm{W}} = \frac{1}{2}\left\{\gamma_\mu\left(\nabla_\mu + \nabla^*_\mu\right) - a\nabla^*_\mu\nabla_\mu\right\} \tag{2.3.11}$$

with the full covariant discrete derivatives in Eq. (2.3.10), allowing to rewrite S_{F} also as

$$\begin{aligned} S_{\mathrm{F}}[U,\overline{\psi},\psi] = (m+4)\sum_x \overline{\psi}(x)\psi(x) - \frac{1}{2a}\sum_{x,\mu}\big[&\overline{\psi}(x)(1-\gamma_\mu)U_\mu(x+a\hat{\mu})\psi(x+a\hat{\mu}) + \\ &+\overline{\psi}(x)(1+\gamma_\mu)U^\dagger_\mu(x-a\hat{\mu})\psi(x-a\hat{\mu})\big] \,. \end{aligned} \tag{2.3.12}$$

This concludes the definition of the QCD action on a finite and discrete lattice, with the path integral representation of its partition function

$$Z = \int [dU][d\overline{\psi}][d\psi] \exp\left\{-S\left[U,\overline{\psi},\psi\right]\right\} \tag{2.3.13}$$

and expectation values of observables

$$\langle \mathcal{O} \rangle = \frac{1}{Z}\int [dU][d\overline{\psi}][d\psi]\mathcal{O}[U,\overline{\psi},\psi] \exp\left\{-S\left[U,\overline{\psi},\psi\right]\right\} \tag{2.3.14}$$

where now $S[U,\overline{\psi},\psi] = S_{\mathrm{G}}[U] + S_{\mathrm{F}}[U,\overline{\psi},\psi]$ depends on the fields, on the bare coupling g_0 and quark masses m_{f}.

We finally mention that we commonly consider (anti-)periodic BCs for bosonic (fermionic) fields in the temporal direction, while the spatial ones are usually taken to be periodic for all the fields. Other possible choices are Dirichlet BCs, where fields assume fixed values at the boundaries; open BCs, removing field interactions across the boundaries, which could be useful to prevent unwanted topological freezing, i.e. trapping in a fixed topological sector; twisted BCs, where fields acquire a phase when crossing the boundary, useful to simulate momentum shifts or handle specific topologies. Other options can also considered for specific applications, e.g. shifted BCs in the context of thermal field theories [61–68], or C* BCs to study QCD+QED on the lattice [69–72].

2.4 Symanzik improvement program

In Lattice QCD [49], the momentum cutoff $\frac{\pi}{a}$ may be interpreted as a new physics scale. This allows to formulate a low-energy effective theory with a continuum action [73–76]

$$S_{\text{eff}} = \int d^4x \, \{\mathcal{L}_0(x) + a\mathcal{L}_1(x) + a^2\mathcal{L}_2(x) + \dots\} \tag{2.4.1}$$

where $\mathcal{L}_0$ is the continuum QCD Lagrangian, and $\mathcal{L}_k$, $k \geq 1$ contain linear combinations of all possible local operators of dimension $4+k$ which are invariant w.r.t. the symmetries of the lattice theory, with coefficients which are usually slowly varying with a (in perturbation theory they are polynomials in $\log a$). For instance, at $O(a)$ the operators contributing to the effective Lagrangian $\mathcal{L}_1$ are

$$\mathcal{O}_1 = \overline{\psi} i\sigma_{\mu\nu} F_{\mu\nu} \psi \,, \quad \mathcal{O}_2 = \overline{\psi} \left(\nabla_\mu \nabla_\nu + \nabla^*_\mu \nabla^*_\nu \right) \psi \,, \tag{2.4.2}$$

$$\mathcal{O}_3 = m \, \mathrm{Tr}\{F_{\mu\nu} F_{\mu\nu}\} \,, \quad \mathcal{O}_4 = m\overline{\psi} \left\{ \gamma_\mu \nabla_\mu - \nabla^*_\mu \gamma_\mu \right\} \psi \,, \quad \mathcal{O}_5 = m^2 \overline{\psi} \psi \tag{2.4.3}$$

where $\sigma_{\mu\nu} = \frac{i}{2}[\gamma_\mu, \gamma_\nu]$. Field equations allow to reduce this list, considering only three independent operators, and we conventionally choose $\mathcal{O}_1$, $\mathcal{O}_3$ and $\mathcal{O}_5$.

2.4.1 $O(a)$-improved Wilson fermions

Let us consider the explicit example of the $O(a)$-improvement for the action of Wilson fermions. In this case, the fields $\mathcal{O}_3$ and $\mathcal{O}_5$ can be re-absorbed in the definitions of the bare coupling constant and of the bare quark masses, both already present in the Wilson action, essentially amounting to a rescaling by factors of the form $1 + O(am_q)$, where $m_q = m_0 - m_c$, m_0 being the bare and m_c the critical masses, as

$$g_0^2 \to g_0^2 (1 + b_g a m_q) \,, \quad m_q \to m_q (1 + b_m a m_q) \,. \tag{2.4.4}$$

The massive $O(a)$-improved Wilson-Dirac operator thus additionally depends only on $\mathcal{O}_1$, namely as [77, 78]

$$D = D_{\text{W}} + a D_{\text{SW}} \,, \tag{2.4.5}$$

where D_{W} is the massive Wilson-Dirac operator introduced in Eq. (2.3.11), and the second term on the r.h.s. of Eq. (2.4.5) is the Sheikholeslami-Wohlert operator

$$D_{\text{SW}} \psi(x) = c_{\text{SW}} \frac{i}{4} \sigma_{\mu\nu} \widehat{F}_{\mu\nu}(x) \psi(x) \,. \tag{2.4.6}$$

In the formula above, the coefficient c_{SW} has been computed at one-loop in perturbation theory [79] and numerically non-perturbatively [80]. It is also possible to use the alternative expression for D_{SW} [81]

$$D_{\text{SW}} + (4 + m_0) \to (4 + m_0) \exp\left\{ \frac{D_{\text{W}}}{(4 + m_0)} \right\} = (4 + m_0) \exp\left\{ \frac{c_{\text{SW}}}{4 + m_0} \frac{i}{4} \sigma_{\mu\nu} \widehat{F}_{\mu\nu} \right\} , \tag{2.4.7}$$

where $\widehat{F}_{\mu\nu}(x)$ is the symmetric lattice field strength tensor

$$\widehat{F}_{\mu\nu}(x) = \frac{1}{8a^2}\{Q_{\mu\nu}(x) - Q_{\nu\mu}(x)\}\,, \tag{2.4.8}$$

with

$$\begin{aligned} Q_{\mu\nu}(x) = {} & U_\mu(x)\,U_\nu(x+a\hat{\mu})\,U_\mu^\dagger(x+a\hat{\nu})\,U_\nu^\dagger(x) \\ & + U_\nu(x)\,U_\mu^\dagger(x-a\hat{\mu}+a\hat{\nu})\,U_\nu^\dagger(x-a\hat{\mu})\,U_\mu(x-a\hat{\mu}) \\ & + U_\mu^\dagger(x-a\hat{\mu})\,U_\nu^\dagger(x-a\hat{\mu}-a\hat{\nu})\,U_\mu(x-a\hat{\mu}-a\hat{\nu})\,U_\nu(x-a\hat{\nu}) \\ & + U_\nu^\dagger(x-a\hat{\nu})\,U_\mu(x-a\hat{\nu})\,U_\nu(x+a\hat{\mu}-a\hat{\nu})\,U_\mu^\dagger(x)\,. \end{aligned} \tag{2.4.9}$$

We finally note that, after eliminating all the redundant terms, the only remaining independent term in the $O(a)$ correction to $\mathcal{L}_0$ is $\mathcal{O}_1$. Since this counterterm explicitly violates chiral symmetry, no $O(a)$ lattice artifacts are present for Ginsparg-Wilson fermions.

2.4.2 Field improvement

A similar representation as Eq. (2.4.1) holds also for local fields, which can be represented as a linear combination of fields with different mass dimensions transforming under the same lattice symmetry, e.g. $\phi_{\text{eff}} = \phi_0 + a\phi_1 + O(a^2)$. The connected n-point correlation function $C(x_1,\ldots,x_n) = \langle\phi(x_1)\ldots\phi(x_n)\rangle_{\text{c}}$ can be expanded as

$$\begin{aligned} C(x_1,\ldots,x_n) = \langle\phi_0(x_1)\ldots\phi_0(x_n)\rangle_{\text{c},0} + a\Bigg[& \sum_{k=1}^{n}\langle\phi_0(x_1)\ldots\phi_1(x_k)\ldots\phi_0(x_n)\rangle_{\text{c},0} \\ & - \int d^4y\,\langle\phi_0(x_1)\ldots\phi_0(x_n)\mathcal{L}_1(y)\rangle_{\text{c},0}\Bigg] + O(a^2) \end{aligned} \tag{2.4.10}$$

where the connected expectation values $\langle\ldots\rangle_{\text{c},0}$ are computed with the only contribution of the Lagrangian $\mathcal{L}_0$ to the action in the path integral. The improvement of the action alone is therefore insufficient to cancel all the $O(a)$ terms in the expansion shown in Eq. (2.4.10). To fully achieve $O(a)$-improvement in correlation functions, fields must also be improved by tuning the coefficients of the $O(a)$ counterterms introduced during the redefinition of local fields. Only by optimizing both the action and the fields can a full cancellation of $O(a)$ discretization effects be obtained. For instance, for the improved axial current

$$(A_{\text{eff}})_\mu^a = A_\mu^a + c_{\text{A}}(g_0)a\frac{\partial_\mu + \partial_\mu^*}{2}P^a\,, \quad P^a = \overline{\psi}\gamma_5\frac{1}{2}T^a\psi\,, \tag{2.4.11}$$

the coefficient c_{A} is tuned for $O(a)$-improvement of correlation functions involving A_μ^a.

2.4.3 Improvement and renormalization

To complete the discussion of $O(a)$-improvement, we include the definition of renormalization for the improved theory. After defining improved coupling, masses and fields,

non-perturbative renormalization follows as described in Subsection 1.2.1. If we are instead interested in computing the running of renormalized parameters, we need to define their improved renormalization constants. We can start from the redefinitions of the improved action and fields, amounting to Eqs. (2.4.4) and e.g. (2.4.11), to then introduce the improved renormalizations of the unimproved coupling and mass

$$g_R^2 = Z_g\left(g_0^2(1+b_g a m_q), a\mu\right) g_0^2(1+b_g a m_q)\,, \tag{2.4.12}$$

$$m_R = Z_m\left(g_0^2(1+b_g a m_q), a\mu\right) m_0(1+b_m a m_q) \tag{2.4.13}$$

The renormalization constants can be properly tuned by choosing a set of renormalization conditions, which can be defined non-perturbatively as already described in Section 1.2. Improved renormalization constants can be defined for the fields as well. For instance, by requiring that the PCAC relation, see Eqs. (1.4.16) and (1.4.18), holds up to $O(a^2)$ errors, we can also tune the multiplicative renormalization constant for the axial current, defined as

$$(A_R)_\mu^a = (1+b_{\mathrm{A}} a m_q) Z_{\mathrm{A}}\left(g_0^2(1+b_g a m_q), a\mu\right)\,. \tag{2.4.14}$$

2.5 Computational Strategies

In addition to its theoretical foundations, Lattice QCD requires advanced, precise and efficient computational strategies. These include numerical linear algebra, Monte Carlo simulations, and massively parallel High Performance Computing. A thorough understanding of such numerical methods is not just a technical requirement, but an indispensable element in driving progress at the cutting edge of theoretical physics. In this Section we provide a general (but far from comprehensive) overview, with additional details in Ref. [82] and Appendix A.

2.5.1 Pseudofermion fields and locality

The formulation of Lattice QCD in Euclidean time allows for a statistical interpretation of expectation values of observables, as in Eq. (2.3.14). In general, scalar and bosonic correlators can be studied by directly employing statistical methods. On the other hand, even if possible in theory, fermions cannot practically be simulated on a lattice, since they are Grassmann variables and therefore computationally inaccessibly expensive. Luckily, the fermionic action is quadratic and thus it can be analytically integrated out, leading to an effective bosonic theory which can be numerically simulated from

$$S_{\mathrm{G}}^{\mathrm{eff}}[U] = S_{\mathrm{G}}[U] + S_{\mathrm{F}}^{\mathrm{eff}}[U]\,, \quad S_{\mathrm{F}}^{\mathrm{eff}}[U] = -\ln\det D[U]\,, \tag{2.5.1}$$

where S_{G} is the local, purely gluonic action, see Eq. (2.2.5). The effective action depends non-locally on the bosonic fields to which fermions are coupled, making numerical

computations very time-consuming. In fact, the Dirac operator is a $V \times V$ sparse matrix[6] for each flavor, making the direct computation of $\det D$ practically unfeasible. The apparent loss of locality will be further discussed in the context of multilevel simulations [1, 4, 83–88], where it is restored up to small non-local terms which can be separately treated, see Chapter 4.

Let us first consider an even number of degenerate flavors, e.g. $N_{\mathrm{f}} = 2$, so that

$$Z = \int [dU] \, (\det D[U])^2 \, e^{-S_{\mathrm{G}}[U]} \tag{2.5.2}$$

and the effective gluonic action is always positive definite, allowing for a statistical interpretation of the above path integral. The standard way to treat the generation of gauge field configurations in this case, with an alternative provided by the multilevel algorithms described in Chapter 4, is to introduce additional bosonic complex *pseudofermion* fields ϕ to represent the effective fermionic action. For instance, for $N_{\mathrm{f}} = 2$ we define[7]

$$(\det D[U])^2 = \det Q[U]^2 = \int [d\phi^\dagger][d\phi] e^{-S_{\mathrm{PF}}[U,\phi^\dagger,\phi]} \,, \tag{2.5.4}$$

$$S_{\mathrm{PF}}[U,\phi^\dagger,\phi] = a^8 \sum_{x,y} \phi^\dagger(x) Q[U]^{-2}(x,y) \phi(y) \tag{2.5.5}$$

where $Q = \gamma_5 D = Q^\dagger$ due to γ_5-hermiticity of D, i.e. $D^\dagger = \gamma_5 D \gamma_5$.

Field configurations can thus be generated with methods widely used e.g. for thermal systems in statistical mechanics, with importance sampling used to generate field configurations following a specific probability distribution $\propto e^{-S}$, with S being the Euclidean classical action we want to simulate, in this case equal to

$$S[U,\phi^\dagger,\phi] = S_{\mathrm{G}}[U] + S_{\mathrm{PF}}[U,\phi^\dagger,\phi] \,. \tag{2.5.6}$$

In Appendix A we properly define Markov chains and describe their properties, while also introducing the Metropolis-Hastings [91, 92] and the Hybrid Monte Carlo [93] (HMC) simulation algorithms, useful for importance sampling. Instead, here we focus on describing the HMC algorithm in the context of QCD. Once we are able to correctly generate field configurations, we can approximately study expectation values as

$$\langle \mathcal{O} \rangle = \frac{1}{Z} \int [dU][d\phi^\dagger][d\phi] \mathcal{O}[U] e^{-S[U,\phi^\dagger,\phi]} = \frac{1}{N} \sum_{n=1}^{N} \mathcal{O}[U_i] + O\left(\frac{1}{\sqrt{N}}\right) , \tag{2.5.7}$$

[6] This holds true at least for all the discretizations of the fermionic action we reviewed here, for which the locality of the action is not spoiled.

[7] State-of-the-art simulations employ a similar representation, applying multiple frequency splitting steps to the quark determinant as

$$|\det D|^2 = \det\{DD^\dagger + \mu^2\} \times \det\left\{\frac{DD^\dagger}{DD^\dagger + \mu^2}\right\} \tag{2.5.3}$$

and representing each factor with a different pseudofermion field [89, 90].

from a representative ensemble $\{U_1 \to \cdots \to U_N\}$, where each configuration is distributed as $U_i \sim P[U, \phi^\dagger, \phi] = \frac{1}{Z} e^{-S[U,\phi^\dagger,\phi]}$. The last term in Eq. (2.5.7) is the statistically interpretable associated error, detailed in Appendix A.3.

2.5.2 Hybrid Monte Carlo in Lattice QCD

The HMC algorithm [93] is one of the most efficient strategies to simulate Lattice QCD known at present, allowing us to generate gauge field configurations with any target probability distribution, for us $\propto e^{-S}$, with S in Eq. (2.5.6), regardless of its normalization, performing global updates of the field configuration with high acceptance rates. For simplicity, let us denote as $\Phi = \{U_\mu, \phi^\dagger, \phi\}$ the collection of fields upon which the action S depends.

The HMC algorithm is based on the Hamiltonian formalism. We can introduce a normally distributed auxiliary field $\pi^a_\mu(x)$ with $Z_\pi = \int [d\pi] \exp\{-\frac{1}{2} \sum_{x,\mu,a} \pi^a_\mu(x)^2\}$ as partition function, allowing us to rewrite

$$\langle \mathcal{O} \rangle = \frac{1}{Z} \int [d\Phi] \mathcal{O}[\Phi] e^{-S[\Phi]} \frac{Z_\pi}{Z_\pi} = \frac{1}{Z_H} \int [d\Phi][d\pi] e^{-H[\Phi,\pi]} \mathcal{O}[\Phi] \tag{2.5.8}$$

where

$$Z_H = Z_\pi Z = \int [d\Phi][d\pi] e^{-H[\Phi,\pi]}, \quad H[\Phi,\pi] = \frac{1}{2} \sum_{x,\mu,a} \pi^a_\mu(x)^2 + S[\Phi]. \tag{2.5.9}$$

We can now consider fields to depend on an additional, auxiliary variable τ, which we interpret as the simulation time, while $\pi(\tau, x)$ are the conjugate moments of $\Phi(\tau, x)$ w.r.t. $H[\Phi, \pi]$ (hence the quadratic action for π). The fields satisfy Hamilton equations

$$\begin{aligned} \frac{dU_\mu(\tau,x)}{d\tau} &= \frac{\delta H[\Phi,\pi]}{\delta \pi_\mu(\tau,x)} = \pi_\mu(\tau,x) U_\mu(x), \\ \frac{d\pi_\mu(\tau,x)}{d\tau} = -\frac{\delta H[\Phi,\pi]}{\delta \Phi_\mu(\tau,x)} &= -\frac{\delta S[\Phi]}{\delta \Phi_\mu(\tau,x)} = -\frac{\delta S_{\mathrm{G}}[U]}{\delta U_\mu(\tau,x)} - \frac{\delta S_{\mathrm{PF}}[U,\phi^\dagger,\phi]}{\delta U_\mu(\tau,x)} \\ &\equiv -(\mathcal{F}_{\mathrm{G}})_\mu(\tau,x) - (\mathcal{F}_{\mathrm{PF}})_\mu(\tau,x) \end{aligned} \tag{2.5.10}$$

which we might refer to as Molecular Dynamics (MD) equations as well, along which H is a constant of motion, i.e. $\frac{dH[\Phi,\pi]}{d\tau} = 0$. Therefore, an Euclidean field theory in d dimensions with action $S[\Phi]$ corresponds to a classical system with potential $S[\Phi]$ in $(d+1)$ dimensions. Notice that the expectation values of observables $\mathcal{O} = \mathcal{O}[\Phi]$ are correctly independent of the values of the auxiliary field $\pi(x)$ and of the simulation time τ. Therefore, since we are interested in such observables only, generating configurations distributed with $P_H[\Phi,\pi] = \frac{1}{Z_H} e^{-H[\Phi,\pi]}$ is equivalent to doing so with $P_S[\Phi] = \frac{1}{Z_H} \int [d\pi] e^{-H[\Phi,\pi]} = \frac{1}{Z} e^{-S[\Phi]}$.

In Appendix A we provide additional details on the integration of such equations. Hardly solved analytically, numerical integration schemes are required to integrate the

MD equations, prime examples being the leapfrog or Omelyan integrators [94] of different orders (i.e. with different scalings of the error as powers of the integration step). A single global and coherent update of the field configuration consists in the following scheme.

1. A field $\pi^{(0)}(x)$ is generated with Gaussian probability $P_G[\pi] = \frac{1}{Z_\pi} e^{-\frac{1}{2}\sum_{x,\mu,a}\pi_\mu^a(x)^2}$ i.e. with quadratic action in moments, independently from previous configurations.

2. The starting configuration $\Phi^{(0)}(x)$ must be set. The first configuration of the Markov chain can be arbitrarily defined, since results will not depend on this choice. For each following step, $\Phi^{(0)}(x)$ will be set as $\Phi(x)$ at the previous step.

3. Set the initial conditions for MD equations at $\tau = 0$ as $\Phi^{(0)}(x) \to \Phi(0,x)$ and $\pi^{(0)}(x) \to \pi(0,x)$. After fixing τ_0 and $\delta\tau$, the system is evolved until $\tau = \tau_0$ by integrating out MD equations with the chosen integrator with step $\delta\tau$.

4. The proposed configuration $(\Phi', \pi') = (\Phi(\tau_0, x), \pi(\tau_0, x))$ would be automatically accepted if MD equations were exactly integrated. To account for integration errors and ensure detailed balance condition (necessary to provide an ergodic algorithm, spanning correctly the whole configuration space with no periodicities), an accept-reject step is applied with acceptance probability

$$P_A((\Phi^{(0)}, \pi^{(0)}) \to (\Phi', \pi')) = \min\left[1, e^{-\Delta H}\right], \quad \Delta H = H[\Phi', \pi'] - H[\Phi^{(0)}, \pi^{(0)}]. \tag{2.5.11}$$

Being an extensive quantity, $\Delta H \propto V$, with a proportionality coefficient of order $(\delta\tau)^4$. Thus, there exist values of $\delta\tau$ sufficiently small (but not too much, in order to avoid unnecessarily long and expensive integrations in a region where autocorrelations are already negligible) to reach good levels of acceptance probability (usually between 70% and 90%). Notice also that the algorithm designed above is ergodic and it has the correct fixed point distribution, as proved in Appendix A.1.3.

We note that for chirally breaking discretizations, such as Wilson fermions, $\det D$ is not necessarily a positive definite quantity. Generally, there might exist regions in configuration space where we encounter negative (exceptional) eigenvalues of D. In such cases, the presence of an odd number of non-degenerate quarks might spoil the positivity of the effective action and therefore its statistical interpretation. The general strategy [95–97] is to introduce a rational approximation (Zolotarev rational function) of $1/\sqrt{Q^2}$ for the single quark determinants, e.g. for the strange quark determinant in $N_f = 2 + 1$ simulatons (i.e. with two light degenerate quarks, in addition to a heavier strange quark), with the small remainder of such approximation that can be included in the observable as part of a reweighting procedure, as described in Subsections 4.2.2 and 4.4.4 in the different context of multilevel simulations but with a similar philosophy.

Before concluding this discussion, we stress that pseudofermion fields are impractical due to large fluctuations causing low acceptance rates in the HMC, especially at small quark masses [98]. Using the frequency-splitting strategy introduced in Ref. [99], see also

Appendix H, eventually leads to sensible improvements. Also, besides the generation of field configurations, the other expensive part of Lattice QCD calculations is performing measurements, detailed in Appendix A.2. In Appendix A.1.4, we additionally discuss another recent simulation strategy, i.e. master-field simulations [81, 100].

2.6 The Signal-to-Noise ratio problem

Leveraging state-of-the-art techniques, numerical computations of hadronic correlation functions suffer from exponential loss of significance, i.e. signal-to-noise (StN) ratios of hadronic correlation function decrease exponentially with the time separation of the sources [101, 102]. The number of configurations required to reach a given statistical precision thus increases with the square of that exponential factor, see also Ref. [85]. For the case of connected Wick contractions, the reason for this behavior lies in the fact that variances of generic hadronic correlators scale as powers of the quark propagator, which (configuration by configuration) decreases approximatively as $\exp\{-m_\pi|x-y|/2\}$ at asymptotically large distances $|x-y|$, while their expectation values decay much faster. A notable exception, detailed below, is given by the propagators of non-singlet pseudoscalar mesons, where the same pion states contribute both to the variance and signal. Many computations at the forefront of research in Lattice QCD need to face this issue, such as the Hadronic Vacuum Polarization and the Light-by-Light scattering contributions to the muon $(g-2)$, see Subsection 3.3.1, the amplitudes of leptonic and semileptonic B decays, masses and matrix elements of (multi) baryons states.

Let us provide an explicit example to clarify the issue, for a connected pseudoscalar propagator, defined in terms of interpolating operators $P = \overline{d}\gamma_5 u$, $\overline{P} = \overline{u}\gamma_5 d$ as

$$\langle P(y)\overline{P}(x)\rangle_c = -\langle D^{-1}(x,y)\gamma_5 D^{-1}(y,x)\gamma_5\rangle \tag{2.6.1}$$

$$= \langle Q^{-1}(x,y)Q^{-1}(y,x)\rangle = \langle Q^{-1}(y,x)\left[Q^{-1}(y,x)\right]^\dagger\rangle, \tag{2.6.2}$$

where $Q = \gamma_5 D = Q^\dagger$. The statistical observable

$$W_\pi = \sum_{\mathbf{x}} \mathrm{Tr}\Big\{Q^{-1}(y,x)\left[Q^{-1}(y,x)\right]^\dagger\Big\} = \sum_{\mathbf{x},a,b}\left|Q^{-1}_{ab}(y,x)\right|^2 > 0 \tag{2.6.3}$$

is positive definite. Using Eqs. (1.4.23) and the fact that the lightest particles with pseudoscalar quantum numbers are the pions, we can rewrite Eq. (2.6.3) as

$$\begin{aligned} W_\pi = \sum_{\mathbf{x}}\langle P(y)\overline{P}(x)\rangle_c &= \sum_{\mathbf{x}}\sum_c \int \frac{d^3\mathbf{p}}{(2\pi)^3\, 2\omega_{\mathbf{p}}}\langle 0|P(y)|\pi^c(p)\rangle\,\langle\pi^c(p)|\overline{P}(x)|0\rangle + (\dots) \\ &= \frac{|G_\pi|^2}{2m_\pi}e^{-m_\pi|x_0-y_0|} \propto e^{-m_\pi|x_0-y_0|} + (\dots) \end{aligned} \tag{2.6.4}$$

where $G_\pi = \langle 0|P(0)|\pi(0)\rangle$, and the dots represent exponentially suppressed contributions from heavier states. The variance associated to this estimator is defined as usual as

$\sigma^2_{W_\pi} = \langle W_\pi^2 \rangle - \langle W_\pi \rangle^2$. A trick can be used to calculate more easily the first term: in order to obtain the desired Wick contractions within the correlator, we can add two additional unphysical flavors u', d' to the theory, with a flavor-diagonal action. In this way, there will be no Wick contraction between W_π defined in terms of u, d and W_π defined from u', d':

$$\langle W_\pi^2 \rangle = \langle P_{ud}(y)\overline{P}_{ud}(x)\, P_{u'd'}(y)\overline{P}_{u'd'}(x)\rangle = \langle [P_{ud}(y)P_{u'd'}(y)]\left[\,\overline{P}_{ud}(x)\overline{P}_{u'd'}(x)\right]\rangle\,. \tag{2.6.5}$$

The identity written as in Eqs. (1.4.23) can then be inserted in the middle of the last term. The lightest states that have the same quantum numbers as $[P_{ud}(y)P_{u'd'}(y)]$ and $\left[\overline{P}_{ud}(x)\overline{P}_{u'd'}(x)\right]$ are formed by two pions, so that $\langle W_\pi^2 \rangle \propto e^{-2m_\pi|x_0-y_0|}$ but with a different coefficient than $\langle W_\pi \rangle^2$, so that also

$$\sigma^2_{W_\pi} = \langle W_\pi^2 \rangle - \langle W_\pi \rangle^2 \propto e^{-2m_\pi|x_0-y_0|} + (\dots)\,. \tag{2.6.6}$$

By combining this result with Eq. (2.6.4), the desired StN for the zero-momentum non-singlet pseudoscalar meson contribution can be obtained as

$$\frac{W_\pi(y_0,x_0)}{\sigma_{W_\pi}(y_0,x_0)} \propto \text{const} + (\dots)\,. \tag{2.6.7}$$

This particular example has been instructive in order to understand how to proceed to compute StNs, but it is a notable exception to the StN problem mentioned above, since its StN is constant and not exponentially decaying. In fact, in this particular case the same states (pions) contribute to both the signal and the variance, making the two contributions cancel out when computing the StN. In a more general scenario, the states contributing to the variance are lighter than those saturating the signal, making StN exponentially decreasing with the time distance of the sources.

We want to emphasize the crucial rôle of Eq. (2.6.3) in this context. In this equation, W_π is written as a sum of positive terms whose averages and errors are exponentially decreasing with the distance in the same way. Being W_π a positive definite estimator with variance $\sigma_{W_\pi} \simeq W_\pi$, within Monte Carlo simulations big cancellations cannot happen, i.e. W_π must be positive definite configuration by configuration. This in turn implies that the sum over spatial indices can be dropped out to write

$$Q^{-1}_{ab}(x,y) \propto e^{-\frac{m_\pi}{2}|x-y|} \tag{2.6.8}$$

which is numerically verified at large distances, $|x-y| > 1\,\text{fm}$. From the free theory it would be expected that $Q^{-1}_{ab}(x,y) \propto e^{-m|x-y|}$, where m is the quark mass. The fact that Eq. (2.6.8) holds is in agreement with the GMOR relation, see Eq. (1.4.28), according to which $m_\pi \propto \sqrt{\frac{m}{\Lambda_{\text{QCD}}}}\Lambda_{\text{QCD}} \ll \Lambda_{\text{QCD}}$. This means that the quark propagator's exponential suppression is a strong signal of the presence of SSB in the theory, since without it $Q^{-1}_{ab}(x,y) \propto e^{-\frac{\Lambda_{\text{QCD}}}{2}|x-y|}$ is expected to hold. Ultimately, the StN problem is a direct consequence of the pions being light.

We now show some examples of StN problems in physically interesting calculations.

1. The disconnected pseudoscalar propagator takes the form $\sum_{\mathbf{x}}\langle P_{uu}(x)P_{dd}(y)\rangle$. The lightest states contributing to its signal are still pions, but in this case the vacuum contributes to its variance, which in turn receives a constant constribution. Therefore, the StN decays like $e^{-m_\pi|x_0-y_0|}$.

2. It is interesting to also consider baryon interpolating operators, which can be written as $N = \left[(u^a)^T C\gamma_5 d^b\right] d^c\epsilon^{abc}$, where $C = i\gamma_0\gamma_2$. The nucleon two-point function at zero momentum receives the largest asymptotic contributions from the nucleon of mass M_N, while the lightest states contributing to its variance are formed by 3 pions. In this case, the StN is exponentially decreasing like $e^{-\left(M_N-\frac{3}{2}m_\pi\right)|x_0-y_0|}$. Note that $M_N \simeq \Lambda_{\mathrm{QCD}}$ and, if SSB was not present i.e. $m_\pi \simeq \Lambda_{\mathrm{QCD}}$ too, the StN would not as problematic as it is for the physical case, in which SSB is indeed present and $m_\pi \ll \Lambda_{\mathrm{QCD}}$. This problem becomes even more severe for correlation functions of fields with higher baryon number.

3. In the computation of the hadronic contributions to a_μ, a particularly bad StN problem is present for the dominant connected light-quark contribution and for the disconnected one. In fact, the non-singlet (isovector) vector two-point function at zero momentum, i.e. the light connected contribution to the two-point function of two electromagnetic currents in the isosymmetric limit, scales with the mass M_ρ of the ρ meson, while the corresponding variance overlaps with a two-pion state, with a resulting exponentially decreasing StN $\propto e^{-(M_\rho-m_\pi)|x_0-y_0|}$. In the singlet case, the exponential degradation is again worse due to the vacuum contribution to the variance.

4. Non-zero momentum correlators are one of the basic building blocks entering the Wick contractions of hadronic and semileptonic decays. They suffer from exponential degradation of StN ratios as well, e.g. for the case of pseudoscalar mesons decays the StN $\propto e^{-(E_\pi(\mathbf{p})-m_\pi)|x_0-y_0|}$.

Variance reduction strategies need to be devised in order to tackle this problem. For a given observable $\mathcal{O}$, it is often possible to define another observable $\mathcal{O}'$ such that

$$\langle\mathcal{O}'\rangle = \langle\mathcal{O}\rangle\,, \quad \sigma_{\mathcal{O}'} \ll \sigma_{\mathcal{O}} \tag{2.6.9}$$

i.e. the desired expectation value can be obtained with much smaller statistical errors. In Appendix A.2 we briefly review random sources [82, 103], allowing to reduce statistical fluctuations thanks to volume averages. Additional refinements can be made, e.g. combining this strategy with low-mode averaging [104–106], with additional care to be put in the estimation of single-trace propagators and differences of propagator traces, see Ref. [99] and the discussion in Appendix H. In Chapter 4 we study in depth a different proposal, namely multilevel algorithms, exploiting the locality of the theory to achieve exponential improvements in StNs.

Chapter 3

Spectral densities and Inverse problems

Spectral densities play an important rôle in particle physics, since they are related to physically interesting quantities such as multiparticle cross sections and decay rates, as well as non-static properties of the quark-gluon plasma [107–110]. We are interested in their non-perturbative extraction from first principles in the framework of Lattice QCD. For this purpose, in Section 3.1, we introduce the Källén-Lehmann representation, relating spectral densities with Euclidean time correlation functions that can be measured on the lattice. The extraction of spectral densities from the Euclidean time dependence of correlation functions entails an *inverse problem*, which is discussed in Section 3.2. Several examples of spectral densities within the context of QCD are finally presented in Section 3.3, with further details provided in Appendix C. The solution to this problem constitutes one of the two original contributions of this Thesis, and it is discussed in Chapter 5. Appendix B complements this discussion by describing an alternative method to extract infinite-volume scattering amplitudes at energies below three or more particle thresholds from their finite-volume counterparts, accessible on the lattice.

3.1 Spectral representations

In this Section we focus on deriving the representation of Euclidean correlators in terms of spectral functions. In this view, we describe an important relation in particle physics, namely the Källén–Lehmann formula, from which we derive the representation of Euclidean time correlators as *generalized Laplace transforms* of spectral densities. We refer to Refs. [111–115] for a more complete introduction to these topics.

3.1.1 Källén–Lehmann representation

Let us consider the Euclidean two-point function of a renormalized (composite) operator $\mathcal{O}$. We can rewrite the (non-ordered) two-point function considering the completeness

relation on the entire Hilbert space

$$\mathbb{1} = \sum\!\!\!\!\!\!\int_n |n\rangle\langle n| \tag{3.1.1}$$

where the sum runs over any complete set of states, including integrals over continuous labels like momenta as well as sums over discrete ones, and the identity written as $1 = \int d^4q\, \delta^4(q - p_n)$, obtaining

$$\langle 0|\mathcal{O}^\dagger(x)\mathcal{O}(y)|0\rangle \;\; = \int \frac{d^4p}{(2\pi)^3} e^{ip(x-y)}\theta(p_0)\rho(p) \tag{3.1.2}$$

in terms of the spectral density

$$\rho(p) = (2\pi)^3 \sum\!\!\!\!\!\!\int_n \delta^4(p_n - p)\,|\langle 0|\mathcal{O}(0)|n\rangle|^2 \equiv (2\pi)^3\langle 0|\mathcal{O}^\dagger(0)\delta^4(p - \mathbb{P})\mathcal{O}(0)|0\rangle \tag{3.1.3}$$

where $\mathbb{P}$ is the QCD four-momentum operator and $\rho(p)$ is a function of p^2 only. Note that the definition of this quantity is independent of the spacetime metric. Typically, the lowest one-particle states of mass m are manifest in ρ by the presence of a δ-function at $p^2 = m^2$, while a continuum of multiparticle states contributes at energies larger than the multiparticle threshold, $p^2 > \omega_{\text{thr}}^2 = (2m)^2$. Possible additional δ functions from bound states might be present in the intermediate range $m^2 < p^2 < \omega_{\text{thr}}^2$.

Considering now the time-ordered two-point function of the same operator $\mathcal{O}$ in Eq. (3.1.2), the Källen-Lehman representation [116–118] directly follows by inserting the identity written as $1 = \int_0^\infty d\mu^2\, \delta(\mu^2 - p^2)$, obtaining

$$\langle 0|T\{\mathcal{O}^\dagger(x)\mathcal{O}(y)\}|0\rangle = \int_0^\infty d\mu^2\, \rho(\mu) D(x - y, \mu^2) \tag{3.1.4}$$

in terms of the Feynman spacetime free propagator

$$D(x, \mu^2) = \int \frac{d^4p}{(2\pi)^4} \frac{e^{ipx}}{p^2 + \mu^2} \tag{3.1.5}$$

allowing us to physically interpret the spectral density as effectively "measuring" the density of states in the interval $[s, s + ds]$ via $\rho(\sqrt{s})ds$.
This discussion can be generalized to any n-point function of arbitrary operators. An additional property for the specific case above of vacuum expectation values with two operators $\mathcal{O}^\dagger(x)$ and $\mathcal{O}(y)$ is that the scalar spectral density $\rho(p)$ is real and positive.

3.1.2 Generalized Laplace transform representation

We now want to rewrite the time-momentum representation of the correlation function projected to definite spatial momentum $\mathbf{p}$

$$C(x_0 - y_0, \mathbf{p}) = \int d^3\mathbf{x}\, e^{-i\mathbf{p}\cdot(\mathbf{x}-\mathbf{y})} \left\langle 0 \left| T\left\{\mathcal{O}^\dagger(x)\mathcal{O}(y)\right\}\right| 0\right\rangle \tag{3.1.6}$$

in terms of its spectral density. Using the Källén-Lehmann representation in Eq. (3.1.4) and the known integral [119]

$$\int_{-\infty}^{\infty} \frac{dp_0}{2\pi}\, e^{ip_0 x_0}\, \frac{1}{p_0^2 + |\mathbf{p}|^2 + \mu^2} = \frac{1}{2\omega_{\mathbf{p}}} e^{-\omega_{\mathbf{p}}|x_0|}\,, \quad \omega_{\mathbf{p}}^2 = \mu^2 + |\mathbf{p}|^2\,, \tag{3.1.7}$$

we derive

$$\begin{aligned} C(x_0 - y_0, \mathbf{p}) &= \int_{-\infty}^{\infty} \frac{dp_0}{2\pi} e^{ip_0(x_0-y_0)} \int_0^{\infty} d\mu^2 \frac{\rho(\omega_{\mathbf{p}})}{p_0^2 + \omega_{\mathbf{p}}^2} \\ &= \int_0^{\infty} d\mu^2 \frac{1}{2\omega_{\mathbf{p}}} e^{-\omega_{\mathbf{p}}|x_0-y_0|} \rho(\mu) \end{aligned} \tag{3.1.8}$$

implying

$$C(x_0 - y_0, \mathbf{p}) = \int_0^{\infty} d\omega\, e^{-\omega|x_0-y_0|} \rho\left(\sqrt{\omega^2 - |\mathbf{p}|^2}\right). \tag{3.1.9}$$

If we are interested in the case of zero spatial momentum, $\mathbf{p} = \mathbf{0}$, then

$$C(x_0, \mathbf{0}) = \int_0^{\infty} d\omega\, e^{-\omega|x_0|} \rho(\omega) \tag{3.1.10}$$

which is the desired relation.

Subtraction of UV divergences

A consequence of the positivity of the spectral density and of the Källén-Lehmann representation in Eq. (3.1.4) is that the vacuum polarization

$$\Pi(p^2) \equiv i \int d^4x\, e^{-ip(x-y)} \langle 0|T\left\{\mathcal{O}^\dagger(x)\mathcal{O}(y)\right\}|0\rangle = \int_0^{\infty} d\mu^2 \frac{\rho(\mu)}{p^2 + \mu^2} \tag{3.1.11}$$

cannot decay faster than the bare propagator as $p^2 \to +\infty$. Indeed, it is not guaranteed that $\Pi(p^2)$, nor the spectral density, vanish at all as $p^2 \to +\infty$.

In general, correlation functions might contain contact terms, which are associated with power-like UV divergences in the corresponding spectral densities, and thus in $\Pi(p^2)$. In order to define finite correlation functions and their associated spectral densities, we need to explicitly remove these UV divergences, modifying Eq. (3.1.11) accordingly [113]. To this end, we define the n-subtracted vacuum polarization $\Pi_{s,n}(p^2)$, $n \in \mathbb{N}\backslash\{0\}$, from

$$\Pi(p^2) = \sum_{k=0}^{n-1} c_k (-p^2)^k + (-p^2)^n \Pi_{s,n}(p^2)\,, \tag{3.1.12}$$

where the subtraction coefficients c_k can be derived through the following iterative, explicit subtraction of UV divergences. The idea is that each subtraction applied to $\Pi(p^2)$ improves its convergence by an additional power of $1/\mu^2$, eventually compensating any divergence after n steps. We start by applying one subtraction to Eq. (3.1.11), namely requiring that c_0 satisfies (i.e. defining implicitly c_0 from)

$$\Pi(p^2) - c_0 = (-p^2) \int_0^{\infty} d\mu^2\, \frac{\rho(\mu)}{\mu^2(p^2 + \mu^2)} \;\to\; c_0 = \Pi(0) = \int_0^{\infty} d\mu^2\, \frac{\rho(\mu)}{\mu^2}\,. \tag{3.1.13}$$

The rest of the coefficients can be analogously found in an iterative way, e.g.

$$\Pi(p^2) - c_0 - (-p^2)c_1 = (-p^2)^2 \int_0^\infty d\mu^2 \, \frac{\rho(\mu)}{\mu^4(p^2+\mu^2)} \;\to\; c_1 = \int_0^\infty d\mu^2 \, \frac{\rho(\mu)}{\mu^4} \,. \tag{3.1.14}$$

In general, we find

$$c_k = \int_0^\infty d\mu^2 \, \frac{\rho(\mu)}{(\mu^2)^{k+1}} \,, \tag{3.1.15}$$

implying

$$\Pi_{s,n}(p^2) = \int_0^\infty d\mu^2 \, \frac{\rho(\mu)}{(\mu^2)^n(p^2+\mu^2)} \tag{3.1.16}$$

which can also be rewritten in terms of a subtracted spectral density $\rho_{s,n}(\mu)$ as

$$\Pi_{s,n}(p^2) = \int_0^\infty d\mu^2 \, \frac{\rho_{s,n}(\mu)}{p^2+\mu^2} \,, \quad \rho_{s,n}(\mu) \equiv \frac{\rho(\mu)}{(\mu^2)^n} \,. \tag{3.1.17}$$

The above results lead to a subtracted version of the Källén–Lehmann representation

$$\left\langle 0 \middle| T\left\{\mathcal{O}^\dagger(x)\mathcal{O}(y)\right\} \middle| 0 \right\rangle = \int \frac{d^4p}{(2\pi)^4} e^{ip(x-y)} \left[\sum_{k=0}^{n-1} c_k(-p^2)^k + (-p^2)^n \Pi_{s,n}(p^2) \right] \tag{3.1.18}$$

which can be equivalently rewritten as

$$\left\langle 0 \middle| T\left\{\mathcal{O}^\dagger(x)\mathcal{O}(y)\right\} \middle| 0 \right\rangle = \sum_{n=0}^{n-1} c_k \, \Box^k \, \delta^4(x-y) + \int \frac{d^4p}{(2\pi)^4} e^{ip(x-y)} (-p^2)^n \Pi_{s,n}(p^2) \,. \tag{3.1.19}$$

As expected, contact terms are responsible for the divergence of the correlation function at $x = y$. Once they are removed, the resulting correlator is finite, and the corresponding subtracted vacuum polarization $\Pi_{s,n}$ is multiplied by $(-p^2)^n$.

The representation of Euclidean correlators as *generalized* Laplace transforms of spectral densities follows by inserting Eq. (3.1.17) inside Eq. (3.1.19) and proceeding similarly to Eqs. (3.1.9) and (3.1.10). We find that

$$C(x_0, \mathbf{p}) = \int_0^\infty d\omega \, e^{-\omega|x_0|} (\omega^2 - |\mathbf{p}|^2)^n \rho_{s,n}\left(\sqrt{\omega^2 - |\mathbf{p}|^2}\right) \,, \tag{3.1.20}$$

while at $\mathbf{p} = 0$ we have

$$C(x_0, \mathbf{0}) = \int_0^\infty d\omega \, e^{-\omega|x_0|} \, \omega^{2n} \rho_{s,n}(\omega) \,. \tag{3.1.21}$$

3.2 The inverse problem

Euclidean time correlation functions in configuration space have been shown to be related to spectral densities via Eqs. (3.1.9), (3.1.10), (3.1.20) and (3.1.21), collectively labeled as generalized Laplace transforms. The possibility of inverting these equations, solving the associated *inverse problem*, would allow us to directly estimate $\rho(\omega)$ and $\rho_{s,n}(\omega)$

from the knowledge of the corresponding correlation functions. Notice that in Lattice QCD the correlation functions are only known on the Euclidean time axis, and therefore standard methods to perform this inversion, such as the textbook Bromwhich integral (also referred to as inverse Mellin formula) [120, 121], are not a viable strategy, as they involve an impractical analytic continuation.

Many physical observables in particle physics can be expressed through integral relations of the form

$$P = \int_0^\infty d\omega\, \kappa(\omega)\rho(\omega) \tag{3.2.1}$$

where $\rho(\omega)$ is a spectral density, whereas $\kappa(\omega)$ is a known analytic kernel that contains information on the physical process of interest. When κ is chosen to be a smooth, peaked function around an additional kinematic variable, such as the center of a Gaussian or a Breit-Wigner (alternatively referred to as Lorentzian or Cauchy) function, see Eqs. (5.4.1) and (3.3.11) respectively, the quantity P is referred to as a *smeared* spectral density [122].

Smearing also arises as a technical necessity when extracting *finite-volume spectral densities* [123], as is the case in Lattice QCD applications [124,125]. Since the finite volume causes the spectrum to be discretized, the spectral densities are weighted sums of δ functions located at the finite-volume spectrum. Both the weights and the spectrum receive power-like finite-volume corrections when at least two particles are involved. The relation with their infinite-volume counterpart is known, up to exponentially small systematic errors, only in limited kinematic regions and for a small number of particles [50–54,126–142], see also Refs. [54,142] for recent reviews and Appendix B for more details. Therefore, in lattice applications the width of the smearing kernel can only approach zero *after* taking the infinite-volume limit, where these δ functions become denser and denser at energies above threshold, reproducing the continuum of states. Notice that the presence of a non-zero smearing width has the beneficial effect of exponentially suppressing FVEs on spectral densities [143].

Having in mind Lattice QCD applications, where we directly extract correlation functions in configuration space, a much more natural representation for Eq. (3.2.1) would ideally be of the form

$$P = \int_0^\infty dt\, K(t)C(t) \tag{3.2.2}$$

where $C(t)$ is the correlation function related to the spectral density $\rho(\omega)$ through a generalized Laplace transform, possibly including any necessary UV subtractions. Whether this rewriting can be explicitly carried out avoiding an explicit inversion of the generalized Laplace transforms depends on the analytic properties of the kernel $\kappa(\omega)$.

In fact, in order to find the function K s.t. $\int_0^\infty d\omega\, \kappa(\omega)\rho(\omega) = \int_0^\infty dt\, K(t)C(t)$ holds, we need to study the analytic continuation of the kernel $\kappa(\omega)$, which could have non-analyticities such as poles ω_i in the complex plane. By introducing $\gamma > \max_i \mathrm{Re}(\omega_i)$, and assuming that a standard Laplace transform relates $\rho(\omega)$ and $C(t)$ as in Eq. (3.1.10), we can analytically solve the inverse Laplace transform for $\kappa(\omega)$ through the standard

Bromwhich integral as

$$\kappa(\omega) = \int_0^\infty dt\, K(t) e^{-\omega t}\,, \quad K(t) = \frac{1}{2\pi i} \lim_{\Lambda\to\infty} \int_{\gamma-i\Lambda}^{\gamma+i\Lambda} dE\, e^{Et} \kappa(E) \tag{3.2.3}$$

in order to rewrite Eq. (3.2.1) as

$$P = \int_0^\infty d\omega\, \rho(\omega)\, \frac{1}{2\pi} \int_{-\infty}^\infty dE\, \kappa(E) \int_0^\infty dt\, e^{-(\omega-\gamma)t} e^{iEt}\,. \tag{3.2.4}$$

Recalling that spectral densities have branch cuts starting from ω_{thr}, the exponential factor in Eq. (3.2.4) gives a suppression that makes the integrals converge as long as $\gamma \leq \omega_{\text{thr}}$, allowing to reach Eq. (3.2.2) and effectively solving the only apparent inverse problem. If $\gamma > \omega_{\text{thr}}$, other strategies must be devised to solve the inverse problem of extracting $\rho(\omega)$ from the knowledge of $C(t)$ on the Euclidean time axis only. We defer to Chapter 5 the discussion of a possible solution to the inverse problem.

3.3 Spectral densities and the inverse problem in QCD

To conclude this Chapter, we present several phenomenologically relevant examples of spectral densities within the context of QCD, along with a discussion of the potential inverse problem that may need to be solved.

3.3.1 The anomalous magnetic moment of the muon

Leptonic magnetic moments g are among the most accurate experimentally measured quantities in high energy physics, reaching astonishing accuracies of 0.13 parts per trillion for the electron g_e [144] and 0.20 (0.14 expected) parts per million [145] for the muon g_μ, while the rapid decay of the tau lepton prevents a precise experimental measurement of g_τ. The non-relativistic limit of the Dirac equation predicts $g = 2$ for all leptons, with quantum loop effects leading to small, calculable and measurable deviations parametrized by the anomalous magnetic moment $a = (g-2)/2$. Besides being more sensitive than a_e to New Physics contributions, a lot of new research has recently involved the estimation of a_μ [146] due to a persisting deviation between experimental measurements [145, 147–152] and Standard Model predictions [30, 153]. Most of the theory uncertainty of a_μ is currently dominated by $O(\alpha^2)$ Hadron Vacuum Polarization (HVP) contributions and the much smaller Hadronic Light-by-Light (HLbL).

The first principles approach for computing the hadronic contributions to a_μ is given by Lattice QCD [146, 154–157] . The HVP tensor in Euclidean time

$$\Pi_{\mu\nu}(q) = \int d^4x\, e^{iqx} \langle V_\mu^{\text{em}}(x) V_\nu^{\text{em}}(0)\rangle = (q_\mu q_\nu - \delta_{\mu\nu} q^2)\Pi(q^2) \tag{3.3.1}$$

is defined in terms of the zero-momentum two-point function

$$C(t) = \frac{1}{3} \sum_{k=1}^3 \int d^3\mathbf{x}\, \langle V_k^{\text{em}}(t,\mathbf{x}) V_k^{\text{em}}(0)\rangle \tag{3.3.2}$$

of two electromagnetic currents

$$V_\mu^{em} = i \sum_{\mathrm{f}=1}^{N_\mathrm{f}} q_\mathrm{f} \overline{\psi}_\mathrm{f} \gamma_\mu \psi_\mathrm{f} \tag{3.3.3}$$

where q_f is the charge of the quark with flavor f. Exploiting the usual Källén-Lehmann representation, the leading hadronic contribution to the vacuum polarization $\Pi(q^2)$ can be rewritten via a once-subtracted dispersion relation as

$$\Pi(q^2) - c_0 = q^2 \int_0^\infty ds \, \frac{\rho(\sqrt{s})}{s(s+q^2)} \tag{3.3.4}$$

where $c_0 = \Pi(0)$, see Eq. (3.1.13), and $\rho(\omega)$ is the spectral density associated to the Euclidean two-point correlation function projected to zero momentum through

$$C(t) = \int_0^\infty d\omega \, e^{-\omega t} \omega^2 \rho(\omega) \, . \tag{3.3.5}$$

The $O(\alpha^2)$ HVP contribution to a_μ can be written as [158]

$$a_\mu^{\mathrm{HVP,LO}} = \left(\frac{\alpha}{\pi}\right)^2 \int_0^\infty ds \, K_E(s) 4\pi^2 [\Pi(s) - \Pi(0)] \tag{3.3.6}$$

in terms of the analytically computable kernel

$$K_E(s) = \frac{1}{m_\mu^2} \hat{s} Z(\hat{s})^3 \frac{1 - \hat{s} Z(\hat{s})}{1 + \hat{s} Z(\hat{s})^2} \, , \quad Z(\hat{s}) = -\frac{\hat{s} - \sqrt{\hat{s}^2 + 4\hat{s}}}{2\hat{s}} \, , \quad \hat{s} = \frac{s}{m_\mu^2} \, . \tag{3.3.7}$$

In order to derive the time-momentum representation of Eq. (3.3.6), as detailed for Eqs. (3.2.1) and (3.2.2), it is crucial that the real part of the pole of the kernel $K_E(s)$ in Eq. (3.3.7) at $1 + \hat{s} Z(\hat{s})^2 = 0$ i.e. $s = -4m_\mu^2$ is lower than the multiparticle threshold $(2m_\pi)^2$, which is indeed the case. As shown in Refs. [154, 158], Eq. (3.3.6) can then be written as

$$\begin{aligned} a_\mu^{\mathrm{HVP,LO}} &= 4\alpha^2 m_\mu \int_0^\infty dt \, t^3 C(t) \tilde{K}(t) \, , \\ \tilde{K}(t) &= \frac{2}{m_\mu t^3} \int_0^\infty \frac{d\omega}{\omega} K_E(\omega^2) \left[\omega^2 t^2 - 4 \sin^2 \frac{\omega t}{2} \right] . \end{aligned} \tag{3.3.8}$$

Therefore, a_μ^{HVP} can be extracted from first principles in Lattice QCD by measuring Eq. (3.3.5) on the lattice and using Eq. (3.3.8), circumventing the inverse problem. Note that a similar analysis can be done for the much smaller HLbL contribution [159] and for the NLO contributions to the HVP [160].

The main hindrance in achieving a precision on a_μ^{HVP} at the permille level, required to obtain uncertainties comparable with the experimental ones, is the necessity to reduce the statistical uncertainty on the dominant connected light-quark contribution $a_\mu^{\mathrm{HVP}}(ud)$, which is calculated in the isosymmetric limit $m_u = m_d$. As detailed in Section 2.6, the correlation function in Eq. (3.3.2) is affected by an exponentially decreasing StN with the temporal distance of the two electromagnetic currents, affecting the evalutation of Eq. (3.3.8) at large distances. A possible solution to this problem is studied in Chapter 4.

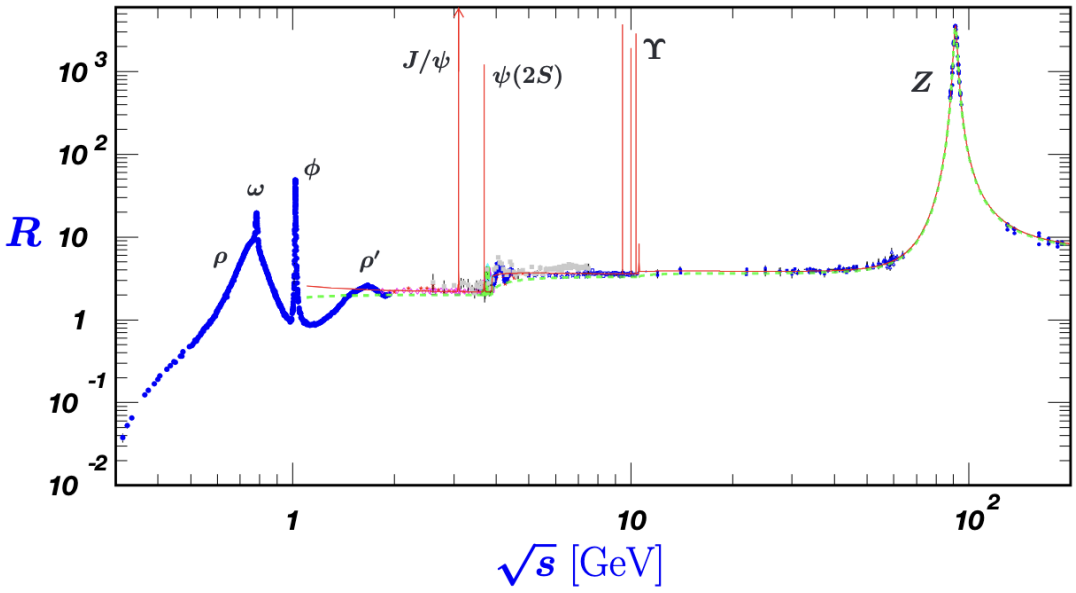

Figure 3.1: World data [161, 162] on the R-ratio in Eq. (3.3.9), with the green dashed curve representing a naïve quark-parton model prediction, while the solid red one is a 3-loop perturbative QCD prediction.

3.3.2 The R-ratio

The spectral density $\rho(\omega)$ is related to the experimentally measurable R-ratio

$$\rho(\omega) = \frac{R(\omega)}{12\pi^2}\,, \quad R(\sqrt{s}) = \frac{\sigma(e^+e^- \to \text{hadrons}, s)}{\sigma(e^+e^- \to \mu^+\mu^-, s)} = \frac{\sigma(e^+e^- \to \text{hadrons}, s)}{4\pi\alpha^2(s)/3s} \tag{3.3.9}$$

shown in Fig. 3.1. Not only it is an important input for important physics applications, entering e.g. the computation of a_μ and of the running of the electromagnetic coupling, but it is an energy-dependent probe of the theory, allowing e.g. to study the ρ meson resonance. This is interesting also in light of the recent discrepancies in the experimental measurements of the $e^+e^- \to \pi^+\pi^-$ channel by BaBar [163, 164], KLOE [165–168] and CMD-3 [169]. This channel dominates the R-ratio at low energies and it is an important input for the dispersive approach to compute a_μ [153,170]. In order to better understand these tensions, a long-term goal of our study is the extraction of the smeared inclusive R-ratio, defined as

$$\rho_\sigma(\omega) = \int_0^\infty d\omega'\, \delta_\sigma(\omega, \omega')\rho(\omega')\,, \quad \rho_\sigma(\omega) \xrightarrow{\sigma\to 0} \rho(\omega)\,. \tag{3.3.10}$$

This defines a quantity that can be compared with smeared experimental data for the R-ratio, while also being suitable for direct extraction from Lattice QCD, as long as very small values of σ are avoided. A widely adopted choice for the smearing kernel is

the Breit-Wigner function

$$\delta_\sigma(\omega,\omega') = \frac{\sigma}{\pi}\frac{1}{(\omega-\omega')^2+\sigma^2} \tag{3.3.11}$$

which manifests two poles at $\omega' = \omega \pm i\sigma$ with $\mathrm{Re}(\omega') = \omega$. As long as we are interested in computing Eq. (3.3.10) at $\omega > \omega_{\mathrm{thr}}$, the extraction of this quantity from the knowledge of the correlation function on the Euclidean time axis in Eq. (3.3.2) relies on our ability to solve the inverse problem in Eq. (3.3.5), which is absent in case we want to extract ρ_σ at $\omega < \omega_{\mathrm{thr}}$.

3.3.3 Other examples

Here we briefly review other phenomenologically interesting cases of spectral densities and the related inverse problems, deferring to Appendix C a more detailed discussion.

Deep inelastic scattering (DIS) is the study of collisions of high-energy hard leptons with fixed hadronic targets via virtual photon exchange. The leptonic and hadronic contributions factorize in the corresponding cross section, allowing to study them separately. More in particular, the Euclidean two-point function of two electromagnetic currents inserted between nucleon single-particle stable QCD states is related to the hadronic tensor via a Laplace transform [107]. The possibility of inverting this relation would allow the extraction of the nucleon structure functions in which the hadronic tensor can be decomposed. These functions enter e.g. the unpolarized cross section for the inclusive process $(e + p \to e' + \text{hadrons})$.

The study of *semileptonic decays of heavy hadrons* (e.g. for B and D mesons, containing heavy b and c quarks respectively) is of crucial importance in the context of particle physics, e.g. in unitarity tests of the CKM matrix. Since leptons only interact via the weak force, the cross section can again be factorized in its leptonic and hadronic contributions, related via a Laplace transform to the Euclidean two-point function of two flavor-changing currents $V_\mu = \overline{q}\gamma_\mu(1-\gamma_5)Q$ with one light and one heavy flavor, associated to the spinors q and Q respectively, inserted between stable single-particle QCD states for a heavy hadron containing Q. The total, inclusive decay rate can be written as a smeared version of the hadronic tensor, with a kernel defined in terms of a θ function restricting the energies to the kinematically accessible ones, namely those below the energy of the decaying particle [107, 108, 171, 172]. Inclusive τ-decays can be described in a similar fashion [173]. The impossibility to analytically continue such θ function through the Bromwhich integral in Eq. (3.2.3) requires the solution of an inverse problem.

Non-static properties of the quark-gluon plasma i.e. *QCD transport coefficients* can be extracted from hadronic spectral densities at finite temperature [109]. For instance, the shear viscosity in $SU(3)$ gluodynamics can be extracted by evaluating at the origin the derivative of a spectral density, which is related to a two-point function of the energy-momentum tensor by a slightly modified Laplace transform to take into account thermal effects [110, 174–177].

Chapter 4

Multi-level Integration

In Chapter 2, we highlighted the pressing need to address the exponential loss of statistical precision in correlation functions at large distances, a problem that arises in Euclidean Quantum Field Theories when states contributing to the variance are lighter than those contributing to the central value, see the discussion in Section 2.6. With the primary goal of improving the precision in the computations of hadron propagators, we can design many variance reduction techniques. One simple but wasteful idea is to simply employ more computer power. Since the error on averaged quantities typically scales with the inverse square root of the number of configurations used, achieving a desired statistical precision with an exponentially decreasing StN requires the number of configurations to increase with the square of that exponential factor. This leads to simulations that become prohibitively expensive as the StN problem worsens. The multilevel strategy instead exploits the locality of the theory to design new estimators that share the same expectation value as the desired, target observable, but with a much lower variance, achieving exponential improvements. Additionally, the possibility of performing independent updates on local subdomains of the lattice can be exploited in master-field simulations at large volumes, described in Appendix A.1.4.

In Section 4.1 we introduce the general strategy in the simple framework of purely bosonic theories, where both the action and the observables depend locally on the integration variables. The StN problem can be avoided by measuring independently the local building blocks of the observables, rather than computing one global integral, leading to an impressive acceleration of the simulations and fully solving the problem in some cases.

The case of full Lattice QCD with fermions requires additional care. As mentioned in Chapter 2, see Subsection 2.5.1, fermions must be analytically integrated out in the QCD path integral in order to perform numerical simulations, leading to an effective gauge theory where the manifest locality of the action and of the observables is lost, since the fermion determinant and propagators are non-local functionals of the background gauge field. This is the reason why multilevel algorithms for systems with fermions are not straightforward. A recent proposal [83–88] for a one-dimensional domain decomposition

is discussed in Section 4.2, allowing for a block factorization of the fermion determinant in Lattice QCD that leads to an effective bosonic theory with a local action in the block gauge, pseudofermion and multiboson fields. Together with the factorization of the fermion observables, this paves the way for multilevel simulations of QCD. The theoretical factorization is also complemented in Section 4.3 by a variance analysis to show the effectiveness of multilevel algorithms for the connected and disconnected contributions used in Ref. [88]. The first novel contribution of this Thesis, published in Refs. [1, 4], is finally presented in Section 4.4, where we describe the extension of the factorization of the fermion determinant to the case of a four-dimensional domain decomposition. A few appendices complete the discussion.

4.1 Multilevel in bosonic theories

In this Section we want to provide a general introduction to multilevel algorithms by studying them for simpler theories than that of QCD with fermions, discussed in the rest of this Chapter. Before addressing the case of bosonic theories, which is the main topic of this introduction, we briefly provide an intuitive argument. Let us consider the computation of a factorized multi-dimensional integral, which can be expressed as the product of lower-dimensional ones. Mimicking the case of lattice simulations, we estimate this integral using Monte Carlo methods, and we require a fixed target statistical precision to be reached on the final result. In this case, it is clear that the cost of directly computing the multi-dimensional integral – with the integrand being the product of the factorized lower-dimensional ones and thus involving multiple integration variables – is significantly larger than the cost of calculating the product of independently estimated lower-dimensional integrals. Having this simple example in mind, let us now describe the case of purely bosonic theories.

Multilevel integration schemes can leverage the locality of non-Abelian pure gauge theories to achieve exponential error reduction, effectively solving StN problems. The gluonic action in Eq. (2.2.5) is local, involving nearest neighbor interactions, and thus factorizable. However, in order to apply the multilevel integration scheme, the observables must be factorizable as well. For instance, Wilson loops, relevant for studying the potential of a static $q\overline{q}$ pair and quark confinement, meet this requirement. These loops are path-ordered products of link variables, such as those along a plane rectangular path C in the time and space directions with extensions t and ℓ, defined as $W_C[U] = \mathrm{Tr}\{\prod_{l\in C} U_l\}$. They are affected by the StN problem, as

$$\langle W_C[U]\rangle \propto e^{-\sigma A}, \quad \langle W_C[U] W_C[U]^\dagger\rangle \propto \text{const} \tag{4.1.1}$$

where $A = t \times \ell$ is the area spanned by the loop, and σ is the string tension. A similar problem enters the computation of the two-point function of Polyakov loops $P(x)$, Wilson loops with the path being a straight line in the negative time direction passing

through x. It turns out that it is possible to write in an explicitly factorized form [178]

$$\begin{aligned} W_C[U] &= \mathbb{L}(0)_{\alpha\gamma} \left\{ \mathbb{T}(0)\mathbb{T}(a)\dots\mathbb{T}(T-a) \right\}_{\alpha\beta\gamma\delta} \mathbb{L}(T)^*_{\beta\delta} , \\ P(x)^* P(x+R\hat{1}) &= \left\{ \mathbb{T}(0)\mathbb{T}(a)\dots\mathbb{T}(T-a) \right\}_{\alpha\alpha\gamma\gamma} , \end{aligned} \tag{4.1.2}$$

where $\mathbb{L}(x_0)$ and $\mathbb{T}(x_0)$ are the local line and two-links operators, defined as

$$\mathbb{L}(x_0)_{\alpha\beta} = \left\{ U_1(x)\dots U_1(x+(\ell-a)\hat{1}) \right\}_{\alpha\beta} , \quad \mathbb{T}(x_0)_{\alpha\beta\gamma\delta} = U_0(x)^*_{\alpha\beta} U_0(x+\ell\hat{1})_{\gamma\delta} \tag{4.1.3}$$

respectively, with $x = (x_0, 0, 0, 0)$. The factorization of the observables W_C and P allows to design a multilevel algorithm, where sublattice averages are estimated stochastically and independently. Specifically, we can alternate global updates with updates inside the thick time slices of interest to estimate local expectation values, which are then employed to compute global averages, achieving the desired exponential error reduction.
These techniques have been combined with a careful analysis of global lattice symmetries to decompose the partition function into sectors with fixed quantum numbers and to define local averages. This approach was introduced in Ref. [179] for a one-dimensional harmonic oscillator and later applied in Ref. [180] to study glueballs in a pure Yang-Mills theory.

4.2 Multilevel in fermionic theories

Since fermions are Grassmann variables, their direct simulation on the lattice is computationally expensive, leading to the practical necessity of analytically integrating out fermionic degrees of freedom in the QCD path integral. The resulting simulated theory is an effective gauge theory with non-local interactions between gauge fields located in distant regions of the lattice, since both the propagator and the determinant of the Dirac matrix are non-local functionals of the background gauge field over the entire lattice, even if the Dirac matrix only contains nearest-neighbor interactions. Yet, intuition suggests that these non-local interactions should be weaker as distances increase, and in this Section we show that it is actually the case by presenting the most recent results on the factorization of the fermion determinant (up to small non-local terms) achieved with the one-dimensional domain decomposition proposed in Refs. [83–88]. As shown in Refs. [83, 85, 87], a local approximation of the quark propagator (and thus of relevant observables) can also be designed, but for the moment we focus on the fermion determinant only.

We begin with the one-dimensional lattice decomposition shown in Fig. 4.1, which consists in three non-overlapping thick time-slices Λ_0^{e}, Λ_1 and Λ_0^{o} such that both Λ_0^{e} and Λ_0^{o} are disconnected, since they only interact with themselves and with Λ_1. The Dirac matrix is

$$D = \begin{pmatrix} D_{\Lambda_0^{\mathrm{e}},\Lambda_0^{\mathrm{e}}} & D_{\Lambda_0^{\mathrm{e}},\Lambda_1} & 0 \\ D_{\Lambda_1,\Lambda_0^{\mathrm{e}}} & D_{\Lambda_1,\Lambda_1} & D_{\Lambda_1,\Lambda_0^{\mathrm{o}}} \\ 0 & D_{\Lambda_0^{\mathrm{o}},\Lambda_1} & D_{\Lambda_0^{\mathrm{o}},\Lambda_0^{\mathrm{o}}} \end{pmatrix} , \tag{4.2.1}$$

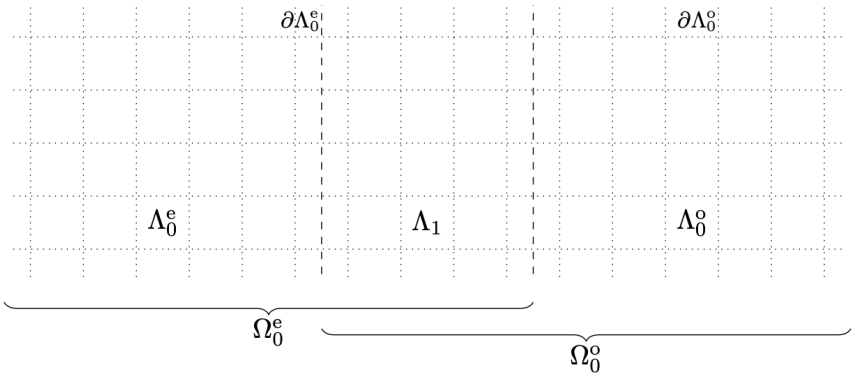

Figure 4.1: One-dimensional domain decomposition in thick time-slices. We slightly changed the notation of the original works [83–86,88] in order to match the most recent one of Refs. [1,4]. Results from previous References are recovered by substituting $\Lambda_0^{\mathrm{e}} \leftrightarrow \Lambda_0$, $\Lambda_0^{\mathrm{o}} \leftrightarrow \Lambda_2$.

where the subscript of an operator indicates the domain where the operator is restricted, e.g. $D_{\Lambda_0^{\mathrm{e}}}$ is the Wilson–Dirac operator restricted to the domain Λ_0^{e} with Dirichlet boundary conditions imposed on its external boundaries. When the subscript of the operator has two domains separated by a comma, this indicates a hopping term among these two domains, see Appendix D. The determinant of this matrix can be studied by applying twice a Schur decomposition, see Appendix E, following the same procedure described in Refs. [84, 85]. In this way, we find

$$\det D = \frac{1}{\det\left[P_{\Lambda_0^{\mathrm{e}}} D_{\Omega_0^{\mathrm{e}}}^{-1} P_{\Lambda_0^{\mathrm{e}}}\right] \det\left[P_{\Lambda_0^{\mathrm{o}}} D_{\Omega_0^{\mathrm{o}}}^{-1} P_{\Lambda_0^{\mathrm{o}}}\right] \det D_{\Lambda_1}^{-1}} \det W \tag{4.2.2}$$

where $\Omega_0^{\mathrm{e,o}} = \Lambda_0^{\mathrm{e,o}} \bigcup \Lambda_1$, or equivalently

$$\det D = \frac{\det D_{\Omega_0^{\mathrm{e}}} \det D_{\Omega_0^{\mathrm{o}}}}{\det D_{\Lambda_1}} \det W\,, \quad W = \begin{pmatrix} 1 & P_{\Lambda_0^{\mathrm{e}}} D_{\Omega_0^{\mathrm{e}}}^{-1} D_{\Lambda_1,\Lambda_0^{\mathrm{o}}} \\ P_{\Lambda_0^{\mathrm{o}}} D_{\Omega_0^{\mathrm{o}}}^{-1} D_{\Lambda_1,\Lambda_0^{\mathrm{e}}} & 1 \end{pmatrix}. \tag{4.2.3}$$

The projectors $P_{\Lambda_0^{\mathrm{e}}}$, $P_{\Lambda_0^{\mathrm{o}}}$ are defined in Appendix D, while Appendix F describes an alternative way to derive this formula that yields useful intermediate results for the case of a multi-dimensional domain decomposition[1]. Note that these results only depend on the form of the Dirac matrix in Eq. (4.2.1), regardless of the number of dimensions of the lattice decomposition and of the particular discretization. We can rewrite

$$\det W = \det(1-\omega)\,, \quad \omega = P_{\partial\Lambda_0^{\mathrm{e}}} D_{\Omega_0^{\mathrm{e}}}^{-1} D_{\Lambda_1,\Lambda_0^{\mathrm{o}}} P_{\partial\Lambda_0^{\mathrm{o}}} D_{\Omega_0^{\mathrm{o}}}^{-1} D_{\Lambda_1,\Lambda_0^{\mathrm{e}}}\,, \tag{4.2.4}$$

where the operator ω propagates a quark from the inner boundary $\partial\Lambda_0^{\mathrm{e}}$ of Λ_0^{e} to Λ_0^{o} and back to $\partial\Lambda_0^{\mathrm{e}}$. At large values of the thickness Δ of Λ_1, it is therefore exponentially

[1] Results from these Appendices can be directly applied to the domain decomposition discussed in the main text by substituting $\Lambda_0^{\mathrm{e}} \leftrightarrow \Lambda_0$, $\Lambda_0^{\mathrm{o}} \leftrightarrow \Lambda_2$.

suppressed as $e^{-m_\pi \Delta}$. If we neglect its contribution on the r.h.s. of Eq. (4.2.3), the quark determinant shows a fully factorized dependence on the gauge field in Λ_0^{e} and Λ_0^{o}. It means that, for the first three determinants in Eq. (4.2.3), the goal has been reached: $\det D_{\Lambda_1}$ depends on the gauge field in the block Λ_1, $\det D_{\Omega_0^{\mathrm{e}}}$ on the gauge field in Ω_0^{e} and $\det D_{\Omega_0^{\mathrm{o}}}$ on the gauge field in Ω_0^{o}. The small remaining determinant $\det(1-\omega)$ still depends on the gauge field over the whole lattice, but its suppression allows it to be approximated, including the remainder in the observable in order to have an exact algorithm.

4.2.1 Multiboson action

As reviewed in Appendix D of Ref. [84], a generalization of Lüscher's original multiboson proposal [181] to complex matrices [182–184] starts by approximating the function $1/z$, with $z \in \mathbb{C}$, by the polynomial

$$P_N(z) \equiv \frac{1 - R_{N+1}(z)}{z} = c_N \prod_{k=1}^{N} (z - z_k) \,, \tag{4.2.5}$$

where N is chosen to be even, the N roots of $P_N(z)$ are obtained by requiring that the remainder polynomial R_{N+1} satisfies $R_{N+1}(0) = 1$, and c_N is an irrelevant numerical constant. The roots z_k can be chosen to lie on an ellipse passing through the origin of the complex plane with center 1 and foci $1 \pm c$,

$$u_k = 1 - z_k = \cos\left(\frac{2\pi k}{N+1}\right) + i\sqrt{1-c^2}\,\sin\left(\frac{2\pi k}{N+1}\right), \quad k = 1, \ldots, N \,. \tag{4.2.6}$$

Approximating the inverse determinant of $(1-\omega)$ with Eq. (4.2.5), we obtain

$$\det(1-\omega) = \frac{\det\left[1 - R_{N+1}(1-\omega)\right]}{\prod_{k=1}^{N/2} \det\left[(u_k - \omega)^\dagger (u_k - \omega)\right]} = \frac{\det\left[1 - R_{N+1}(1-\omega)\right]}{\prod_{k=1}^{N/2} \det\left(W^\dagger_{\sqrt{u_k}} W_{\sqrt{u_k}}\right)} \tag{4.2.7}$$

where

$$W_z = \begin{pmatrix} z P_{\partial\Lambda_0^{\mathrm{e}}} & P_{\partial\Lambda_0^{\mathrm{e}}} D^{-1}_{\Omega_0^{\mathrm{e}}} D_{\Lambda_1, \Lambda_0^{\mathrm{o}}} \\ P_{\partial\Lambda_0^{\mathrm{o}}} D^{-1}_{\Omega_0^{\mathrm{o}}} D_{\Lambda_1, \Lambda_0^{\mathrm{e}}} & z P_{\partial\Lambda_0^{\mathrm{o}}} \end{pmatrix} . \tag{4.2.8}$$

The determinants in Eqs. (4.2.2) and (4.2.7) can finally be represented by introducing auxiliary local pseudofermion fields in the domains Λ_1, Ω_0^{e} and Ω_0^{o} and multiboson fields [181–186] on the inner boundaries of Λ_0^{e} and Λ_0^{o} to study $\det W$. For instance, for two degenerate quark flavors

$$\begin{aligned} \frac{\det D^2}{\det\left[1 - R_{N+1}(1-\omega)\right]^2} = C \int [d\phi_0^{\mathrm{e}}][d\phi_0^{\mathrm{e}\,\dagger}] e^{-\left|D^{-1}_{\Omega_0^{\mathrm{e}}} \phi_0^{\mathrm{e}}\right|^2} \int [d\phi_0^{\mathrm{o}}][d\phi_0^{\mathrm{o}\,\dagger}] e^{-\left|D^{-1}_{\Omega_0^{\mathrm{o}}} \phi_0^{\mathrm{o}}\right|^2} \times \\ \times \int [d\phi_1][d\phi_1^\dagger] e^{-\left|D^{-1}_{\Lambda_1} \phi_1\right|^2} \prod_{k=1}^{N/2} \left\{ \int [d\chi_k][d\chi_k^\dagger] e^{-\left|W_{\sqrt{u_k}} \chi_k\right|^2} \right\} \end{aligned} \tag{4.2.9}$$

where C is an irrelevant numerical constant. Each pseudofermion field ϕ_0^{e}, ϕ_1, ϕ_0^{o} is confined to the corresponding region Λ_0^{e}, Λ_1, Λ_0^{o} respectively, while the N multiboson fields χ_k live on the outer boundaries of region Λ_1. The explicit factorization of the multiboson action can be shown by expanding the product $W_{\sqrt{u_k}}\chi_k$ and decomposing $\chi_k = \eta_k + \xi_k$, with $\eta_k = P_{\partial\Lambda_0^{\mathrm{e}}}\chi_k$ and $\xi_k = P_{\partial\Lambda_0^{\mathrm{o}}}\chi_k$, ultimately implying the factorization of the dependence of the bosonic action from the gauge field in the two disconnected blocks Λ_0^{e} and Λ_0^{o}.

4.2.2 Reweighting factor

The expectation value of a generic observable $\mathcal{O}$ can be expressed as

$$\langle \mathcal{O} \rangle = \frac{\langle \mathcal{O}\, \mathcal{W}_N \rangle_N}{\langle \mathcal{W}_N \rangle_N}\,, \quad \mathcal{W}_N = \det[1 - R_{N+1}(1-\omega)]\,, \tag{4.2.10}$$

where $\langle\cdot\rangle_N$ indicates the expectation value for an importance sampling with N multibosons in the action. A locally factorizable approximation for the quark propagator has been detailed in Refs. [83, 85, 87], and a different one can be derived starting from the factorization of the fermion determinant, as described in Appendix F, allowing to introduce a factorized approximation $\mathcal{O}^{\mathrm{fact}}$ of $\mathcal{O}$. We find

$$\langle \mathcal{O} \rangle = \frac{\langle \mathcal{O}\mathcal{W}_N \rangle_N}{\langle \mathcal{W}_N \rangle_N} = \langle \mathcal{O}^{\mathrm{fact}} \rangle_N + \frac{\langle \mathcal{O}\mathcal{W}_N - \mathcal{O}^{\mathrm{fact}} \langle \mathcal{W}_N \rangle_N \rangle_N}{\langle \mathcal{W}_N \rangle_N}\,. \tag{4.2.11}$$

Since both the action and the (approximated) observable are factorized, the expectation value $\langle \mathcal{O}^{\mathrm{fact}} \rangle_N$ can be computed with a multilevel algorithm by generating gauge field configurations from the multiboson action, while all other quantities can be extracted with a standard one-level Monte Carlo e.g.

$$\mathcal{W}_N = \det\left[1 - R_{N+1}(1-\omega)\right] = \frac{\int [d\eta][d\eta^\dagger] e^{-\left|(1-R_{N+1})^{-1}\eta\right|^2}}{\int [d\eta][d\eta^\dagger] e^{-\eta^\dagger \eta}}\,. \tag{4.2.12}$$

To sum up, the gauge field dependence of the fermion determinant can be factorized by combining a domain decomposition with a multiboson representation of the (small) interaction among gauge fields on distant blocks. The resulting action is local in the block scalar and gauge fields and can be simulated by variants of the standard HMC algorithm. The remainder can be approximated up to a required precision, and it is included in the observable as the reweighting factor in Eq. (4.2.10).

4.2.3 Equivalence to the Schwarz alternating procedure

It can be shown that the above procedure in equivalent to the introduction of a properly defined Schwarz alternating procedure (SAP) [187–191]. The strategy was originally formulated to solve elliptic linear differential equations in an iterative way, but its application for our purposes is (as mostly common nowadays) as preconditioner for difference

operators (e.g. the discretized Laplace operator). It consists in employing the *multiplicative SAP* as a preconditioner for D, and starts by approximately solving the linear system $D\psi = \eta$ in two steps:

1. solve the equation in $\Omega_0^{\mathrm{e}} = \Lambda_0^{\mathrm{e}} \cup \Lambda_1$:

$$\psi_0 = D^{-1}_{\Lambda_0^{\mathrm{e}}}(\mathbb{1} - P_{\Lambda_0^{\mathrm{o}}})\eta\,, \quad \eta_0 = \eta - D\psi_0 = P_{\Lambda_0^{\mathrm{o}}}\eta - D_{\Lambda_0^{\mathrm{o}},\Lambda_1} D^{-1}_{\Lambda_0^{\mathrm{e}}}(\mathbb{1} - P_{\Lambda_0^{\mathrm{o}}})\eta\,; \tag{4.2.13}$$

2. solve the equation in $\Omega_0^{\mathrm{o}} = \Lambda_0^{\mathrm{o}} \cup \Lambda_1$:

$$\psi_1 = D^{-1}_{\Lambda_0^{\mathrm{o}}}(\mathbb{1} - P_{\Lambda_0^{\mathrm{e}}})\eta_0\,, \quad \eta_1 = \eta - D(\psi_0 + \psi_1) = -D_{\Lambda_0^{\mathrm{e}},\Lambda_1} D^{-1}_{\Lambda_0^{\mathrm{o}}}(\mathbb{1} - P_{\Lambda_0^{\mathrm{e}}})\eta_0\,. \tag{4.2.14}$$

The SAP converges if we iterate the above two steps, but here we only apply each of them once to construct the desired preconditioner from $\psi_0 + \psi_1 \equiv M_{\mathrm{sap}}\eta$, i.e.

$$M_{\mathrm{sap}} = D^{-1}_{\Lambda_0^{\mathrm{e}}}(\mathbb{1} - P_{\Lambda_0^{\mathrm{o}}}) + D^{-1}_{\Lambda_0^{\mathrm{o}}}(\mathbb{1} - P_{\Lambda_0^{\mathrm{e}}})P_{\Lambda_0^{\mathrm{o}}} - D^{-1}_{\Lambda_0^{\mathrm{o}}} D_{\Lambda_0^{\mathrm{o}},\Lambda_1} D^{-1}_{\Lambda_0^{\mathrm{e}}}(\mathbb{1} - P_{\Lambda_0^{\mathrm{o}}}) \tag{4.2.15}$$

which satisfies

$$\det(DM_{\mathrm{sap}}) = \det(1 - \omega)\,, \tag{4.2.16}$$

directly allowing us to recover Eq. (4.2.2) through $\det D = \det(DM_{\mathrm{sap}})/\det M_{\mathrm{sap}}$. This allows us to effectively interpret the matrix $\hat{W}$ in Eqs. (4.2.3) and (4.2.4) as a preconditioner, isolating all the terms suppressed at least as $O\left(e^{-m_\pi \Delta}\right)$. We note that the equivalence of the two approaches was discovered only after Ref. [84] was published, and it is therefore not mentioned there.

4.3 Variance analysis

We can now show the potential of the two-level Monte Carlo integration proposed in Refs. [83–86] for the one-dimensional factorization reviewed in the previous Section. We perform a separate variance analysis for both connected and disconnected contributions for data generated in Ref. [88], see also Ref. [99], extending these results on the isovector vector current in QCD also to other channels, proving the effectiveness of the proposed strategy where a StN problem is present.

4.3.1 Lattice setup

For the gluonic action, we consider the Wilson discretization in Eq. (2.2.5), while for quarks we opt for $O(a)$-improved Wilson-Dirac fermions with $c_{\mathrm{SW}} = 1.90952$, see Eqs. (2.4.5) and (2.4.6), with boundary conditions being periodic (anti-periodic) for the gluonic (fermionic) fields in time, and periodic in space for all fields. We consider QCD with $N_{\mathrm{f}} = 2 + 1$ sea quarks and a lattice of size 96×48^3, with lattice spacing $a = 0.065$ fm (i.e. $\beta = 6/g_0^2 = 5.3$) taken from Ref. [40]. The spatial size L of the lattice is so that $m_\pi L \geq 4$ with $m_\pi \simeq 270$ MeV. We study two-point functions involving the local

discretization of scalar (S) and pseudoscalar (P) densities, as well as of vector (V_k) and axial (A_k) currents[2]. If needed, the required finite renormalization constant can be included later on, e.g. the renormalization factor $Z^l_{\mathrm{V,sub}} = 0.74636(70)$ can be taken from Table 4 of Ref. [192]. In the following analysis, we only focus on the light-connected and disconnected Wick contractions, as they are the most problematic concerning the statistical error and the StN problem. In fact, for the light-connected one the StN at large time distances $|x_0|$ decays $\propto e^{-(M_\rho - m_\pi)|x_0|}$, while for the disconnected case the situation is even worse due to constant QCD vacuum contributions to its variance.

Details of multilevel analysis

The active regions are two disconnected thick time-slices in $x_0/a \in [0, 40) \cup [48, 88)$, while the inactive ones are in $x_0/a \in [40, 48) \cup [88, 96)$. Their thickness $\Delta \approx 0.5$ fm was found [88] to be large enough to suppress contributions in ω in Eq. (4.2.4), allowing to employ a relatively small number $N = 12$ of multiboson fields to approximate it. The generation of configurations involves $n_0 = 25$ level-0 global configurations separated by 48 molecular dynamics units (MDUs), so that in practice they can be considered statistically uncorrelated [40, 193]. For each one of them, $n_1 = 10$ configurations, spaced by 16 MDUs, were independently generated in the two disconnected active regions.

Estimators. The *light-connected* contraction is calculated by inverting the Wilson-Dirac operator on local sources defined on fixed time-slices y_0. The light-connected estimator $\bar{g}_c(x_0, y_0)$ is summed over the sink space-position and averaged over the space-position of the local sources. For the purposes of the variance analysis, we consider $N_s = 216$ local sources at $y_0/a = 32$. Instead, the difference $(l - s)$ of light and strange *disconnected* contractions[3] is determined via split-even random-noise estimators, see Ref. [99] and Appendix H. Single-propagator traces are estimated by averaging over a large number of Gaussian random sources, namely 768, tuned in Ref. [99] so that the random-noise contribution to the variance of the vector channel becomes negligible w.r.t. its gauge noise. The best estimator $\bar{g}_d(x_0, y_0)$ for the disconnected two-point function for fixed source and sink time-slices is ultimately obtained by combining such averages and by subtracting the vacuum contributions[4].

We can finally extract the best estimators by averaging the estimators $\bar{g}(x_0, y_0) = \bar{g}_c(x_0, y_0)$, $\bar{g}_d(x_0, y_0)$, computed at different source position y_0, over all available sources. For this purpose, for the connected case we introduce $N_s = 32$ additional sources for each

[2] Additional operators need to be considered to include $O(a)$-improvement.

[3] When computing the leading order HVP contribution to $(g-2)_\mu$, the disconnected diagrams enter only through this difference, which can be conveniently generated generated via a frequency-splitting strategy, see Ref. [99] and Appendix H. Here we focus on this term only, but for all the cases where the full computation of the light and strange disconnected contributions is required, the strange one can be separately computed, either directly or via and additional splitting.

[4] Doing so even when they are expected to vanish helps reduce fluctuations in variance estimators.

$y_0/a \in \{8, 16, 24, 56, 64, 72, 80\}$, while for the disconnected one $y_0/a \in [0, 95]$, as single-propagator traces are estimated at all time slices. We employ a weighted average, where any choice of the weights would lead to a correct estimate for the central value but we are interested in those leading to the smallest errors. Taking into account the fact that in multilevel algorithms the variance of the estimator is not translationally invariant nor symmetric in time for generic x_0 and y_0, we can exploit the correlator time-reflection symmetry to define the weighted average

$$\bar{g}(x_0) = \frac{1}{\mathcal{N}} \sum_{y_0} \left[\bar{g}_\mu(x_0 + y_0, y_0) + \bar{g}_\mu(T - x_0 - y_0, T - y_0) \right] , \tag{4.3.1}$$

$$\bar{g}_\mu(x_0, y_0) = \bar{g}(x_0, y_0)\mu(x_0, y_0) \ , \quad \mathcal{N} = \sum_{y_0} \left[\mu(x_0 + y_0, y_0) + \mu(T - x_0 - y_0, T - y_0) \right] \tag{4.3.2}$$

where we set the weights as $\mu(x_0, y_0) = \sigma_{\bar{g}}^{-2}(x_0, y_0)$. Our choice could be improved by using the full covariance matrix for different y_0.

Reweighting. In a two-level algorithm, statistical estimators for each level-0 configuration are computed from the reweighting procedure in Eq. (4.2.10) by averaging over the n_1^2 combinations of level-1 fields obtained by combining the n_1 configurations generated at level-1 in the two independent, disconnected, active regions. We can define

$$\langle \mathcal{O} \rangle = \frac{\langle \widetilde{\mathcal{O}}_\alpha \rangle_N}{\langle \widetilde{w}_\alpha \rangle_N} , \quad \widetilde{\mathcal{O}}_\alpha = \frac{1}{n_1^2} \sum_{i,j=1}^{n_1} w_\alpha^{ij} \mathcal{O}_\alpha^{ij} , \quad \widetilde{w}_\alpha = \frac{1}{n_1^2} \sum_{i,j=1}^{n_1} w_\alpha^{ij} , \quad \alpha = 1, \dots, n_0 \tag{4.3.3}$$

where $\mathcal{O}_\alpha^{ij}$ corresponds to the α-th level-0 measurement of the observable $\mathcal{O}$ on the configuration obtained by combining the i-th level-1 configuration in the first active region with the j-th in the second one, for $i, j = 1, \dots, n_1$. Instead, w_α^{ij} is a level-1 estimate of the reweighting factor in Eq. (4.2.10), whose contribution is separately estimated stochastically with 2 random sources, that are enough for its contribution to the statistical error to be negligible. With $\langle \cdot \rangle_N$ we indicate averages computed with N multibosons in the action, as in Eq. (4.2.10), and we set $\langle \widetilde{x}_\alpha \rangle_N \equiv \frac{1}{n_0} \sum_{\alpha=1}^{n_0} \widetilde{x}_\alpha$. In order to single out the variance reduction only due to the two-level averaging, we compute the ratios of connected variances at different values of n_1 with the corresponding ones from CLS configurations[5], which were generated with a conventional one-level HMC with $N_s = 216$ random sources located at $y_0/a = 32$ as well. For the disconnected ones, we instead normalize variances w.r.t. that at $n_1 = 1$. To study cases with $n_1 < 10$, we construct several replicas using the same data as for $n_1 = 10$, both for the correlator and the reweighting factor. The first replica combines the first n_1 configurations from two independent regions, with additional replicas formed analogously where possible. For example, for $n_1 = 3$, we generate three replicas by pairing the first, second, and third triplets of configurations from each region. Since any residual covariance between the configurations at level-1 reduces the maximal two-level gain $1/n_1^2$, in order to reduce

[5] `https://wiki-zeuthen.desy.de/CLS/CLS`

auto-correlations, for $n_1 = 3$ we also explore an alternative combination, labeled as $n_1 = 3^*$. In this case, we combine configurations differently, e.g. forming the first triplet from the first, fourth and seventh configurations from both regions, and similarly for the remaining triplets. These replicas provide independent estimates of variances and correlators, which are averaged only after completing the reweighting. While the central value of the variance remains unchanged, its error is smaller i.e. oscillations are reduced, a difference being clearly visible when comparing $n_1 = 1$ to CLS data.

The translational average in Eq. (4.3.1) and the reweighting in Eq. (4.3.3) are independent from each other and lead (up to multiplicative renormalization and charge factors to be included at a later stage if needed) to the best estimator

$$g(x_0) = \frac{\langle \widetilde{g}(x_0) \rangle_N}{\langle \widetilde{w} \rangle_N} \,. \tag{4.3.4}$$

4.3.2 Results of the analysis

In Fig. 4.2 we show the ratio of variances of the *light-connected* vector (vv), axial (aa) scalar (ss) and pseudoscalar (pp) correlators for $n_1 = 1, 2, 3, 3^*, 6, 10$ w.r.t. standard one level HMC (CLS data), as a function of the source-sink temporal separation. Horizontal dashed lines represent the maximum variance reduction for two-level algorithms in the absence of correlations between level-1 configurations, i.e. $1/n_1^2$.
In order to correctly read the plots, first recall that the width of the inactive region is 8 in units of the lattice spacing, and that multilevel algorithms break an otherwise exact periodicity in the temporal direction also for the variance estimators. For the connected pseudoscalar and scalar densities, we note the absence of any variance reduction pattern with respect to standard algorithms, indicating that they do not benefit from multilevel. Instead, a substantial gain from the two-level integration scheme can be observed for the vector and axial currents, especially in the central region of the plots. This reproduces the known result for the vector current [88], while constitutes a theoretically expected but numerically novel result for the axial one. The reason for this behavior is that, as long as we consider short-distance correlators, i.e. focusing on the left part of the plots, we are only combining configurations within the same active or inactive region, or at most from neighboring active and inactive regions. Therefore, the exponential gain is not expected, nor it is found, within this region. Instead, considering correlators which are spaced at least by the time extent of the inactive region, and moving to larger distances i.e. in the region where the StN problem is more strongly felt, we eventually start combining configurations from two different active regions. The ideal exponential gain in statistics proportional to n_1^2 would be saturated only if correlation between level-1 configurations was absent, which is practically never the case. Furthermore, since the StN problem is more important for the axial connected correlator than it is for the vector one, and since the tuning of n_1 was performed in Ref. [88] specifically for the latter, increasing n_1 is expected to further improve the quality of axial data.

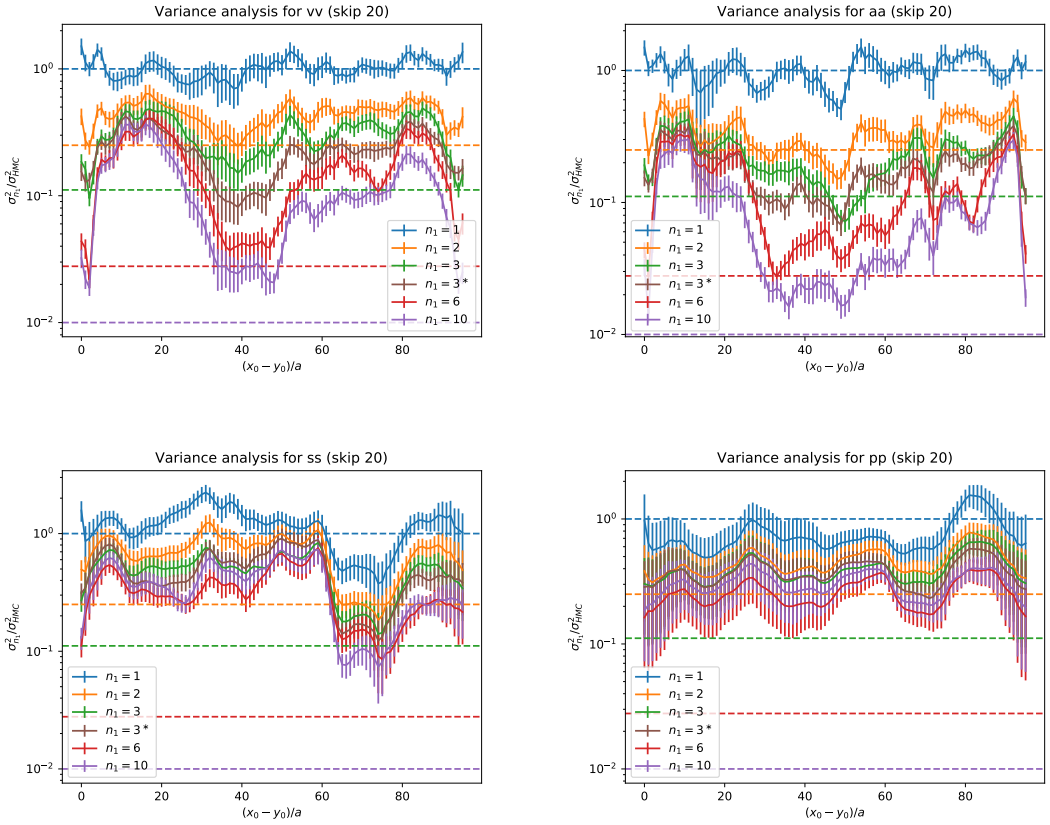

Figure 4.2: Variance analysis for the isovector *light-connected* vector (vv), axial (aa), scalar (ss) and pseudoscalar (pp) correlators. In the vertical axis we show the ratio of variances between multilevel with different values of n_1 (number of level-1 updates) and standard HMC algorithms (CLS data), with the relative source-sink separation on the horizontal line. Horizontal dashed lines represent the maximum variance reduction which can be obtained by two-level integration in the absence of correlations between level-1 configurations, namely $1/n_1^2$. We skipped the 20-th configuration since it was found to be exceptional.

Our variance analysis for the subtracted, *disconnected* contributions is instead displayed in Fig. 4.3, where we normalize the variance ratios w.r.t. the standard $n_1 = 1$ case. The variances are relative to the estimators before performing the weighted temporal average, at a fixed value of the source temporal position $y_0/a = 32$, in order to better disentangle the effects of multilevel from those stemming from the temporal average. From these plots, we can clearly appreciate once again the benefits of the multilevel algorithm for the axial and vector correlators: in the two active regions, $x_0/a \in [0, 40) \cup [48, 88)$, the expected multilevel scaling is manifest through a rapid drop in the variance just outside the frozen domains. As already noted for the connected case, increasing n_1 might lead to further improvements in the axial channel, while multilevel does not seem to

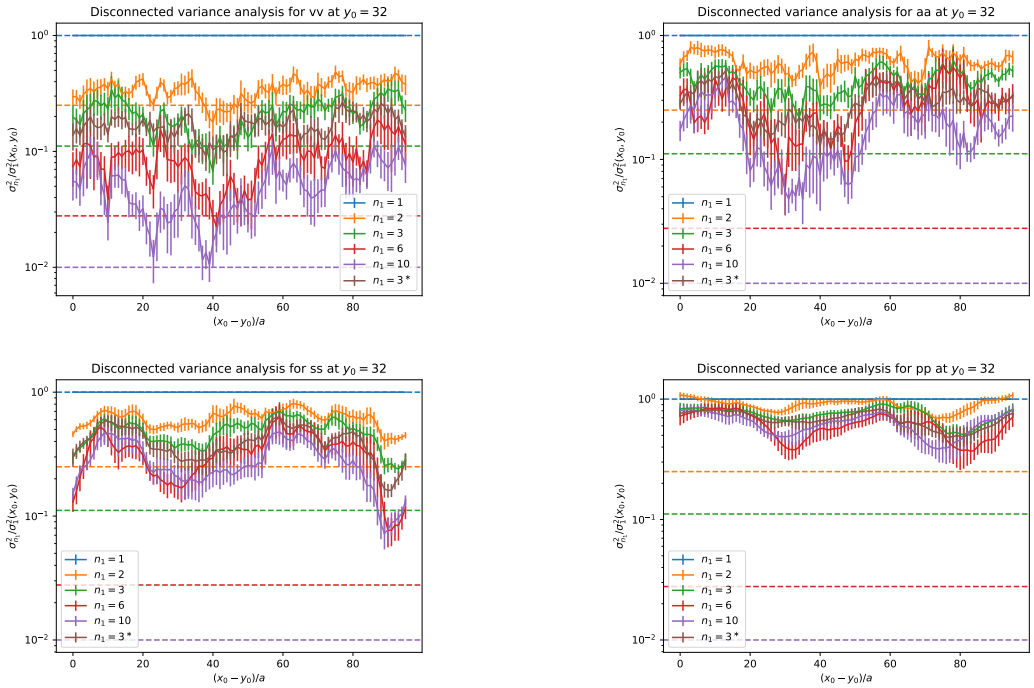

Figure 4.3: Variance analysis for the disconnected vector, axial, scalar and pseudoscalar $(l-s)$ contributions *before* taking the translational average with $y_0/a = 32$, using all 768 Gaussian random sources. The inactive regions are in $x_0/a \in [40, 48) \cup [88, 96)$.

provide significant gains for the scalar and pseudoscalar correlators. Overall, the effect of the multilevel algorithm is to effectively decrease the variance of the estimators when the source and the sink are located in two different active regions, at large source-sink time separation, if and where a StN problem is present, similarly to what has been observed for the connected case. We also note that multilevel might not be optimal for observables as $(l-s)$, mostly affected by the low modes which are sensitive to the gauge-field configuration over the whole lattice. Its scaling is instead expected to improve in the computation of the higher modes, e.g. the remaining strange contribution, and even more for the hopping term [99], although the absolute value of the corresponding contributions to the propagator might be small.

4.4 Four-dimensional factorization

In this Section we present the first original contribution of this Thesis, published in Refs. [1, 4]. Here, we closely follow the presentation in those references to extend the factorization of the fermion determinant to the case of a four-dimensional domain decomposition. Before starting with the discussion, we recall a few relevant aspects of lattice gauge theories which will be relevant in the following discussion. Even though

it is possible to define different expressions for the lattice Dirac operator D, here we are only interested in local ones. As desribed in Subsection 2.5.1, this manifest locality is spoiled once we analytically integrate out the Grassman variables representing the fermionic degrees of freedom, resulting in a global contribution $S_{\mathrm{F}}^{\mathrm{eff}}[U]$ to the effective gluonic action in Eq. (2.5.1)

$$S_{\mathrm{G}}^{\mathrm{eff}}[U] = S_{\mathrm{G}}[U] + S_{\mathrm{F}}^{\mathrm{eff}}[U]\,, \quad S_{\mathrm{F}}^{\mathrm{eff}}[U] = -\ln\det D[U]\,, \tag{4.4.1}$$

thus limiting our ability of directly simulating fermions on the lattice, where S_{G} is the local, purely gluonic action, see Eq. (2.2.5). In principle, we would expect the notion of locality not to be completely lost, but rather masked out by the complicated functional $\ln\det D[U]$. Intuitively, we would reasonably assume that it is possible to approximate it as the sum of local contributions also for a domain decomposition in more than one dimension, with an extra term which is anticipated to be tiny since the effective link interaction decreases with their distance. Here we show how our intuition can be formalized. We introduce a meticolously chosen overlapping four-dimensional domain decomposition of the lattice which allows to derive a block-decomposition of the fermion determinant. We also show that this result is a (not-so-straightforward) generalization of the one-dimensional factorization, presented in Section 4.2 and proposed a few years ago [83, 84], see also [190, 194], and that has already been extensively tested numerically [83–88]. Similarly to the one-dimensional case, the remaining global contribution is studied by means of a multiboson representation, with the resulting multiboson action also factorized. The small residual global term can be regarded as a reweighting factor to be included in the observable, but in principle we could also drop it out and correct this approximation via an accept-reject step.

4.4.1 Four-dimensional domain decomposition of the lattice

We consider a four-dimensional hyperrectangular lattice of spacing a and lengths L_μ in the directions labeled by $\mu = 0, \ldots, 3$. We employ some of the notation adopted for the one-dimensional case in Section 4.2 and proceed with the following steps.

1. We start by dividing the lattice in a domain Λ_0 made of hyperrectangular blocks embedded in a thick frame Λ_1. In the two-dimensional representation shown in Fig. 4.4, the blocks are represented by red squares, while the grey region is the frame. By construction Λ_0 is a disconnected domain which can be decomposed as $\Lambda_0 = \bigcup_{\hat{a}} \Lambda_0^{\hat{a}}$, where the label $\hat{a}$ identifies the single hyperrectangle, see Appendix G for its definition. The domain Λ_1 spans the entire lattice and it is connected[6], differently from the one-dimensional decomposition. Typically the linear extension B_μ of the blocks in each direction μ can be of a few fermi, while the thicknesses of the frame b_μ are typically of 0.5 fm or so.

[6]It is possible to introduce an even-odd decomposition of the domain Λ_0, so that the union of the even and the odd blocks plays the same rôle as the domains Λ_0^{e} and Λ_0^{o} in the one-dimensional decomposition in Section 4.2, while the frame Λ_1 corresponds to the homologous one.

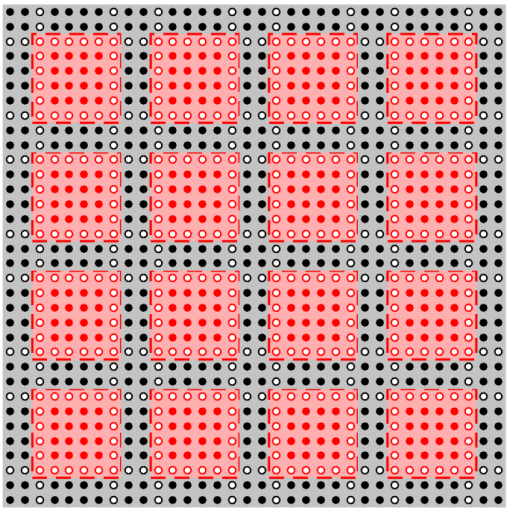

Figure 4.4: Two-dimensional representation of the basic domain decomposition of the lattice in the disconnected domain Λ_0 (red square blocks) and the globally connected one Λ_1 (grey thick frame). The empty circles indicate the domain of hyperplanes $\partial\Pi$, see main text, with the red and black circles indicating $\partial\Lambda_0$ and $\partial\Pi_1$ respectively.

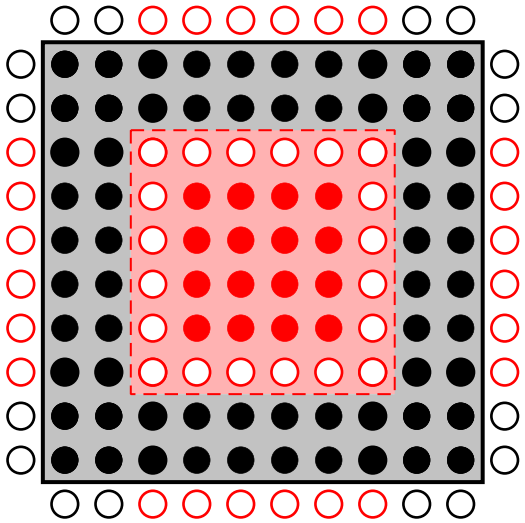

Figure 4.5: A "framed domain" $\Omega_0^{\hat{a}}$ made by the union of a hyperrectangle $\Lambda_0^{\hat{a}}$ (red) and its frame $\Phi_1^{\hat{a}}$ (grey). The points of its exterior boundary $\partial\Omega_0^{\hat{a}*}$ are indicated with open circles outside the continuous black line. The red circles represents sites belonging to $\partial\Lambda_0$, while black circles are used for sites in $\partial\Pi_1$ and in particular in $\partial\bar{\Omega}_0^{\hat{a}*}$.

2. Following Refs. [84,194], for each block $\Lambda_0^{\hat{a}}$ we introduce $\partial\Lambda_0^{\hat{a}}$ as the inner boundary of the block (open red circles in Fig. 4.4), defined as the set of points in $\Lambda_0^{\hat{a}}$ at a distance a from the closest points of the lattice outside the block, the latter being the exterior boundary $\partial\Lambda_0^{\hat{a}*}$. The sub-block $\bar{\Lambda}_0^{\hat{a}} = \Lambda_0^{\hat{a}} \backslash \partial\Lambda_0^{\hat{a}}$ is therefore the set of the inner points of $\Lambda_0^{\hat{a}}$ (closed red circles in the same Figure). Analogously to Λ_0, it is also useful to define $\partial\Lambda_0 = \bigcup_{\hat{a}} \partial\Lambda_0^{\hat{a}}$ and $\bar{\Lambda}_0 = \bigcup_{\hat{a}} \bar{\Lambda}_0^{\hat{a}}$. The various boundary faces that form $\partial\Lambda_0$ belong to hyperplanes with normal directions parallel to the axes of the lattice (open circles in Fig. 4.4) which are spaced alternatively by B_μ and b_μ along each direction μ. Their ensemble defines the domain $\partial\Pi$, which can be decomposed as $\partial\Pi = \partial\Lambda_0 \cup \partial\Pi_1$, where $\partial\Pi_1$ is represented by black open circles in Fig. 4.4. Note that $\partial\Pi_1 \in \Lambda_1$ and that $\bar{\Lambda}_1 = \Lambda_1 \backslash \partial\Pi_1$ is a disconnected domain.

3. Each block $\Lambda_0^{\hat{a}}$ has an associated "frame" $\Phi_1^{\hat{a}}$ defined as the grey region around it, see Fig. 4.5 for a graphic representation and Appendix G for its precise definition. The set of blocks $\Phi_1^{\hat{a}}$ clearly forms an overlapping domain decomposition of Λ_1. The "framed" counterpart of $\Lambda_0^{\hat{a}}$ is given by $\Omega_0^{\hat{a}} = \Lambda_0^{\hat{a}} \cup \Phi_1^{\hat{a}}$, with obvious modifications for the blocks near the boundaries of the lattice, depending on the boundary conditions adopted. The blocks $\Omega_0^{\hat{a}}$ form an overlapping domain decomposition of the entire

lattice L, see Fig. 4.4, similarly to what happens in the one-dimensional case. Finally, we define $\partial\Omega_0^{\hat{a}*}$ as the exterior boundary of $\Omega_0^{\hat{a}}$, see Fig. 4.5 for a graphic representation and Appendix G for its definition, and $\partial\bar{\Omega}_0^{\hat{a}*} = \partial\Omega_0^{\hat{a}*} \cap \partial\Pi_1$ as its subdomain belonging to $\partial\Pi_1$ (black open circles in Fig. 4.5).

We conclude with a few, trivial but relevant observations. First of all, we note that the two domains Λ_0 and Λ_1 only interact through the internal boundaries $\partial\Lambda_0^{\hat{a}}$ of each local cell. Additionally, the disconnected domain $\partial\Lambda_0$ is formed by the disjoint union of local boundaries $\partial\Lambda_0^{\hat{a}}$, which lie on orthogonal hyperplanes, the union of which forms the global, connected domain $\partial\Pi$. Different internal boundaries are then connected through the global, disconnected domain $\partial\Pi_1 = \partial\Pi\backslash\partial\Lambda_0$.
In the next Subsections we will need the projection operators to the subspace of quark fields supported on the various sub-lattices, see Appendix D for their definitions. We will indicate them with the symbol $\mathbb{P}$ associated to a subscript indicating the sub-lattice considered, e.g. $\mathbb{P}_{\Lambda_0^{\hat{a}}}$ for the block $\Lambda_0^{\hat{a}}$.

4.4.2 Block decomposition of the fermion determinant

In this Subsection, we want to discuss the block-factorization of $\det D$ resulting from the domain decomposition defined in the previous Subsection. We can consider D to be the Wilson–Dirac operator [15, 77, 78], see Subsections 2.3.2 and 2.4.1, but in principle we only require it to be local.
The idea is to apply two consecutive Schur decompositions for the domain decomposition described above. At first, we decompose the entire lattice as

$$L = \partial\Lambda_0 \cup \left(\bar{\Lambda}_0 \cup \Lambda_1\right) \tag{4.4.2}$$

and, accordingly, we rewrite D as a 2×2 block matrix. Using Eq. (E.1.4) we have

$$\det D = \det D_{\bar{\Lambda}_0} \det D_{\Lambda_1} \det \tilde{D}_{\partial\Lambda_0} \,, \tag{4.4.3}$$

where[7]

$$\tilde{D}_{\partial\Lambda_0} = \bar{D}_{\partial\Lambda_0} - D_{\partial\Lambda_0,\Lambda_1} D_{\Lambda_1}^{-1} D_{\Lambda_1,\partial\Lambda_0} \tag{4.4.4}$$

and

$$\bar{D}_{\partial\Lambda_0} = D_{\partial\Lambda_0} - D_{\partial\Lambda_0,\bar{\Lambda}_0} D_{\bar{\Lambda}_0}^{-1} D_{\bar{\Lambda}_0,\partial\Lambda_0} = \sum_{\hat{a}} \bar{D}_{\partial\Lambda_0^{\hat{a}}} \,. \tag{4.4.5}$$

By noticing that

$$D_{\partial\Lambda_0,\Lambda_1} = \sum_{\hat{a}} D_{\partial\Lambda_0^{\hat{a}},\Phi_1^{\hat{a}}} \,, \qquad D_{\Lambda_1,\partial\Lambda_0} = \sum_{\hat{a}} D_{\Phi_1^{\hat{a}},\partial\Lambda_0^{\hat{a}}} \,, \tag{4.4.6}$$

[7] Note that $\tilde{D}_{\partial\Lambda_0}$ corresponds to the effective Wilson–Dirac operator, once the Grassmann field variables in $\bar{\Lambda}_0$ and Λ_1 have been integrated out in the path integral. Analogous considerations apply to other Schur complements throughout this Section, see the discussion in Appendix F for further details.

it is clear that

$$D_{\partial\Lambda_0,\Lambda_1} D_{\Lambda_1}^{-1} D_{\Lambda_1,\partial\Lambda_0} = \sum_{\hat{a},\hat{a}'} D_{\partial\Lambda_0^{\hat{a}},\Phi_1^{\hat{a}}} D_{\Lambda_1}^{-1} D_{\Phi_1^{\hat{a}'},\partial\Lambda_0^{\hat{a}'}} \,. \tag{4.4.7}$$

Then, in order to isolate all the local contributions from links in the same (framed) domain $\Omega_0^{\hat{a}}$, we can apply a second decomposition as $\Lambda_1 = \Phi_1^{\hat{a}} \cup (\Lambda_1 \backslash \Phi_1^{\hat{a}})$. The corresponding Schur decomposition of D_{Λ_1}, written in the 2×2 blocked form, allows us to rewrite its inverse as in Eq. (E.1.3). This in turn implies that

$$\mathbb{P}_{\Phi_1^{\hat{a}}} D_{\Lambda_1}^{-1} = D_{\Phi_1^{\hat{a}}}^{-1} - D_{\Phi_1^{\hat{a}}}^{-1} D_{\Phi_1^{\hat{a}},\partial\bar{\Omega}_0^{\hat{a}*}} D_{\Lambda_1}^{-1} \,, \tag{4.4.8}$$

$$D_{\Lambda_1}^{-1} \mathbb{P}_{\Phi_1^{\hat{a}}} = D_{\Phi_1^{\hat{a}}}^{-1} - D_{\Lambda_1}^{-1} D_{\partial\bar{\Omega}_0^{\hat{a}*},\Phi_1^{\hat{a}}} D_{\Phi_1^{\hat{a}}}^{-1} \,. \tag{4.4.9}$$

By inserting Eqs. (4.4.8) and (4.4.9) in Eq. (4.4.7), we obtain

$$\tilde{D}_{\partial\Lambda_0} = \hat{D}_{\partial\Lambda_0} - \hat{D}_{\partial\Lambda_0,\partial\Pi_1} D_{\Lambda_1}^{-1} \hat{D}_{\partial\Pi_1,\partial\Lambda_0} \tag{4.4.10}$$

where

$$\hat{D}_{\partial\Lambda_0,\partial\Pi_1} = -\sum_{\hat{a}} D_{\partial\Lambda_0^{\hat{a}},\Phi_1^{\hat{a}}} D_{\Phi_1^{\hat{a}}}^{-1} D_{\Phi_1^{\hat{a}},\partial\bar{\Omega}_0^{\hat{a}*}} \,, \tag{4.4.11}$$

$$\hat{D}_{\partial\Pi_1,\partial\Lambda_0} = -\sum_{\hat{a}} D_{\partial\bar{\Omega}_0^{\hat{a}*},\Phi_1^{\hat{a}}} D_{\Phi_1^{\hat{a}}}^{-1} D_{\Phi_1^{\hat{a}},\partial\Lambda_0^{\hat{a}}} \,, \tag{4.4.12}$$

and

$$\hat{D}_{\partial\Lambda_0} = \hat{D}^{\mathrm{d}}_{\partial\Lambda_0} + \hat{D}^{\mathrm{h}}_{\partial\Lambda_0} \tag{4.4.13}$$

with

$$\hat{D}^{\mathrm{d}}_{\partial\Lambda_0} = \sum_{\hat{a}} \hat{D}_{\partial\Lambda_0^{\hat{a}}} \,, \qquad \hat{D}^{\mathrm{h}}_{\partial\Lambda_0} = \sum_{\hat{a}\neq\hat{a}'} \hat{D}_{\partial\Lambda_0^{\hat{a}},\partial\Lambda_0^{\hat{a}'}} \,, \tag{4.4.14}$$

and

$$\hat{D}_{\partial\Lambda_0^{\hat{a}}} = \bar{D}_{\partial\Lambda_0^{\hat{a}}} - D_{\partial\Lambda_0^{\hat{a}},\Phi_1^{\hat{a}}} D_{\Phi_1^{\hat{a}}}^{-1} D_{\Phi_1^{\hat{a}},\partial\Lambda_0^{\hat{a}}} \,, \tag{4.4.15}$$

$$\begin{aligned} \hat{D}_{\partial\Lambda_0^{\hat{a}},\partial\Lambda_0^{\hat{a}'}} = -\frac{1}{2} D_{\partial\Lambda_0^{\hat{a}},\Phi_1^{\hat{a}}} \Big[& D_{\Phi_1^{\hat{a}}}^{-1} - D_{\Phi_1^{\hat{a}}}^{-1} D_{\Phi_1^{\hat{a}},\partial\bar{\Omega}_0^{\hat{a}*}} D_{\Phi_1^{\hat{a}'}}^{-1} + \\ & D_{\Phi_1^{\hat{a}'}}^{-1} - D_{\Phi_1^{\hat{a}}}^{-1} D_{\partial\bar{\Omega}_0^{\hat{a}'*},\Phi_1^{\hat{a}'}} D_{\Phi_1^{\hat{a}'}}^{-1} \Big] D_{\Phi_1^{\hat{a}'},\partial\Lambda_0^{\hat{a}'}} \,. \end{aligned} \tag{4.4.16}$$

Before proceeding further, it is already interesting to notice that $\hat{D}_{\partial\Lambda_0^{\hat{a}}}$ is the Schur complement of $D_{\Omega_0^{\hat{a}}}$ w.r.t. the decomposition $\Omega_0^{\hat{a}} = \partial\Lambda_0^{\hat{a}} \cup [\bar{\Lambda}_0^{\hat{a}} \cup \Phi_1^{\hat{a}}]$, and that the hopping terms among the blocks $D_{\partial\Lambda_0^{\hat{a}},\partial\Lambda_0^{\hat{a}'}}$ are suppressed with the thicknesses of the frame. To manipulate the last sum on the r.h.s. of Eq. (4.4.10), we can define the Schur complement

$$\hat{D}_{\partial\Pi_1} = D_{\partial\Pi_1} - D_{\partial\Pi_1,\bar{\Lambda}_1} D_{\bar{\Lambda}_1}^{-1} D_{\bar{\Lambda}_1,\partial\Pi_1} \,. \tag{4.4.17}$$

Since $\partial\bar{\Omega}_0^{\hat{a}*} \in \partial\Pi_1$, in Eq. (4.4.10) we can replace $D_{\Lambda_1}^{-1}$ with its projection on $\partial\Pi_1$, which in turn is equal to $\hat{D}_{\partial\Pi_1}^{-1}$. Therefore, if we define the block matrix

$$\hat{W} = \begin{pmatrix} \hat{D}_{\partial\Lambda_0} & \hat{D}_{\partial\Lambda_0,\partial\Pi_1} \\ \hat{D}_{\partial\Pi_1,\partial\Lambda_0} & \hat{D}_{\partial\Pi_1} \end{pmatrix}, \tag{4.4.18}$$

it is immediate to see that

$$\det \hat{W} = \det \hat{D}_{\partial\Pi_1} \det \tilde{D}_{\partial\Lambda_0} . \tag{4.4.19}$$

By remembering that

$$\det D_{\Lambda_1} = \det D_{\bar{\Lambda}_1} \det \hat{D}_{\partial\Pi_1} , \tag{4.4.20}$$

we can rewrite Eq. (4.4.3) as

$$\det D = \det D_{\bar{\Lambda}_0} \det D_{\bar{\Lambda}_1} \det \hat{W} . \tag{4.4.21}$$

4.4.3 Preconditioning of $\hat{W}$

In order to accomplish our initial aim of factorizing $\det D$, we still need to factorize $\det \hat{W}$. By taking inspiration from the one-dimensional example, we would like to precondition $\hat{W}$ so as to remain with a matrix which deviates from the identity by off-diagonal blocks which are suppressed with the thicknesses of the frame. To this aim we first notice that each block of the diagonal part $\hat{D}^{\mathrm{d}}_{\partial\Lambda_0}$ in Eq. (4.4.14) depends on the gauge field in each (framed) block, while the elements of the off-diagonal component $\hat{D}^{\mathrm{h}}_{\partial\Lambda_0}$ are suppressed with the thicknesses of the frame and depend on the gauge field in Λ_1 only. Differently from the one-dimensional case, here $\hat{D}_{\partial\Lambda_0}$ is not the only operator that appears in $\hat{W}$. We have to consider additional block matrices, e.g. $\hat{D}_{\partial\Pi_1}$, because the domain Λ_1 is not disconnected i.e. factorized. We emphasize that the operator $\hat{D}_{\partial\Pi_1}$ may also be decomposed in blocks similarly to $\hat{D}_{\partial\Lambda_0}$, but it is not useful for the factorization strategy discussed here, having in mind a multilevel application where we would keep the gauge configuration in Λ_1 frozen during level-1 updates.

The structure of $\hat{D}_{\partial\Lambda_0}$ suggests the definition of a preconditioned operator $\overline{W}_1$ as

$$\hat{W} = \begin{pmatrix} \hat{D}^{\mathrm{d}}_{\partial\Lambda_0} & 0 \\ 0 & \hat{D}_{\partial\Pi_1} \end{pmatrix} \cdot \overline{W}_1 , \quad \overline{W}_z = \left(\begin{array}{c|c} z\mathbb{P}_{\partial\Lambda_0} + [\hat{D}^{\mathrm{d}}_{\partial\Lambda_0}]^{-1} \hat{D}^{\mathrm{h}}_{\partial\Lambda_0} & \overline{W}_{\partial\Lambda_0,\partial\Pi_1} \\ \hline \overline{W}_{\partial\Pi_1,\partial\Lambda_0} & z\mathbb{P}_{\partial\Pi_1} \end{array} \right), \tag{4.4.22}$$

for $z \in \mathbb{C}$, and

$$\overline{W}_{\partial\Lambda_0,\partial\Pi_1} = \sum_{\hat{a}} \mathbb{P}_{\partial\Lambda_0^{\hat{a}}} D^{-1}_{\Omega_0^{\hat{a}}} D_{\Phi_1^{\hat{a}},\partial\bar{\Omega}_0^{\hat{a}*}} , \quad \overline{W}_{\partial\Pi_1,\partial\Lambda_0} = \hat{D}^{-1}_{\partial\Pi_1} \hat{D}_{\partial\Pi_1,\partial\Lambda_0} . \tag{4.4.23}$$

Notice that the off-diagonal blocks of $\overline{W}_z$ act on a subspace of $\partial\Pi$ identified by the projector $P_{\partial\Pi} = P_{\partial\Lambda_0} + P_{\partial\Pi_1}$ defined in Appendix D. Differently from $\mathbb{P}_{\partial\Lambda_0}$ and $\mathbb{P}_{\partial\Pi_1}$,

the projectors $P_{\partial\Lambda_0}$ and $P_{\partial\Pi_1}$ include the appropriate projectors on the spinor index for the inner and outer boundaries of $\Lambda_0^{\hat{a}}$ and $\Omega_0^{\hat{a}}$ respectively. From Eq. (E.1.5), it follows

$$\det \overline{W}_1 = \det W_1 \,, \qquad \text{where} \qquad W_z = P_{\partial\Pi}\, \overline{W}_z\, P_{\partial\Pi} \,, \tag{4.4.24}$$

with the dimensionality of the matrix W_z being smaller by essentially a factor 2 w.r.t. that of $\overline{W}_z$. By combining Eqs. (4.4.21), (4.4.22) and (4.4.24) we finally obtain

$$\det D = \frac{1}{\det D_{\Lambda_1}^{-1} \prod_{\hat{a}} \left[\det D_{\Phi_1^{\hat{a}}} \det D_{\Omega_0^{\hat{a}}}^{-1} \right]} \det W_1 \tag{4.4.25}$$

that leads directly to

$$S_{\mathrm{F}}^{\mathrm{eff}}[U] = -\sum_{\hat{a}} \ln\det D_{\Omega_0^{\hat{a}}} + \sum_{\hat{a}} \ln\det D_{\Phi_1^{\hat{a}}} - \ln\det D_{\Lambda_1} - \ln\det W_1 \,. \tag{4.4.26}$$

The dependence of $\det D$ on the gauge-field configuration in the active region Λ_0 is fully factorized if we only focus on the denominator of Eq. (4.4.25), since each factor can be independently computed. Though, a small but (still) not negligible global contribution comes from the numerator of the last expression in Eq. (4.4.21), written in terms of a matrix W_1 that acts on the fermion fields on the domain of the hyperplanes $\partial\Pi$ only. The off-diagonal blocks of W_1 are suppressed with the thicknesses of the frame of the blocks and depend on the gauge field in Λ_1 only.

Recovery of the one-dimensional result

Before addressing the factorization of the remaining term $\det W_1$, we would like to make more sense of this result by showing how it is a (not-so-trivial) generalization of the one-dimensional case that was first discussed in Ref. [84]. We can apply a one-dimensional domain decomposition, as shown in Fig. 4.6, and adopt the same exact strategy that we described in Subsection 4.4.1.

1. First, we identify the local domains $\Lambda_0^{\hat{a}}$ as thick time-slices and their union as the disconnected active region $\Lambda_0 = \bigcup_{\hat{a}} \Lambda_0^{\hat{a}}$. The rest of the lattice forms the inactive domain Λ_1, which is now a disconnected union of thick time-slices.

2. We define the internal boundaries of each block and their union respectively as $\partial\Lambda_0^{\hat{a}}$ and $\partial\Lambda_0$. Trying to connect the internal boundaries of different slices, we notice that we do not need to include any additional lattice site, i.e. in this case $\partial\Pi_1 = \partial\Lambda_0$ and the domain $\partial\Pi_1$ is actually empty. Thus, the only block of W_z that is now present is the upper-left one, connecting different local slices $\Lambda_0^{\hat{a}}$.

3. We can finally define the frame $\Phi_1^{\hat{a}}$ for each local slice and the respective local (framed) slice $\Omega_0^{\hat{a}} = \Lambda_0^{\hat{a}} \cup \Phi_1^{\hat{a}}$. We notice that the union of all the frames takes exactly twice into account each thick time-slice of the domain Λ_1.

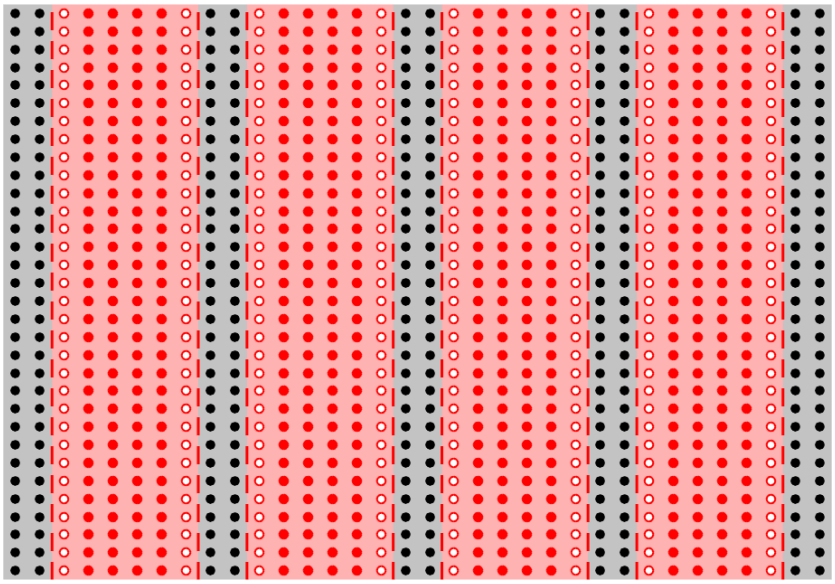

Figure 4.6: One-dimensional domain decomposition of the lattice in thick time-slices in the disconnected domains Λ_0 (red slices) and Λ_1 (grey slices). The empty circles indicate the domain of hyperplanes $\partial\Pi$, that in this case coincides with the internal boundary $\partial\Lambda_0$ of Λ_0.

We can now apply an even-odd decomposition of $\Lambda_0^{\hat{a}}$, i.e. considering $\hat{a} \in \{\mathrm{e}, \mathrm{o}\}$. Since $\det D_{\Phi_1^{\mathrm{e}}} = \det D_{\Phi_1^{\mathrm{o}}} = \det D_{\Lambda_1}$, from Eq. (4.4.25) we recover the one-dimensional result in Eq. (4.2.3). We want to point out that the four-dimensional generalization of this result is not straightforward due to the presence of two additional complications, namely Λ_1 being a connected domain, and the presence of the domain $\partial\Pi_1$ and of the off-diagonal terms of $\hat{W}$.

4.4.4 Multiboson factorization of $\det W_1$

We now focus on factorizing the remaining global term $\det W_1$. For large enough thicknesses of the frame Λ_1, we expect W_1 to have a large spectral gap, a fact which makes it effective to express its determinant through a polynomial approximation of W_1^{-1}. As reviewed in Section 4.2, see Eq. (4.2.7), we can introduce a proper polynomial P_N of even order N to approximate the inverse determinant as

$$\det \overline{W}_1 = \frac{\det\left[1 - R_{N+1}(\overline{W}_1)\right]}{\det P_N(\overline{W}_1)} = C \prod_{k=1}^{N/2} \det{}^{-1}\left[\overline{W}_{u_k}^{\dagger}\, \overline{W}_{u_k}\right], \tag{4.4.27}$$

where C is an irrelevant numerical constant, $\overline{W}_z$ is defined in Eq. (4.4.22) and u_k are defined in Eq. (4.2.6). It follows that

$$\frac{\det D}{\det[1 - R_{N+1}(W_1)]} \propto \frac{\det D_{\Lambda_1}}{\prod_{\hat{a}}\left[\det D_{\Phi_1^{\hat{a}}} \det D_{\Omega_0^{\hat{a}}}^{-1}\right] \prod_{k=1}^{N/2} \det\left[W_{u_k}^{\dagger}\, W_{u_k}\right]}, \tag{4.4.28}$$

where we have replaced $\overline{W}_{u_k}$ with W_{u_k} by using again the first relation in Eq. (4.4.24) which, for $z \neq 1$, is valid up to an irrelevant multiplicative constant. The first product in the denominator on the r.h.s. is local and can thus be included in the effective gluonic action via standard pseudofermions, see Subsection 2.5.1, defined in individual blocks.

Multiboson action

Each of the $N/2$ factors in the last product in the denominator of the r.h.s. of Eq. (4.4.28) can be represented up to an irrelevant multiplicative constant, as

$$\frac{1}{\det\left[W_{u_k}^\dagger\, W_{u_k}\right]} \propto \int d\chi_k d\chi_k^\dagger\, e^{-|W_{u_k}\chi_k|^2}\,. \tag{4.4.29}$$

The $N/2$ multiboson fields χ_k live on the projection of $\partial\Pi$ defined by $P_{\partial\Pi}$ and we can decompose them as $\chi = \chi_{\partial\Lambda_0} + \chi_{\partial\Pi_1}$, with $\chi_{\partial\Lambda_0} = P_{\partial\Lambda_0}\chi$ and $\chi_{\partial\Pi_1} = P_{\partial\Pi_1}\chi$, resulting in

$$\begin{aligned} |W_z\chi|^2 = \sum_{\hat{a}} \Big| P_{\partial\Lambda_0^{\hat{a}}} \Big[z\,\chi_{\partial\Lambda_0} + [\hat{D}^{\rm d}_{\partial\Lambda_0^{\hat{a}}}]^{-1} \hat{D}^{\rm h}_{\partial\Lambda_0}\chi_{\partial\Lambda_0} + D^{-1}_{\Omega_0^{\hat{a}}}\, D_{\Phi_1^{\hat{a}},\partial\bar{\Omega}_0^{\hat{a}*}}\chi_{\partial\Pi_1} \Big] \Big|^2 \\ + \Big| z\,\chi_{\partial\Pi_1} + W_{\partial\Pi_1,\partial\Lambda_0}\chi_{\partial\Lambda_0} \Big|^2\,. \end{aligned} \tag{4.4.30}$$

The term on the second line of the r.h.s of Eq. (4.4.30) depends on the gauge field in Λ_1 only. The gauge field within the domain Λ_0 appears only on the first line. As a result, *the dependence of the multiboson action from the gauge field in the blocks $\Lambda_0^{\hat{a}}$ is factorized*. Moreover, all contributions in Eq. (4.4.30) are highly suppressed with the thicknesses of the frame. This implies that the order N of the multi-boson polynomial can be rather low, i.e. of the order of ten or so [84].

Reweighting factor

We can now proceed to apply the reweighting procedure exactly as detailed for the one-dimensional case, see Eq. (4.2.10), obtaining

$$\frac{\det D}{\mathcal{W}_N} \propto \frac{1}{\det D_{\Lambda_1} \prod_{\hat{a}} \left[\det D_{\Phi_1^{\hat{a}}} \det D_{\Omega_0^{\hat{a}}}\right] \prod_{k=1}^{N/2} \det\left(W_{u_k}^\dagger W_{u_k}\right)}\,, \tag{4.4.31}$$

which can be estimated analogously to Eq. (4.2.9), with

$$\mathcal{W}_N = \det\{1 - R_{N+1}(W_1)\} \propto \frac{1}{\det\left\{W_1^{-1} \prod_{k=1}^{N/2} [W_{u_k}^\dagger]^{-1} W_{u_k}^{-1}\right\}}\,, \tag{4.4.32}$$

a representation which suggests the random noise estimator

$$\mathcal{W}_N = \frac{\int [d\eta][d\eta^\dagger] e^{-\xi^\dagger W_1^{-1}\xi}}{\int [d\eta][d\eta^\dagger] e^{-\eta^\dagger\eta}}\,, \qquad \xi = \prod_{k=1}^{N/2} W_{u_k}^{-1}\eta\,. \tag{4.4.33}$$

Given a certain factorization of the observable [83,85,87], expectation values can then be computed exactly as in Eq. (4.2.11) by including this reweighting factor in the definition of the observable. As already noted, in Appendix F we provide a procedure to obtain such factorized approximation starting from the factorization of the fermion determinant, regardless of the dimensions of the domain decomposition. In order to show explicitly the achieved factorization, we can define the multiboson action

$$S_{\mathrm{mb}}[\chi,\chi^\dagger,U] = |W_z\chi|^2 = \sum_{\hat{a}} S^{\hat{a}}_{\mathrm{mb}}[\chi,\chi^\dagger,U_{\Omega^{\hat{a}}_0}] + S^r_{\mathrm{mb}}[\chi,\chi^\dagger,U]\,, \tag{4.4.34}$$

where

$$S^{\hat{a}}_{\mathrm{mb}}[\chi,\chi^\dagger,U_{\Omega^{\hat{a}}_0}] = \left|P_{\partial\Lambda^{\hat{a}}_0}\Big[z\,\chi_{\partial\Lambda_0} + \hat{D}^{-1}_{\partial\Lambda^{\hat{a}}_0}\hat{D}^{\mathrm{h}}_{\partial\Lambda_0}\chi_{\partial\Lambda_0} + D^{-1}_{\Omega^{\hat{a}}_0}\,D_{\Phi^{\hat{a}}_1,\partial\bar{\Omega}^{\hat{a}*}_0}\chi_{\partial\Pi_1}\Big]\right|^2 \tag{4.4.35}$$

and

$$S^r_{\mathrm{mb}}[\chi,\chi^\dagger,U] = \left|z\,\chi_{\partial\Pi_1} + W_{\partial\Pi_1,\partial\Lambda_0}\chi_{\partial\Lambda_0}\right|^2. \tag{4.4.36}$$

The averages $\langle\cdot\rangle_N$ can now be computed with the factorized fermionic effective action

$$\begin{aligned} S^{\mathrm{eff},N}_{\mathrm{F}}[U,\{\chi_k,\chi^\dagger_k\}_{k=1}^{N/2}] = \sum_{\hat{a}}\left\{-\ln\det D_{\Omega^{\hat{a}}_0} + \sum_{k=1}^{N/2} S^{\hat{a}}_{\mathrm{mb}}[\chi_k,\chi^\dagger_k,U_{\Omega^{\hat{a}}_0}]\right\} \\ + \sum_{\hat{a}}\ln\det D_{\Phi^{\hat{a}}_1} - \ln\det D_{\Lambda_1} + \sum_{k=1}^{N/2} S^r_{\mathrm{mb}}[\chi_k,\chi^\dagger_k,U]\,. \end{aligned} \tag{4.4.37}$$

Our initial goal has been achieved: the dependence of the fermion determinant on the gauge field configuration in the active region has been fully factorized, see Eq. (4.4.31), up to the small reweighting term in Eq. (4.4.33) that can be included in the observable, implying that the fermionic effective action can be rewritten as in Eq. (4.4.37). On one hand, each term in the sum on the first line only depends on the gauge field configuration in the (framed) local domain $\Omega^{\hat{a}}_0$ and therefore it can be computed independently from the others, see Eq. (4.4.35). On the other hand, the remaining global contributions in the second line, see Eq. (4.4.36), only depend on the gauge field configuration in the inactive region, and are therefore constant if we only update links in the active domains.

Besides a purely theoretical interest for studying the factorization of $\det D$, the factorization we presented in this Section could in principle have many possible applications. It would certainly pave the way to multilevel intergation schemes, which have been shown as a promising variance reduction strategy for addressing the StN problem, mitigating the exponential StN degradation in physically relevant correlators, particularly in the challenging long-distance regime. The four-dimensional factorization discussed here would also facilitate master-field simulations [81,100,195], see also Appendix A.1.4, with the block-local accept/reject step in the HMC solving the problem of the increasing numerical precision needed for larger and larger volumes. It would allow for highly efficient parallelizations of Monte Carlo algorithms, also on heterogeneous architectures, by reducing very significantly the rate of data exchange among different (blocks of) computer nodes where the various domains of the lattice are mapped to, while possibly improving also the sampling in flow-based generative models [196–198].

Chapter 5

Spectral densities from Euclidean lattice correlation functions

Many phenomenologically relevant observables can be extracted either from spectral densities $\rho(\omega)$ or their smearing with theoretically known kernels $\kappa(\omega)$

$$\rho_\kappa = \int_\omega \rho(\omega)\kappa(\omega)\,. \tag{5.0.1}$$

Lattice QCD is the only known framework that allows to study their non-perturbative extraction from first principles, see Chapters 1 and 2. On the lattice, we can estimate correlation functions such as generic zero-momentum two-point functions[1]

$$C(t) = \int d^3\mathbf{x}\,\langle \mathcal{O}_1(t,\mathbf{x})\mathcal{O}_2(0)\rangle\,. \tag{5.0.2}$$

As discussed in Chapter 3, a Laplace transform

$$C(t) = \int_\omega \rho(\omega)e^{\omega t}\,, \quad \int_\omega \equiv \int_0^\infty d\omega \tag{5.0.3}$$

relates these correlators to spectral densities $\rho(\omega)$, whose support is $[\omega_{\text{thr}}, \infty)$, where $\omega_{\text{thr}} > 0$ for theories with a mass gap. For the case when UV subtractions are required, this expression can be generalized as in Eq. (3.1.21). An inverse problem is therefore present in all the cases where we are interested in directly extracting spectral densities, or when the kernel has poles at $\omega > \omega_{\text{thr}}$, preventing Eq. (5.0.1) from being rewritten through standard techniques, see Eq. (3.2.4), as an integral in the time-momentum representation, more suitable for lattice computations. This problem is further complicated by the intrinsically noisy, finite and discrete nature of lattice data. The practical solution adopted in state-of-the-art studies relies on the numerical Backus-Gilbert procedure and

[1] This discussion can be generalized to the case of a non-zero momentum projection, see Eqs. (3.1.9) and (3.1.20). Our results are fully generic, and the derivation presented here can be straightforwardly applied to any n-point function, involving multiple Euclidean-time separations.

its generalizations [107, 108, 123, 124, 199], see also Refs. [200–211] for alternative strategies and Refs. [125, 173, 212–221] for some concrete applications.

In this Chapter, we are mainly interested in deriving the details of this inversion, which is the second original contributions of this Thesis. Building on a broad mathematical literature [119, 121, 222–249], we closely follow and extend the discussion in Refs. [2, 3, 6] to review our strategy to perform the exact, analytic inversion both in the continuum and on a discrete lattice, respectively discussed in Sections 5.1 and 5.2. In Section 5.3 we instead address the delicate issue of estimating statistical and systematic errors in the context of spectral reconstructions. We conclude by presenting in Section 5.4 preliminary numerical results, extending our previous analysis published in Ref. [5].

5.1 Continuous inverse problems

In this Section, our main focus is the derivation of the analytic solution to the inverse Laplace transform in Eq. (5.0.3) in the continuum. Generalizations to the cases of smeared and subtracted spectral densities can be obtained analogously.

5.1.1 The inverse Laplace transform

Our starting point is Eq. (5.0.3) i.e. we need to compute the inverse Laplace transform (ILT) [222–224] of Euclidean time correlation functions. For this purpose, we introduce the orthonormal *time basis* $\{|t\rangle\}$, $t \in \mathbb{R}^+$, on the vector space $V_{\mathcal{T}}$ of real functions with support on $\mathbb{R}^+$. We define the inner product and resolution of the identity on $V_{\mathcal{T}}$ as

$$\langle f|g\rangle = \int_t f(t)g(t)\,, \quad \mathbb{1} = \int_t |t\rangle\langle t|\,, \quad \int_t \equiv \int_0^\infty dt\,. \tag{5.1.1}$$

We can now introduce a second space $V_{\mathcal{E}}$, spanned by the non-orthogonal *energy basis* $\{|\omega\rangle\}$, $\omega \in \mathbb{R}^+$, with coordinates in the time basis[2]

$$\langle t|\omega\rangle = \langle \omega|t\rangle = e^{-\omega t} \tag{5.1.2}$$

reproducing the kernel of the Laplace transform. We now define the non-diagonal metric

$$\langle \omega|\omega'\rangle = \int_t \langle \omega|t\rangle\langle t|\omega'\rangle = \frac{1}{\omega+\omega'} \equiv \mathcal{H}(\omega,\omega') \tag{5.1.3}$$

which corresponds to the Carleman operator [225]. We can rewrite the inverse problem in Eq. (5.0.3) on this basis as

$$|C\rangle = \int_\omega \rho(\omega)|\omega\rangle\,, \quad C(t) = \langle t|C\rangle \tag{5.1.4}$$

[2] We consider t, ω to be dimensionless variables, e.g. by rescaling all physical times and energies by a common reference scale.

which can equivalently be written as a Fredholm integral equation of the first kind

$$\langle\omega|C\rangle = \int_{\omega'} \mathcal{H}(\omega,\omega')\rho(\omega') \tag{5.1.5}$$

which must be solved in order to extract $\rho(\omega)$. Before inverting $\mathcal{H}$, we first need to diagonalize it, and we do so by introducing the *Mellin basis* $\{|s\rangle\}$, $s \in \mathbb{R}$, defined as

$$u_s(t) = \langle t|s\rangle \equiv \frac{e^{is\log(t)}}{\sqrt{2\pi t}}\,. \tag{5.1.6}$$

As shown in Appendix I.1, this is an orthonormal basis satisfying

$$\langle\omega|s\rangle = \int_t e^{-tw}\,u_s(t) = \lambda_s\,u_{-s}(w) = \lambda_s\,u_s^*(w)\,, \quad \lambda_s \equiv \Gamma\left(\frac{1}{2}+is\right) \tag{5.1.7}$$

where $\Gamma(z)$ is the Euler Gamma function. This allows us to write

$$\langle\omega|t\rangle = e^{-\omega t} = \int_s u_s(\omega)\lambda_s^* u_s(t)\,, \quad \int_s \equiv \int_{-\infty}^{\infty} ds \tag{5.1.8}$$

and to diagonalize $\mathcal{H}$, since

$$\mathcal{H}(\omega,\omega') = \int_s \langle\omega|s\rangle\langle s|\omega'\rangle = \int_s u_s^*(\omega)|\lambda_s|^2 u_s(\omega')\,, \quad |\lambda_s|^2 = \frac{\pi}{\cosh(\pi s)} \in [0,\pi]\,. \tag{5.1.9}$$

We note that from Eq. (5.1.8) we could define the eigenfunctions of the Laplace transform operator

$$\ell_s^{\pm}(t) = \frac{1}{\sqrt{2}}\left[u_s(t) \pm \frac{\lambda_s}{|\lambda_s|}u_s^*(t)\right], \quad \int_\omega \ell_s^{\pm}(\omega)e^{-\omega t} = \pm|\lambda_s|\ell_s^{\pm}(t) \tag{5.1.10}$$

through which Eq. (5.0.3) could be directly diagonalized and inverted. From Eq. (5.1.10), it also follows that the Laplace transform is a bounded and self-adjoint operator with purely absolutely continuous spectrum, $\pm|\lambda_s| \in [-\sqrt{\pi},+\sqrt{\pi}]$ of multiplicitly one. Similarly, Eq. (5.1.9) implies that $\mathcal{H}$ is a bounded operator with spectrum of multiplicity two. Additionally, analogously to the case of the Fourier transform, despite the representation in terms of the complex Mellin basis, the integral in Eq. (5.1.9) is real, and in Appendix I.1 we show an equivalent representation in terms of a real basis. Another consequence of Eq. (5.1.9) is that we need to define $V_{\mathcal{E}} \equiv L^2(0,\infty,d\omega)$ in order to work with convergent quantities. Since the Laplace transform is a self-adjoint operator on $L^2(0,\infty,dx)$ with norm $\sqrt{\pi}$ [247], we also restrict ourselves to $V_{\mathcal{T}} \equiv L^2(0,\infty,dt)$.
The problem of inverting Eq. (5.1.8), or equivalently Eq. (5.1.10), is mathematically ill-posed in the Hadamard sense [232] (a unique solution to the inverse problem exists, but the inverse Laplace operator is not a continuous functional operator, i.e. the solution does not depend continuously on data), due to the rapid exponential decay of the eigenvalues $|\lambda_s|^2$ as $|s| \to \infty$. As pointed out by Tikhonov [226, 227, 232], this does not imply the absence of a solution, which can be retrieved by temporarily introducing

a regulating parameter to perform the ill-posed inversion, to then remove it after the inversion has been completed. For simplicity, we introduce the Tikhonov regularization

$$\mathcal{H}_\alpha = \mathcal{H} + \alpha\mathcal{I}\,, \quad \mathcal{H}_\alpha^{-1}(\omega,\omega') = \int_s u_s^*(\omega)\frac{1}{|\lambda_s|^2+\alpha}u_s(\omega')\,, \quad \alpha > 0 \tag{5.1.11}$$

but in principle any real, symmetric and positive-definite regulating functional would work [5]. We can then introduce a smeared Dirac δ function as

$$\delta_\alpha(\omega,\omega') = \int_{\omega''}\mathcal{H}(\omega,\omega'')\mathcal{H}_\alpha^{-1}(\omega'',\omega') = \langle\omega|S_\alpha|\omega'\rangle = \int_s u_s^*(\omega)\frac{|\lambda_s|^2}{|\lambda_s|^2+\alpha}u_s(\omega') \tag{5.1.12}$$

which recovers $\delta(\omega-\omega')$ in $V_\mathcal{E}$ in the limit of $\alpha\to 0$, see Eq. (I.1.3), and where we introduced

$$S_\alpha = \int_s \frac{|s\rangle\langle s|}{|\lambda_s|^2+\alpha}\,. \tag{5.1.13}$$

We can now invert Eq. (5.1.8), ending up with

$$\rho(\omega) = \lim_{\alpha\to 0}\rho_\alpha(\omega)\,, \quad \rho_\alpha(\omega) = \langle\omega|S_\alpha|C\rangle = \int_{\omega'}\delta_\alpha(\omega,\omega')\rho(\omega') = \int_t g_\alpha(t|\omega)C(t) \tag{5.1.14}$$

from which it is clear that ρ_α can be interpreted as a smeared spectral density as in Eq. (5.0.1) with $\kappa = \delta_\alpha$. In the equation above, since in practice we only know $|C\rangle$ in the time basis, we inserted the completeness relation in Eq. (5.1.1), obtaining the coefficients

$$g_\alpha(t|\omega) = \langle\omega|S_\alpha|t\rangle = \int_s u_s^*(\omega)\frac{\lambda_s}{|\lambda_s|^2+\alpha}u_s^*(t)\,. \tag{5.1.15}$$

These coefficients are real, since $s\in\mathbb{R}$, and they can be numerically computed, thanks to the rapid fall-off of the numerator at large s [229]. Note that a similar property is shared by the smeared Dirac δ in Eq. (5.1.12). In Fig. 5.1 we provide a concrete example, where we highlight the geometrical distribution of the zeros of the coefficients and of δ_α, stemming from that of the basis functions u_s and ultimately related to the $x\to 1/x$ symmetry of the continuum integration domain $(0,\infty)$ detailed in Appendix I.1, see Eq. (I.1.11). We also note that a completely equivalent definition of ρ_α is

$$\rho_\alpha(\omega) = e^{\omega t_0}\int_{t_0}^\infty dt\, g_\alpha(t-t_0|\omega)C(t) \quad \forall\, t_0 \geq 0\,. \tag{5.1.16}$$

We emphasize that Eq. (5.1.14) is the desired solution: the spectral density can be extracted from the Euclidean time dependence of $C(t)$ by integrating it out with the analytically known, real and computable coefficients in Eq. (5.1.15). A numerical example and proof of convergence of the solution as $\alpha\to 0$ for

$$\rho(\omega) = \sqrt{1-4\frac{m_\pi^2}{\omega^2}}\frac{\Gamma_\rho}{(\omega-M_\rho)^2+\Gamma_\rho^2}\,, \quad \{m_\pi, M_\rho, \Gamma_\rho\} = \{135, 776, 140\}\,\text{MeV} \tag{5.1.17}$$

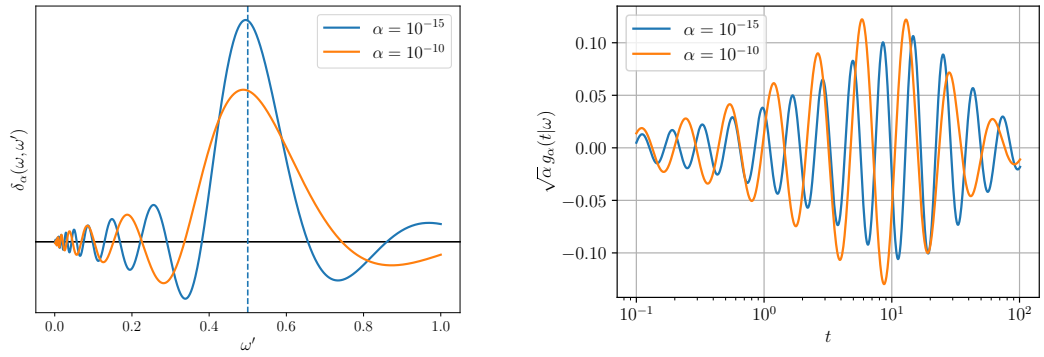

(a) Smeared Dirac δ as a function of the energy. Notice the distribution of the peaks along the horizontal axis.

(b) Coefficients as in Eq. (5.1.15) rescaled with $\sqrt{\alpha}$ as a function of time. Notice the logarithmic scale along the horizontal axis.

Figure 5.1: Smeared Dirac δ (a) and coefficients rescaled with $\sqrt{\alpha}$ (b), see Eqs. (5.1.12) and (5.1.15) respectively, at fixed $\omega = 0.5$.

is provided in Fig. 5.2a, where we compare different reconstructions of $\rho_\alpha(\omega)$ for a few values of α. It can be appreciated that, as we decrease α, the reconstructed spectral density approaches the correct one in Eq. (5.1.17), also shown in the same plot. Such convergence can be understood also from the fact that ρ_α can alternatively be found by expanding $\rho_\alpha(\omega) = \int_t g'_\alpha(t) e^{-\omega t}$ on the exponentially suppressed basis given by the coefficients in Eq. (5.1.2) and minimizing the distance

$$d[\rho, \rho_\alpha] = \int_\omega [\rho(\omega) - \rho_\alpha(\omega)]^2 + \alpha \int_t g'_\alpha(t)^2 = \int_\omega [\rho(\omega) - \rho_\alpha(\omega)]^2 + \alpha \langle C | S_\alpha^2 | C \rangle \quad (5.1.18)$$

with respect to $g'_\alpha(t)$, ending up with

$$g'_\alpha(t) = \int_{t'} \mathcal{A}_\alpha^{-1}(t, t') C(t') \quad (5.1.19)$$

where

$$\mathcal{A}_\alpha = \mathcal{A} + \alpha \mathcal{I}\,, \quad \mathcal{A}(t, t') = \int_\omega e^{-\omega(t+t')} = \frac{1}{t + t'}\,, \quad \langle t | S_\alpha | t' \rangle = \mathcal{A}_\alpha^{-1}(t, t')\,. \quad (5.1.20)$$

This is equivalent to Eq. (5.1.14), since

$$\rho_\alpha(\omega) = \int_{t,t'} e^{-\omega t'} \mathcal{A}_\alpha^{-1}(t', t) C(t')\,, \quad g_\alpha(t|\omega) = \int_{t'} e^{-\omega t'} \mathcal{A}_\alpha^{-1}(t', t)\,. \quad (5.1.21)$$

Also the smeared δ function can be expanded on this exponentially suppressed basis as $\delta_\alpha(\omega, \omega') = \int_t \langle \omega | S_\alpha | t \rangle \langle t | \omega' \rangle$, with the choice of the coefficients $\langle \omega | S_\alpha | t \rangle$ minimizing $d[\delta, \delta_\alpha]$ [231, 232] at fixed ω' and reproducing the solution in Eq. (5.1.12).

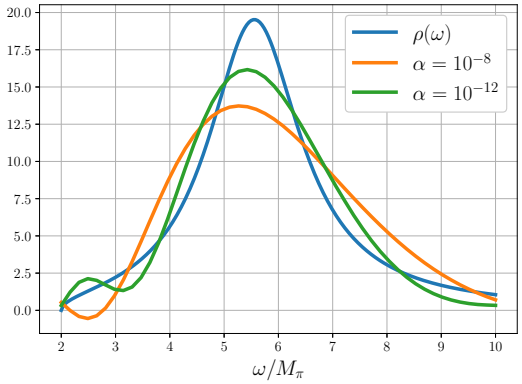

(a) Continuum reconstruction, see Eq. (5.1.14).

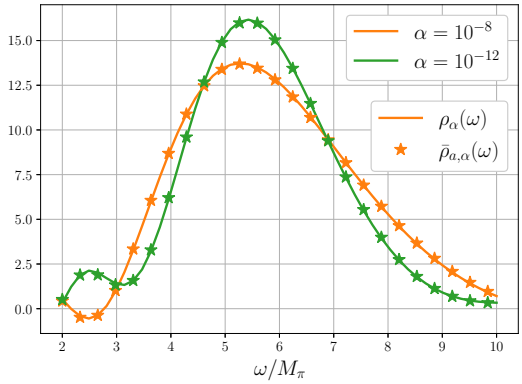

(b) Discrete reconstruction, see Eq. (5.2.12).

Figure 5.2: Spectral reconstructions, with $\rho(\omega)$ defined as in Eq. (5.1.17). The fluctuations at small values of α are a direct consequence of those in δ_α, see Fig. 5.1a.

5.1.2 Smeared spectral densities

The equations above can be straightforwardly generalized to the extraction of smeared spectral densities, of great interest in QFTs. For their extraction, we can treat the smearing kernel[3] in complete analogy with Eq. (5.1.2), i.e. by replacing $|\omega\rangle$ in Eq. (5.1.14) with the vector

$$|\kappa\rangle \equiv \int_\omega \kappa(\omega)|\omega\rangle\,. \tag{5.1.22}$$

The smeared spectral density is then simply found from integrating out Eq. (5.1.14) with $\kappa(\omega)$, namely[4]

$$\rho_\kappa = \lim_{\alpha\to 0}\rho_{\kappa,\alpha}\,, \quad \rho_{\kappa,\alpha} = \langle\kappa|S_\alpha|C\rangle = \int_t g_{\kappa,\alpha}(t)C(t)\,, \quad g_{\kappa,\alpha}(t) = \int_\omega \kappa(\omega)g_\alpha(t|\omega)\,. \tag{5.1.23}$$

In order to obtain this solution, we first extracted the spectral density ρ_α smeared with a specific kernel δ_α induced by the regularization procedure, required to perform the ill-posed ILT, to then compute the additional smearing w.r.t. the desired kernel κ. The solution in Eq. (5.1.23) directly allows us to interpret $\rho_{\kappa,\alpha}$ in the opposite direction, namely as if the kernel $\kappa(\omega)$ had first been smeared with δ_α, to later compute the numerically accessible smearing of ρ with the resulting kernel $\kappa_\alpha(\omega) = \int_{\omega'}\delta_\alpha(\omega,\omega')\kappa(\omega')$. We must therefore ensure that $\kappa(\omega) \in L^2(0,\infty,d\omega)$ as well, which is also sufficient to ensure that the integral defining ρ_κ converges. This kernel can therefore be additionally interpreted as the solution of yet another least-square problem, minimizing $d[\kappa,\kappa_\alpha]$,

[3] In general, $\kappa(\omega)$ (and ρ_κ as a consequence) may depend on additional variables, like the mass of the decaying particle for rates, or the center of the Gaussian kernel for smeared densities. For better readibility, here we omit them from the notation.

[4] Even though Eq. (5.1.16) provides an equivalent solution for ρ, the additional dependence on $e^{\omega t_0}$ requires careful consideration when applying smearing. To ensure the integrals converge, further constraints on the choice of κ may be required.

where κ has been expanded on the exponentially suppressed basis and regulated in the same way as before. This exact philosophy is adopted in many Lattice QCD applications [5, 107, 123–125, 199, 204, 212, 215] to approximate the kernel by computing its expansion on a finite and discrete set of basis elements.

5.1.3 Subtracted spectral densities

In relativistic field theories, the convergence and uniqueness of the solutions above are guaranteed by our a priori theoretical knowledge[5] on the validity of the representation[6] in Eq. (5.0.3). For theories with a mass gap $\omega_{\text{thr}} > 0$ such as QCD, the IR regime is automatically regulated. In the UV region instead we should be more careful, as short-distance singularities might spoil convergence of integrals of correlators at small t. Practically, whenever $\rho(\omega) \notin L^2(0,\infty,d\omega)$, modifications of Eq. (5.1.14) must be studied. For instance, for the isovector vector two-point function studied in QCD and projected at zero spatial momentum, $C(t)$ in Eq. (5.0.3) scales proportionally to $1/t^3$ at short times, i.e. $\rho(\omega)$ scales as ω^2 at large energies.

As detailed in Subsection 3.1.2, the relation between the correlator and the spectral density is slightly modified into

$$C(t) = \int_\omega \rho_{\mathsf{s}}(\omega)\omega^{2k}e^{-\omega t} \tag{5.1.24}$$

with $k \neq 0$, i.e. a Laplace transform as in Eq. (5.0.3) where now $\rho(\omega) = \omega^{2k}\rho_{\mathsf{s}}(\omega)$, with $\rho_{\mathsf{s}}(\omega) \in L^2(0,\infty,d\omega)$ and where the additional power-like dependence is related to UV divergences. In order to address this problem, we can first generalize Eq. (5.1.7) as

$$\int_t e^{-\omega t}t^b u_s(t) = \lambda_{s,b}\, u_s^*(\omega)\omega^{-b}\,, \quad b > -\frac{1}{2}\,, \quad \lambda_{s,b} = \Gamma\left(\frac{1}{2}+b+is\right). \tag{5.1.25}$$

Our strategy to perform the inversion consists now in exploiting the additional factor ω^{-b} on the r.h.s. of Eq. (5.1.25) to cancel out the power-like dependence in Eq. (5.1.24). In fact, we can expand

$$\rho_{\mathsf{s}}(\omega) = \int_s (\rho_{\mathsf{s}})_s u_s^*(\omega)\,, \quad (\rho_{\mathsf{s}})_s \equiv \int_s u_s(\omega)\rho_{\mathsf{s}}(\omega) \tag{5.1.26}$$

to rewrite Eq. (5.1.25) as

$$C(t) = \int_s (\rho_{\mathsf{s}})_s \int_\omega u_s^*(\omega)e^{-\omega t}\omega^{2k} = \int_s (\rho_{\mathsf{s}})_s\, t^{-2k}\lambda_{s,2k}^* u_s(t) \tag{5.1.27}$$

which implies that

$$\int_t t^{2k}\frac{1}{\lambda_{s,2k}^*}u_s^*(t)C(t) = (\rho_{\mathsf{s}})_s\,. \tag{5.1.28}$$

[5] In the absence of such prior knowledge, we should refer to the most general conditions under which $C(t)$ may be interpreted as the Laplace transform of another function [239].

[6] Depending on the quantum numbers, when several densities appear in the parametrization of the correlator, one should consider the appropriate linear combinations to satisfy Eq. (5.0.3).

Before inserting it in Eq. (5.1.26), we follow a similar procedure as above to regularize this expression, considering the replacement $1/\lambda^*_{s,2k} \to \lambda_{s,p}/(\lambda_{s,p}\lambda^*_{s,2k} + \alpha)$ and defining the solution as

$$\rho_{\mathfrak{s}}(\omega) = \lim_{\alpha\to 0} \int_t g_\alpha(t|\omega, p, 2k) C(t)\,, \quad g_\alpha(t|\omega, p, q) = t^q \int_s \frac{u^*_s(\omega)\lambda_{s,p} u^*_s(t)}{\lambda_{s,p}\lambda^*_{s,q} + \alpha} \tag{5.1.29}$$

in terms of the generalized coefficients $g_\alpha(t|\omega, p, q)$, defined $\forall\, p > -1/2$. Notice that in practice this strategy allows to define a family of solutions not only in p but also at different values of q for which the expressions, such as the t-integral in Eq. (5.1.29), are well-defined and convergent. Experimenting with the values of p and q might be beneficial in some practical calculations. We additionally note the power-like t-dependence of the generalized coefficients in Eq. (5.1.29), which (as expected) suppresses UV divergences at short times.

Clearly, smeared regulated spectral densities can be extracted by combining the two methods presented here. In Appendix I.3, we discuss a possible application of this formalism to rewrite smeared spectral densities as integrals of correlation functions in the time-momentum representation.

5.2 Discrete inverse problems

In Lattice QCD, $C(t)$ is sampled at discrete Euclidean times $t = an$, where $n \in \mathbb{N}$ and a is the lattice spacing. Additionally, the correlator at finite a, $\overline{C}_a(t)$, suffers from discretization errors, typically of $O(a^2)$, which we do not address here. When numerical simulations are used to estimate $\overline{C}_a(t)$, n is also limited to $n \in [0, t_{\max}/a]$ at finite $t_{\max}$, and $\overline{C}_a(t)$ is affected by statistical errors. We defer the discussion of these two aspects to the following Section, while here we focus on generalizing the results derived so far in the continuum to the ideal case of $n \in \mathbb{N}$.

Although our goal is to find an exact analytic formula, one might initially consider discrete samples of the coefficients to apply a discretized version of the continuum solutions. Given the geometric distribution of the zeros of the basis functions u_s and therefore of the coefficients, as highlighted in Fig. 5.1b, an optimal adaptation to the discrete case would be achieved by replacing the integral over time with a sum spanning geometrically distributed data [243], which however is evidently not usable in lattice field theories. Instead, using the available evenly spaced data would induce large discretization errors due to the large oscillations of the coefficients at short times. Notice that these wild fluctuations are unavoidably present also in Eq. (5.1.16), where $C(t)$ is integrated with $g_\alpha(t - t_0)$ for $t \in (t_0, \infty)$.

In order to obtain an exact formula for the discrete case, we proceed similarly to the continuum. For simplicity, we consider the unsubtracted case. We begin by computing the analogue of Eq. (5.1.5), obtaining the Fredholm equation of the first kind

$$a \sum_{t=t_{\min}}^{\infty} e^{-\omega t} \overline{C}_a(t) = \int_{\omega'} \overline{\mathcal{H}}_a(\omega, \omega')\rho(\omega')\,, \quad t_{\min} \geq a \tag{5.2.1}$$

in terms of the modified Carleman operator[7]

$$\overline{\mathcal{H}}_a(\omega,\omega') = a\sum_{t=t_{\min}}^{\infty} e^{-(\omega+\omega')t} = \frac{a\, e^{-(\omega+\omega')t_{\min}}}{1-e^{-a(\omega+\omega')}}\,. \tag{5.2.2}$$

In order to invert Eq. (5.2.1), we need to diagonalize $\overline{\mathcal{H}}_a$. To this aim, we introduce a different operator, namely the infinite Hilbert matrix

$$\overline{\mathcal{A}}_a(t,t') = \frac{a}{t+t'+2t_{\min}}\,, \quad t,t' = 0,a,2a,\dots \tag{5.2.3}$$

which is the analogue of the operator $\mathcal{A}$ in Eq. (5.1.20) in the continuum[8], and it is related to $\overline{\mathcal{H}}_a$ by

$$\int_{\omega'} \overline{\mathcal{H}}_a(\omega,\omega')e^{-a\omega'(n+\tau)} = a\sum_{m=0}^{\infty} \overline{\mathcal{A}}_a(na,ma)e^{-a\omega(m+\tau)}\,. \tag{5.2.4}$$

Following Refs. [2, 3, 6], see also Appendix I.2, we can determine the eigenfunctions $v_s(\omega,a)$, $s\in\mathbb{R}^+$ of $\overline{\mathcal{H}}_a$ from the eigenvectors $\overline{v}_s(n,a)$ of $\overline{\mathcal{A}}_a$ by

$$|\lambda_s| v_s(\omega,a) = a\sum_{n=0}^{\infty} e^{-a\omega(n+\tau)}\overline{v}_s(an,a) \tag{5.2.5}$$

where we introduced $\tau \equiv t_{\min}/a$. Using Eq. (5.2.4), it can be shown that $\overline{v}_s(t,a)$ diagonalizes $\overline{\mathcal{A}}_a$ if and only if $v_s(\omega,a)$ diagonalizes $\overline{\mathcal{H}}_a$, and that they share the same eigenvalues. Building on known mathematical results [242], in Appendix I.2 we show that the functions

$$\overline{v}_s(t,a) \equiv \frac{|\lambda_s|^3}{\sqrt{a}|N_s|}\,{}_3F_2\left(\begin{matrix} -\frac{t}{a}, \frac{1}{2}+is, \frac{1}{2}-is \\ 1, 2\tau \end{matrix}\,\middle|\, 1\right), \tag{5.2.6}$$

$$v_s(\omega,a) = \sqrt{a}z\frac{|\lambda_s|^2}{|N_s|}\,{}_2F_1\left(\begin{matrix} \frac{1}{2}+is, \frac{1}{2}-is \\ 2\tau \end{matrix}\,\middle|\, -z\right)e^{-a\omega(\tau-1)}\,, \quad z = \frac{e^{-a\omega}}{1-e^{-a\omega}} \tag{5.2.7}$$

where ${}_qF_p$ are the hypergeometric functions [119] and

$$N_s = \sqrt{2\pi}\frac{\Gamma(-2is)\lambda_s}{\Gamma\left(2\tau-\frac{1}{2}+is\right)\Gamma(2\tau)}\,, \tag{5.2.8}$$

are eigenfunctions of $\overline{\mathcal{A}}_a$ and $\overline{\mathcal{H}}_a$ respectively, satisfying

$$a\sum_{m=0}^{\infty} \overline{\mathcal{A}}_a(na,ma)\overline{v}_s(ma,a) = |\lambda_s|^2\overline{v}_s(na,a)\,, \tag{5.2.9}$$

$$\int_{\omega'} \overline{\mathcal{H}}_a(\omega,\omega')v_s(\omega',a) = |\lambda_s|^2 v_s(\omega,a)\,. \tag{5.2.10}$$

[7] We omit the explicit dependence on $t_{\min}$.

[8] The action of the operator $\mathcal{A}$ is defined by applying the Laplace transform followed by its dual operator, whereas $\mathcal{H}$ results from applying these operators in the reverse order. This in turn implies that the functional form of $\mathcal{H}$ changes due to $\int_t \to a\sum_t$ in the definition of $\mathcal{H}\to\overline{\mathcal{H}}_a$, while the space of functions on which it acts is unchanged. Instead, the functional form of the operator $\mathcal{A}$ is the same as in the continuum, but it acts on a different (discrete) space.

Surprisingly, they share the same exponentially suppressed eigenvalues $|\lambda_s|^2$ as their continuum counterparts, now with $s \in \mathbb{R}^+$ and with no degeneracy of the spectrum. Also, they form separate orthonormal and complete sets [244–246], acting respectively on $\ell^2(\mathbb{Z}^+)$ and $L^2(0,\infty,d\omega)$, see footnote 8. A smeared δ function at finite a can be introduced also in the discrete case by replacing $u_s(\omega)$ with $v_s(\omega,a)$ in Eq. (5.1.12), i.e. by regularizing $\overline{\mathcal{H}}_a$ à-là-Tikhonov with $\overline{\mathcal{H}}_{a,\alpha} = \overline{\mathcal{H}}_a + \alpha\mathcal{I}$, obtaining

$$\overline{\delta}_{a,\alpha}(\omega,\omega') = \int_{\omega''} \overline{\mathcal{H}}^{-1}_{a,\alpha}(\omega,\omega'')\overline{\mathcal{H}}_a(\omega'',\omega') = \int_{s\in\mathbb{R}^+} v_s(\omega,a)\frac{|\lambda_s|^2}{|\lambda_s|^2+\alpha}v_s(\omega',a) \tag{5.2.11}$$

which again satisfies $\overline{\delta}_{a,\alpha}(\omega,\omega') \xrightarrow{\alpha\to 0} \delta(\omega-\omega')\ \forall\, a$. The spectral density at finite lattice spacing can then be recovered on a lattice with infinite time extent from the limit

$$\rho(\omega) = \lim_{\alpha\to 0}\overline{\rho}_{a,\alpha}(\omega)\,, \quad \overline{\rho}_{a,\alpha}(\omega) = \int_{\omega'}\overline{\delta}_{a,\alpha}(\omega,\omega')\rho(\omega') = a\sum_{t=t_{\min}}^{\infty}\overline{g}_{a,\alpha}(t|\omega)C(t) \tag{5.2.12}$$

written in terms of the real coefficients

$$\overline{g}_{a,\alpha}(t|\omega) = \int_{s\in\mathbb{R}^+}\frac{v_s(\omega,a)|\lambda_s|\overline{v}_s(t,a)}{|\lambda_s|^2+\alpha}\,, \tag{5.2.13}$$

which remarkably holds $\forall\, t_{\min} \geq a$. Taking $t_{\min} = a$ i.e. $\tau = 1$, Eq. (5.2.7) simplifies to

$$v_s(\omega,a) \equiv \sqrt{2\pi a}\frac{u_s(1-e^{-a\omega})}{|N_s|}e^{-a\omega}|\lambda_s|^2{}_2F_1\left(\begin{matrix}\frac{1}{2}+is,\frac{3}{2}+is\\ 2\end{matrix}\,\middle|\, e^{-a\omega}\right) \tag{5.2.14}$$

with

$$N_s = \sqrt{2\pi}\frac{\Gamma(-2is)\lambda_s}{(\frac{1}{2}-is)\lambda_s^*}\,, \tag{5.2.15}$$

which in Appendix I.2 is shown to satisfy

$$v_s(\omega,a) = \sqrt{a}\,\frac{2\mathrm{Re}[u_s(a\omega)N_s]}{|N_s|}\left(1+O(a^2\omega^2)\right)\,, \tag{5.2.16}$$

i.e. it approaches the expected real linear combination of continuum eigenfunctions $u_s(\omega)$, $u_s^*(\omega)$ to recover the correct orthonormality relation. We also expect $O(a^2\omega^2)$ discretization effects, i.e. enhanced in the UV region. In Fig. 5.3, the coefficients in Eq. (5.2.13) with $t_{\min} = a$ are compared to their continuum counterpart in Eq. (5.1.15) for fixed values of α and ω. As anticipated and as it is clear from Fig. 5.3a, in the IR (UV) regime the discrepancies between the continuum and discrete coefficients are reduced (enhanced). As we decrease the lattice spacing, these discretization errors start to be negligible even in the short t regime.

Even though the discretization errors are particularly pronounced at small times for the individual coefficients, they remain minimal for the resulting spectral density.

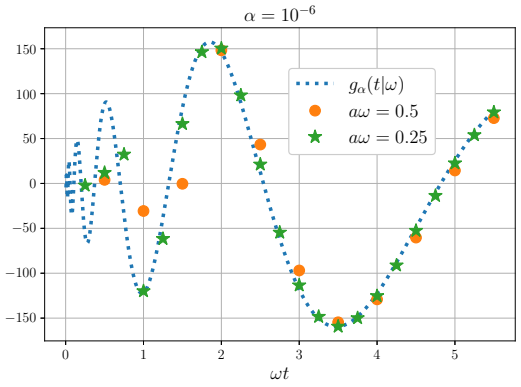

(a) Continuum (blue, dotted line) and discrete coefficients at different values of the lattice spacing a, while α and the physical value of ω are fixed.

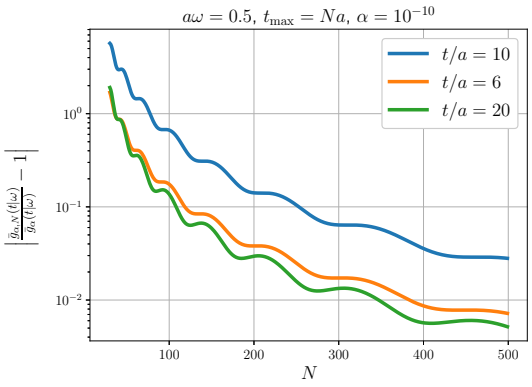

(b) The relative errors on the computation of discrete coefficients at finite N w.r.t. our results in Eq. (5.2.13) approach 0 as $N \to \infty$.

Figure 5.3: Comparison of discrete coefficients $\overline{g}_{a,\alpha}$, with their continuum (a) and finite-N counterparts (b), g_α and $\overline{g}_{\alpha,N}$ respectively. See Eqs. (5.1.15), (5.2.13) and (5.2.17) for the corresponding definitions. Plots taken from Ref. [6].

Indeed, the solution in Eq. (5.2.12) with the choice of coefficients in Eq. (5.2.13) minimizes a functional similar to Eq. (5.1.18) for the continuum case. To be more precise, we can expand $\overline{\rho}_{a,\alpha}(\omega) = a\sum_{n=0}^{N-1} e^{-\omega(na+t_{\min})}\overline{g}'_{a,\alpha}(na)$ and minimize

$$d_N[\rho,\overline{\rho}_{a,\alpha}] = \int_\omega \left[\rho(\omega) - a\sum_{n=0}^{N-1}\overline{g}'_{a,\alpha}(na)e^{-\omega(na+t_{\min})}\right]^2 + \alpha a\sum_{n=0}^{N-1}\overline{g}'_{a,\alpha}(na)^2 \tag{5.2.17}$$

with respect to $\overline{g}'_{a,\alpha}(na)$. In the limit $N \to \infty$, we end up recovering our solution in Eq. (5.2.12), which can be equivalently written as

$$\overline{\rho}_{a,\alpha}(\omega) = \lim_{\alpha\to 0} a^2 \sum_{n,m=0}^{\infty} e^{-\omega(na+t_{\min})}\overline{\mathcal{A}}^{-1}_{a,\alpha}(na,ma)\overline{C}_a(na+t_{\min})\,, \quad \overline{\mathcal{A}}_{a,\alpha} = \overline{\mathcal{A}}_a + \alpha\mathcal{I} \tag{5.2.18}$$

which coincides with the above one in Eq. (5.2.12) since

$$\overline{g}_{a,\alpha}(t|\omega) = a\sum_{t'=0}^{\infty} e^{-\omega(t'+t_{\min})}\overline{\mathcal{A}}^{-1}_{a,\alpha}(t',t)\,. \tag{5.2.19}$$

The main difficulties in the discrete derivation are due to the differences both in the functional forms and in the spaces on which the operators $\overline{\mathcal{H}}_a$ and $\overline{\mathcal{A}}_a$ act, which instead coincide in the continuum case for $\mathcal{H}$ and $\mathcal{A}$. In the limit $\alpha \to 0$, the functional in Eq. (5.2.17) approaches 0, a fact that can be interpreted as the recovery of the exact solution even at a fixed value of a, showing the beneficial effect on the reconstruction of discretization errors on the coefficients. The only residual source of discretization errors, in this case, would then be that related to the correlation function alone. In principle,

as proposed in Ref. [207], we could even remove this source of errors by taking the limit $\lim_{a\to 0} \overline{C}_a(t)$ beforehand, to then linearly combine C with $\overline{g}_{\Delta t,\alpha}$ at any chosen discrete but fixed set of physical times, for arbitrary choices of the physical temporal interval Δt.

We additionally notice that the proposal in Refs. [124, 250, 251] is based on the minimization of a similar functional as that in Eq. (5.2.17) with a fixed, finite number N of terms of the exponential basis on which the spectral density is expanded, and with additional refinements due to the choice of different regulators. By choosing the Tikhonov regulator also for that case, in Fig. 5.3b we show that the coefficients corresponding to the numerical solution of Eq. (5.2.17) at fixed N approach our results as $N \to \infty$. In Appendix I.4, we show a possible application of this strategy to the computation of integrals of correlation functions.

5.3 Errors

Any quantity numerically computed through Lattice QCD simulations is inherently affected by statistical errors stemming from the Monte Carlo estimates of path integral averages via importance sampling. In the presence of statistical fluctuations, the rapid oscillations of the coefficients in Eq. (5.1.15) or Eq. (5.2.13) might amplify statistical errors in the reconstructed (smeared) spectral density. Retrieving the exact solution relies on properly accounting for all the cancellations arising when the correlation function, a smooth function of time, is integrated with such wildly oscillating coefficients. These delicate cancellations might also be spoiled by other systematic errors that affect correlation functions computed on the lattice, such as their knowledge only on a finite temporal extent. In this Section, we examine statistical and systematic effects. Note that one benefit of the formalism developed in Section 5.1 is that these two error sources can be analyzed independently.

As it has already been observed in Fig. 5.1b, increasing the ILT regulator reduces the magnitude of the oscillations in the coefficients. This may help lower the variance, but also broadens the width of the smeared Dirac δ in Eq. (5.1.12), with which ρ is convoluted. The presence of a non-zero but fixed regulating parameter can therefore be incorporated in the definition of the observables we extract, and the $\alpha \to 0$ limit might be studied (if needed) after all extrapolations to physical, continuum and infinite-volume limits have been taken.

5.3.1 Statistical errors

As described above, in any Lattice QCD computation the correlation functions are estimated with their statistical errors. We consider the case of a two-point function

$$C(t) = \langle \widetilde{\mathcal{O}}(t)\mathcal{O}^\dagger(0)\rangle = \int_\omega e^{-\omega t}\rho(\omega)\,, \quad \widetilde{\mathcal{O}}(t) = \int d^3\mathbf{x}\,\mathcal{O}(t,\mathbf{x}) \tag{5.3.1}$$

projected to zero-momentum, assuming for simplicity that $\langle \mathcal{O} \rangle = 0$ and that no UV subtraction is needed. We can follow similar arguments as those outlined in Subsection 3.1.2 to represent its covariance

$$\mathrm{Cov}(t,t') = \langle \widetilde{\mathcal{O}}(t)\mathcal{O}^\dagger(0)\widetilde{\mathcal{O}}(t')\mathcal{O}^\dagger(0)\rangle - C(t)C(t') \tag{5.3.2}$$

as a double Laplace transform

$$\mathrm{Cov}(t,t') = \int_{\omega\omega'} e^{-\omega t}[\rho_2(\omega,\omega') - \rho(\omega)\rho(\omega')]e^{-\omega' t'} \equiv \int_{\omega\omega'} e^{-\omega t}\rho_{\mathsf{c}}(\omega,\omega')e^{-\omega' t'} \tag{5.3.3}$$

where

$$\langle \widetilde{\mathcal{O}}(t)\mathcal{O}^\dagger(0)\widetilde{\mathcal{O}}(t')\mathcal{O}^\dagger(0)\rangle = \int_{\omega\omega'} e^{-\omega t}\rho_2(\omega,\omega')e^{-\omega' t'} \tag{5.3.4}$$

and where, for the purposes of this discussion, we take $\rho_2(\omega,\omega') \in L^2(\mathbb{R}^+\times\mathbb{R}^+, d\omega\, d\omega')$, so that also[9] $\rho_{\mathsf{c}}(\omega,\omega') \in L^2(\mathbb{R}^+\times\mathbb{R}^+, d\omega\, d\omega')$. Given the linearity of the solution in Eq. (5.1.14), the errors (at fixed α) straightforwardly propagate as

$$\mathcal{C}_\alpha(\omega,\omega') = \int_{tt'} g_\alpha(t|\omega)\mathrm{Cov}(t,t')g_\alpha(t'|\omega') \xrightarrow{\alpha\to 0} \rho_{\mathsf{c}}(\omega,\omega') \tag{5.3.5}$$

with the variance of $\rho_\alpha(\omega)$ being $\mathcal{C}_\alpha(\omega,\omega)$. By integrating out this equation with any desired kernel $\kappa(\omega)$, we obtain the estimate for the variance on the corresponding smeared spectral densities as

$$\mathcal{C}_\alpha(\kappa) = \int_{t,t'} g_{\kappa,\alpha}(t)\mathrm{Cov}(t,t')g_{\kappa,\alpha}(t') \xrightarrow{\alpha\to 0} \int_{\omega\omega'} \kappa(\omega)\rho_{\mathsf{c}}(\omega,\omega')\kappa(\omega')\,. \tag{5.3.6}$$

Different models for the covariance matrix can be defined and inserted to predict their effect on the errors of the corresponding reconstruction. Below, we provide a few examples[10], but a detailed study of different effects with real data still needs to be done.
For instance, inspired by the asymptotic exponential decay of correlation functions in QFTs which applies also to the covariance matrix, we formulate the ansatz

$$\mathrm{Cov}(t,t') = e^{-m(t+t')} \quad \text{i.e.} \quad \rho_{\mathsf{c}}(\omega,\omega') = \delta(\omega-m)\delta(\omega'-m) \tag{5.3.7}$$

which implies that

$$\mathcal{C}_\alpha(\kappa) \xrightarrow{\alpha\to 0} [\kappa(m)]^2\,. \tag{5.3.8}$$

In this case, no particular issue arises in the reconstruction, even in the $\alpha \to 0$ limit[11]. If we were to consider instead a diagonal covariance matrix, we would obtain

$$\mathrm{Cov}(t,t') = e^{-m(t+t')}\delta(t-t') \quad \to \quad \mathcal{C}_\alpha(\omega,\omega') = \int_s \frac{u_s^*(\omega-m)u_s(\omega'-m)}{|\lambda_s|^2+\alpha} \tag{5.3.9}$$

[9] Recall that, in order for Eq. (5.3.1) to be inverted, we require $\rho(\omega) \in L^2(0,\infty,d\omega)$.

[10] A few numerical consistency checks have been performed, although they are not included here.

[11] The corresponding StN $= \rho_\kappa/\kappa(m)$ would have a specific behavior w.r.t. the additional parameters on which κ can depend, e.g. the center or the width of a Gaussian.

with a diverging $\alpha \to 0$ limit. This also implies that

$$\mathcal{C}_\alpha(\kappa) = \int_s \frac{\kappa_s(m)^* \kappa_s(m)}{|\lambda_s|^2 + \alpha}\,, \quad \kappa_s(m) \equiv \int_\omega \kappa(\omega) u_s(\omega - m)\,. \tag{5.3.10}$$

The $\alpha \to 0$ divergence in the errors of the reconstructed spectral density in Eq. (5.3.9) can be mitigated and potentially cured by particular choices of smearing kernels, specifically those for which $\kappa_s(m)$ decays faster than $|\lambda_s|$ as $|s| \to \infty$, i.e. provided at least that their ILT exists. Taking the extreme case of uncorrelated data with $m = 0$ in Eq. (5.3.9), we would obtain $\mathcal{C}_\alpha(\omega, \omega') = \lim_{\alpha\to 0} \mathcal{H}_\alpha^{-1}(\omega, \omega')$, necessarily diverging when smearing is not included. We note that the diagonal contributions ($t = t'$) in covariance matrices enhance the oscillations of the coefficients in the linear combinations in Eqs. (5.3.5) and (5.3.6), while the inclusion of off-diagonal elements ($t \neq t'$) mitigates them.
We might also consider the case of a constant contribution to the error, interesting e.g. for disconnected correlation functions whose variance mixes with the vacuum. By considering $m = 0$ in Eq. (5.3.7), we obtain

$$\mathrm{Cov}(t, t') = 1 \quad \to \quad \rho_{\mathsf{c}}(\omega, \omega') = \delta(\omega)\delta(\omega')\,, \quad \mathcal{C}_\alpha(\kappa) \xrightarrow{\alpha\to 0} [\kappa(0)]^2\,. \tag{5.3.11}$$

While these formulae are promising, only a test on real data can verify their validity, as deviations from the assumptions made here are likely in practical applications.

5.3.2 Systematic errors

The formalism of Section 5.1 allows us to study different sources of systematic errors separately, and here we mainly focus on those induced by a finite temporal domain $t_{\max}$. We also comment on rounding errors and the choice of a non-zero regulating parameter.

Finite temporal domain

We can consider the case where the correlator $C(t)$ is only known on a finite temporal range $t \in [0, t_{\max}]$, e.g. the typical time subdomain accessible to lattice simulations, where we suppose that non-zero temperature effects are negligible. With this restriction, the operator to be inverted becomes

$$\int_0^{t_{\max}} dt\, e^{-(\omega+\omega')t} = \frac{1 - e^{-t_{\max}(\omega+\omega')}}{\omega + \omega'}\,. \tag{5.3.12}$$

At fixed $\alpha > 0$ and considering the continuous solution in Eq. (5.1.14), the systematic error due to the restriction to $t \in [0, t_{\max}]$ of the time integral is

$$\rho_\alpha(\omega) - \rho_{\alpha, t_{\max}}(\omega) = \int_s \frac{u_s^*(\omega)\lambda_s}{|\lambda_s|^2 + \alpha} \int_{t_{\max}}^\infty dt\, u_s^*(t) C(t)\,. \tag{5.3.13}$$

In field theories with a mass gap $\omega_{\mathrm{thr}} > 0$, the large-time behavior of correlation functions is bounded by $0 \leq |C(t)| \leq |C(t_{\max})| e^{-\omega_{\mathrm{thr}}(t - t_{\max})}$ for $t > t_{\max}$. From this bound, we find

$$\left| \int_{t_{\max}}^\infty dt\, C(t) u_s^*(t) \right| \leq \frac{|C(t_{\max})|}{\sqrt{2\pi\omega_{\mathrm{thr}}}\sqrt{\omega_{\mathrm{thr}} t_{\max}}}\,, \tag{5.3.14}$$

which leads, with little additional algebra, to

$$|\rho_\alpha(\omega) - \rho_{\alpha,t_{\max}}(\omega)| \leq \frac{|C(t_{\max})|}{2\pi\sqrt{\omega\omega_{\rm thr}}\sqrt{\omega_{\rm thr}t_{\max}}} \int_s \frac{|\lambda_s|}{|\lambda_s|^2+\alpha}\,. \tag{5.3.15}$$

This bound is finite as long as $\alpha > 0$ and exponentially suppressed by $|C(t_{\max})|$. A bound that applies independently of α can be derived from this result by using

$$\int_s \frac{|\lambda_s|}{|\lambda_s|^2+\alpha} \leq \int_s |\lambda_s| = \frac{\Gamma\left(\frac{1}{4}\right)^2}{\sqrt{2}\pi}\,, \quad \forall\,\alpha > 0\,. \tag{5.3.16}$$

Instead, from the concrete assumption $C(t) = c\,e^{-\omega_{\rm thr}t}$ at $t \geq t_{\max}$, we obtain

$$\int_{t_{\max}}^{\infty} dt\, u_s^*(t)C(t) = c\,u_s(\omega_{\rm thr})\lambda_s^*(\omega_{\rm thr}t_{\max})\,, \tag{5.3.17}$$

where $\lambda_s^*(x) \equiv \Gamma\left(\frac{1}{2} - is, x\right)$ is the upper incomplete Γ-function. The resulting systematic error

$$\rho_\alpha(\omega) - \rho_{\alpha,t_{\max}}(\omega) = c\int_s \frac{u_s^*(\omega)\lambda_s u_s(\omega_{\rm thr})}{|\lambda_s|^2+\alpha}\lambda_s^*(x)\,, \tag{5.3.18}$$

is bounded and exponentially suppressed in $x = \omega_{\rm thr}t_{\max}$, and it can be calculated explicitly provided that $\omega_{\rm thr}$ and c are known. A bound which applies $\forall\,\alpha > 0$ can again be introduced using Eq. (5.3.16), obtaining

$$|\rho_\alpha(\omega) - \rho_{\alpha,t_{\max}}(\omega)| \leq c\frac{\Gamma\left(\frac{1}{4}\right)^2}{2\pi\sqrt{2\pi}}\frac{\mathrm{Erfc}[\sqrt{\omega_{\rm thr}t_{\max}}]}{\sqrt{\omega_{\rm thr}t_{\max}}}\,. \tag{5.3.19}$$

As a consequence, the systematic difference between $\rho_\alpha(\omega)$ and the spectral density calculated by restricting the time interval in Eq. (5.1.14) to $[0, t_{\max}]$ vanishes exponentially in $\omega_{\rm thr}t_{\max}$. This is not sufficient for the thermal theory, where one should instead diagonalize the appropriate finite-temperature metric, similar to that in Eq. (5.3.12).

Fixing α a priori

The presence of a non-zero regulating parameter is associated to an additional smearing with δ_α, as seen in Section 5.1. In principle, we can keep $\alpha > 0$ fixed (even during the continuum extrapolation) and include this additional smearing as a part of the definition of the observables we want to extract. The $\alpha \to 0$ limit can then be studied only at the end of our calculations. Different choices of α are associated with observables affected by systematic biases of various sizes. We emphasize that any choice is valid, but we might want to set the value of α a priori by minimizing the associated systematic bias, leading to a final extraction which is closer to its true value, see also Appendix I.4. Thus, our focus here is on quantifying systematic errors stemming from any fixed choice of $\alpha > 0$, either via a direct estimate or a bound, both of which are in principle computable from lattice data.

Double reconstruction. We can directly estimate the systematic errors stemming from $\alpha > 0$. Given the solution of $\rho_\alpha(\omega)$ in Eq. (5.1.14), we introduce the corresponding approximated correlation function

$$C_\alpha(t) \equiv \int_\omega e^{-\omega t}\rho_\alpha(\omega) = \int_{t'} \delta_\alpha(t,t')C(t') \tag{5.3.20}$$

so that the difference

$$C(t) - C_\alpha(t) = \int_\omega e^{-\omega t}[\rho(\omega) - \rho_\alpha(\omega)] = \alpha \int_{t'} C(t') \int_s \frac{u_s(t)u_s^*(t')}{|\lambda_s|^2 + \alpha} \tag{5.3.21}$$

allows the systematic error $[\rho(\omega) - \rho_\alpha(\omega)]$ to be estimated via an additional ILT, e.g.

$$\rho(\omega) - \rho_\alpha(\omega) = \lim_{\beta\to 0} \int_t C(t) g_{\alpha,\beta}(t|\omega)\,, \quad g_{\alpha,\beta}(t|\omega) = \alpha \int_s \frac{u_s^*(\omega)\lambda_s u_s^*(t)}{(|\lambda_s|^2+\alpha)(|\lambda_s|^2+\beta)}\,. \tag{5.3.22}$$

Note that the integration of Eq. (5.3.22) with $\kappa(\omega)$ yields the estimate of the systematic error on the corresponding smeared ρ_κ. This strategy can be straightforwardly generalized to arbitrary regulating functionals.

Bound. We can also derive an upper bound for the difference $\rho_\kappa - \rho_{\kappa,\alpha}$ for the case of smeared spectral densities. Using the Schwartz inequality, we can isolate the effects of the approximate reconstruction from its physics content. In particular, we can define

$$\kappa_\alpha(\omega) \equiv \int_{\omega'} \delta_\alpha(\omega,\omega')\kappa(\omega')\,, \quad \rho_{\kappa,\alpha} = \int_\omega \kappa_\alpha(\omega)\rho(\omega) \tag{5.3.23}$$

so that a possible bound on the systematic error can be computed as

$$\begin{aligned} |\rho_\kappa - \rho_{\kappa,\alpha}|^2 &= \left| \int_\omega [\kappa(\omega) - \kappa_\alpha(\omega)]\rho(\omega) \right|^2 \\ &\leq \left(\int_\omega [\kappa(\omega) - \kappa_\alpha(\omega)]^2 \gamma(\omega) \right) \left(\int_\omega \rho(\omega)^2 \gamma(\omega)^{-1} \right) \end{aligned} \tag{5.3.24}$$

where $\gamma(\omega)$ is an arbitrary weight function that can be introduced to ensure the convergence of the second contribution, thereby also limiting the possible kernels for which this bound applies. We note that the first term is a measure of the systematic differences associated to the kernel reconstruction at fixed α, and it can be computed exactly. Instead, the second term encodes physical information on the spectral density and it can be estimated independently. For instance, if ρ allows to set $\gamma(\omega) = 1$, the first term is

$$\int_\omega [\kappa(\omega) - \kappa_\alpha(\omega)]^2 = \alpha^2 \int_{\omega\omega'} \kappa(\omega)\kappa(\omega') \int_s \frac{u_s^*(\omega)u_s(\omega')}{(|\lambda_s|^2+\alpha)^2} \tag{5.3.25}$$

and the second one might be approximated as

$$\int_\omega \rho(\omega)^2 \approx \int_\omega \rho_\alpha(\omega)^2 = \int_{tt'} C(t)C(t') \int_s \frac{u_s^*(t)|\lambda_s|^2 u_s(t')}{(|\lambda_s|^2+\alpha)^2}\,. \tag{5.3.26}$$

Alternatively, one may use sum rules or experimental data, if available.

Rounding errors

The formalism developed to treat statistical errors proves to be useful also in understanding how rounding errors, which affect all numerical simulations, impact spectral reconstructions. The case of constant noise has already been considered, see Eq. (5.3.11), so we can try to model rounding errors as white, uncorrelated noise, e.g.

$$\mathrm{Cov}(t,r) = \epsilon\eta(t)\eta(r)\,, \quad \langle\eta\rangle = 0\,, \quad \langle\eta(t)\eta(r)\rangle = \delta(t-r) \tag{5.3.27}$$

where we consider ϵ to be the machine precision, e.g. $\epsilon \approx 10^{-16}$ for double precision. In this case, we would obtain

$$\mathcal{C}_\alpha(\omega,\omega') = \epsilon \int_s u_s^*(\omega) \frac{|\lambda_s|^2}{(|\lambda_s|^2+\alpha)^2} u_s(\omega') \tag{5.3.28}$$

which does not converge in the $\alpha \to 0$ limit. To mitigate the effect of rounding, one might consider a restriction of the interval in s up to a maximum value s_{MAX}, with a similar effect achieved by imposing $\alpha \leq |\lambda_{s_{\mathrm{MAX}}}|^2$. Note that specific choices of the smearing kernel could also improve the reconstruction by mitigating the impact of rounding errors.

5.4 Preliminary numerical results: spectral densities from multilevel

In this Section, we present a preliminary study, extending our results published in Ref. [5] for the isovector vector spectral density, obtained from the corresponding Euclidean correlator estimated with high accuracy in Ref. [88] using the multilevel algorithm, see Chapter 4, with the same lattice setup described in Section 4.3. We recall that $n_0 = 25$ independent global (level-0) updates of the field configuration were alternated with $n_1 = 10$ level-1 updates of the local thick time-slices only, in order to achieve an exponential gain in the StN. The local, unimproved discretization of the vector current was used, and we take the renormalization factor Z_V at $\beta = 5.3$ from Ref. [192].

The underlying spectral density that we consider here corresponds to the light isovector contribution to the R-ratio, whose phenomenological importance has been highlighted in Subsection 3.3.2 and whose non-perturbative determination from first principles QCD is an active area of research [214]. In order to extract it from our finite-volume lattice setup, a smearing procedure is necessary, and we choose[12] to do it through the introduction of a non-zero Tikhonov regulating parameter α, extracting its smeared

[12] We recall that our procedure directly allows to extract the smearing of spectral densities with any other choice of the kernel, see also Eq. (3.3.10), e.g. the Gaussian kernel that we considered in our previous study of Ref. [5]

$$\rho_\sigma(\omega) \equiv \int_{\omega'} \mathfrak{G}_\sigma(\omega,\omega')\rho(\omega')\,, \quad \mathfrak{G}_\sigma(\omega,\omega') = \frac{1}{\sqrt{2\pi\sigma^2}} \exp\left\{-\frac{(\omega-\omega')^2}{2\sigma^2}\right\} \tag{5.4.1}$$

which reproduces a δ function in the limit $\sigma \to 0$. In this case, finite-volume effects are expected to be of order $O(e^{-\sigma L})$ as long as $\sigma \lesssim m_\pi$ [143]. In this case, Eq. (5.4.2) becomes $\rho(\omega) = \lim_{\sigma\to 0}\lim_{L\to\infty}\rho_\sigma(\omega)$.

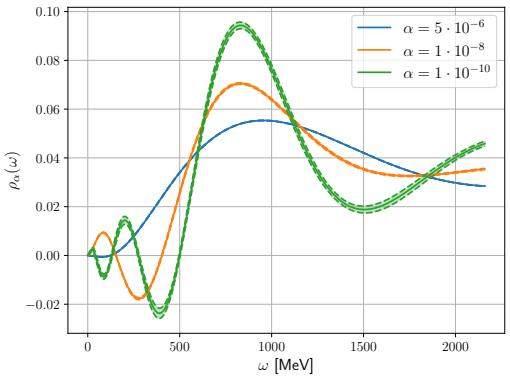

Figure 5.4: Light quark isovector vector spectral density $\rho_\alpha(\omega)$ from multilevel data at $N_f = 2 + 1$, as a function of ω and at different values of α.

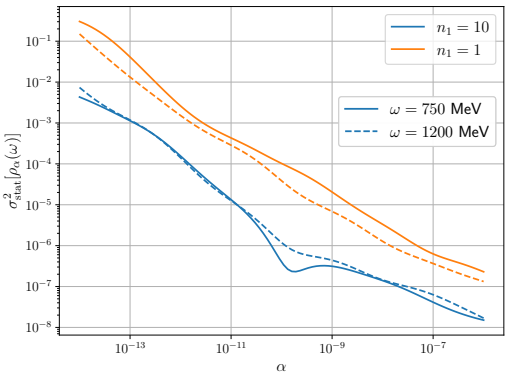

Figure 5.5: Scaling of the statistical errors on the reconstruction of $\rho_\alpha(\omega)$, see Eq. (5.3.5), as a function of α and for different choices of ω and n_1.

version with δ_α, namely ρ_α, see Eqs. (5.1.14) and (5.1.12)[13]. Notice that $\rho_\alpha(\omega)$ always implicitly depends on the spatial length L of the lattice, and the infinite-volume spectral density can only be recovered through the ordered double-limit

$$\rho(\omega) = \lim_{\alpha \to 0} \lim_{L \to \infty} \rho_\alpha(\omega) \tag{5.4.2}$$

where only the infinite-volume smeared spectral density, $\lim_{L\to\infty} \rho_\alpha(\omega)$, defines a valid quantity to be compared with smeared experimental data.

In Fig. 5.4 we show the extraction of the spectral density with our best multilevel data-set at $n_1 = 10$ for a few fixed values of α, as a function of the energy, which ranges from 0 up to $a\omega \simeq 0.9$. The behavior of the reconstruction with α can be understood from that of the smearing kernel δ_α, shown in Fig. 5.1a. Small values of α correspond to a narrow smearing width, with denser oscillations at small energies which visibly affect the reconstructed spectral density. At larger values of α, instead, such fluctuations are reduced in the IR region, with a larger smearing width that causes a smoother reconstruction. These oscillations are always less wild in the UV region, where they have a smaller impact on ρ_α. This behavior is also evident in Fig. 5.2a.
Similarly to Ref. [5], we can also observe a peak, which is compatible with the presence of a resonance, but further refinements are required to overcome the present limitations due to e.g. the unphysical pion mass, finite-volume [143] and discretization effects.

Although only slightly noticeable, in Fig. 5.4 the statistical errors on the reconstruction increase as we decrease α. The overall scaling of the coefficients with $\sqrt{\alpha}$ observed in Fig. 5.1b might qualitatively explain this behavior. In fact, even small statistical fluctuations of the correlation functions might get amplified in the delicate linear

[13] To be more precise, the smearing kernel is that induced by the discrete coefficients, and not by δ_α, which is instead defined from the continuum solution. Although different, these functions qualitatively share the same fluctuating features that we are interested in.

combinations with the oscillating coefficients, resulting in large statistical errors of the reconstructed spectral densities. In order to investigate this effect, in Fig. 5.5 we show the behavior of the square of statistical errors as a function of α for different values of ω, comparing also $n_1 = 10$ with $n_1 = 1$ cases to study the impact of multilevel on the reconstruction.
Considering any fixed values of α and ω, by comparing the multilevel results ($n_1 = 10$, blue lines) with classical, one-level algorithms ($n_1 = 1$, orange lines), at the energies we probe we observe a gain in the statistical error from multilevel, which agrees with our previous findings in Ref. [5]. This gain is more pronounced at low energies, where multilevel is expected to be more beneficial: with a number of configurations which is $n_1 = 10$ times larger, the observed gain in the statistical errors of ρ_α ranges between 30 and 80. The difference from the ideal $n_1^2 = 100$ gain in the scaling of the statistical errors was already observed in Ref. [88] and in Section 4.3 for the variance of $C(t)$, and it is compatible with the presence of a residual correlation among level-1 configurations. Even if smaller, the advantage of multilevel can also be observed at higher energies, since a more accurate estimation of correlation functions, although more effective in the IR region, typically leads to reduced errors in the linear combinations with the coefficients. Furthermore, we can appreciate that the behavior of the errors at fixed n_1 remains relatively consistent across different energy ranges, likely due to the interplay of IR and UV effects within the linear combination. A better theoretical and numerical understanding of these effects will be relevant to discriminate whether multilevel algorithms might play an important rôle also in the context of spectral reconstructions.

Before concluding this Chapter, we want to briefly discuss possible further developments of the topics discussed here. Our continuum solution allows for systematic studies of discretization effects, which can now be treated similarly to what was shown in Section 2.4 for the Symanzik improvement program. Instead, the study of finite-volume effects on spectral densities can be addressed employing the Lüscher formalism. Additionally, our discrete formula has been shown to be the one that minimizes discretization errors with evenly-distributed data, lacking the ideally geometrically-distributed data that would be best suited for a straightforward discretization of the continuum formula. Moreover, the behavior of statistical errors is still an active area of study, both theoretically and numerically. A comprehensive analysis of these effects lies beyond the scope of this Thesis and is deferred for future investigations, in order to achieve our long-term goal of accurately extracting spectral densities from Euclidean time correlation functions.

Conclusions and outlook

Smeared spectral densities from physics-motivated kernels provide access to phenomenologically relevant observables, such as inclusive hadronic cross sections, semi-leptonic decay rates, or non-static properties of the quark-gluon plasma, among others. In this Thesis, we have addressed two stumbling blocks that affect their non-perturbative extraction from first principles in QCD. As Lattice QCD is currently the only established framework for the first-principle study of this theory in its non-perturbative regime, we focus on extracting spectral densities from the Euclidean time dependence of correlation functions estimated in Lattice QCD.

The first issue we tackled has been that of deriving an explicit, analytic, integral solution of spectral densities in terms of Euclidean correlation functions. The problem can be phrased as that of computing an inverse Laplace transform, a notoriously ill-posed inverse problem that must be addressed in all cases where we are interested in directly extracting spectral densities. When their convolution with analytically known kernels is needed, an inverse problem is present whenever those kernels show non-analyticities, such as poles that extend beyond multiparticle thresholds.
The main contribution of this Thesis in this context is the explicit, analytical solution to perform this extraction. Spectral densities, as well as their smeared and subtracted versions, are expressed as the integral of correlation functions with analytically known, real and computable coefficients. This formalism has improved our comprehension of different sources of error, allowing for independent analysis of statistical errors and those induced by a finite temporal extent. The analytical control of the solution also offers a deeper understanding and potential quantification of discretization and finite-volume effects on spectral densities, which can be inferred from those of the correlation functions. Furthermore, we have derived an analytical solution to the discrete problem that maintains the remarkable property of being exact for any value of the lattice spacing on an infinite lattice.

In addition, we have addressed the StN problem that affects the computation of several correlation functions related to phenomenologically interesting quantities. In multilevel algorithms, the locality of the theory is exploited in order to achieve a beneficial exponential gain in the StN. However, the manifest locality is compromised once fermionic degrees of freedom are integrated out. The resulting non-local dependence of the fermion determinant on the gauge field limits our ability to simulate Lattice

QCD with fermions through multilevel algorithms. To address this, we have carefully defined a four-dimensional domain decomposition of the lattice, restoring the manifest locality of the theory, up to a small, non-local remainder which can be easily included into observables through a reweighting procedure. Using a one-dimensional domain decomposition, the effectiveness of this approach as a variance reduction technique has also been demonstrated in preliminary tests, including spectral reconstructions of the R-ratio.

Although many technical challenges remain to be addressed, our results represent a substantial theoretical advancement toward achieving competitive extractions of spectral densities, which is our ultimate, long-term goal.

Appendix A

Computational strategies in Lattice QCD

In this Appendix, we extend the discussion of computational strategies for Lattice QCD of Section 2.5. We refer to Ref. [82] for additional details.

The path integral formalism, paired with the Wick rotation to the Euclidean metric, allows for a statistical interpretation of expectation values of observables. For simplicity, let us consider a real scalar field ϕ with Euclidean space-time action $S[\phi]$. Identifying $p[\phi] = \frac{1}{Z}e^{-S[\phi]}$, and defining the partition function $Z = \int [d\phi]e^{-S[\phi]}$ with $[d\phi] = \prod_x d\phi(x)$, it is possible to study path integral averages of observables $\mathcal{O} = \mathcal{O}[\phi]$

$$\langle \mathcal{O} \rangle = \int [d\phi] p[\phi] \mathcal{O}[\phi] \tag{A.0.1}$$

so that Lattice QCD resembles a classical statistical system, where the states (the field configurations) have a definite probability. All the following algorithms are based on the assumption that such a probabilistic representation of the theory exists[1]. Given a representative ensemble, namely a set of fields $\{\phi_1, \ldots, \phi_N\}$ where each configuration satisfies $\phi_i \sim p[\phi]$ such that the number of fields in a region $\mathcal{R}$ is $\int_{\mathcal{R}} [d\phi] p[\phi] + O\left(\frac{1}{\sqrt{N}}\right)$,

[1] In the case of full QCD, slight modifications to the above discussion must be made. Being Grassmann variables, fermionic degrees of freedom must be integrated out before computing expectation values for a probability distribution $p[U]$ depending only on the gauge field configuration U. For instance, for two degenerate quarks we have a similar representation as Eq. (A.0.1)

$$\langle \mathcal{O} \rangle = \int [dU] p[U] \mathcal{O}[U] \,, \quad p[U] = \frac{1}{Z} \{\det D[U]\}^2 e^{-S_{\mathrm{G}}[U]} \tag{A.0.2}$$

in terms of the standard gluonic action $S_{\mathrm{G}}[U]$, of the Dirac operator D, and of the partition function

$$Z = \int [dU] \{\det D[U]\}^2 e^{-S_{\mathrm{G}}[U]} \,, \quad [dU] = \prod_{x,\mu} dU_\mu(x) \,. \tag{A.0.3}$$

If an additional, non-degenerate quark is added, its determinant is commonly treated by means of rational approximations [95–97].

we can estimate the expectation value in Eq. (A.0.1) as

$$\langle \mathcal{O} \rangle = \frac{1}{N} \sum_{i=1}^{N} \mathcal{O}[\phi_i] + O\left(\frac{1}{\sqrt{N}}\right) \tag{A.0.4}$$

with the last term representing statistical errors. Note that translational symmetry is preserved by periodic boundary conditions (which are the most common choice, except for anti-commuting quark fields having anti-periodic ones in time) and can be exploited to further reduce statistical errors, profiting from available data on the full lattice.

The statistical interpretation of expectation values of observables allows us to generate field configurations employing strategies which are common for thermal systems in statistical mechanics, such as importance sampling to generate field configurations given their probability distribution $\propto e^{-S}$, with S being the Euclidean classical action. In Section A.1, we briefly introduce the concept of Markov chains before describing two algorithms to achieve the above task, namely the Metropolis-Hastings [91, 92] and the Hybrid Monte Carlo [93] ones. A more recent simulation paradigm is also discussed, namely master-field simulations [81, 100] at large volumes. Given a representative ensemble, Section A.2 in dedicated to the discussion of measurement strategies. These simulation algorithms also allow for a statistical interpretation of the associated errors, whose computation is detailed in Section A.3.

A.1 Simulation strategies: Monte Carlo and beyond

In this Section, we are interested in the generation of a representative field ensemble given the underlying probability distribution of the field(s).

A.1.1 Markov chains

Let us consider a set of states $\{\phi_k\}_{k=1}^{N}$ and define the following quantities:

- $P_{jk} \equiv P(\phi_j \to \phi_k)$ is the transition probability from state ϕ_j to ϕ_k;
- a_k is the probability that the initial state is ϕ_k;
- $P_{jk}^{(n)}$ is the probability that, starting from the state ϕ_j, the final state after n transitions is ϕ_k;
- $f_{jk}^{(n)}$ is the probability that, starting from the state ϕ_j, the state ϕ_k is reached for the first time after n steps.

We can define a *Markov chain* as a discrete stochastic process where the probability of obtaining the sequence of states ϕ_1, ϕ_2, …, ϕ_n is given by

$$P(\phi_1, \phi_2, \ldots, \phi_n) = a_1 \times P(\phi_1 \to \phi_2) \times \cdots \times P(\phi_{n-1} \to \phi_n)\,. \tag{A.1.1}$$

The state ϕ_j is called *ergodic* if it is

1. *recurrent*, i.e. $f_{jj} \equiv \sum_{n=1}^{\infty} f_{jj}^{(n)} = 1$;

2. *aperiodic*, i.e. $\nexists\, t > 1$: $P_{jj}^{(n)} = 0 \;\forall\, n \neq vt$ for some v;

3. *not null*, i.e. it has a finite average return time $\mu \equiv \sum_{n=1}^{\infty} n f_{jj}^{(n)} < \infty$.

Ergodic Markov chains are Markov chains with all ergodic states[2]. Starting from a state within a Markov chain, the latter is called *irreducible* if any other state that can be reached is still within the same chain. It can be proven that for ergodic and irreducible Markov chains a unique equilibrium probability distribution $\pi_k = \lim_{n\to\infty} P_{jk}^{(n)} \;\forall\, j$ always exists, which is invariant i.e. $\pi_k = \sum_i \pi_i P_{ik}$.
As described before, we are interested in generating field configurations with a given proability distribution. A possible way to define a Markov chain that, in the limit of large Markovian time, reaches a target probability distribution $\mathcal{P}_i = \frac{R_i}{\sum_j R_j}$ with $R_i \geq 0$ $\forall\, i$ (in our case, $R_i = R[\phi_i] = e^{-S[\phi_i]}$) is given by the *detailed balance condition*

$$R_i P_{ij} = R_j P_{ji}\,. \tag{A.1.2}$$

As seen above, if the Markov chain is ergodic, namely if $\inf_{\phi_j,\phi_k} P_{jk} > 0$, then it has a unique, invariant fixed point distribution. We can take

$$P_{jk} = P_M(\phi_j \to \phi_k) + \delta(\phi_i - \phi_k)\left[1 - \int [d\phi] P_M(\phi_i - \phi)\right], \quad P_M \geq 0 \tag{A.1.3}$$

such that $\int [d\phi_k] P_{jk} = 1 \;\forall\, \phi_j$. If P_M satisfies the detailed balance condition

$$P_S(\phi_j) P_M(\phi_j \to \phi_k) = P_S(\phi_k) P_M(\phi_k \to \phi_j)\,, \tag{A.1.4}$$

then P_S is the fixed point probability distribution for the Markov chain defined with P_{jk} as transition probability. Here P_S is the analogous of $\mathcal{P}$, defining R in Eq. (A.1.2).

A.1.2 Metropolis-Hastings

In order to generate an arbitrary distribution, the detailed balance condition must be met, see Eq. (A.1.2). To do so, we can employ the Metropolis-Hastings algorithm [91,92]:

1. given an initial state ϕ_j, we propose ϕ_k with any probability Q_{jk};

2. we accept ϕ_k with acceptance probability $A_{jk} = \min\left[1, \frac{R_k Q_{kj}}{R_j Q_{jk}}\right]$.

For the case of a real scalar field, we need to consider the detailed balance condition in Eq. (A.1.4). We choose $P_M(\phi_j \to \phi_k) = P_C(\phi_j \to \phi_k) P_A(\phi_j \to \phi_k)$ where $P_C(\phi_j \to \phi_k)$ and $P_A(\phi_j \to \phi_k)$ are respectively the probability of proposing and accepting a new

[2]It can be proven that the states of a Markov chain are all of the same kind, namely it is sufficient for one state to be ergodic for all of the states of the same Markov chain to be ergodic as well, i.e. for the entire Markov chain to be ergodic.

configuration ϕ_k. The detailed balance condition in Eq. (A.1.4) can be satisfied $\forall\, P_C$ with a similar choice as for A_{jk} above, namely taking $P_A(\phi_j \to \phi_k) = \min\left[1, \frac{P_S(\phi_k)P_C(\phi_k\to\phi_j)}{P_S(\phi_j)P_C(\phi_j\to\phi_k)}\right]$. If P_C is symmetric, i.e. if $P_C(\phi_j \to \phi_k) = P_C(\phi_k \to \phi_j)$, we find

$$P_A(\phi_j \to \phi_k) = \min\left[1, e^{-\Delta S}\right], \quad \Delta S = S[\phi_k] - S[\phi_j]\,. \tag{A.1.5}$$

The Metropolis-Hastings algorithm then consists of the following steps:

1. the initial configuration ϕ_0 can be generated arbitrarily, since the results are independent of this choice;

2. starting from the current configuration ϕ_n, we need to formulate a proposal ϕ'_n for the update of the field. A possible choice is to fix a lattice point x' and define $\phi'_n(x) = \phi_n(x) + \delta_{x,x'}\Delta\left(r - \frac{1}{2}\right)$, with $\Delta > 0$ and r a random number uniformly distributed in $[0, 1)$, i.e. with a uniform and symmetric P_C. This proposal is therefore accepted with a probability given by P_A in Eq. (A.1.5). Notice the locality of the algorithm: at each step, the proposed configuration differs from the previous one at most by the field configuration in one point. If the action is local, this observation greatly simplifies the computation of ΔS in Eq. (A.1.5).

3. One sweep corresponds to a single iteration of the previous proposal step with the corresponding update or reject for all the points x' of our lattice. The observables can be computed at each sweep, to then estimate

$$\langle \mathcal{O} \rangle \simeq \frac{1}{N - n_{\text{therm}}} \sum_{n=n_{\text{therm}}}^{N} \mathcal{O}[\phi_n] + O\left(\frac{1}{\sqrt{N - n_{\text{therm}}}}\right) \tag{A.1.6}$$

   where n_{therm} denotes the number of sweeps skipped before starting the measurements, allowing to perform them once the probability distribution has thermalized i.e. reached the desired equilibrium one.

Notice that an ideal Markov chain thermalizes rapidly, keeping a high acceptance rate at a low computational cost, while also having negligible autocorrelations.

A.1.3 Hybrid Monte Carlo

The field updates studied for the Metropolis-Hastings algorithm above are local, implying a slow exploration of the configuration space. Furthermore, local algorithms usually show increasing autocorrelations with the dimensionality of the system. It is therefore useful to design a way to perform global updates which are also coherent to avoid low acceptance rates. The Hybrid Monte Carlo (HMC) algorithm [93] satisfies these requirements.
The HMC algorithm relies on the Hamiltonian formalism, and here we present it for the simple case of a real, scalar theory, with the generalization to non-Abelian gauge theories similar to what we presented in Subsection 2.5.2 for the case of Lattice QCD with fermions. We can follow the same steps detailed for that case, and here we recall

that the fields ϕ of the theory, with Euclidean time action $S[\phi]$, and the auxiliary conjugate moments π with quadratic action, satisfy Hamilton equations in Eq. (2.5.10) with simulation time τ, which we rewrite for our case as[3]

$$\begin{aligned} \frac{d\phi(\tau,x)}{d\tau} &= \frac{\delta H[\phi,\pi]}{\delta\pi(\tau,x)} = \pi(\tau,x)\,, \\ \frac{d\pi(\tau,x)}{d\tau} &= -\frac{\delta H[\phi,\pi]}{\delta\phi(\tau,x)} = -\frac{\delta S[\phi]}{\delta\phi(\tau,x)} \equiv -\mathcal{F}(\tau,x)\,. \end{aligned} \tag{A.1.7}$$

Integration of Molecular Dynamics equations

Since MD equations in Eq. (A.1.7), see also Eq. (2.5.10), cannot be solved exactly for any arbitrary form of the action, and thus of the force $\mathcal{F}$, their numerical solution is required. Different integration schemes have been devised, the most common ones being for instance the leap-frog and Omelyan integrators [94] of different orders (i.e. with different scalings of the error as powers of the integration step). In order to provide an explicit example, we present the leap-frog integrator (LPF). We first need to divide the integration interval $[0,\tau_0]$ in N_0 sub-intervals of size $\delta\tau$ such that $\tau_0 = \delta\tau\, N_0$. Note that MD equations imply

$$\begin{aligned} \pi(\tau+\delta\tau) &= \pi(\tau) - \delta\tau\,\mathcal{F}(\tau) + O\left(\delta\tau^2\right)\,, \\ \phi(\tau+\delta\tau) &= \phi(\tau) + \delta\tau\,\pi(\tau) + O\left(\delta\tau^2\right) \end{aligned} \tag{A.1.8}$$

which can be rewritten up to $O\left(\delta\tau^2\right)$ errors also as

$$\begin{aligned} \begin{pmatrix} \pi(\tau+\delta\tau) \\ \phi(\tau) \end{pmatrix} &= \begin{pmatrix} \pi(\tau) - \delta\tau\,\mathcal{F}(\tau) \\ \phi(\tau) \end{pmatrix} \equiv I_\pi(\delta\tau) \begin{pmatrix} \pi(\tau) \\ \phi(\tau) \end{pmatrix}\,, \\ \begin{pmatrix} \pi(\tau) \\ \phi(\tau+\delta\tau) \end{pmatrix} &= \begin{pmatrix} \pi(\tau) \\ \phi(\tau) + \delta\tau\,\pi(\tau) \end{pmatrix} \equiv I_\phi(\delta\tau) \begin{pmatrix} \pi(\tau) \\ \phi(\tau) \end{pmatrix}\,. \end{aligned} \tag{A.1.9}$$

The LPF integration strategy consists in alternating updates of the fields π and ϕ as

$$\begin{pmatrix} \pi(\tau_0) \\ \phi(\tau_0) \end{pmatrix} = I_{\mathrm{LPF}}(N_0,\delta\tau) \begin{pmatrix} \pi(0) \\ \phi(0) \end{pmatrix} \tag{A.1.10}$$

with[4]

$$I_{\mathrm{LPF}} = \left[I_\pi\left(\frac{\delta\tau}{2}\right) I_\phi(\delta\tau) I_\pi\left(\frac{\delta\tau}{2}\right) \right]^{N_0} = I_\pi\left(\frac{\delta\tau}{2}\right) \left[I_\phi(\delta\tau) I_\pi(\delta\tau) \right]^{N_0-1} I_\phi(\delta\tau) I_\pi\left(\frac{\delta\tau}{2}\right)\,. \tag{A.1.11}$$

[3] For each lattice site, the field $\pi(x)$ in Subsection 2.5.2 was element of the symmetry group algebra, while in this simple case it simply is a scalar (number). In the computation of the derivatives in Eq. (A.1.7), for the non-Abelian case we have additional indices and need to correctly consider the non-commuting group structure.

[4] In principle, it is possible to define I_{LPF} also as $I_{\mathrm{LPF}} = \left[I_\phi\left(\frac{\delta\tau}{2}\right) I_\pi(\delta\tau) I_\phi\left(\frac{\delta\tau}{2}\right) \right]^{N_0}$. These two choices lead to compatible results, and we simply pick one to define the HMC algorithm.

Despite H not being exactly conserved, since MD equations are not exactly solved, the LPF integrator (as others also employed in Lattice QCD) is a *symplectic* integrator, i.e.

- it is time-reversible: $I_{\mathrm{LPF}}(N_0, -\delta\tau) I_{\mathrm{LPF}}(N_0, \delta\tau) = 1 \ \forall\, N_0,\ \delta\tau$;
- it conserves phase-space measure: $[d\pi(\tau_0)][d\phi(\tau_0)] = [d\pi(0)][d\phi(0)]$

implying the conservation of a shadow Hamiltonian $\widetilde{H}[\phi, \pi] = H[\phi, \pi] + O\left(\delta\tau^2\right)$ along the time evolution defined by the LPF integrator.

The algorithm

We can now define the HMC algorithm, as done in Subsection 2.5.2, summarized below for the choice of a leapfrog integrator to solve MD equations in Eqs. (A.1.9). A single global and coherent update of the field configuration consists in the following scheme.

1. A field $\pi_0(x)$ is generated with Gaussian probability $P_G[\pi] = \frac{1}{Z_\pi} e^{-\frac{1}{2}\sum_x \pi(x)^2}$ i.e. with quadratic action in moments, independently of previous configurations.

2. The starting configuration $\phi_0(x)$ must be set. The first configuration of the Markov chain can be arbitrarily defined, since results do not depend on this choice (as it happened for the Metropolis-Hastings algorithm). For each step following the first, $\phi_0(x)$ is instead set as the one reached at the previous step.

3. We need to set initial conditions for MD equations at $\tau = 0$: $\phi_0(x) \to \phi(0, x)$, $\pi_0(x) \to \pi(0, x)$. After fixing τ_0 and $\delta\tau$, the system is evolved until $\tau = \tau_0$ by integrating out MD equations with the LPF integrator with step $\delta\tau$. The transition probability is

$$P_{\mathrm{LPF}}((\phi_0, \pi_0) \to (\phi', \pi')) = \delta(\phi' - \phi(\tau_0))\delta(\pi' - \pi(\tau_0))\,. \tag{A.1.12}$$

4. The proposed configuration $(\phi', \pi') = (\phi(\tau_0, x), \pi(\tau_0, x))$ would be accepted if MD equations were exactly integrated. To account for integration errors and ensure detailed balance, an accept-reject step is applied with acceptance probability

$$P_A((\phi_0, \pi_0) \to (\phi', \pi')) = \min\left[1, e^{-\Delta H}\right], \quad \Delta H = H[\phi', \pi'] - H[\phi_0, \pi_0]\,. \tag{A.1.13}$$

We shall now prove that the algorithm designed above is ergodic and it has the correct fixed point distribution. In fact, the resulting transition probability for ϕ is

$$P_M(\phi \to \phi') = \int [d\pi][d\pi'] P_G[\pi] P_{\mathrm{LPF}}((\phi, \pi) \to (\pi', \phi'))\, P_A((\phi, \pi) \to (\phi', \pi'))\,, \tag{A.1.14}$$

so that $P_S[\phi] P_M(\phi \to \phi') = P_S[\phi'] P_M(\phi' \to \phi)$ i.e. P_M satisfies the detailed balance condition in Eq. (A.1.4) with respect to the desired distribution $P_S[\phi] = \frac{1}{Z} e^{-S[\phi]}$. This ensures that the transition probability defined in Eq. (A.1.3), with P_M defined in Eq. (A.1.14), has the correct fixed point distribution.

A.1.4 Master-field simulations

A widely adopted strategy in Lattice QCD is that of master-field simulations [81, 100]. Numerical simulations of Euclidean lattice field theories usually proceed by generating an ensemble of representative fields through a Markov process, as detailed above. The ensemble averages of the observables of interest then provide stochastic estimates of their field-theoretical expectation values. The idea here is both simple and very promising: if theories are simulated on very large lattices, accurate results for the expectation values may be obtained from a single representative field by applying averages of expectation values on small, local and (ideally completely) independent blocks.

In Lattice QCD, the field variables in distant regions of a physically large lattice fluctuate largely independently, a property that may be referred to as *stochastic locality*. It is possible to compute translational averages over the entire lattice

$$\langle\!\langle \mathcal{O}(x) \rangle\!\rangle \equiv \frac{1}{V} \sum_z \mathcal{O}(x+z) = \langle \mathcal{O}(x) \rangle + O\left(V^{-1/2}\right). \tag{A.1.15}$$

and their errors

$$\begin{aligned} \langle (\langle\!\langle \mathcal{O}(x) \rangle\!\rangle - \langle \mathcal{O}(x) \rangle)^2 \rangle &= \frac{1}{V} \sum_y \langle \mathcal{O}(y)\mathcal{O}(0) \rangle_c = \frac{1}{V} \left[\sum_{|y| \le R} \langle \mathcal{O}(y)\mathcal{O}(0) \rangle_c + O\left(e^{-mR}\right) \right] \\ &= \frac{1}{V} \left[\sum_{|y| \le R} \langle\!\langle \mathcal{O}(y)\mathcal{O}(0) \rangle\!\rangle_c + O\left(e^{-mR}\right) + O\left(V^{-1/2}\right) \right], \end{aligned} \tag{A.1.16}$$

where m describes the exponential decay of the correlator at large distances, while

$$\sum_{|y| \le R} \langle\!\langle \mathcal{O}(y)\mathcal{O}(0) \rangle\!\rangle_c = \frac{1}{V} \sum_{|y| \le R} \sum_z \left[\mathcal{O}(y+z) - \langle\!\langle \mathcal{O}(y) \rangle\!\rangle \right] \left[\mathcal{O}(z) - \langle\!\langle \mathcal{O}(0) \rangle\!\rangle \right] \tag{A.1.17}$$

and the $O\left(e^{-mR}\right)$, $O\left(V^{-1/2}\right)$ terms are respectively the systematic and statistical contributions to the error of the error. Translational averages thus allow us to define unbiased estimators for expectation values and to estimate the corresponding errors up to exponentially small statistical uncertainties, and with power-like volume effects which are negligible as long as we consider very large lattices. These FVEs might dominate over other smaller but less controlled FVEs, eventually allowing to ignore them, as detailed below for some of the many interesting applications of master-field simulations.

Topology fixing. The topological charge density $q(x)$ defines the topological charge of the gauge field $Q = \int d^4x\, q(x)$, see Eq. (1.1.10). The $SU(3)$ group has a non-trivial topology and in the continuum formulation of the gauge theory its phase space is divided into disjoint regions which are labeled by distinct values of Q. If the theory is studied on a lattice, it turns out that the links' phase space is not disjoint: regions with a different Q from its continuum limit correspond to a small probability e^{-S}, i.e. at sufficiently small

lattice spacing configurations do not cross regions with fixed Q. Therefore, Lattice QCD must be simulated with the correct fixed topology, even though QCD is not a theory with a fixed topology, thus introducing unphysical FVEs in the simulations. In fact, fixed-topology simulations give results for local correlation functions that differ from their exact field-theoretical values by terms of $O(V^{-1})$. Yet, in master-field simulations these effects are parametrically smaller[5] than the statistical errors of $O(V^{-1/2})$. This shows that master-field simulations can provide a solution to the infamous topology-freezing problem in Lattice QCD if the physical size of the lattice is large enough.

HMC. The use of global operations seems to be unnatural in local theories, but it should be reconsidered when very large lattices are simulated. For instance, global operations are necessary to evaluate ΔH in the accept-reject step of the HMC algorithm, correcting for the inexact numerical integration of MD equations. Due to floating point errors with alternating signs, $\Delta H \propto \sqrt{V}\epsilon^p$ (rather than $V\epsilon^p$), where ϵ is the step size of the MD integrator of order p. The acceptance probability is computed as $\min\left[1, e^{-\Delta H}\right]$, which means that we need $\epsilon \propto V^{-\frac{1}{2p}}$ for a reasonable acceptance rate. Furthermore, the computation of ΔH is affected by a loss of significance.
These problems are caused by the use of global operations and can be therefore avoided by updating the field variables in a small, local block (sub-lattice) while keeping the other field variables fixed. In this way, the error on the accept-reject step are proportional to the (small) volume of this block, even if more accept-reject steps are needed in order to update the field configuration on the whole lattice. The localization of the simulation is relatively straightforward for a pure gauge theory, but it is highly non-trivial in presence of the sea quarks. In Chapter 4 a one-dimensional division of the lattice in (thick) time slices allows to solve this issue for fermionic theories, alongside with our new proposal for localizing the algorithm with a four-dimensional domain decomposition.

A.2 Measurement strategies: the computation of quark propagators

Besides the generation of gauge-field configurations, the most time-consuming aspect of a full Lattice QCD study is the measurement part, namely the computation of quark propagators. This ultimately amounts to inverting the Dirac equation

$$D\psi(x) = \eta(x) \tag{A.2.1}$$

with the massive lattice Dirac operator D, the known source $\eta(x)$ and the desired solution $\psi(x)$. The usual method to solve this linear equation is to minimize the residue

$$r(x) = \eta(x) - D\varphi(x) \tag{A.2.2}$$

[5]Note that, if a single representative field is generated, all the computational work is done in the thermalization phase required for the Markov chain to reach its fixed point. In order to reduce the cost, the fields are usually initialized from thermalized configurations on smaller lattices through reflections at the lattice planes, allowing for fixed-topology effects to be of $O(V^{-1})$ and not larger.

of the approximated solution $\varphi(x)$. This can be achieved by applying iterative methods, the most common ones being Krylov-space solvers such as (generalized) conjugate gradient methods. The solution ψ_n at the n-th step is found as the one with minimal norm of the residue $r_n = \eta - D\psi_n$ within the n-th dimensional Krylov space $\mathcal{K}_n$, which is the complex linear space generated by η, $D\eta$, $D^2\eta$, ..., $D^{n-1}\eta$. For instance, the generalized conjugate gradient method leads to the solution

$$\psi_n = \sum_{l=0}^{n-1} \sum_{j=0}^{l} c_l \, a_{lj} \, r_j \tag{A.2.3}$$

with known coefficients $\{c_l\}_{l=0}^{n-1}$ and $\{a_{lj}\}_{l=0,\dots,n-1}^{j=0,\dots,l}$ from

$$r_n = \eta - \sum_{l=0}^{n-1} \langle \chi_l, \eta \rangle \chi_l \,, \quad \chi_l = \sum_{j=0}^{l} a_{lj} D \, r_j \tag{A.2.4}$$

where $r_0 = \eta$ and $\{\chi_l\}_{l=0}^{n-1}$ is any orthonormal basis of $D\mathcal{K}_n$, and usually $n \in [16, 32]$.

A.2.1 Preconditioning

A common strategy to substantially improve the convergence properties of the iterative methods used to invert the Dirac equation is to precondition the initial equation, i.e. to solve a slightly modified one $LDR\phi = L\eta$ for ϕ, to then recover the solution as $\psi = R\phi$, with ideally $D \approx L^{-1}R^{-1}$. A common choice for the Wilson–Dirac operator is to apply even-odd preconditioning. We can apply an even-odd lattice decomposition and compute

$$D = \begin{pmatrix} D_{\mathrm{ee}} & D_{\mathrm{eo}} \\ D_{\mathrm{oe}} & D_{\mathrm{oo}} \end{pmatrix}, \quad L = \begin{pmatrix} 1 & -D_{\mathrm{eo}} D_{\mathrm{oo}}^{-1} \\ 0 & 1 \end{pmatrix}, \quad R = \begin{pmatrix} 1 & 0 \\ -D_{\mathrm{oo}}^{-1} D_{\mathrm{oe}} & 1 \end{pmatrix} \tag{A.2.5}$$

with the diagonal blocks D_{ee}, D_{oo} defined as the projection of the initial matrix to even, odd domains, thus avoiding mixing different lattice points and being easy to invert. The preconditioned system amounts to inverting

$$LDR = \begin{pmatrix} \hat{D} & 0 \\ 0 & D_{\mathrm{oo}} \end{pmatrix}, \quad \hat{D} = D_{\mathrm{ee}} - D_{\mathrm{eo}} D_{\mathrm{oo}}^{-1} D_{\mathrm{oe}} \tag{A.2.6}$$

where inverting the Schur complement $\hat{D}$ is usually 2× or 3× faster than doing so for D. Another common choice is to define a preconditioner through the Schwarz alternating procedure [187–191], see also Subsection 4.2.3.

A.2.2 Low-mode deflation

As already detailed in Subsection 1.4.2, the spontaneous breaking of chiral symmetry is related to the low modes of the Dirac operator through the Banks-Casher relation, see Eq. (1.4.30). It is both physically intuitive and numerically recommended at small

quark masses to treat these modes independently of the other ones. The idea is to project and exactly compute the solution on the space spanned by the first (smallest) few eigenvalues. The solution on the remaining space can be found by solving a better-conditioned system with standard, iterative algorithms.
The computation of the lowest eigenvalues and the corresponding eigenvectors might get prohibitively expensive, since the required computer time grows rapidly with the lattice volume[6]. In order to overcome this issue, a deflation strategy has been defined that does not require the exact knowledge of the low modes. It is possible to study the solution projected on the subspace generated by any set $\{\phi_k\}_{k=1}^N$ of N orthonormal quark fields, with $P\psi = \sum_{k=1}^N \phi_k \langle \phi_k | \psi \rangle$. Defining the projectors

$$P_L = 1 - DP(PDP)^{-1}P\,, \quad P_R = 1 - P(PDP)^{-1}PD \tag{A.2.7}$$

and the projections

$$\psi_{\|} = (1 - P_R)\psi\,, \quad \psi_{\perp} = P_R\eta\,, \quad \eta_{\|} = (1 - P_L)\eta\,, \quad \eta_{\perp} = P_L\eta \tag{A.2.8}$$

we can split the Dirac equation into two decoupled equations

$$D\psi_{\|} = \eta_{\|}\,, \quad D\psi_{\perp} = \eta_{\perp}\,. \tag{A.2.9}$$

The solution $\psi_{\|} = P(PDP)^{-1}\eta$ can be easily found, and $\psi_{\perp}$ can be computed with standard iterative methods through the inversion of $\hat{D} = P_L D(1 - P)$ (usually with an additional preconditioning step), a system which might be better conditioned than D, depending on how much $1 - P$ effectively approximates the subspace spanned by the low modes of $D^\dagger D$. A possible strategy is to introduce a domain decomposition of the lattice in non-overlapping blocks to define P as the projector on a set of orthonormal fields on each block. In this case, an important rôle is played by the property of *local coherence* [82], i.e. the requirement of $O(V)$ low modes of the Dirac operator aligning to a lower dimensional linear space on each small block of lattice points.

A.2.3 Random sources

The main idea of using random sources [82, 103] is to exploit the decoupling of link variables in distant regions of a large lattice to average over almost independently sampled hadron propagators computed at a set of stochastically selected and distant source points, reducing statistical fluctuations but increasing computational costs, since quark propagators must be recomputed at each point. Random sources can be regarded as

[6] Recall the Banks-Casher relation $\lim_{\lambda\to 0}\lim_{m\to 0}\lim_{V\to\infty}\rho(\lambda, m) = \frac{1}{\pi}\Sigma$, see Eq. (1.4.30), where $\Sigma = -\lim_{m\to 0}\lim_{V\to\infty}\langle \overline{u}u\rangle$ is the quark condensate, $\rho(\lambda, m) = \frac{1}{V}\sum_{k=1}^{\infty}\langle \delta(\lambda - \lambda_k)\rangle$ is the average spectral density of the eigenvalue $\lambda = \lambda_k + im$ of the Dirac operator with mass m, and λ_k are the eigenvalues of the massless Dirac operator. It follows that the number of low modes of $D^\dagger D$ with eigenvalues $\alpha_k = m^2 + \lambda_k^2 \leq M^2$ is $\nu(M, m) \simeq \frac{2}{\pi}\Lambda\Sigma V$, $\Lambda^2 = M^2 - m^2$. Since $\nu(M, m) \sim V$, an effective deflation of the Dirac equation requires $O(V)$ deflated modes, with $O(V^2)$ cost.

a set of additional fields that are decoupled from the dynamical ones (the degrees of freedom of the theory). Therefore, physical quantities are independent of the details of the generation of such sources. For Gaussian random fields, for instance, we can consider a multiplet of pseudo-fermion fields on the fixed-time spatial lattice $\{\eta_i(\mathbf{x})\}_{i=1}^{N_s}$ with quadratic action $S_s[\eta] = \sum_{i=1}^{N_s}\langle\eta_i,\eta_i\rangle$ such that $\langle\eta_i(\mathbf{x})\eta_j(\mathbf{y})^\dagger\rangle_s = \delta_{ij}\delta_{\mathbf{x}-\mathbf{y}}$. We randomly generate the source fields with probability density $\propto e^{-S_s[\eta]}$ for each gauge-field configuration in a representative field ensemble. We consider observables $\mathcal{O}[U,\eta]$ depending both on the gauge field U and on the random sources η, easily recovering (using Wick's theorem, as long as $\mathcal{O}[U,\eta]$ is a polynomial in η) ordinary (non-stochastic) observables by integrating out the sources. For instance

$$\mathcal{O} = \frac{1}{N_s}\sum_{i=1}^{N_s}\sum_{\mathbf{x},\mathbf{y}}\eta_i(\mathbf{x})^\dagger S(x,y)\big|_{x_0=y_0}\eta_i(\mathbf{y})\,, \quad \langle\mathcal{O}\rangle_s = \sum_{\mathbf{x}}\mathrm{Tr}\{S(x,x)\} \tag{A.2.10}$$

allowing the trace in the last equation to be estimated stochastically. These sources allow to reduce statistical fluctuations thanks to volume averages, being beneficial in many cases e.g. for the computation of the pion propagator. Additional refinements can be made, e.g. combining this strategy with low-mode averaging [104–106], with additional care to be put for the estimation of single-trace propagators and differences of propagator traces for disconnected correlation functions, see Ref. [99] and the discussion in Appendix H. In general, we emphasize the need to carefully analyze the variance of any proposed stochastic observable before applying random source methods in order to achieve a good scaling of statistical errors with the lattice volume.

A.3 Statistical analysis

Building on the results discussed so far, we are now able to extract physical observables from Lattice QCD simulations. Besides, we must be able to provide a consistent error estimation, since any measurement without the knowledge of its uncertainty is completely meaningless. This is based on correct error propagation, which usually is a non-trivial task due to non-linearities in the measurement process. Resampling techniques, such as the jackknife or the bootstrap methods, allow to estimate errors with minimal efforts with the assumption of negligible correlations, while the slightly more involved Γ-method [252] is always able to provide a conservative error estimate. We are now going to describe these strategies, and for further discussions on this topic we refer to Refs. [253,254]. Also, for practical purposes, the error analysis in this Thesis has been performed with the `pyobs` package [255].

Let us consider N measurements $\mathcal{O}_i$ of an observable $\mathcal{O}$ performed at the equilibrium configurations ϕ_i, i.e. $\mathcal{O}_i = \mathcal{O}[\phi_i]$, $i = 1,\dots,N$. It follows that

$$\overline{\mathcal{O}} \equiv \frac{1}{N}\sum_{i=1}^{N}\mathcal{O}_i = \langle\mathcal{O}\rangle + O\left(\frac{1}{\sqrt{N}}\right), \quad \langle\mathcal{O}\rangle \equiv \frac{1}{Z}\int[d\phi]e^{-S[\phi]}\mathcal{O}[\phi]\,, \quad \langle\overline{\mathcal{O}}\rangle = \langle\mathcal{O}\rangle \tag{A.3.1}$$

defines an unbiased estimator for the mean value of observables, where the average $\langle\overline{\mathcal{O}}\rangle$ can only be computed assuming ideally either an infinitely long Markov chains with different starting configurations and sequences of random number, or a single infinitely long Markov chain with infinitely-many samples. Uncorrelated measurements satisfy $\langle\mathcal{O}_i\mathcal{O}_j\rangle = \langle\mathcal{O}_i\rangle\langle\mathcal{O}_j\rangle \;\forall\, i \neq j$. Their errors and the corresponding unbiased estimator are

$$\sigma^2_{\overline{\mathcal{O}}} = \frac{\sigma^2_{\mathcal{O}}}{N}\,, \quad \Delta^2_{\overline{\mathcal{O}}} = \frac{1}{N}\times\frac{1}{N-1}\sum_{i=1}^{N}\left(\mathcal{O}_i - \overline{\mathcal{O}}\right)^2\,, \quad \langle\Delta^2_{\overline{\mathcal{O}}}\rangle = \sigma^2_{\overline{\mathcal{O}}}\,. \tag{A.3.2}$$

For correlated measurements, i.e. such that $\langle\mathcal{O}_i\mathcal{O}_j\rangle \neq \langle\mathcal{O}_i\rangle\langle\mathcal{O}_j\rangle$, it is useful to introduce the autocorrelation function and its corresponding estimator as

$$\Gamma_{\mathcal{O}}(t) = \langle\mathcal{O}_i\mathcal{O}_{i+t}\rangle - \langle\mathcal{O}\rangle^2\,, \quad \overline{\Gamma}_{\mathcal{O}}(t) = \frac{1}{N-t}\sum_{i=1}^{N-t}\left(\mathcal{O}_i - \overline{\mathcal{O}}\right)\left(\mathcal{O}_{i+t} - \overline{\mathcal{O}}\right)\,. \tag{A.3.3}$$

In a homogeneous Markov chain, transition probabilities are independent of markovian time (number of update steps performed since the initial configuration). The autocorrelation function is independent from markovian time as well, so that

$$\sigma^2_{\overline{\mathcal{O}}} = \frac{\sigma^2_{\mathcal{O}}}{N}2\tau^{\mathcal{O}}_{\text{int}}\,, \quad \tau^{\mathcal{O}}_{\text{int}} = \frac{1}{2}\left[1 + 2\sum_{i=1}^{N-1}\frac{\Gamma_{\mathcal{O}}(t)}{\Gamma_{\mathcal{O}}(0)}\right] \tag{A.3.4}$$

with the corresponding estimators

$$\Delta^2_{\overline{\mathcal{O}}} = \frac{\Delta^2_{\mathcal{O}}}{N}2\overline{\tau}^{\mathcal{O}}_{\text{int}}\,, \quad \overline{\tau}^{\mathcal{O}}_{\text{int}} = \frac{1}{2}\left[1 + 2\sum_{i=1}^{N-1}\frac{\overline{\Gamma}_{\mathcal{O}}(t)}{\overline{\Gamma}_{\mathcal{O}}(0)}\right]. \tag{A.3.5}$$

Based on Eq. (A.3.4), the effect of the quantity $2\tau^{\mathcal{O}}_{\text{int}}$ can be interpreted as an effective correction to the naïve estimate of the error $\sigma^2_{\overline{\mathcal{O}}} = \sigma^2_{\mathcal{O}}/N$ due to the presence of correlation. Assuming uncorrelated measurements, where $2\tau^{\mathcal{O}}_{\text{int}} = 1$, we would correctly retrieve this estimate, while the presence of correlations implies $2\tau^{\mathcal{O}}_{\text{int}} > 1$, reducing the number of effectively independent samples.

A.3.1 The jackknife method

For the moment, let us assume that the measurements $\mathcal{O}_i$ are uncorrelated (otherwise, see the following discussion of the Γ-method). This can be achieved either by skipping or by binning (averaging) measurements once every $2\tau^{\mathcal{O}}_{\text{int}}$ steps. Suppose we want to estimate a function $F(\langle a\rangle, \langle b\rangle)$, with a, b being primary observables, such as Wilson loops, quark-line diagrams or any other function of the gauge field, from which physical quantities as F can eventually be obtained. From the central limit theorem it follows that

$$\overline{a} \equiv \frac{1}{N}\sum_{i=1}^{N} a_i = \langle a\rangle + O\left(\frac{1}{\sqrt{N}}\right)\,, \quad \overline{b} \equiv \frac{1}{N}\sum_{i=1}^{N} b_i = \langle b\rangle + O\left(\frac{1}{\sqrt{N}}\right) \tag{A.3.6}$$

implying

$$\begin{aligned}\overline{F} &= F(\overline{a},\overline{b}) = F(\langle a\rangle + (\overline{a}-\langle a\rangle), \langle b\rangle + (\overline{b}-\langle b\rangle)) \\ &= F(\langle a\rangle,\langle b\rangle) + \left.\frac{\partial F}{\partial a}\right|_{\langle a\rangle,\langle b\rangle}(\overline{a}-\langle a\rangle) + \left.\frac{\partial F}{\partial b}\right|_{\langle a\rangle,\langle b\rangle}(\overline{b}-\langle b\rangle) + O\left(\frac{1}{\sqrt{N}}\right).\end{aligned} \tag{A.3.7}$$

We can estimate the corresponding variance from

$$\sigma_F^2 = \left(\left.\frac{\partial F}{\partial a}\right|_{\langle a\rangle,\langle b\rangle}\right)^2 \sigma_{\overline{a}}^2 + \left(\left.\frac{\partial F}{\partial b}\right|_{\langle a\rangle,\langle b\rangle}\right)^2 \sigma_{\overline{b}}^2 + 2\left(\frac{\partial F}{\partial a}\frac{\partial F}{\partial b}\right)\Big|_{\langle a\rangle,\langle b\rangle} \mathrm{Cov}(\overline{a},\overline{b}) \tag{A.3.8}$$

with $\mathrm{Cov}(\overline{a},\overline{b}) = \langle(\overline{a}-\langle a\rangle)(\overline{b}-\langle b\rangle)\rangle$. This method does not seem too appealing nor it is practical for arbitrarily complicated functions of any number of primary observables. For this reason, an alternative and more sensible procedure was developed: the jackknife method. We introduce the jackknife variables for primary observables

$$\begin{gathered} a_k^J \equiv \frac{1}{N-1}\sum_{i=1,i\neq k}^{N} a_i = \overline{a} - \frac{a_k-\overline{a}}{N-1} \quad \rightarrow \quad \overline{a}^J = \overline{a}\,, \\ [\Delta_{\overline{a}}^J]^2 \equiv \frac{N-1}{N}\sum_{k=1}^{N}\left(a_k^J - \overline{a}^J\right)^2 = \Delta_{\overline{a}}^2 \end{gathered} \tag{A.3.9}$$

i.e. it is possible to compute their mean and error to retrieve the exact same values of those of primary observables. The value of this method resides in the fact that this property holds true also for jackknife variables of derived observables, i.e.

$$\begin{gathered} F_k^J = F\left(a_k^J\right) \quad \rightarrow \quad \overline{F}^J = F\left(\overline{a}^J\right) = F(\overline{a}) = \overline{F}\,, \\ \left[\Delta_{\overline{F}}^J\right]^2 \equiv \frac{N-1}{N}\sum_{k=1}^{N}\left(F_k^J - \overline{F}^J\right)^2 = \Delta_{\overline{F}}^2 \end{gathered} \tag{A.3.10}$$

as well as for derived observables depending on more variables, allowing for a simple computation of the error for arbitrary composite functions.

A.3.2 The Γ- method

The jackknife method is based on the assumption of the absence of autocorrelation in the measurements. Here we are going to provide a simple, executive summary of the more general Γ-method, detailed in Ref. [252]. The aim is to explicitly estimate the value of $\overline{\tau}_{\mathrm{int}}^{\mathcal{O}}$ as the integral of the autocorrelation function in Eq. (A.3.4) in order to correctly estimate errors, avoiding the often imprecise assumption of absence of autocorrelation. In order to do so, we exploit a property of the autocorrelation function, namely its exponential decay at large markovian times t. Let τ be the finite characteristic timescale of the exponential decay of Γ, such that $\Gamma(t) \propto e^{-|t|/\tau}$ at large t. We can now introduce an upper bound $t = W$ to truncate the integral, with the resulting truncation error being estimated by integrating the tail, using the exponential decay as an approximation for

the autocorrelation function. The resulting error will be twofold, one of a systematic and the other of a statistical nature, with the corresponding approximate estimates behaving like $e^{-W/\tau}$ and $2\sqrt{W/N}$ respectively. The idea is to determine the optimal value W^* of W that minimizes the absolute value of the sum of these two contributions. Note that the quantity $2W^*$ plays a similar rôle to the bin length B in the binning procedure, where the systematic error on the error estimate behaves like τ/B, both for the ordinary binning and for the jackknife strategies, while the statistical error on the error is $\sqrt{2B/N}$. Also for this case it is possible to find the optimal value of the bin size and of the corresponding total error. The advantages of the Γ-method, with its explicit analysis of autocorrelation functions, with respect to binning, can be understood from the resulting behavior of the systematic error on the error, decaying much faster in the first case (exponentially) than in the second one (like $1/W$). This in turn allows for a better estimator of the error on the error.

Appendix B

Quantization condition

Lattice QCD simulations are defined in a finite volume, causing the QCD spectrum to become discrete. Therefore, generic zero-momentum correlation functions[1]

$$C(x_0) = \int d^3\mathbf{x}\, \langle \mathcal{O}^\dagger(x_0, \mathbf{x}) \mathcal{O}(0) \rangle \tag{B.0.1}$$

can be represented in a finite-volume of spatial length L as

$$C(x_0; L) = \sum_n C_n(L) e^{-E_n(L)|x_0|}\,, \quad C_n(L) = |\langle 0|\mathcal{O}(0)|n\rangle|^2 \tag{B.0.2}$$

in terms of the finite-volume spectrum $E_n(L)$ and matrix elements $C_n(L)$. The associated spectral density is then

$$\rho(\omega; L) = \sum_n C_n(L) \delta(\omega - E_n(L))\,. \tag{B.0.3}$$

In the low-energy regime, the finite-volume spectrum and matrix elements can be directly computed from lattice correlation functions. For instance, single-particle states can be safely extracted from a fit of the exponential temporal dependence of Eq. (B.0.2), since they are affected only by exponentially suppressed finite-volume effects (FVEs), due to virtual pions propagating in periodic systems. In typical Lattice QCD applications, where $m_\pi L \geq 4$, their magnitude is generally around or below a few percent. In the following discussion, these terms will be neglected. Multiparticle states are much more sensitive to the exponential increase of the StN described in Section 2.6, requiring more sophisticated alternatives for their extraction, such as the the GEVP [256] method, or a solution to the StN problem, such as multilevel algorithms [1, 4, 83–88]. Additionally, when at least two particles are involved, the finite-volume spectrum and matrix elements show instead power-like FVEs that cannot be neglected.

As shown in the seminal works of Refs. [50, 51] for the case of two-to-two scattering in a scalar theory at energies below the inelastic threshold, the finite-volume dependence

[1] The discussion is straightforwardly generalizable to higher momenta projections, which we do not address here for simplicity.

of the spectrum can be directly related to infinite-volume amplitudes. This relation is often referred to as *quantization condition* and it holds up to terms that are exponentially suppressed in the spatial volume. In this Appendix, we briefly review this case. Note that a similar correspondence is also valid for matrix elements [52].

Since we are focusing on FVEs, we set the QFT in a torus of spatial length L and infinite temporal length. We follow the derivations in Refs. [53, 54], considering the case of $2 \to 2$ scattering at energies strictly *below* the inelastic threshold. In this kinematic regime, the s-channel is the only one that involves the exchange of virtual particles that can potentially go on-shell. Once the theory is set in a finite volume, momenta are discretized and the integrals over the momenta of virtual particles become discrete sums. The differences of finite-volume sums and infinite-volume integrals can be studied through the Poisson summation formula, which in one dimension reads

$$\frac{1}{L}\sum_{n\in\mathbb{Z}} g\left(k_n\right) = \int \frac{dk}{2\pi} g(k) + \sum_{l\neq 0}\int \frac{dk}{2\pi} e^{iLlk} g(k)\,, \quad k_n = \frac{2\pi}{L} n\,. \tag{B.0.4}$$

The last term on the r.h.s. of this equation represents the sum-integral difference for the function $g(k)$, which decreases exponentially as $L \to \infty$ for analytic functions, while for other cases its decay is power-like. These non-analiticities are related to the presence of particles propagating within internal loops that may potentially go on-shell. Therefore, for the case we are studying, power-like FVEs can only arise in the s-channel, whose contribution can be explicitly isolated exploiting the non-perturbative Bethe-Salpeter equation. This separation allows to study the sum-integral difference between finite and infinite-volume contributions using the Poisson summation formula, as described above. In 1+1 dimensions, we can express the finite-volume scattering amplitude as

$$\mathcal{M}_{2L}(s) = \frac{8q\sqrt{s}}{\cot\delta\left(q\right) + \cot\phi\left(q, L\right)}\,, \quad q = \frac{1}{2}\sqrt{s - 4m^2} \tag{B.0.5}$$

for a process with two particles with total initial energy $\sqrt{s}$ in their center-of-mass frame. Above, we introduced $\phi(q, L)$ by rewriting the sum-integral difference as

$$\cot\phi(q, L) = \frac{x}{\pi}\left[\sum_n - \mathrm{PV}\int dn\right]\frac{1}{x^2 - n^2}\,, \quad x = \frac{qL}{2\pi}\,, \tag{B.0.6}$$

while the infinite-volume scattering phase shift $\delta(q)$ is related to the infinite-volume scattering matrix $\mathcal{M}_2$ through

$$\mathrm{Re}\big(\mathcal{M}_2^{-1}\big)(s) = \frac{q\cot\delta(q)}{8q^2\sqrt{s}}\,. \tag{B.0.7}$$

The finite-volume spectrum is thus given by all the solutions to the quantization condition

$$\cot\delta(q) + \cot\phi(q, L) = 0 \quad \text{i.e.} \quad 2\delta(q) + qL = 2\pi n\,, n \in \mathbb{Z} \tag{B.0.8}$$

where $\delta(q)$ encodes infinite-volume dynamics and $\phi(q, L)$ finite-volume kinematics. In the 3+1 dimensional case, a careful estimation of the sum-integral difference leads to a similar quantization condition as in Eq. (B.0.8) of the form

$$\det\left[\mathcal{M}_2^{-1}(q) + F_2^{i\epsilon}(q, \mathbf{P}, L)\right] = 0 \tag{B.0.9}$$

where the determinant is computed in the space of angular momentum in the center-of-mass frame of the two on-shell particles with spatial momentum $\mathbf{P}$. We note that we can again clearly separate the infinite-volume dynamics contribution of $\mathcal{M}_2$ from the finite-volume kinematic effects, encoded in $F_2^{i\epsilon}$, which is a matrix of geometric functions in angular momentum space that encodes how angular momentum states mix due to the reduced symmetry of the finite-volume system, generalizing to the $3+1$ dimensional case the term $\cot\phi(q, L)$. Similar arguments hold for FVEs in matrix elements [52, 53].

Incredible progress has been and is being made in generalizing these quantization conditions to more and more difficult cases [53, 54, 126–142]. For instance, two particles with different masses and spins can be studied as well, and all the relevant cases involving 2 initial particles have been analyzed, see Ref. [142] for a review on this topic. The more complicated case of 3 particles is an active area of research, recently reviewed in Ref. [54]. It is based upon the knowledge of the 2-particle scattering, and it is limited to specific energy ranges as well. Extensions to 4 scattering particles would then be based on the full knowledge of 2 and 3 scattering particles, with increasing difficulties arising in the definition of the corresponding quantization conditions, hindering the study (through these finite-volume methods, at least) of phenomenologically interesting processes such as $B \to \pi\pi$, where the threshold for producing more than 30 pions is open.

Appendix C

Spectral densities and the inverse problem in QCD

In this Appendix, we provide more details on the examples of spectral densities in Quantum Chromodynamics (QCD) discussed in Chapter 3, discussing the inverse problems to be solved in the cases of deep inelastic scattering, semileptonic inclusive decays of heavy hadrons, and the extraction of transport coefficients in thermal QCD.

C.1 Deep inelastic scattering

Deep inelastic scattering (DIS) is the study of collisions of high-energy ("deep") hard leptons with fixed hadronic targets via virtual photon exchange (energies are far below than those needed to produce a Z-boson). The kinematics of the process is described in Fig. C.1, where a hard lepton with mass m_ℓ carrying initial momentum k collides with a hadron with mass M and momentum p through the exchange of a hard spacelike photon with momentum q s.t. $Q^2 = -q^2 > 0$, producing a final hadronic state X with mass M_X which is usually not detected, thus allowing us to obtain information only on total (inclusive) rates. The scattering process is deep as $Q^2 \gg M_X^2 \gg m_\ell^2$. We are interested in the unpolarized cross section in the nucleon rest-frame

$$d\sigma = \frac{e^4}{Q^4} \int \frac{d^3\mathbf{k}'}{(2\pi)^3 2\omega_{\mathbf{k}'}} \frac{4\pi L^{\mu\nu} W_{\mu\nu}(p, k-k')}{2k^0\, 2M} \tag{C.1.1}$$

where the leptonic tensor

$$L^{\mu\nu} = 2(k^\mu k'^\nu + k^\nu k'^\mu - g^{\mu\nu} k \cdot k') \tag{C.1.2}$$

and the hadronic one

$$W_{\mu\nu}(p,q) = \frac{1}{4\pi n_\lambda} \sum_\lambda \int d^4x\, e^{iqx} \langle N, \mathbf{p}, \lambda | V_\mu^{\rm em}(x) V_\nu^{\rm em}(0) | N, \mathbf{p}, \lambda \rangle \tag{C.1.3}$$

$$= F_1 \cdot \left(-g_{\mu\nu} + \frac{q_\mu q_\nu}{q^2}\right) + \frac{F_2}{p\cdot q} \left(p_\mu - \frac{(p\cdot q) q_\mu}{q^2}\right)\left(p_\nu - \frac{(p\cdot q) q_\nu}{q^2}\right) \tag{C.1.4}$$

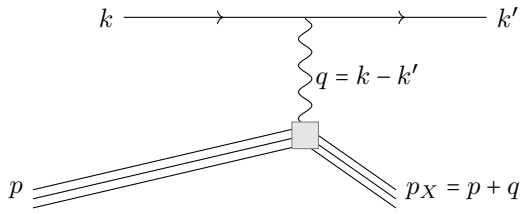

Figure C.1: Deep Inelastic Scattering of a proton colliding with a hard lepton, carrying initial momenta p and k respectively, via the exchange of a virtual, space-like photon with momentum q.

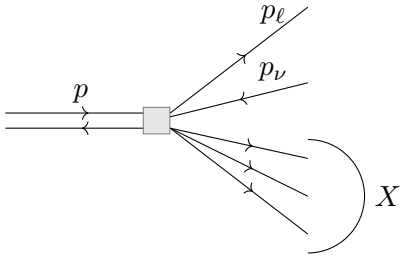

Figure C.2: Semileptonic weak decay of a heavy meson $H_Q \to \ell + \overline{\nu}_\ell + X$, with the initial meson H_Q carrying momentum p and the final lepton ℓ and antineutrino $\overline{\nu}_\ell$ with momenta p_ℓ and p_ν respectively.

are factorized. In Eq. (C.1.3), $|N, \mathbf{p}, \lambda\rangle$ is a stable single-particle QCD state for a nucleon with flavor label N, total three-momentum $\mathbf{p}$ and projection λ of the spin along the z-direction. The total number of spin states n_λ is 2 for a nucleon, while $V_\mu^{\rm em}$ is the electromagnetic current defined in Eq. (3.3.3), and F_1, F_2 are structure functions, depending only on the scalar quantities q^2 and $(p \cdot q)$. The unpolarized cross section for the inclusive process $(e + p \to e' + \text{hadrons})$ depends on these as

$$\frac{d^2\sigma}{dx\,dy} = \frac{e^4 M q^0}{2\pi Q^4}\left[xyF_1 + (1-y)F_2\right] \tag{C.1.5}$$

where the *Bjorken-x* is $x = \frac{Q^2}{2Mq^0}$ and $y = \frac{(p\cdot q)}{(p\cdot k)} = \frac{q^0}{k^0}$ is the fractional energy loss of the lepton in the nucleon reference system. The hadronic tensor can be extracted directly from the Euclidean time correlation function projected to definite spatial momentum $\mathbf{p_x}$ [107]

$$C_{\mu\nu}(\tau, \mathbf{p_x}; \mathbf{p}) = \frac{1}{4\pi n_\lambda} e^{-\omega_{\mathbf{p}}\tau} \int d^{\mathbf{3}}\mathbf{x}\, e^{i(\mathbf{p}-\mathbf{p_x})\cdot\mathbf{x}} \sum_\lambda \langle N, \mathbf{p}, \lambda | J_\mu^{\rm em}(\tau, \mathbf{x}) J_\nu^{\rm em}(0) | N, \mathbf{p}, \lambda\rangle \tag{C.1.6}$$

by inverting the Laplace transform

$$C_{\mu\nu}(\tau, \mathbf{p_x}; \mathbf{p}) = \int_0^\infty dp_x^0\, e^{-p_x^0\tau} W_{\mu\nu}(p, p_x - p)\,. \tag{C.1.7}$$

Our ability to perform the inverse transform of Eq. (C.1.7) would allow a direct estimate of the spectral density $W_{\mu\nu}$, from which the structure functions of the nucleon F_1 and F_2 can be extracted, from the knowledge of the correlation function in Euclidean time, measured e.g. from lattice simulations.

C.2 Semileptonic decays of heavy hadrons

The study of semileptonic decays of heavy hadrons H_Q containing a heavy quark Q (such as B and D mesons, containing one b and c quark respectively) represents a rel-

atively clean environment to test the Standard Model since these decays involve both a quark transition and a lepton in the final state. For instance, we can think of the decay $H_Q \to \ell \overline{\nu}_\ell X$ shown in Fig. C.2, where X represents any hadronic state compatible with the decay. Inclusive semileptonic decays of heavy mesons (e.g. B and D) allow to extract the Cabibbo-Kobayashi-Maskawa (CKM) matrix elements, and the presence of discrepancies [30] between their current inclusive and exclusive experimental measurements (by LHCb, Belle, Belle II, BaBar) call for urgent theoretical predictions of e.g. $|V_{cb}|$ [171] and $|V_{ub}|$, allowing to test CP violations in the Standard Model by studying the unitarity of the CKM matrix.

For the case shown in Fig. C.2, as it happened for DIS it is possible to factorize the leptonic and hadronic contributions to the differential decay width [107]

$$\frac{d^3\Gamma}{dE_\ell\, dq^2\, dq^0} = \frac{G_F^2 |V_{Qq}|^2}{8\pi^3} L^{\mu\nu} W_{\mu\nu}^{H_Q \to X} \tag{C.2.1}$$

where G_F is the Fermi constant, E_ℓ is the lepton energy, $q = p_\ell + p_\nu$ so that $q^2 > 0$ and q^0 are the $\ell - \overline{\nu}_\ell$ invariant mass and energy respectively. The leptonic tensor here is

$$L^{\mu\nu} = p_\ell^\mu p_\nu^\nu + p_\ell^\nu p_\nu^\mu - (p_\ell \cdot p_\nu) g^{\mu\nu} - i\epsilon^{\mu\nu\rho\sigma} p_{\ell,\rho} p_{\nu,\sigma}\,, \tag{C.2.2}$$

while the hadronic tensor is

$$W_{\mu\nu}^{H_Q \to X}(v,q) = \frac{1}{2M_{H_Q}} \int d^4x\, e^{-iqx} \langle H_Q, \mathbf{p} | J_\mu^\dagger(x) J_\nu(0) | H_Q, \mathbf{p} \rangle \tag{C.2.3}$$

where $v^\mu = p_H^\mu / M_{H_Q}$ is the four-velocity of the stable single-particle QCD state $|H_Q, \mathbf{p}\rangle$ for the heavy hadron H_Q containing the heavy quark Q, with total three-momentum $\mathbf{p}$, while $J_\mu = \overline{q}\gamma_\mu(1-\gamma_5)Q$ is the flavor-changing current with one light and one heavy flavor, associated to the spinors q and Q respectively. The hadronic tensor $W_{\mu\nu}$ can again be decomposed into structure functions. It can also be interpreted as a transition spectral function and related via a Laplace transform [107]

$$C_{\mu\nu}^{H_Q \to X}(\tau, \mathbf{p_x}; \mathbf{p}) = \int_0^\infty dp_x^0\, e^{-p_x^0 \tau} W_{\mu\nu}^{H_Q \to X}(p, p_x - p) \tag{C.2.4}$$

to the Euclidean time correlation function projected to definite spatial momentum $\mathbf{p_x}$

$$C_{\mu\nu}^{H_Q \to X}(\tau, \mathbf{p_x}; \mathbf{p}) = \frac{1}{2M_{H_Q}} e^{-\omega_{\mathbf{p}}\tau} \int d^3\mathbf{x}\, e^{i(\mathbf{p}-\mathbf{p_x})\cdot\mathbf{x}} \langle H_Q, \mathbf{p} | J_\mu^\dagger(\tau, \mathbf{x}) J_\nu(0) | H_Q, \mathbf{p} \rangle\,. \tag{C.2.5}$$

Our ability to extract $W_{\mu\nu}^{H_Q \to X}$ from $C_{\mu\nu}^{H_Q \to X}$ again would allow us to compute the corresponding structure functions.

Notice the strict analogy between the formulae for this and the DIS case. As a matter of fact, these two examples can be straightforwardly generalized in order to extract total decays or transition rates into final states with any number of hadrons (i.e. considering all out-states with a given set of QCD quantum numbers). These quantities are integrated out w.r.t. hadronic degrees of freedom, but in principle they can be differential w.r.t. non-hadronic degrees of freedom such as those related to photons or leptons. We refer to Ref. [107] for further details.

C.2.1 Total inclusive semileptonic decay rates

The specific case where one is interested in extracting total inclusive semileptonic decay rates has been studied in Ref. [108], see also Chapter 3 of Ref. [172]. Taking as an example inclusive decays $B_s \to \ell\overline{\nu}_\ell X$, they are characterized by a sum over all possible final states allowed by the kinematics of the specific $\overline{b} \to \overline{c}$ weak transition, with the state X possibly including multiparticle states besides single-particle ones (such as D_s). The differential decay rate, already given in Eq. (C.2.1), can be integrated out in order to obtain the total decay rate as

$$\Gamma = \frac{G_F^2|V_{cb}|^2}{24\pi^3}\int_0^{{\mathbf{q}_{\rm max}}^2} d\mathbf{q}^2\,\sqrt{\mathbf{q}^2}\sum_{l=0}^{2}\overline{X}^{(l)}(\mathbf{q}^2)\,, \quad \overline{X}^{(l)}(\mathbf{q}^2) = \int_{\omega_{\rm min}}^{\omega_{\rm max}} d\omega\, X^{(l)}(\mathbf{q}^2,\omega) \quad \text{(C.2.6)}$$

where ω and $\mathbf{q}$ are the energy and three-momentum of the final-state hadron respectively, $\omega_{\rm min} = \sqrt{M_{D_s}^2+\mathbf{q}^2}$, $\omega_{\rm max} = M_{B_s} - \sqrt{\mathbf{q}^2}$, ${\mathbf{q}_{\rm max}}^2 = \frac{M_{B_s}^2 - M_{D_s}^2}{4M_{B_s}^2}$ and where

$$\begin{aligned} X^{(0)}(\mathbf{q}^2,\omega) &= \mathbf{q}^2 W_{00}^{B_s\to X} + \sum_i (q_i^2 - \mathbf{q}^2) W_{ii}^{B_s\to X} + \sum_{i\neq j} q^i W_{ij}^{B_s\to X} q^j\,, \\ X^{(1)}(\mathbf{q}^2,\omega) &= -q_0 \sum_i q^i (W_{0i}^{B_s\to X} + W_{i0}^{B_s\to X})\,, \quad X^{(2)}(\mathbf{q}^2,\omega) = q_0^2 \sum_i W_{ii}^{B_s\to X}\,. \end{aligned} \quad \text{(C.2.7)}$$

Inclusive hadronic decays of the τ lepton have been studied in Ref. [173], obtaining

$$\Gamma_{ud}^{(\tau)} = \frac{G_F^2|V_{ud}|^2 m_\tau^2}{16\pi}\int_0^1 ds\,(1-s)^2\left[(1+2s)\rho_T(s) + \rho_L(s)\right] \quad \text{(C.2.8)}$$

where the integration variable is $s = q^2/m_\tau^2$. The transverse and longitudinal spectral form factors, $\rho_T(s)$ and $\rho_L(s)$ respectively, are given by the decomposition of the spectral density tensor

$$\rho_{ud}^{\mu\nu}(q) = \langle 0|J_{ud}^\mu(0)(2\pi)^3\delta^4(\mathbb{P}-q)J_{ud}^\nu(0)|0\rangle = (q^\mu q^\nu - q^2 g^{\mu\nu})\rho_T(q^2) + q^\mu q^\nu \rho_L(q^2) \quad \text{(C.2.9)}$$

with the current $J_{ud}^\mu = \overline{u}\gamma^\mu(1-\gamma_5)d$ and the QCD 4-momentum operator $\mathbb{P}$. This spectral density is the inverse Laplace transform of the correlation function at positive Euclidean time $\tau > 0$ and projected to fixed spatial momentum $\mathbf{q}$

$$C_{ud}^{\mu\nu}(\tau,\mathbf{q}) = \int d^3\mathbf{x}\, e^{-i\mathbf{q}\cdot\mathbf{x}}\langle 0|J_{ud}^\mu(\tau,\mathbf{x})J_{ud}^\nu(0)^\dagger|0\rangle = \int_0^\infty d\omega\, e^{-\omega\tau}\rho_{ud}^{\mu\nu}(\omega,\mathbf{q})\,. \quad \text{(C.2.10)}$$

It is now even clearer that a procedure to extract the spectral densities, represented above by the hadronic tensor $W_{\mu\nu}^{H_Q\to X}$ and by $\rho_{ud}^{\mu\nu}$, from measurements of Euclidean time correlation functions, denoted above as $C_{\mu\nu}^{H_Q\to X}$ and $C_{ud}^{\mu\nu}$, is of primary importance, also for the study of semileptonic decays. If we want to compute hadronic structure functions, then the inverse Laplace transform of Eqs. (C.2.4) or (C.2.10) must be directly solved. If we are interested instead into inclusive hadronic decay widths, Eqs. (C.2.6) and (C.2.8) must be solved. We note that in both equations the integration interval is limited by the

kinematics of the process to energies below M_B and m_τ respectively, effectively inserting a Heaviside step-function, whose inverse Laplace transform cannot be analytically computed[1]. As discussed in Section 3.2, this prevents us from rewriting the integrals in Eqs. (C.2.6) and (C.2.8) in the time-momentum representation, necessitating the inverse problem to be addressed in a different way.

C.3 QCD transport coefficients

Non-static properties of the quark-gluon plasma i.e. *QCD transport coefficients* can be extracted from hadronic spectral densities at finite temperature as well [109]. For instance, the *shear viscosity* in $SU(3)$ gluodynamics is given by [110, 174–176]

$$\eta(T) = \pi \left.\frac{d\rho}{d\omega}\right|_{\omega=0} \tag{C.3.1}$$

at temperature $T = 1/L_0 = 1/\beta$, where the spectral density $\rho(\omega)$ is related to the two-point function of the energy-momentum tensor

$$C(x_0) = L_0^5 \int d^3\mathbf{x}\, \langle \overline{T}_{12}(0)\overline{T}_{12}(x_0,\mathbf{x})\rangle\,, \quad \overline{T}_{\mu\nu} = F^a_{\mu\alpha}F^A_{\nu\alpha} - \frac{1}{4}\delta_{\mu\nu}F^a_{\rho\sigma}F^a_{\rho\sigma} \tag{C.3.2}$$

by a slightly modified Laplace transform of the form

$$C(x_0) = L_0^5 \int_0^\infty d\omega\, \rho(\omega) \frac{\cosh[\omega(L_0/2 - x_0)]}{\sinh[\omega L_0/2]} \tag{C.3.3}$$

to take into account thermal effects.

[1] It can be seen for instance by inserting the representation

$$\theta(M_B - \omega) = -\frac{1}{2\pi\epsilon}\lim_{\epsilon\to 0}\int_{-\infty}^{\infty}\frac{dx}{x + i\epsilon}e^{ix(M_B-\omega)} \tag{C.2.11}$$

inside the Bromwhich integral in Eq. (3.2.3).

Appendix D

Projectors on inner boundaries

Starting from the action

$$S = \sum_{x,y} \overline{\psi}(y) D(y,x) \psi(x) \,, \tag{D.0.1}$$

where D has the form described in Subsections 2.3.2 or 2.4.1, it is possible to extract the explicit form of hopping terms, which are only due to D_{W} in Eq. (2.3.11) or Eq. (2.4.5):

$$D(x, x + a\hat{\mu}) = -U_\mu(x) \frac{1-\gamma_\mu}{2} \,,\; D(x, x - a\hat{\mu}) = -U_\mu^\dagger(x) \frac{1+\gamma_\mu}{2} \tag{D.0.2}$$

and there is no hopping between lattice points whose distance is larger than one lattice spacing in any direction of the lattice. Projectors on the inner boundary $\partial\Lambda_i$ of the domain Λ_i are defined as

$$P_{\partial\Lambda_i} D_{\Lambda_{i,j}} = D_{\Lambda_{i,j}} P_{\partial\Lambda_j} \,,\; i \neq j \tag{D.0.3}$$

and are such that

$$\begin{aligned} D_{\partial\Lambda_i}\psi(x) = -\vartheta_{\Lambda_i}(x) \sum_{\mu=0}^{3} \Big[& \frac{1-\gamma_\mu}{2} \vartheta_{\Lambda_i^*}(x + a\hat{\mu}) U_\mu(x) \psi(x + a\hat{\mu}) \\ & + \frac{1+\gamma_\mu}{2} \vartheta_{\Lambda_i^*}(x - a\hat{\mu}) U_\mu(x - a\hat{\mu})^\dagger \psi(x - a\hat{\mu}) \Big] \,, \end{aligned} \tag{D.0.4}$$

where $\partial\Lambda_i^*$ is the external boundary of the domain Λ_i, Λ_i^* is the union of nearest neighbors of Λ_i and ϑ_Λ is the characteristic function relative to the domain Λ. Therefore

$$P_{\partial\Lambda_i}\psi(x) = \begin{cases} 0, & \text{if } x \notin \partial\Lambda_i \\ \frac{1+\gamma_\mu}{2}, & \text{if } x \in \partial\Lambda_i,\; x + a\hat{\mu} \in \partial\Lambda_i^* \\ \frac{1-\gamma_\mu}{2}, & \text{if } x \in \partial\Lambda_i,\; x - a\hat{\mu} \in \partial\Lambda_i^* \\ 0, & \text{otherwise} \end{cases} \,. \tag{D.0.5}$$

Appendix E

LU factorization of the block-banded Wilson-Dirac operator

The LU factorization for block banded matrices leads to the simple result for the Wilson–Dirac operator [257]

$$\begin{pmatrix} D_{\Lambda_{0,0}} & D_{\Lambda_{0,1}} & 0 & \dots \\ D_{\Lambda_{1,0}} & D_{\Lambda_{1,1}} & D_{\Lambda_{1,2}} & \dots \\ 0 & D_{\Lambda_{2,1}} & D_{\Lambda_{2,2}} & \\ \vdots & & & \ddots \end{pmatrix} = \begin{pmatrix} 1 & B_0 & 0 & \dots \\ 0 & 1 & B_1 & \dots \\ 0 & 0 & 1 & \\ \vdots & & & \ddots \end{pmatrix} \begin{pmatrix} A_0 & 0 & 0 & \dots \\ D_{\Lambda_{1,0}} & A_1 & 0 & \dots \\ 0 & D_{\Lambda_{2,1}} & A_2 & \\ \vdots & & & \ddots \end{pmatrix}, \tag{E.0.1}$$

where A_i, B_i are defined uniquely in terms of the $D_{\Lambda_{i,j}}$ by the recursion relations

$$A_i = D_{\Lambda_{i,i}} - D_{\Lambda_{i,i+1}} A_{i+1}^{-1} D_{\Lambda_{i+1,i}}\,, \quad B_i = D_{\Lambda_{i,i+1}} A_{i+1}^{-1}\,, \quad (i = 0, \dots, T-2)\,, \tag{E.0.2}$$

whereas $A_{T-1} = D_{\Lambda_{T-1,T-1}}$. Using the factorization in Eq. (E.0.1), the linear system $D\psi = \eta$ can be easily solved, again leading to recursion relations. It is useful to consider the case where the source η is non-zero only on one thick time-slice Λ_k. Solutions for sources on multiple time slices can be obtained by superposition. The system

$$\begin{pmatrix} 1 & B_0 & 0 & \dots & \\ 0 & 1 & B_1 & \dots & \\ 0 & 0 & 1 & & \\ \vdots & & & \ddots & \\ 0 & & & & 1 \end{pmatrix} \begin{pmatrix} \chi_0 \\ \chi_1 \\ \vdots \\ \\ \chi_{T-1} \end{pmatrix} = \begin{pmatrix} 0 \\ \vdots \\ \eta_k \\ \vdots \\ 0 \end{pmatrix} \tag{E.0.3}$$

is solved by

$$\chi_i = \begin{cases} \left[\prod_{j=i}^{k-1} (-B_j) \right] \eta_k & i < k \\ \eta_k & i = k \\ 0 & i > k \end{cases} \tag{E.0.4}$$

taking the obvious ordered product. Using Eq. (E.0.2) we can rewrite

$$\prod_{j=i}^{k-1}(-B_j)\,\eta_k = (-)^{k-i}\,(D_{\Lambda_{i,i+1}}A_{i+1}^{-1})\,\ldots\,(D_{\Lambda_{k-1,k}}A_k^{-1})\,\eta_k\,, \tag{E.0.5}$$

where for $i < k$ the χ_i have support only on the boundaries. By solving the system

$$\begin{pmatrix} A_0 & 0 & 0 & \ldots \\ D_{\Lambda_{1,0}} & A_1 & 0 & \ldots \\ 0 & D_{\Lambda_{1,2}} & A_2 & \\ \vdots & & & \ddots \end{pmatrix}\begin{pmatrix} \psi_0 \\ \vdots \\ \\ \psi_{T-1} \end{pmatrix} = \begin{pmatrix} \chi_0 \\ \vdots \\ \\ \chi_{T-1} \end{pmatrix}, \tag{E.0.6}$$

we obtain the final result

$$\psi_0 = A_0^{-1}\,\chi_0\,, \quad \psi_i = A_i^{-1}(\chi_i - D_{\Lambda_{i,i-1}}\psi_{i-1})\,, \quad (i = 1,\ldots,T-1)\,. \tag{E.0.7}$$

As for the χ_i, the second term in the parentheses in Eq. (E.0.7) lives on the boundaries. The matrix A_i^{-1} propagates these two contributions into the center of the thick time-slice.

E.1 The 2×2 case

The previous derivation for the 2×2 block-banded Wilson-Dirac operator

$$D = \begin{pmatrix} D_{\Lambda_{0,0}} & D_{\Lambda_{0,1}} \\ D_{\Lambda_{1,0}} & D_{\Lambda_{1,1}} \end{pmatrix} = \begin{pmatrix} I & D_{\Lambda_{0,1}}D_{\Lambda_{1,1}}^{-1} \\ 0 & I \end{pmatrix}\begin{pmatrix} S_{\Lambda_{0,0}} & 0 \\ D_{\Lambda_{1,0}} & D_{\Lambda_{1,1}} \end{pmatrix}, \tag{E.1.1}$$

where the Schur complement is defined as

$$S_{\Lambda_{0,0}} = D_{\Lambda_{0,0}} - D_{\Lambda_{0,1}}D_{\Lambda_{1,1}}^{-1}D_{\Lambda_{1,0}}\,, \tag{E.1.2}$$

leads to

$$D^{-1} = \begin{pmatrix} S_{\Lambda_{0,0}}^{-1} & -S_{\Lambda_{0,0}}^{-1}D_{\Lambda_{0,1}}D_{\Lambda_{1,1}}^{-1} \\ -D_{\Lambda_{1,1}}^{-1}D_{\Lambda_{1,0}}S_{\Lambda_{0,0}}^{-1} & D_{\Lambda_{1,1}}^{-1} + D_{\Lambda_{1,1}}^{-1}D_{\Lambda_{1,0}}S_{\Lambda_{0,0}}^{-1}D_{\Lambda_{0,1}}D_{\Lambda_{1,1}}^{-1} \end{pmatrix} \tag{E.1.3}$$

and

$$\det D = \det D_{\Lambda_{0,0}}\det S_{\Lambda_{0,0}} = \det D_{\Lambda_{1,1}}\det S_{\Lambda_{1,1}} \tag{E.1.4}$$

where $S_{\Lambda_{1,1}}$ is the equivalent of the Schur complement in Eq. (E.1.2) but computed with respect to $\Lambda_{1,1}$. Thanks to Eq. (E.1.1), this formula can be equivalently rewritten as

$$\det\begin{pmatrix} D_{\Lambda_{0,0}} & D_{\Lambda_{0,1}} \\ D_{\Lambda_{1,0}} & D_{\Lambda_{1,1}} \end{pmatrix} = \det D_{\Lambda_{0,0}}\det D_{\Lambda_{1,1}}\det\begin{pmatrix} \mathbb{1} & D_{\Lambda_{0,0}}^{-1}D_{\Lambda_{0,1}} \\ D_{\Lambda_{1,1}}^{-1}D_{\Lambda_{1,0}} & \mathbb{1} \end{pmatrix}. \tag{E.1.5}$$

It is worth noting that $S_{\Lambda_{0,0}}^{-1}$ is the exact block in the block inverse of D. By putting the Schur complement in the bottom-right block, the analogous formula can be written as

$$D^{-1} = \begin{pmatrix} D_{\Lambda_{0,0}}^{-1} + D_{\Lambda_{0,0}}^{-1}D_{\Lambda_{0,1}}S_{\Lambda_{1,1}}^{-1}D_{\Lambda_{1,0}}D_{\Lambda_{0,0}}^{-1} & -D_{\Lambda_{0,0}}^{-1}D_{\Lambda_{0,1}}S_{\Lambda_{1,1}}^{-1} \\ -S_{\Lambda_{1,1}}^{-1}D_{\Lambda_{1,0}}D_{\Lambda_{0,0}}^{-1} & S_{\Lambda_{1,1}}^{-1} \end{pmatrix}. \tag{E.1.6}$$

with $S_{\Lambda_{1,1}}$ defined as in Eq. (E.1.2) but with $1 \leftrightarrow 0$.

Appendix F

Path integral derivation of fermion determinant factorization

This Appendix describes an alternative way to derive Eq. (4.2.3), while also providing useful intermediate results for the case of a multidimensional domain decomposition. Additionally, it outlines a strategy to achieve an approximate factorization of the propagator starting from that of the fermion determinant.

We consider a lattice domain decomposition in non-overlapping domains Λ_0, Λ_1, Λ_2, with Λ_0 and Λ_2 being disconnected, and a local definition of the Dirac matrix D, e.g. the Wilson–Dirac operator in Eq. (2.3.11) or its $O(a)$-improved counterpart in Eq. (2.4.5). We can represent it as

$$D = \begin{pmatrix} D_{\Lambda_0} & D_{\Lambda_0,\Lambda_1} & 0 \\ D_{\Lambda_1,\Lambda_0} & D_{\Lambda_1} & D_{\Lambda_1,\Lambda_2} \\ 0 & D_{\Lambda_2,\Lambda_1} & D_{\Lambda_2} \end{pmatrix} \tag{F.0.1}$$

where the hopping terms D_{Λ_i,Λ_j}, $i \neq j$ are defined in Appendix D. We are interested in estimating the fermion determinant

$$\det D = \int [d\overline{\psi}][d\psi] e^{-\overline{\psi} D \psi} \tag{F.0.2}$$

which can be computed by first integrating out fermions in $\bar{\Lambda}_0 \bigcup \Lambda_1 \bigcup \bar{\Lambda}_2$, where we define $\bar{\Lambda}_0 = \Lambda_0 \backslash \partial\Lambda_0$ and $\partial\Lambda_0$ is the inner border of the domain Λ_0 and analogous relations hold for $\bar{\Lambda}_2$. This process is equivalent to treating fermions inside the borders $\partial\Lambda_0$ and $\partial\Lambda_2$ as constant external source terms in the gaussian integration. Then, the remaining integration can be performed, yielding

$$\det D = \det D_{\bar{\Lambda}_0} \det D_{\Lambda_1} \det D_{\bar{\Lambda}_2} \det \tilde{D}\,, \tag{F.0.3}$$

where

$$\tilde{D} = \begin{pmatrix} \tilde{D}_{\partial\Lambda_0} & \tilde{D}_{\partial\Lambda_0,\partial\Lambda_2} \\ \tilde{D}_{\partial\Lambda_2,\partial\Lambda_0} & \tilde{D}_{\partial\Lambda_2} \end{pmatrix},$$

$$\begin{aligned} \tilde{D}_{\partial\Lambda_0} &= D_{\partial\Lambda_0} - D_{\partial\Lambda_0,\bar{\Lambda}_0} D^{-1}_{\bar{\Lambda}_0} D_{\bar{\Lambda}_0,\partial\Lambda_0} - D_{\partial\Lambda_0,\Lambda_1} D^{-1}_{\Lambda_1} D_{\Lambda_1,\partial\Lambda_0}\,, \\ \tilde{D}_{\partial\Lambda_0,\partial\Lambda_2} &= -D_{\Lambda_{0,1}} D^{-1}_{\Lambda_1} D_{\Lambda_{1,2}}\,,\ \tilde{D}_{\partial\Lambda_2,\partial\Lambda_0} = -D_{\Lambda_{2,1}} D^{-1}_{\Lambda_1} D_{\Lambda_{1,0}}\,, \\ \tilde{D}_{\partial\Lambda_2} &= D_{\partial\Lambda_2} - D_{\partial\Lambda_2,\bar{\Lambda}_2} D^{-1}_{\bar{\Lambda}_2} D_{\bar{\Lambda}_2,\partial\Lambda_2} - D_{\partial\Lambda_2,\Lambda_1} D^{-1}_{\Lambda_1} D_{\Lambda_1,\partial\Lambda_2}\,. \end{aligned} \tag{F.0.4}$$

Therefore, it is possible to rewrite

$$\det D = \det D_{\bar{\Lambda}_0} \det \tilde{D}_{\partial\Lambda_0} \det D_{\bar{\Lambda}_2} \det \tilde{D}_{\partial\Lambda_2} \det D_{\Lambda_1} \det W\,, \tag{F.0.5}$$

which is equivalent to Eq. (4.2.3) since

$$\det D_{\bar{\Lambda}_0} \det \tilde{D}_{\partial\Lambda_0} = \det D_{\Omega_0} \det D^{-1}_{\Lambda_1}\,, \quad \det D_{\bar{\Lambda}_2} \det \tilde{D}_{\partial\Lambda_2} = \det D_{\Omega_2} \det D^{-1}_{\Lambda_1} \tag{F.0.6}$$

and

$$W = \begin{pmatrix} 1 & \tilde{D}^{-1}_{\partial\Lambda_0} \tilde{D}_{\partial\Lambda_0,\partial\Lambda_2} \\ \tilde{D}^{-1}_{\partial\Lambda_2} \tilde{D}_{\partial\Lambda_2,\partial\Lambda_0} & 1 \end{pmatrix} \tag{F.0.7}$$

is the same as W_1 in Eq. (4.2.8) since $\tilde{D}^{-1}_{\partial\Lambda_0} = P_{\partial\Lambda_0} D^{-1}_{\Omega_0} P_{\partial\Lambda_0}$ and $\tilde{D}^{-1}_{\partial\Lambda_2} = P_{\partial\Lambda_2} D^{-1}_{\Omega_2} P_{\partial\Lambda_2}$. Note that the procedure we just described only depends on the form of the Dirac matrix, regardless of the dimensionality of the lattice decomposition.

F.1 Factorizing the vector-meson two-point function

Assuming exact isospin symmetry, we can define the two-point correlation function

$$\langle V^a_\mu(x) V^b_\nu(y) \rangle = -\left. \frac{\partial^2 \ln Z[J]}{\partial J^a_\mu(x) \partial J^b_\nu(y)} \right|_{J=0} \tag{F.1.1}$$

of two isovector vector currents $V^a_\mu = \overline{\psi} i T^a \psi$, where T^a is a matrix in the algebra of $SU(2)$, and in the definition of the partition function we introduced a source term

$$S[U,\overline{\psi},\psi] \to S[U,\overline{\psi},\psi;J] = S[U,\overline{\psi},\psi] + \sum_x J^a_\mu(x) V^a_\mu(x) \gamma_\mu \psi\,, \tag{F.1.2}$$

$$Z[J] = \int [dU][d\overline{\psi}][d\psi] e^{-S[U,\overline{\psi},\psi;J]} \tag{F.1.3}$$

where

$$S[U,\overline{\psi},\psi] = S_{\mathrm{G}}[U] + S_{\mathrm{F}}[U,\overline{\psi},\psi]\,, \quad S_{\mathrm{F}}[U,\overline{\psi},\psi] = \overline{\psi} D \psi \tag{F.1.4}$$

is the QCD discrete action, see Eq. (2.3.14). Note that Eq. (F.1.2) amounts to

$$D \to D + J^a_\mu i T^a \gamma_\mu\,. \tag{F.1.5}$$

Without factorizing the determinant, we would retrieve the standard, unfactorized result

$$\left. \frac{\partial^2 \det D}{\partial J^a_\mu(x) \partial J^b_\nu(y)} \right|_{J=0} = \det D \times \mathrm{Tr}\big\{ T^a \gamma_\mu D^{-1}(x,y) T^b \gamma_\nu D^{-1}(y,x) \big\}\,. \tag{F.1.6}$$

We can introduce the partition function corresponding to the approximate factorization of $\det D$ with N multiboson fields in Eq. (4.2.9)[1]

$$Z_N = \int [dU] e^{-S_{\mathrm{G}}[U]} \prod_{\mathrm{f}=u,d,s,\ldots} [d\chi_{\mathrm{f}}] \frac{\det D^{\mathrm{f}}_{\Omega_0^{\mathrm{e}}} \det D^{\mathrm{f}}_{\Omega_0^{\mathrm{o}}}}{\det D_{\Lambda_1}} e^{-S_{\mathrm{mb}}[\chi^{\mathrm{f}}]} \tag{F.1.7}$$

in terms of the factorized multiboson action $S_{\mathrm{mb}}[\chi] = \sum_{k=1}^{N/2} \|W_{\sqrt{u_k}}\, \chi\|^2$. Thanks to the factorization of the fermion determinant, we can obtain an approximated factorized observable as

$$\left.\frac{\partial^2 \ln Z}{\partial J^a_\mu(x) \partial J^b_\nu(y)}\right|_{J=0} = \left\langle \frac{\partial S_{\mathrm{mb}}}{\partial J^a_\mu(x)} \frac{\partial S_{\mathrm{mb}}}{\partial J^b_\nu(y)} \right\rangle_{J=0} + \mathcal{O}\left(e^{-N m_\pi \Delta}\right) \tag{F.1.8}$$

up to exponentially suppressed terms in the width Δ of the inactive region Λ_1.

[1] The notation of this Section differs from that of the first part of this Appendix simply by the substitutions $\Lambda_0 \leftrightarrow \Lambda_0^{\mathrm{e}}$, $\Lambda_2 \leftrightarrow \Lambda_0^{\mathrm{o}}$ in order to match that used in Chapter 4.

Appendix G

Basic domains in four-dimensional domain decomposition

To easily label the various subdomains considered in Section 4.4, it is useful to introduce a non-overlapping domain decomposition of the lattice so that the entire lattice L is decomposed as

$$L = \bigcup_{\hat{a}} \Gamma^{\hat{a}}\,, \tag{G.0.1}$$

where $\Gamma^{\hat{a}}$ is a basic hyperrectangular cell, see Fig. G.1 for a 2-dimensional representation. Each cell has dimension $G_\mu = B_\mu + b_\mu$ in the direction μ and it is uniquely identified by the position of its lower-left corner, given in four-dimensional Cartesian coordinates (in

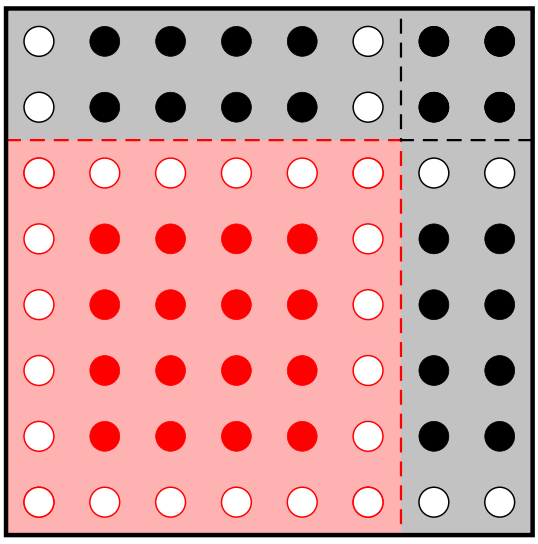

Figure G.1: Two-dimensional representation of a basic cell $\Gamma^{\hat{a}}$.

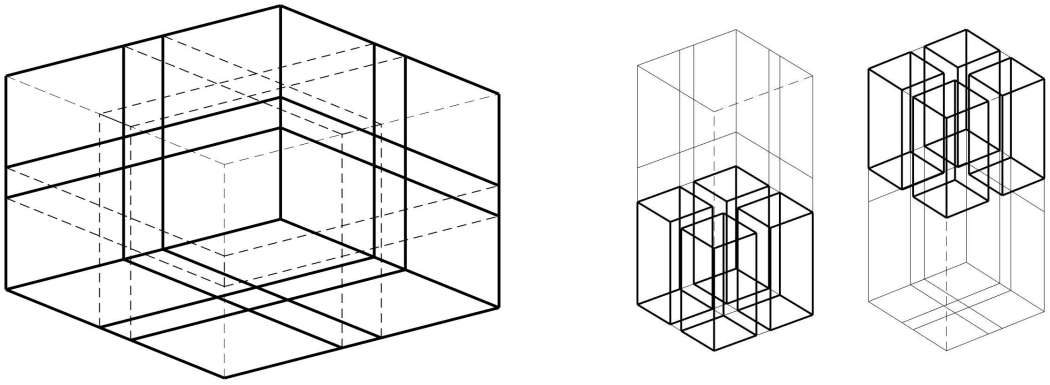

(a) 3-dimensional lattice. **(b)** Λ_0

Figure G.2: 3-dimensional domain decomposition.

units of G_μ) by $\hat{a} = \{a_0, a_1, a_2, a_3\}$, where

$$a_\mu = 0, \dots, \frac{L_\mu}{G_\mu} - 1 \,, \qquad \mu = 0, \dots, 3 \,, \tag{G.0.2}$$

where L_μ is the length of the lattice along direction μ. As a result, the global lattice coordinates of the lower-left point of the basic cell are given by $x_\mu = G_\mu \cdot a_\mu$ (no summation over repeated indices is meant here).

To map the blocks of the decomposition in Fig. 4.4 to the basic cells, the latter are further decomposed in 2^4 blocks as depicted in Fig. G.1. Within each cell, the 16 blocks can be identified by their local Cartesian coordinates in each direction μ, i.e. by $\hat{d} = (d_0, d_1, d_2, d_3)$ with $d_\mu = 0, 1$. In particular, the lower-left block ($\hat{d} = \hat{0}$) of $\Gamma^{\hat{a}}$ identifies the block $\Lambda_0^{\hat{a}}$ of Λ_0, shown in a 3-dimensional representation in Fig. G.2, with their lower-left corners coinciding. The other blocks of the basic cell belong to Λ_1, and the coordinates of their lower-left point are given by $x_\mu = G_\mu \cdot a_\mu + B_\mu \cdot d_\mu$ with $\hat{d} \neq \hat{0}$. For each block $\Lambda_0^{\hat{a}}$, its "frame" $\Phi_1^{\hat{a}}$ is shown in Fig. 4.5, and the "framed" domain $\Omega_0^{\hat{a}}$ are

$$\Gamma^{\hat{a}} = \Lambda_0^{\hat{a}} \bigcup_{\substack{\hat{d} \neq \hat{0} \\ d_\mu = 0,1}} \Lambda_1^{(\hat{a}, \hat{d})} \,, \quad \Phi_1^{\hat{a}} = \bigcup_{\substack{(\hat{c}, \hat{d}) \neq (\hat{0}, \hat{0}) \\ c_\mu, d_\mu = 0,1 \,|\, (d-c)_\mu = 0,1}} \Lambda_1^{(\hat{a}-\hat{c}, \hat{d})} \,, \quad \Omega_0^{\hat{a}} = \Lambda_0^{\hat{a}} \cup \Phi_1^{\hat{a}} \,. \tag{G.0.3}$$

The framed domain $\Omega_0^{\hat{a}}$ is made of 3^4 blocks with the obvious modifications for the blocks near the boundaries of the lattice depending on the boundary conditions adopted. The blocks $\Phi^{\hat{a}}$ clearly form an overlapping domain decomposition of the entire domain Λ_1. Analogously, the blocks $\Omega_0^{\hat{a}}$ form an overlapping domain decomposition of the entire lattice L, similarly to what happens in the one-dimensional case [84, 85].

Appendix H

Frequency-splitting of single-propagator traces

In this Appendix we review the frequency-splitting strategy, developed in Ref. [99] and employed to compute the disconnected contractions in Ref. [88] and in Section 4.3. We start with a theoretical introduction, to then show a preliminary numerical analysis.

Single-propagator traces (SPTs) are the most elementary fermion Wick contractions, e.g. entering the computations of the η' propagator, $K \to \pi\pi$ decays and a_μ^{HVP} among many other physically interesting quantities. Random noise estimators of SPTs are commonly used to profit from volume averages, see Subsection A.2.3, but they are numerically expensive since the quark propagator must be re-computed at each lattice point to then average over a large number of random-noise fields, in order to suppress the random noise variance which would otherwise dominate over the gauge noise. The idea of frequency-splitting (FS) is to propose a family of stochastic estimators of SPTs that reduces the computational cost by a factor 10 up to 100 (depending on the fermion bilinear) and whose variances are dominated by gauge noise (as ultimately desirable).

The connected correlation function of a generic disconnected Wick contraction made of two sub-diagrams $W_0(0)$, $W_1(x) \in \mathbb{R}$ is

$$\mathcal{C}_{W_1W_0} = \langle [W_1(x) - \langle W_1(x)\rangle]\,[W_0(0) - \langle W_0(0)\rangle]\rangle \tag{H.0.1}$$

with variance

$$\begin{aligned}\sigma^2_{\mathcal{C}_{W_1W_0}} &= \left\langle [W_1(x) - \langle W_1(x)\rangle]^2\,[W_0(0) - \langle W_0(0)\rangle]^2 \right\rangle - \mathcal{C}^2_{W_1W_0} \\ &\approx \sigma^2_{\mathcal{C}_{W_1}} \cdot \sigma^2_{\mathcal{C}_{W_0}} + \dots \quad \text{at large } |x|\,,\end{aligned} \tag{H.0.2}$$

which factorizes, for large $|x|$, as the product of the variances of single SPT estimators, e.g. $\sigma^2_{\mathcal{C}_{W_0}} = \left\langle [W_0(0) - \langle W_0(0)\rangle]^2 \right\rangle$. A multilevel algorithm could be beneficial if each SPT is computed using random-noise estimators, with the auxiliary field action being factorized, in the case of gauge noise dominating the variance of each sub-diagram.

H.1 Single propagator traces

SPTs can be written as

$$t_{\Gamma,r}(x) = -\frac{a_\Gamma}{a^4}\,\mathrm{Tr}\big\{\Gamma D^{-1}_{m_r}(x,x)\big\}\,, \quad a_\Gamma = \begin{cases} 1 & ,\ \Gamma \in \{\mathbb{1},\gamma_5,\gamma_\mu\gamma_5,\sigma_{\mu\nu}\} \\ -i & ,\ \Gamma = \gamma_\mu \end{cases} \tag{H.1.1}$$

and we are interested in computing

$$\bar{t}_{\Gamma,r}(x_0) = \frac{1}{L^3}\sum_{\mathbf{x}} a^3 t_{\Gamma,r}(x)\,, \quad \text{s.t.} \quad s_{\Gamma,r} = \langle \bar{t}_{\Gamma,r}(x_0)\rangle = a_\Gamma \langle \overline{\psi}_r(x)\Gamma\psi_r(x)\rangle \tag{H.1.2}$$

with variance $\sigma^2_{\bar{t}_{\Gamma,r}}$. We can define its random-noise estimator as

$$\bar{\tau}_{\Gamma,r}(x_0) = \frac{1}{L^3}\sum_{\mathbf{x}} a^3 \tau_{\Gamma,r}(x)\,, \quad \tau_{\Gamma,r}(x) = -\frac{1}{a^4 N_s}\sum_{i=1}^{N_s}\mathrm{Re}\Big[a_\Gamma \eta_i^\dagger(x)\Gamma\{D^{-1}_{m_r}\eta_i\}(x)\Big] \tag{H.1.3}$$

in terms of random sources

$$\langle \eta^a_\gamma(x)\{\eta^b_\delta(y)\}^\star\rangle = \delta^{ab}\delta_{\gamma\delta}\delta_{xy} \tag{H.1.4}$$

where a, b (γ, δ) are color (spin) indices. This estimator has variance

$$\sigma^2_{\bar{\tau}_{\Gamma,r}} = \sigma^2_{\bar{t}_{\Gamma,r}} - \frac{1}{2L^3N_s}\left\{a_\Gamma^2\sum_{\mathbf{x}} a^3\langle \mathcal{O}_{\Gamma,rr'}(0,\mathbf{x})\mathcal{O}_{\Gamma,r'r}(0)\rangle + \frac{1}{a}\sum_x a^4\langle P_{rr'}(x)P_{r'r}(0)\rangle\right\} \tag{H.1.5}$$

where $P_{rs} = \mathcal{O}_{\gamma_5,rs}$ and the last term is only due to random-noise, scales like a^{-3}, is color-enhanced w.r.t. gauge-noise and due to the π pole scales like m_r^{-1}, giving large contributions to the variances of all bilinears. Numerically, we observe a random-noise contribution to $\sigma^2 \propto N_s^{-1}$ comparable for all bilinears and dominating until the plateau due to gauge-noise is reached, with densities having larger gauge-noise w.r.t. currents.

SPTs can be estimated more effectively via a hopping expansion, isolating the contribution from the high-frequency modes of the quark propagator. The hopping parameter expension (HPE), combined with an even-odd decomposition, leads to

$$D^{-1}_m = M_{2n,m} + D^{-1}_m H^{2n}_m\,, \tag{H.1.6}$$

$$M_{2n,m} = (D_{\mathrm{ee}} + D_{\mathrm{oo}})^{-1}\sum_{k=0}^{2n-1} H^k_m\,, \quad H_m = -\big[D_{\mathrm{eo}}D^{-1}_{\mathrm{oo}} + D_{\mathrm{oe}}D^{-1}_{\mathrm{ee}}\big] \tag{H.1.7}$$

that allows us to rewrite the SPT estimator as

$$\bar{t}_{\Gamma,r}(x_0) = \bar{t}^M_{\Gamma,r}(x_0) + \bar{t}^R_{\Gamma,r}(x_0)\,, \tag{H.1.8}$$

where

$$\bar{t}^M_{\Gamma,r}(x_0) = -\frac{a_\Gamma}{aL^3}\sum_{\mathbf{x}}\mathrm{Tr}\left[\Gamma M_{2n,m_r}(x,x)\right] \tag{H.1.9}$$

can be computed exactly and efficiently at small n, and

$$\bar{t}^R_{\Gamma,r}(x_0) = -\frac{a_\Gamma}{aL^3}\sum_{\mathbf{x}} \mathrm{Tr}\big\{\Gamma\{D^{-1}_{m_r} H^{2n}_{m_r}\}(x,x)\big\} \tag{H.1.10}$$

can be estimated from

$$\tau^R_{\Gamma,r}(x_0) = -\frac{1}{aL^3 N_s}\sum_{\mathbf{x}}\sum_{i=1}^{N_s} \mathrm{Re}\Big\{a_\Gamma\left[\eta_i^\dagger H^n_{m_r}\right](x)\Gamma\left[D^{-1}_{m_r} H^n_{m_r}\eta_i\right](x)\Big\} \tag{H.1.11}$$

via a UV filtering of $H^n_{m_r}$ on both random sources. This is beneficial w.r.t. applying $H^{2n}_{m_r}$ only to one of the two, with the resulting variance roughly halved. The HPE variance reduction proves to be numerically effective, with $\sigma^2_{\bar{\tau}^R} \sim \frac{1}{10\div 100}\sigma^2_{\bar{\tau}}$ for $am_q = 0.3$ and $n = 2$, with a further reduction by $4\div 8$ times (depending on Γ) at $n = 4$. The bulk of the random-noise contribution to $\sigma^2_{\bar{\tau}}$ is due to $M_{2n,m_r}\ \forall\,\Gamma$, with a beneficial effect stemming from the subtraction and exact computation of the remainder. At heavier masses, a larger variance reduction is obtained from the definition of an efficient estimator of $s_{\Gamma,r}$, obtained by combining the exact computation of $\bar{t}^M$ and the stochastic estimation of $\bar{\tau}^R$, with optimal n, N_s which depend on the bilinear and on the final target observable.

H.2 Differences of single-propagator traces

To analyze the contribution to traces in variances from low-frequency modes of quark propagators, we can consider the difference of two SPTs with different masses $m_r \neq m_s$

$$\begin{aligned} t_{\Gamma,rs}(x) \equiv t_{\Gamma,r}(x) - t_{\Gamma,s}(x) &= -\frac{a_\Gamma}{a^4}\,\mathrm{Tr}\big\{\Gamma\{D^{-1}_{m_r}(x,x) - D^{-1}_{m_s}(x,x)\}\big\} \\ &= -\frac{a_\Gamma}{a^4}(m_s - m_r)\,\mathrm{Tr}\big\{\Gamma D^{-1}_{m_r} D^{-1}_{m_s}(x,x)\big\} \end{aligned} \tag{H.2.1}$$

and

$$\begin{aligned} s_{\Gamma,rs} \equiv s_{\Gamma,r} - s_{\Gamma,s} &= a_\Gamma\left\{\langle \mathcal{O}_{\Gamma,rr}(x)\rangle - \langle \mathcal{O}_{\Gamma,ss}(x)\rangle\right\} \\ &= a_\Gamma(m_s - m_r)\sum_y a^4 \langle S_{rs}(y)\mathcal{O}_{\Gamma,rs}(x)\rangle \end{aligned} \tag{H.2.2}$$

where $S_{rs} = \mathcal{O}_{\mathbb{1},rs}$ is the scalar density. We can also introduce

$$\bar{t}_{\Gamma,rs}(x_0) = \frac{1}{L^3}\sum_{\mathbf{x}} a^3 t_{\Gamma,rs}(x)\,. \tag{H.2.3}$$

The standard random-noise estimator

$$\bar{\theta}_{\Gamma,rs}(x_0) = \frac{1}{L^3}\sum_{\mathbf{x}}\theta_{\Gamma,rs}(x)\,,\quad \theta_{\Gamma,rs}(x) = -\frac{(m_s - m_r)}{a^4 N_s}\sum_{i=1}^{N_s}\mathrm{Re}\Big[a_\Gamma \eta_i^\dagger(x)\Gamma\{D^{-1}_{m_r} D^{-1}_{m_s}\eta_i\}(x)\Big] \tag{H.2.4}$$

receives again, as it happened for SPTs, a large, Γ-independent contribution to the variance. We can instead introduce a split-even random-noise estimator

$$\bar{\tau}_{\Gamma,rs}(x_0) = \frac{1}{L^3}\sum_{\mathbf{x}}\tau_{\Gamma,rs}(x)\,,\quad \tau_{\Gamma,rs}(x) = -\frac{(m_s - m_r)}{a^4 N_s}\sum_{i=1}^{N_s}\mathrm{Re}\Big[a_\Gamma\{\eta_i^\dagger D^{-1}_{m_r}\}(x)\Gamma\{D^{-1}_{m_s}\eta_i\}(x)\Big] \tag{H.2.5}$$

which has a smaller, Γ-dependent variance, since both sources η_i, $\eta_i^\dagger$ are UV filtered by D^{-1}. It is found numerically that, for the split-even estimator, $O(10)$ sources are needed to reach the gauge-noise level for $\Gamma = \gamma_5$, and $O(100)$ for $\Gamma = \gamma_\mu$, while the variances are $10 \div 100$ times larger for the standard one. Since the two estimators have the same cost for each source, the split-even is proved to be more efficient.

H.3 Frequency-splitting of single-propagator traces

We can now combine the efficient estimators for SPT at high momenta (masses) analyzed in Section H.1 and for low-frequencies SPT differences discussed in Section H.2, to efficiently estimate SPTs via a *frequency-splitting* (FS) strategy. The FS estimator is defined by adding and subtracting $m-1$ SPTs with increasing masses, to then estimate

$$\bar{\tau}^{\mathrm{FS}}_{\Gamma,r_1}(x_0) = \sum_{k=1}^{m-1} \bar{\tau}_{\Gamma,r_k r_{k+1}} + \bar{\tau}^{R}_{\Gamma,r_m}(x_0) + \bar{t}^{M}_{\Gamma,r_m}(x_0) \tag{H.3.1}$$

via a distinct separation between high momenta, contributing both to the exact computation of $\bar{t}^{M}_{\Gamma,r_m}(x_0)$ (giving the bulk of the standard variance) and the estimate of $\bar{\tau}^{R}_{\Gamma,r_m}(x_0)$, and low-frequencies, present in the efficient estimate of $\bar{\tau}_{\Gamma,r_k r_{k+1}}$ via split-even estimators. Numerical tests for two-point functions can be found in Ref. [99], and here we simply report that $\forall\,\Gamma$ the gauge-noise was reached in a limited and affordable number of evaluations of FS estimators, with the number of sources required to reach gauge-noise being $N_s \sim 1$ for $\Gamma = \mathbb{1}$ and $\Gamma = \gamma_5$; $N_s \sim O(10)$ for $\Gamma = \gamma_5\gamma_k$; $N_s \sim O(100)$ for $\Gamma = \gamma_k$. The FS estimator for the isoscalar vector current used in Section 4.3 is

$$C^{r}_{VV}(x_0) = -\frac{L^3}{3L_0}\sum_{k=1}^{3}\sum_{y_0} a\langle \bar{t}_{\gamma_k,r}(x_0+y_0)\bar{t}_{\gamma_k,r}(y_0)\rangle \tag{H.3.2}$$

where the disconnected is a small contribution to the isoscalar channel at intermediate hadronic distances, but its variance quickly dominates at large distances, calling for an improved estimator to resolve the full correlator at larger distances.

H.4 Preliminary Numerical Results

We now present an ongoing numerical analysis testing the frequency splitting strategy, employing the same lattice setup as that detailed in Subsection 4.3.1 with the goal of estimating the remaining disconnected strange SPT, with the $(l-s)$ contribution having already been computed to the gauge level in Ref. [88]. In particular, the focus of the present analysis is to discriminate between whether applying an additional split would be beneficial in terms of computational cost. We also show a few results to illustrate the concepts above. Note that an optimization strategy has been presented in Ref. [258].

Given N_s sources, we define an estimator for the gauge noise level σ^2_{gnl}, a quantity which is independent of N_s, as

$$\bar{\sigma}^2_{\text{gnl}} = \frac{1}{N_s(N_s-1)} \left(\langle \sum_{i\neq j}^{N_s} \tau_i(x_0)\tau_j(x_0) \rangle - \sum_{i\neq j}^{N_s} \langle \tau_i(x_0) \rangle \langle \tau_j(x_0) \rangle \right) \tag{H.4.1}$$

where τ_i is the stochastic estimator for the SPT. Since σ^2_{gnl} is time-independent, we can also average Eq. (H.4.1) over time, in order to define the best estimator using all available points and sources. Although the number of sources N_s is limited for this preliminary study, in order to extract an estimate of the approximate number of sources needed to saturate the gauge noise level, we additionally consider a fit of the form $\sigma^2 = \sigma^2_{\text{gnl}} + \frac{c_0}{N_s}$ and a subsequent extrapolation. In order to perform a correct comparison, we need to check the convergence of the SPT for the strange contribution alone and compare it with the one of $(s-c)+c$ where we introduce one splitting, computing $(s-c)$ and c independently. A few remarks are due.

- Even if we are interested in the full disconnected contribution, the $(l-s)$ term has already been computed to the gauge level in Ref. [88], and thus we focus on the remaining s contribution. For completeness, we also numerically studied the $(l-s)$, and estimated the full $(l-s)+(s-c)+c$ contributions to the gauge variance, finding no significant change in the following analysis.

- Interestingly, the c contribution for each channel reaches the gauge noise level at a number of sources that is always roughly 10× those needed for $(s-c)$. We keep this ratio fixed, indicating results as $(s-c)+10\times c$.

- Since the gauge noise can only be reached at $N_s = \infty$, we define the gauge noise level to be saturated (stopping criterion) at the number of sources $N_s^\star$ required for the variance to be equal to 1.2× the gauge noise level. At this point, the total noise receives a small stochastic contribution compared to gauge noise (recall that in multilevel simulations we want to be dominated by gauge noise).

To study the s contribution alone, we analyzed 100 configurations with $N_s = 100$ sources, with one configuration analyzed in 931 seconds on average (with 192 cores, it corresponds to 0.50 CPUh per source). Each one of the 100 configurations with $25+250$ sources used for the $(s-c)+10\times c$ contribution was instead analyzed in 1020 seconds (2.176 CPUh per $1+10$ sources). We can finally estimate the total costs to saturate the level of 1.2× gauge noise for the different channels, with the results extracted from Fig. H.1 reported in Table H.1, showing the gain of splitting, since

1. the cost of s with $N_s = 100$ is roughly the same as that of $(s-c)+10\times c$ with $N_s = 25$, making the direct estimate of s roughly 4 times faster for each configuration;

2. the required number of sources $N_s^\star$ is 10 times larger for s than for $(s-c)+10\times c$.

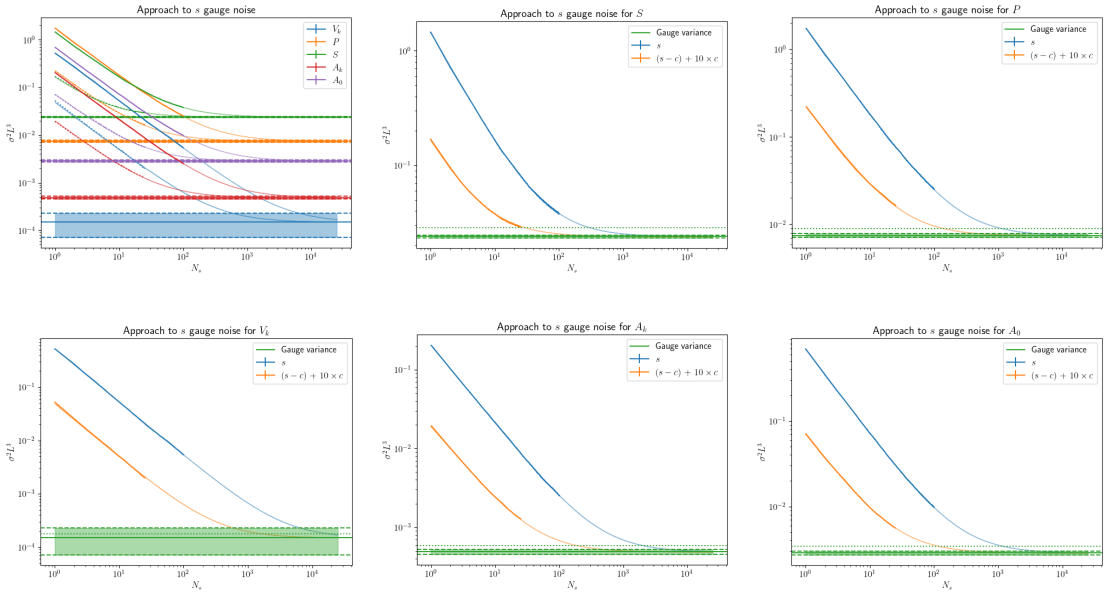

Figure H.1: Comparison of s and $(s-c)+10\times c$ contributions to the variance for different channels S, P, V_k, A_k and A_0, including fits and extrapolations. The horizontal line with errorbars represents the estimate of the gauge noise, while the dashed one with no errorbar is the central value of 1.2× the gauge noise, used to define convergence to the gauge noise level.

Obs	$N_s^\star[s]$	Cost $[s]$	$N_s^\star[(s-c)+10\times c]$	Cost $[(s-c)+10\times c]$
V_k	2×10^4	9930.7	2×10^3	4352.0
P	1×10^3	496.53	1×10^2	217.60
S	3×10^2	148.96	3×10^1	65.28
A_k	2×10^3	993.06	2×10^2	435.20
A_0	1×10^3	496.53	1×10^2	217.60

Table H.1: Estimated costs (CPUh) to compute the s SPT to 1.2× gauge noise level.

We can repeat a similar analysis defining $N_s^\star$ from requiring the variance to reach the gauge noise level of the light contribution $(l-s)+(s-c)+c$, confirming our conclusions. In fact, the estimates of $N_s^\star$, and thus of the cost, are unchanged for V_k ($\Gamma=\gamma_k$), A_k ($\Gamma=\gamma_5\gamma_k$), S ($\Gamma=\mathbb{1}$) and A_0 ($\Gamma=\gamma_5\gamma_0$), while for P ($\Gamma=\gamma_5$) they are 10× lower, both with and without the splitting.

Appendix I

Continuum and discrete inverse problems

In this Appendix, we review useful mathematical relations to perform the ILT, both in the continuum and in the discrete cases. We also provide two examples of applications of our formalism, namely to rewrite smeared spectral densities as integrals of the associated correlation functions in the time-momentum representation, and a procedure to estimate the latter by minimizing the associated discretization errors.

I.1 Properties of the Mellin basis

The *orthogonality* of the basis vectors $\{|s\rangle\}$, defined in Eq. (5.1.6), may be proven by considering the change of variable $\eta = \log(t)$ so that

$$\int_0^\infty dt\, u_s^*(t) u_{s'}(t) = \int_{-\infty}^\infty \frac{d\eta}{2\pi}\, e^{i\eta(s-s')} = \delta(s-s')\,, \tag{I.1.1}$$

while the *completeness* of the basis is guaranteed by

$$\int_s u_s^*(t) u_s(t') = \frac{\delta(\log(t/t'))}{\sqrt{tt'}} = \delta(t-t')\,. \tag{I.1.2}$$

This relation also helps us understand that

$$\lim_{\alpha\to 0} \delta_\alpha(\omega,\omega') = \lim_{\alpha\to 0} \int_s u_s^*(\omega) \frac{|\lambda_s|^2}{|\lambda_s|^2+\alpha} u_s(\omega') = \delta(\omega-\omega')\,. \tag{I.1.3}$$

Analogously to the Fourier transform, also in this case it is possible to work with a basis of *real eigenfunctions*

$$u_s^+(t) = \frac{u_s(t)+u_s^*(t)}{\sqrt{2}} = \frac{\cos(s\log(t))}{\sqrt{\pi t}}\,, \tag{I.1.4}$$

$$u_s^-(t) = \frac{u_s(t)-u_s^*(t)}{\sqrt{2}i} = \frac{\sin(s\log(t))}{\sqrt{\pi t}}\,, \tag{I.1.5}$$

with $s \in \mathbb{R}^+$. They satisfy the orthogonality relations

$$\int_\omega \left[u_s^+(\omega)u_{s'}^+(\omega) \pm u_s^-(\omega)u_{s'}^-(\omega)\right] = \delta(s \mp s')\,, \qquad \int_\omega u_s^\pm(\omega)u_{s'}^\mp(\omega) = 0 \tag{I.1.6}$$

while their completeness stems from

$$\int_{s\in\mathbb{R}^+} u_s^\pm(\omega)u_s^\pm(\omega') = \frac{1}{2}\left[\delta(\omega-\omega') \pm \omega\delta\left(\omega - \frac{1}{\omega'}\right)\right], \qquad \int_{s\in\mathbb{R}^+} u_s^\pm(\omega)u_s^\mp(\omega') = 0 \tag{I.1.7}$$

and it is retrieved in the sense that

$$\int_{s\in\mathbb{R}^+} \left[u_s^+(\omega)u_s^+(\omega') + u_s^-(\omega)u_s^-(\omega')\right] = \delta(\omega-\omega')\,. \tag{I.1.8}$$

In this basis, Carleman's operator in Eq. (5.1.3) becomes

$$\mathcal{H}(\omega,\omega') = \int_{s\in\mathbb{R}^+} |\lambda_s|^2\left[u_s^+(\omega)u_s^+(\omega') + u_s^-(\omega)u_s^-(\omega')\right], \tag{I.1.9}$$

making more explicit the (known) *double degeneracy* of its spectrum. The eigenvalue equation can also be rewritten as

$$\int_{\omega'} \mathcal{H}(\omega,\omega')u_s^\pm(\omega') = |\lambda_s|^2 u_s^\pm(\omega) = \pm\int_{\omega'} \mathcal{G}(\omega,\omega')u_s^\pm(\omega') \tag{I.1.10}$$

where we used the change of variables $\omega' \to 1/\omega'$, which leaves the integration domain unchanged, and we introduced the operator

$$\mathcal{G}(\omega,\omega') = \frac{1}{1+\omega\omega'} = \int_{s\in\mathbb{R}^+} |\lambda_s|^2\left[u_s^+(\omega)u_s^+(\omega') - u_s^-(\omega)u_s^-(\omega')\right]. \tag{I.1.11}$$

This operator breaks the degeneracy of the spectrum of $\mathcal{H}$, directly linked to the invariance of the domain under $x \to 1/x$ symmetry [241]. In fact, for instance the spectrum of the discrete operators is found not to be degenerate, see the next Section. So, if we were to restrict $\omega \in (1,\infty)$, the Mellin basis would not diagonalize neither $\mathcal{H}$ nor $\mathcal{G}$, but only their specific combination

$$\int_1^\infty d\omega' \left[\mathcal{H}(\omega,\omega') - i\mathcal{G}(\omega,\omega')\right]u_s(\omega') = |\lambda_s|^2 u_s(\omega) \tag{I.1.12}$$

with a similar relation holding for $\omega \in (0,1)$. This of course applies to the operator $\mathcal{A}$ in Eq. (5.1.20) as well, which in the continuum has the same functional form as $\mathcal{H}$. Besides the fact that the Mellin basis does not diagonalize anymore $\mathcal{A}$ for $t \in (a, t_{\max})$, the operator to be inverted when a restriction is applied to the time domain is different, see Eq. (5.2.2) for the case of $t/a \in \mathbb{N}$ and Eq. (5.3.12) for the case of $t \in (0, t_{\max})$. In the following Section, we address the first case.

I.2 Properties of the discrete basis

In this Section we examine known properties of the so-called Hilbert matrix to derive the explicit functional form of the $v_s(\omega, a)$ functions in Eq. (5.2.7). We begin from the diagonalization of the (infinite) Hilbert matrix [242] regarded as an operator acting on $\ell^2(\mathbb{Z}^+)$

$$\sum_{n=0}^{\infty} \frac{1}{n+m+\lambda} x_n(\mu,\lambda) = \frac{\pi}{\sin(\pi\mu)} x_m(\mu,\lambda)\,, \quad \lambda \in \mathbb{R}\backslash\mathbb{Z}^- \tag{I.2.1}$$

with $\mu = \frac{1}{2} + is$, by the eigenfunctions

$$x_n(\mu,\lambda) = \sum_{k=0}^{n} \binom{n}{k} (-1)^k \frac{\Gamma(k+\mu)\Gamma(k+1-\mu)}{\Gamma(k+\lambda)\Gamma(k+1)}\,. \tag{I.2.2}$$

By using a known integral representation of Euler's β function and its relation with the Γ function

$$\beta(x,y) = \int_0^1 dr\, r^{x-1}(1-r)^{y-1} = \frac{\Gamma(x)\Gamma(y)}{\Gamma(x+y)}\,, \tag{I.2.3}$$

and the property

$$\sum_{k=0}^{n} \binom{n}{k} x^k = (1+x)^n\,, \tag{I.2.4}$$

with little algebra we derive the following representation in terms of the hypergeometric function ${}_3F_2$ [119]

$$x_n(\mu,\lambda) = \frac{\pi}{\sin(\pi\mu)}\ {}_3F_2\left(\begin{matrix} -n, \mu, 1-\mu \\ 1, \lambda \end{matrix} \middle| 1 \right), \tag{I.2.5}$$

much more suitable for numerical evaluation than Eq. (I.2.2). For $\mu = \frac{1}{2} + is$ the eigenvalues in Eq. (I.2.1) coincide with those in the continuum $|\lambda_s|^2$. Instead the eigenfunctions $x_n(\frac{1}{2} + is, \lambda)$ are related to the so-called continuous dual Hahn polynomials, defined according to [244–246]

$$S_n(x^2; a, b, c) = (a+b)^{(n)}(a+c)^{(n)}\, {}_3F_2\left(\begin{matrix} -n, a+ix, a-ix \\ a+b, a+c \end{matrix} \middle| 1 \right), \tag{I.2.6}$$

with the rising factorial being

$$(x)^{(n)} = \frac{\Gamma(x+n)}{\Gamma(x)}\,, \quad \forall x \in \mathbb{C}/\mathbb{Z}_0^-\,. \tag{I.2.7}$$

They satisfy the orthogonality relation (see e.g. Ref. [244])

$$\begin{aligned} \frac{1}{2\pi} \int_0^{\infty} ds\, |W_s(a,b,c)|^2\, S_m(s^2; a, b, c)\, S_n(s^2; a, b, c) \\ = \Gamma(n+a+b)\Gamma(n+a+c)\Gamma(n+b+c) n!\, \delta_{nm}\,, \end{aligned} \tag{I.2.8}$$

with

$$W_s(a,b,c) = \frac{\Gamma(a+is)\Gamma(b+is)\Gamma(c+is)}{\Gamma(2is)}\,. \tag{I.2.9}$$

By setting $a = b = 1/2$ and $c = \lambda - 1/2$, we obtain a completeness relation for the eigenfunctions of the Hilbert matrix acting on $\ell^2(\mathbb{Z}^+)$

$$\int_0^\infty ds\, \frac{|\lambda_s|^2}{|N_s|^2} x_n\left(\frac{1}{2}+is,\lambda\right) x_m\left(\frac{1}{2}+is,\lambda\right) = \delta_{nm} \tag{I.2.10}$$

with

$$N_s = \sqrt{2\pi}\, \frac{\Gamma(-2is)\lambda_s}{\Gamma\left(\lambda-\frac{1}{2}+is\right)\Gamma(\lambda)} \tag{I.2.11}$$

coinciding with N_s defined in Eq. (5.2.8) if we set $\lambda = 2t_{\min}/a = 2\tau$. Note that, for simplicity and similarly to Section 5.2 for $t_{\min}$, we omit the explicit dependence on λ. Since the Hilbert matrix is typically expressed in terms of integer numbers, we denote its corresponding dimensionful counterpart as $\overline{A}_a$ as in Eq. (5.2.3) with $\lambda = 2t_{\min}/a = 2\tau$, with matrix elements

$$\overline{A}_a(an,am) = \frac{1}{a(n+m+\lambda)}\,. \tag{I.2.12}$$

It may be interpreted as the projection of Eq. (5.1.20) (at $\alpha = 0$) to discrete time coordinates and its normalized eigenfunctions are given by

$$\overline{v}_s(an,a) \equiv \frac{|\lambda_s|}{\sqrt{a}|N_s|} x_n\left(\frac{1}{2}+is,\lambda\right). \tag{I.2.13}$$

Starting from the relation between $\overline{A}_a(t,t')$ and $\overline{\mathcal{H}}_a(\omega,\omega')$

$$a\sum_{n=0} e^{-a\omega(n+\lambda/2)}\overline{A}_a(an,am) = \int_{\omega'} \overline{\mathcal{H}}_a(\omega,\omega')e^{-a\omega'(m+\lambda/2)}\,, \tag{I.2.14}$$

one easily finds that they share the same spectrum

$$\int_{\omega'} \overline{\mathcal{H}}_a(\omega,\omega')v_s(\omega',a) = |\lambda_s|^2\, v_s(\omega,a)\,, \tag{I.2.15}$$

while their eigenfunctions are related as follows

$$|\lambda_s|\, v_s(\omega,a) = a\sum_{n=0}^{\infty} e^{-a\omega(n+\lambda/2)}\overline{v}_s(an,a)\,. \tag{I.2.16}$$

Setting $t_{\min} = a$ i.e. $\lambda = 2 = 2\tau$, from the exclusion of the first time slice $t = 0$, it follows that $an = t - a$ as in Eq. (5.2.13). Their orthogonality stems from the spectral theorem, while their completeness follows from Eq. (I.2.10). Hence, they define a complete orthonormal basis in $L^2(0,\infty,d\omega)$ where $\overline{\mathcal{H}}_a(\omega,\omega')$ is diagonal

$$\overline{\mathcal{H}}_a(\omega,\omega') = \int_0^\infty ds\, v_s(\omega,a)|\lambda_s|^2 v_s(\omega',a)\,. \tag{I.2.17}$$

Now, we briefly study the leading discretization effects of the $v_s(\omega,a)$ functions. By starting from Eq. (I.2.16), after some algebra, we arrive at the integral representation

$$v_s(\omega,a) = \sqrt{a}z\frac{|\lambda_s|^2}{|N_s|}{}_2F_1\left(\begin{matrix}\frac{1}{2}+is,\frac{1}{2}-is\\ \lambda\end{matrix}\,\middle|\, -z\right)e^{-a\omega(\lambda/2-1)}\,,\quad z = \frac{e^{-a\omega}}{1-e^{-a\omega}}\,. \tag{I.2.18}$$

Setting $\lambda = 2$ and using known relations among the hypergeometric function ${}_2F_1$ with different arguments [119], we obtain the equivalent form used in Eq. (5.2.14). From its expansion around $a = 0$, we prove that discretization errors linear in the lattice spacing vanish, and in the continuum limit the functions $v_s(\omega, a)$ tend to the specific linear combination of $u_s(\omega)$ and $u_s^*(\omega)$ given in Eq. (5.2.16). In the alternative basis of real functions in the continuum, $v_s(\omega, a)$ would tend to a combination of $u_s^+(\omega)$ and $u_s^-(\omega)$. Finally, we note that by squaring Eq. (5.2.16) we obtain four terms: $a[u_s(a\omega)u_s^*(a\omega') + u_s^*(a\omega)u_s(a\omega')]$ lead to $\delta(\omega - \omega')$ upon integration over s, while the remaining additional terms, proportional to $u_s(a\omega)u_s(a\omega')$ and $u_s^*(a\omega)u_s^*(a\omega')$, produce a vanishing contribution for $a \to 0$, after integrating in s.

I.3 Applications to a_μ^{HVP}

Here we want to show a possible application of the above formalism to the computation of time-momentum kernels. We consider the exemplary case of the computation of the hadronic contributions to the muon $(g-2)$, detailed in Subsection 3.3.1, providing an alternative strategy than that devised in Ref. [154]. The core of the problem is to rewrite

$$a_\mu^{\mathrm{HVP,LO}} = \int_0^\infty dQ^2\, K(Q^2)[\Pi(Q^2) - \Pi(0)] \tag{I.3.1}$$

in terms of an integral involving the correlation function, exploiting the once-subtracted dispersive relation[1]

$$\Pi(Q^2) - \Pi(0) = Q^2 \int_0^\infty ds \frac{\rho(\sqrt{s})}{s(s+Q^2)} \tag{I.3.2}$$

and

$$C(t) = \int_\omega \rho(\omega)\omega^2 e^{-\omega t}\,. \tag{I.3.3}$$

The idea is the following: we can insert in Eq. (I.3.2) our solution of the inverse problem given in Eq. (5.1.29). If the problem has a solution, as we know it does for this case, we must be able to analytically take the $\alpha \to 0$ limit and rewrite Eq. (I.3.2) as an intergral of $C(t)$ over $t \in \mathbb{R}^+$. This integral can be then inserted in Eq. (I.3.1) in order to compute the desired solution, with the kernel in the time domain given by the remaining analytical integration over Q^2. Here, we show how this procedure is practically feasible by showing how to rewrite Eq. (I.3.2) by means of inverting Eq. (I.3.3).

We can first rewrite Eq. (I.3.2) through the change of variables $s \to \omega^2$. Using our solution in Eq. (5.1.29) with $k = 1$, we find

$$\Pi(Q^2) - \Pi(0) = 2Q^2 \lim_{\alpha\to 0} \int_t t^2 C(t) \int_s \frac{\lambda_{s,b} u_s^*(t)}{\lambda_{s,b}\lambda_{s,2}^* + \alpha} \times \int_\omega u_s^*(\omega) \frac{1}{\omega(\omega^2+Q^2)}\,. \tag{I.3.4}$$

[1] We omit the s in the subscript of $\rho(\omega)$, used in Subsection 5.1.3 to indicate subtracted spectral densities.

We should now rewrite the last integral as an integral over t', ideally extracting $\lambda^*_{s,2}$ to correctly remove unexpected divergences at $|s| \to \infty$ and take the $\alpha \to 0$ limit. Our strategy is to exploit known relations between a function and its Laplace transform, e.g.

$$f(x) = \int_0^\infty dy\, e^{-xy} g(y) \quad \to \quad \int_0^\infty dx\, u_s^*(x) f(x) = \lambda_s^* \int_0^\infty dy\, g(y) u_s(y) \tag{I.3.5}$$

which can be generalized to extract $\lambda^*_{s,2}$ as

$$f(x) = \int_0^\infty dy\, e^{-xy} y^2 g(y) \quad \to \quad \int_0^\infty dx\, u_s^*(x) x^2 f(x) = \lambda^*_{s,2} \int_0^\infty dy\, u_s(y) g(y)\,. \tag{I.3.6}$$

Using the known result [119]

$$\int_0^\infty dy\, e^{-xy} y^2 \frac{1-\cos(Qy)}{Q^2 y^2} = \frac{1}{x(x+Q^2)} \tag{I.3.7}$$

we can rewrite

$$\int_\omega u_s^*(\omega) \frac{1}{\omega(\omega^2+Q^2)} = \lambda^*_{s,2} \int_{t'} u_s(t') \frac{1-\cos(Qt')}{t'^2 Q^2} \tag{I.3.8}$$

which allows us to take the $\alpha \to 0$ limit in Eq. (I.3.4). We can then additionally expand the kernel $[1-\cos(Qt)]$ at small t, as done in Ref. [154], to then proceed analogously. Notice that in principle the same result is recovered by inserting in the unsubtracted polarization scalar

$$\Pi(Q^2) = \int_0^\infty ds \frac{\rho(\sqrt{s})}{s+Q^2} \tag{I.3.9}$$

the unsubtracted result of the ILT in Eq. (5.1.14), using then

$$\int_0^\infty dy\, e^{-xy} \cos(Qy) = \frac{x}{x^2+Q^2} \tag{I.3.10}$$

rather than Eq. (I.3.7) to take the $\alpha \to 0$ limit. The expansion to extract $\Pi(Q^2) - \Pi(0)$ could then be computed only at this point, avoiding it at the level of Eq. (I.3.9).

I.4 Integrals in time with minimal discretization errors

We are now going to address the seemingly different problem of estimating

$$I = \int_0^\infty dt\, C(t) K(t)\,, \tag{I.4.1}$$

where $K(t)$ is analytically known and we sample $C(t)$ as $\overline{C}_a(t)$ on a finite and discrete set of points $t \in \{a, 2a, \ldots, Na = t_{\max}\}$ with $O(a^2)$ discretization errors. We refer to Ref. [6] for further details. Applications include for instance the computation of a (smeared) spectral density, with K being our coefficients, or $a_\mu^{\mathrm{LO,HVP}}$ in the time-momentum representation [154]. One approach is to directly discretize the integral, ending up with

$$I_1 = a \sum_{n=1}^{N} \overline{C}_a(na) K(na) \tag{I.4.2}$$

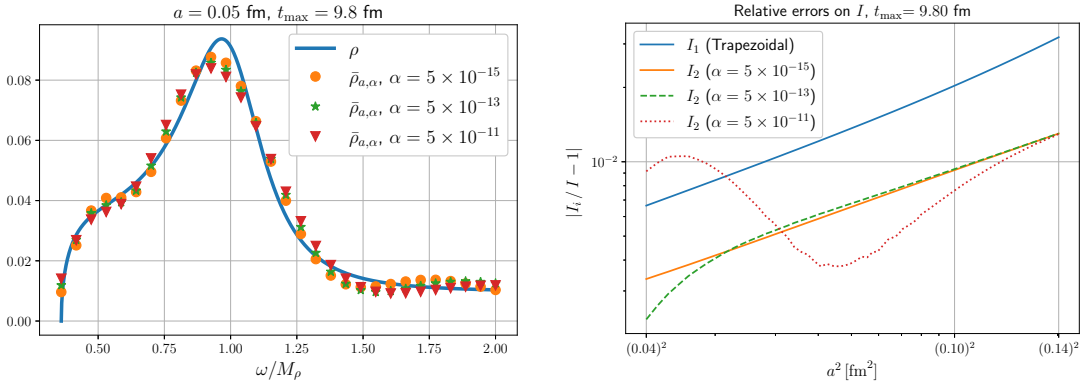

(a) Reconstruction of $\rho(\omega)$

(b) Relative errors on the reconstruction of I

Figure I.1: (a) Reconstruction of the spectral density in Eq. (I.4.6), and (b) relative errors on the reconstruction of the corresponding $I = \int_t C(t)K(t)$ with $K(t) = t^3$ using the two methods in Eq. (I.4.2) and Eq. (I.4.5).

or employing a higher-order discrete estimator of the integral, such as the $O(a)$-improved trapezoidal rule. We could also interpret the original integral as a smeared spectral density, since

$$I = \int_0^\infty dt\, C(t)K(t) = \int_0^\infty d\omega\, \rho(\omega)\kappa[K](\omega) \tag{I.4.3}$$

where the energy-kernel κ is a functional of the time-kernel K. For instance

$$C(t) = \int_0^\infty d\omega\, \rho(\omega)\omega^2 e^{-\omega t} \quad \to \quad \kappa[K](\omega) = \omega^2 \int_0^\infty dt\, e^{-\omega t} K(t)\,. \tag{I.4.4}$$

In principle, this might seem counterintuitive, given all the efforts in analytically inverting the last form of Eq. (I.4.3) to define it in the time domain. Taking inspiration from what has just been studied, its direct discretization might not always be the best discrete solution we can define. For instance, we can directly apply our discrete, analytic formula to extract I as a linear combination of $\overline{C}_a(t)$ with proper coefficients as

$$\rho_\kappa = \lim_{\alpha\to 0} I_2(\alpha) = \lim_{\alpha\to 0} a \sum_{n=1}^{\infty} \overline{g}_{a,\alpha}(na|\kappa)\overline{C}_a(na)\,, \quad \overline{g}_{a,\alpha}(na|\kappa) = \int_\omega \overline{g}_{a,\alpha}(na|\omega)\kappa(\omega)\,, \tag{I.4.5}$$

with the great benefit of allowing us to interpret this solution as the one with minimal discretization errors, becoming negligible as $\alpha \to 0\ \forall\, a$. This statement is necessarily inexact as long as $\alpha > 0$ and with $N < \infty$ points in the above linear combination, with truncation errors which are expected to be exponentially suppressed in $t_{\max}$, see Subsection 5.3.2. In Fig. I.1a we show the results of the reconstruction at different values of α for the correlation function $C(t)$ as in Eq. (I.4.4) with

$$\omega^2\rho(\omega) = \frac{1}{\Gamma_\rho}\sqrt{1 - 4\frac{m_\pi^2}{\omega^2}}\left[\frac{\Gamma_\rho^2}{(\omega - M_\rho)^2 + \Gamma_\rho^2} + \left(\frac{\omega}{3M_\rho}\right)^2\right], \tag{I.4.6}$$

where the values of m_π, M_ρ and Γ_ρ are taken as in Eq. (5.1.17). In Fig. I.1b we compare the relative errors on the estimate of the integral I as a function of the lattice spacing, at a fixed value of $t_{\max}$ and α and for the simple choice $K(t) = t^3$. As expected, the continuum limit is approached with a similar scaling in a^2 for both methods. Every choice of α corresponds to a different reconstructed observable, additionally smeared by $\overline{\delta}_{a,\alpha}$ in Eq. (5.2.11), with different systematic errors w.r.t. its $\alpha \to 0$ limit. The oscillations of the relative errors observed in Fig. I.1b are nothing but a consequence of the fluctuations in $\overline{\delta}_{a,\alpha}$, vanishing as α is sent to 0. From the comparison of the two plots in Fig. I.1, we can appreciate that even small differences in the spectral reconstructions can be significantly amplified in the computation of its smearing, potentially introducing relevant systematic errors when approximating I. Our ideal strategy is then to study the continuum limit at fixed α, which therefore enters the definition of the observable we want to extract. This eliminates the need to account for or quantify any systematic effects related to α, which can nevertheless be estimated a priori to fix a suitable value of α, as detailed in Subsection 5.3.2. The $\alpha \to 0$ limit can then be addressed in the continuum.

Bibliography

[1] L. Giusti and M. Saccardi, *Four-dimensional factorization of the fermion determinant in lattice QCD*, *Phys. Lett. B* **829** (2022) 137103, [arXiv:2203.02247].

[2] M. Bruno, L. Giusti, and M. Saccardi, *Spectral densities from Euclidean lattice correlators via the Mellin transform*, arXiv:2407.04141.

[3] M. Bruno, L. Giusti, and M. Saccardi, "Publication in preparation."

[4] M. Saccardi and L. Giusti, *Four-dimensional domain decomposition for the factorization of the fermion determinant*, *PoS* **LATTICE2022** (2023) 386, [arXiv:2211.06902].

[5] M. Bruno, L. Giusti, and M. Saccardi, *On the prediction of spectral densities from lattice qcd*, *IL NUOVO CIMENTO* **47 C** (2024) 197.

[6] M. Saccardi, M. Bruno, and L. Giusti, "Spectral densities from Euclidean-time lattice correlation functions." Proceeding to the 41st International Symposium on Lattice Field Theory (LATTICE2024), in preparation.

[7] H. Fritzsch, M. Gell-Mann, and H. Leutwyler, *Advantages of the Color Octet Gluon Picture*, *Phys. Lett. B* **47** (1973) 365–368.

[8] M. Gell-Mann, *Symmetries of baryons and mesons*, *Phys. Rev.* **125** (1962) 1067–1084.

[9] M. Gell-Mann, *A Schematic Model of Baryons and Mesons*, *Phys. Lett.* **8** (1964) 214–215.

[10] G. Zweig, *An SU(3) model for strong interaction symmetry and its breaking. Version 1*, .

[11] M. Gell-Mann, *The symmetry group of vector and axial vector currents*, *Physics Physique Fizika* **1** (Jul, 1964) 63–75.

[12] K. G. Wilson, *Renormalization group and critical phenomena. 1. Renormalization group and the Kadanoff scaling picture*, *Phys. Rev. B* **4** (1971) 3174–3183.

[13] K. G. Wilson, *Renormalization group and critical phenomena. ii. phase-space cell analysis of critical behavior*, *Phys. Rev. B* **4** (Nov, 1971) 3184–3205.

[14] K. G. Wilson and J. B. Kogut, *The Renormalization group and the epsilon expansion*, *Phys. Rept.* **12** (1974) 75–199.

[15] K. G. Wilson, *Confinement of quarks*, *Phys. Rev. D* **10** (Oct, 1974) 2445–2459.

[16] J. Schwinger, *ON THE EUCLIDEAN STRUCTURE OF RELATIVISTIC FIELD THEORY*, *Proc. Nat. Acad. Sci.* **44** (1958), no. 9 956–965.

[17] K. Osterwalder and R. Schrader, *Axioms for Euclidean Green's functions*, *Communications in Mathematical Physics* **31** (1973), no. 2 83 – 112.

[18] A. Wightman, *Hilbert's Sixth Problem: Mathematical Treatment of the Axioms of Physics*, *Mathematical Developments Arising from Hilbert Problems, Symposia in Pure Mathematics* **28** (1976) 147–240.

[19] C. A. Baker et al., *An Improved experimental limit on the electric dipole moment of the neutron*, *Phys. Rev. Lett.* **97** (2006) 131801, [hep-ex/0602020].

[20] M. Luscher, R. Narayanan, P. Weisz, and U. Wolff, *The Schrödinger functional: A Renormalizable probe for nonAbelian gauge theories*, *Nucl. Phys. B* **384** (1992) 168–228, [hep-lat/9207009].

[21] M. Lüscher, *Properties and uses of the Wilson flow in lattice QCD*, *JHEP* **08** (2010) 071, [arXiv:1006.4518]. [Erratum: JHEP 03, 092 (2014)].

[22] M. Cè, C. Consonni, G. P. Engel, and L. Giusti, *Non-Gaussianities in the topological charge distribution of the SU(3) Yang–Mills theory*, *Phys. Rev. D* **92** (2015), no. 7 074502, [arXiv:1506.06052].

[23] M. Lüscher, *On the chiral anomaly and the Yang–Mills gradient flow*, *Phys. Lett. B* **823** (2021) 136725, [arXiv:2109.07965].

[24] C. G. Callan, *Broken scale invariance in scalar field theory*, *Phys. Rev. D* **2** (Oct, 1970) 1541–1547.

[25] K. Symanzik, *Small distance behavior in field theory and power counting*, *Commun. Math. Phys.* **18** (1970) 227–246.

[26] T. van Ritbergen, J. Vermaseren, and S. Larin, *The four-loop β-function in quantum chromodynamics*, *Physics Letters B* **400** (May, 1997) 379–384.

[27] D. J. Gross and F. Wilczek, *Asymptotically Free Gauge Theories - I*, *Phys. Rev. D* **8** (1973) 3633–3652.

[28] D. J. Gross and F. Wilczek, *ASYMPTOTICALLY FREE GAUGE THEORIES. 2.*, *Phys. Rev. D* **9** (1974) 980–993.

[29] H. D. Politzer, *Asymptotic Freedom: An Approach to Strong Interactions*, *Phys. Rept.* **14** (1974) 129–180.

[30] **Particle Data Group** Collaboration, S. Navas et al., *Review of particle physics*, *Phys. Rev. D* **110** (2024), no. 3 030001.

[31] **ALPHA** Collaboration, M. Bruno, M. Dalla Brida, P. Fritzsch, T. Korzec, A. Ramos, S. Schaefer, H. Simma, S. Sint, and R. Sommer, *QCD Coupling from a Nonperturbative Determination of the Three-Flavor Λ Parameter*, *Phys. Rev. Lett.* **119** (2017), no. 10 102001, [arXiv:1706.03821].

[32] **Flavour Lattice Averaging Group (FLAG)** Collaboration, Y. Aoki et al., *FLAG Review 2021*, *Eur. Phys. J. C* **82** (2022), no. 10 869, [arXiv:2111.09849].

[33] P. H. Ginsparg and K. G. Wilson, *A Remnant of Chiral Symmetry on the Lattice*, *Phys. Rev. D* **25** (1982) 2649.

[34] H. Neuberger, *Exactly massless quarks on the lattice*, *Physics Letters B* **417** (Jan., 1998) 141–144.

[35] F. Niedermayer, *Exact chiral symmetry, topological charge and related topics*, *Nuclear Physics B - Proceedings Supplements* **73** (Mar., 1999) 105–119.

[36] M. Lüscher, *Exact chiral symmetry on the lattice and the ginsparg-wilson relation*, *Physics Letters B* **428** (June, 1998) 342–345.

[37] M. Gell-Mann, R. J. Oakes, and B. Renner, *Behavior of current divergences under SU(3) x SU(3)*, *Phys. Rev.* **175** (1968) 2195–2199.

[38] G. P. Engel, L. Giusti, S. Lottini, and R. Sommer, *Chiral Symmetry Breaking in QCD with Two Light Flavors*, *Phys. Rev. Lett.* **114** (2015), no. 11 112001, [arXiv:1406.4987].

[39] L. Giusti and M. Lüscher, *Chiral symmetry breaking and the Banks-Casher relation in lattice QCD with Wilson quarks*, *JHEP* **03** (2009) 013, [arXiv:0812.3638].

[40] G. P. Engel, L. Giusti, S. Lottini, and R. Sommer, *Spectral density of the Dirac operator in two-flavor QCD*, *Phys. Rev.* **D91** (2015), no. 5 054505, [arXiv:1411.6386].

[41] T. Banks and A. Casher, *Chiral symmetry breaking in confining theories*, *Nuclear Physics B* **169** (1980), no. 1 103–125.

[42] H. Leutwyler and A. V. Smilga, *Spectrum of Dirac operator and role of winding number in QCD*, *Phys. Rev. D* **46** (1992) 5607–5632.

[43] A. V. Smilga and J. Stern, *On the spectral density of Euclidean Dirac operator in QCD*, *Phys. Lett. B* **318** (1993) 531–536.

[44] K. Cichy, E. Garcia-Ramos, and K. Jansen, *Chiral condensate from the twisted mass Dirac operator spectrum*, *JHEP* **10** (2013) 175, [arXiv:1303.1954].

[45] E. Witten, *Current algebra theorems for the u(1) "goldstone boson"*, *Nuclear Physics B* **156** (1979), no. 2 269–283.

[46] G. Veneziano, *U(1) Without Instantons*, *Nucl. Phys. B* **159** (1979) 213–224.

[47] H. J. Rothe, *Lattice gauge theories: An Introduction*, vol. 43. World Scientific, 1992.

[48] C. Gattringer and C. B. Lang, *Quantum chromodynamics on the lattice*, vol. 788. Springer, Berlin, 2010.

[49] M. Luscher, *Advanced lattice QCD*, in *Les Houches Summer School in Theoretical Physics, Session 68: Probing the Standard Model of Particle Interactions*, pp. 229–280, 2, 1998. hep-lat/9802029.

[50] M. Luscher, *Volume Dependence of the Energy Spectrum in Massive Quantum Field Theories. 1. Stable Particle States*, *Commun. Math. Phys.* **104** (1986) 177.

[51] M. Luscher, *Volume Dependence of the Energy Spectrum in Massive Quantum Field Theories. 2. Scattering States*, *Commun. Math. Phys.* **105** (1986) 153–188.

[52] L. Lellouch and M. Luscher, *Weak transition matrix elements from finite volume correlation functions*, *Commun. Math. Phys.* **219** (2001) 31–44, [hep-lat/0003023].

[53] C. h. Kim, C. T. Sachrajda, and S. R. Sharpe, *Finite-volume effects for two-hadron states in moving frames*, *Nucl. Phys. B* **727** (2005) 218–243, [hep-lat/0507006].

[54] M. T. Hansen and S. R. Sharpe, *Lattice QCD and Three-particle Decays of Resonances*, *Ann. Rev. Nucl. Part. Sci.* **69** (2019) 65–107, [arXiv:1901.00483].

[55] M. Ueding, "Lattice qcd tikz graphics." https://github.com/HISKP-LQCD/lqcd-tikz-graphics, July, 2018.

[56] V. Gribov, *Quantization of non-abelian gauge theories*, *Nuclear Physics B* **139** (1978), no. 1 1–19.

[57] L. D. Faddeev and V. N. Popov, *Feynman Diagrams for the Yang-Mills Field*, *Phys. Lett. B* **25** (1967) 29–30.

[58] H. B. Nielsen and M. Ninomiya, *No Go Theorem for Regularizing Chiral Fermions*, *Phys. Lett. B* **105** (1981) 219–223.

[59] D. B. Kaplan, *A method for simulating chiral fermions on the lattice*, *Physics Letters B* **288** (Aug., 1992) 342–347.

[60] Y. Kikukawa and T. Noguchi, *Low-energy effective action of domain wall fermion and the Ginsparg-Wilson relation*, *Nucl. Phys. B Proc. Suppl.* **83** (2000) 630–632, [hep-lat/9902022].

[61] L. Giusti and H. B. Meyer, *Thermal momentum distribution from path integrals with shifted boundary conditions*, *Phys. Rev. Lett.* **106** (2011) 131601, [arXiv:1011.2727].

[62] L. Giusti and H. B. Meyer, *Thermodynamic potentials from shifted boundary conditions: the scalar-field theory case*, *JHEP* **11** (2011) 087, [arXiv:1110.3136].

[63] L. Giusti and H. B. Meyer, *Implications of Poincare symmetry for thermal field theories in finite-volume*, *JHEP* **01** (2013) 140, [arXiv:1211.6669].

[64] L. Giusti and M. Pepe, *Equation of state of the SU(3) Yang–Mills theory: A precise determination from a moving frame*, *Phys. Lett. B* **769** (2017) 385–390, [arXiv:1612.00265].

[65] M. Dalla Brida, L. Giusti, T. Harris, D. Laudicina, and M. Pepe, *Non-perturbative thermal QCD at all temperatures: the case of mesonic screening masses*, *JHEP* **04** (2022) 034, [arXiv:2112.05427].

[66] M. Bresciani, M. Dalla Brida, L. Giusti, and M. Pepe, *Thermal QCD for non-perturbative renormalization of composite operators*, *PoS* **LATTICE2022** (2023) 364, [arXiv:2211.13641].

[67] M. Bresciani, M. Dalla Brida, L. Giusti, and M. Pepe, *Progresses on high-temperature QCD: Equation of State and energy-momentum tensor*, *PoS* **LATTICE2023** (2024) 192, [arXiv:2312.11009].

[68] L. Giusti, T. Harris, D. Laudicina, M. Pepe, and P. Rescigno, *Baryonic screening masses in QCD at high temperature*, *Phys. Lett. B* **855** (2024) 138799, [arXiv:2405.04182].

[69] B. Lucini, A. Patella, A. Ramos, and N. Tantalo, *Charged hadrons in local finite-volume QED+QCD with C^* boundary conditions*, *JHEP* **02** (2016) 076, [arXiv:1509.01636].

[70] M. Hansen, B. Lucini, A. Patella, and N. Tantalo, *Simulations of QCD and QED with C* boundary conditions*, *EPJ Web Conf.* **175** (2018) 09001, [arXiv:1710.08838].

[71] A. Patella, *QED Corrections to Hadronic Observables*, *PoS* **LATTICE2016** (2017) 020, [arXiv:1702.03857].

[72] M. Hansen, B. Lucini, A. Patella, and N. Tantalo, *Gauge invariant determination of charged hadron masses*, *JHEP* **05** (2018) 146, [arXiv:1802.05474].

[73] K. Symanzik, *Cutoff dependence in lattice ϕ_4^4 theory*, *NATO Sci. Ser. B* **59** (1980) 313–330.

[74] K. Symanzik, *Some topics in quantum field theory*, in *6th International Conference on Mathematical Physics - Congress of Association for Mathematical Physics*, pp. 47–58, 10, 1981.

[75] K. Symanzik, *Continuum limit and improved action in lattice theories: (i). principles and ϕ^4 theory*, *Nuclear Physics B* **226** (1983), no. 1 187–204.

[76] K. Symanzik, *Continuum limit and improved action in lattice theories: (ii). o(n) non-linear sigma model in perturbation theory*, *Nuclear Physics B* **226** (1983), no. 1 205–227.

[77] B. Sheikholeslami and R. Wohlert, *Improved Continuum Limit Lattice Action for QCD with Wilson Fermions*, *Nucl. Phys.* **B259** (1985) 572.

[78] M. Lüscher, S. Sint, R. Sommer, and P. Weisz, *Chiral symmetry and O(a) improvement in lattice QCD*, *Nucl. Phys.* **B478** (1996) 365–400, [hep-lat/9605038].

[79] R. Wohlert, "IMPROVED CONTINUUM LIMIT LATTICE ACTION FOR QUARKS." DESY-97-069, July, 1987.

[80] M. Lüscher, *Chiral symmetry and o(a) improvement in lattice qcd*, *Nuclear Physics B* **478** (Oct., 1996) 365–397.

[81] A. Francis, P. Fritzsch, M. Lüscher, and A. Rago, *Master-field simulations of O(a)-improved lattice QCD: Algorithms, stability and exactness*, *Comput. Phys. Commun.* **255** (2020) 107355, [arXiv:1911.04533].

[82] M. Lüscher, *Computational Strategies in Lattice QCD*, in *Modern perspectives in lattice QCD: Quantum field theory and high performance computing. Proceedings, International School, 93rd Session, Les Houches, France, August 3-28, 2009*, pp. 331–399, 2010. arXiv:1002.4232.

[83] M. Cè, L. Giusti, and S. Schaefer, *Domain decomposition, multi-level integration and exponential noise reduction in lattice QCD*, *Phys. Rev.* **D93** (2016), no. 9 094507, [arXiv:1601.04587].

[84] M. Cè, L. Giusti, and S. Schaefer, *A local factorization of the fermion determinant in lattice QCD*, *Phys. Rev.* **D95** (2017), no. 3 034503, [arXiv:1609.02419].

[85] L. Giusti, M. Cè, and S. Schaefer, *Multi-boson block factorization of fermions*, *EPJ Web Conf.* **175** (2018) 01003, [arXiv:1710.09212].

[86] M. Cè, L. Giusti, and S. Schaefer, *Local multiboson factorization of the quark determinant*, *EPJ Web Conf.* **175** (2018) 11005, [arXiv:1711.01592].

[87] L. Giusti, T. Harris, A. Nada, and S. Schaefer, *Multi-level integration for meson propagators*, in *36th International Symposium on Lattice Field Theory (Lattice 2018) East Lansing, MI, United States, July 22-28, 2018*, 2018. arXiv:1812.01875.

[88] M. Dalla Brida, L. Giusti, T. Harris, and M. Pepe, *Multi-level Monte Carlo computation of the hadronic vacuum polarization contribution to* $(g_\mu - 2)$, *Phys. Lett. B* **816** (2021) 136191, [arXiv:2007.02973].

[89] M. Hasenbusch, *Speeding up the hybrid Monte Carlo algorithm for dynamical fermions*, *Phys.Lett.* **B519** (2001) 177–182, [hep-lat/0107019].

[90] M. Hasenbusch and K. Jansen, *Speeding up lattice QCD simulations with clover improved Wilson fermions*, *Nucl.Phys.* **B659** (2003) 299–320, [hep-lat/0211042].

[91] N. Metropolis, A. W. Rosenbluth, M. N. Rosenbluth, A. H. Teller, and E. Teller, *Equation of state calculations by fast computing machines*, *J. Chem. Phys.* **21** (1953) 1087–1092.

[92] W. K. Hastings, *Monte Carlo Sampling Methods Using Markov Chains and Their Applications*, *Biometrika* **57** (1970) 97–109.

[93] S. Duane, A. D. Kennedy, B. J. Pendleton, and D. Roweth, *Hybrid Monte Carlo*, *Phys. Lett.* **B195** (1987) 216–222.

[94] I. P. Omelyan, I. M. Mryglod, and R. Folk, *Symplectic analytically integrable decomposition algorithms: classification, derivation, and application to molecular dynamics, quantum and celestial mechanics simulations*, *Computer Physics Communications* **151** (2003), no. 3 272 – 314.

[95] D. Mohler and S. Schaefer, *Remarks on strange-quark simulations with Wilson fermions*, *Phys. Rev. D* **102** (2020), no. 7 074506, [arXiv:2003.13359].

[96] A. D. Kennedy, I. Horvath, and S. Sint, *A New exact method for dynamical fermion computations with nonlocal actions*, *Nucl. Phys. B Proc. Suppl.* **73** (1999) 834–836, [hep-lat/9809092].

[97] M. A. Clark and A. D. Kennedy, *The RHMC algorithm for two flavors of dynamical staggered fermions*, *Nucl. Phys. B Proc. Suppl.* **129** (2004) 850–852, [hep-lat/0309084].

[98] M. Luscher and F. Palombi, *Fluctuations and reweighting of the quark determinant on large lattices*, *PoS* **LATTICE2008** (2008) 049, [arXiv:0810.0946].

[99] L. Giusti, T. Harris, A. Nada, and S. Schaefer, *Frequency-splitting estimators of single-propagator traces*, *Eur. Phys. J. C* **79** (2019), no. 7 586, [arXiv:1903.10447].

[100] M. Lüscher, *Stochastic locality and master-field simulations of very large lattices*, *EPJ Web Conf.* **175** (2018) 01002, [arXiv:1707.09758].

[101] G. Parisi, *The Strategy for Computing the Hadronic Mass Spectrum*, *Phys. Rept.* **103** (1984) 203–211.

[102] G. P. Lepage, *The Analysis of Algorithms for Lattice Field Theory*, in *Boulder ASI 1989:97-120*, pp. 97–120, 1989.

[103] **UKQCD** Collaboration, C. Michael and J. Peisa, *Maximal variance reduction for stochastic propagators with applications to the static quark spectrum*, *Phys. Rev.* **D58** (1998) 034506, [hep-lat/9802015].

[104] H. Neff, N. Eicker, T. Lippert, J. W. Negele, and K. Schilling, *On the low fermionic eigenmode dominance in QCD on the lattice*, *Phys. Rev.* **D64** (2001) 114509, [hep-lat/0106016].

[105] L. Giusti, P. Hernandez, M. Laine, P. Weisz, and H. Wittig, *Low-energy couplings of QCD from current correlators near the chiral limit*, *JHEP* **04** (2004) 013, [hep-lat/0402002].

[106] T. A. DeGrand and S. Schaefer, *Improving meson two point functions in lattice QCD*, *Comput. Phys. Commun.* **159** (2004) 185–191, [hep-lat/0401011].

[107] M. T. Hansen, H. B. Meyer, and D. Robaina, *From deep inelastic scattering to heavy-flavor semileptonic decays: Total rates into multihadron final states from lattice QCD*, *Phys. Rev. D* **96** (2017), no. 9 094513, [arXiv:1704.08993].

[108] P. Gambino and S. Hashimoto, *Inclusive Semileptonic Decays from Lattice QCD*, *Phys. Rev. Lett.* **125** (2020), no. 3 032001, [arXiv:2005.13730].

[109] S. Jeon and L. G. Yaffe, *From quantum field theory to hydrodynamics: Transport coefficients and effective kinetic theory*, *Phys. Rev. D* **53** (1996) 5799–5809, [hep-ph/9512263].

[110] H. B. Meyer, *A Calculation of the shear viscosity in SU(3) gluodynamics*, *Phys. Rev. D* **76** (2007) 101701, [arXiv:0704.1801].

[111] S. Weinberg, *The Quantum theory of fields. Vol. 1: Foundations*. Cambridge University Press, 6, 2005.

[112] J. D. Bjorken and S. D. Drell, *Relativistic Quantum Mechanics*. International Series In Pure and Applied Physics. McGraw-Hill, New York, 1965.

[113] H. M. Nussenzveig, *Causality and dispersion relations*, vol. 95. Academic Press, New York, London, 1972.

[114] M. L. Bellac, *Thermal Field Theory*. Cambridge Monographs on Mathematical Physics. Cambridge University Press, 3, 2011.

[115] L. Giusti, "Summary for dispersive relations." Unpublished notes (2024).

[116] G. Kallen, *On the definition of the Renormalization Constants in Quantum Electrodynamics*, *Helv. Phys. Acta* **25** (1952), no. 4 417.

[117] H. Lehmann, *On the Properties of propagation functions and renormalization contants of quantized fields*, *Nuovo Cim.* **11** (1954) 342–357.

[118] G. Kallen, *Quantenelektrodynamik*. New York, Springer, 1972.

[119] I. S. Gradshteyn, I. M. Ryzhik, D. Zwillinger, and V. Moll, *Table of integrals, series, and products; 8th ed.* Academic Press, Amsterdam, 2015.

[120] B. Davies, *Integral transforms and their applications*, vol. 41 of *Texts in Applied Mathematics*. Springer New York, NY, 2012.

[121] B. Davies and B. Martin, *Numerical inversion of the laplace transform: a survey and comparison of methods*, *Journal of Computational Physics* **33** (1979), no. 1 1–32.

[122] E. C. Poggio, H. R. Quinn, and S. Weinberg, *Smearing the Quark Model*, *Phys. Rev. D* **13** (1976) 1958.

[123] J. Bulava and M. T. Hansen, *Scattering amplitudes from finite-volume spectral functions*, *Phys. Rev. D* **100** (2019), no. 3 034521, [arXiv:1903.11735].

[124] M. Hansen, A. Lupo, and N. Tantalo, *On the extraction of spectral densities from lattice correlators*, *Phys. Rev. D* **99** (2019) 094508, [arXiv:1903.06476].

[125] J. Bulava, M. T. Hansen, M. W. Hansen, A. Patella, and N. Tantalo, *Inclusive rates from smeared spectral densities in the two-dimensional O(3) non-linear σ-model*, *JHEP* **07** (2022) 034, [arXiv:2111.12774].

[126] H. B. Meyer, *Lattice QCD and the Timelike Pion Form Factor*, *Phys. Rev. Lett.* **107** (2011) 072002, [arXiv:1105.1892].

[127] C. Lin, G. Martinelli, C. T. Sachrajda, and M. Testa, *$K \to \pi\pi$ decays in a finite volume*, *Nucl. Phys. B* **619** (2001) 467–498, [hep-lat/0104006].

[128] W. Detmold and M. J. Savage, *Electroweak matrix elements in the two nucleon sector from lattice QCD*, *Nucl. Phys. A* **743** (2004) 170–193, [hep-lat/0403005].

[129] N. H. Christ, C. Kim, and T. Yamazaki, *Finite volume corrections to the two-particle decay of states with non-zero momentum*, *Phys. Rev. D* **72** (2005) 114506, [hep-lat/0507009].

[130] M. T. Hansen and S. R. Sharpe, *Multiple-channel generalization of Lellouch-Lüscher formula*, *Phys.Rev.* **D86** (2012) 016007, [arXiv:1204.0826].

[131] V. Bernard, D. Hoja, U. Meißner, and A. Rusetsky, *Matrix elements of unstable states*, *JHEP* **09** (2012) 023, [arXiv:1205.4642].

[132] R. A. Briceño, M. T. Hansen, and A. Walker-Loud, *Multichannel $1 \to 2$ transition amplitudes in a finite volume*, *Phys. Rev.* **D91** (2015), no. 3 034501, [arXiv:1406.5965].

[133] R. A. Briceño, *Two-particle multichannel systems in a finite volume with arbitrary spin*, *Phys. Rev.* **D89** (2014), no. 7 074507, [arXiv:1401.3312].

[134] R. A. Briceño and M. T. Hansen, *Multichannel $0 \to 2$ and $1 \to 2$ transition amplitudes for arbitrary spin particles in a finite volume*, *Phys. Rev.* **D92** (2015), no. 7 074509, [arXiv:1502.04314].

[135] R. A. Briceño and M. T. Hansen, *Relativistic, model-independent, multichannel $2 \to 2$ transition amplitudes in a finite volume*, *Phys. Rev. D* **94** (2016), no. 1 013008, [arXiv:1509.08507].

[136] A. Baroni, R. A. Briceño, M. T. Hansen, and F. G. Ortega-Gama, *Form factors of two-hadron states from a covariant finite-volume formalism*, *Phys. Rev. D* **100** (2019), no. 3 034511, [arXiv:1812.10504].

[137] R. A. Briceño, M. T. Hansen, and A. W. Jackura, *Consistency checks for two-body finite-volume matrix elements: I. Conserved currents and bound states*, *Phys. Rev. D* **100** (2019), no. 11 114505, [arXiv:1909.10357].

[138] **RBC, UKQCD** Collaboration, R. Abbott et al., *Direct CP violation and the $\Delta I = 1/2$ rule in $K \to \pi\pi$ decay from the standard model*, *Phys. Rev. D* **102** (2020), no. 5 054509, [arXiv:2004.09440].

[139] C. Andersen, J. Bulava, B. Hörz, and C. Morningstar, *The $I = 1$ pion-pion scattering amplitude and timelike pion form factor from $N_f = 2 + 1$ lattice QCD*, *Nucl. Phys. B* **939** (2019) 145–173, [arXiv:1808.05007].

[140] **Hadron Spectrum** Collaboration, M. T. Hansen, R. A. Briceño, R. G. Edwards, C. E. Thomas, and D. J. Wilson, *Energy-Dependent $\pi^+\pi^+\pi^+$ Scattering Amplitude from QCD*, *Phys. Rev. Lett.* **126** (2021) 012001, [arXiv:2009.04931].

[141] X. Feng, S. Aoki, S. Hashimoto, and T. Kaneko, *Timelike pion form factor in lattice QCD*, *Phys. Rev.* **D91** (2015), no. 5 054504, [arXiv:1412.6319].

[142] R. A. Briceno, J. J. Dudek, and R. D. Young, *Scattering processes and resonances from lattice QCD*, *Rev. Mod. Phys.* **90** (2018), no. 2 025001, [arXiv:1706.06223].

[143] Bruno, Mattia and Hansen, M.T., "Publicationn preparation."

[144] X. Fan, T. G. Myers, B. A. D. Sukra, and G. Gabrielse, *Measurement of the Electron Magnetic Moment*, *Phys. Rev. Lett.* **130** (2023), no. 7 071801, [arXiv:2209.13084].

[145] **Muon g-2** Collaboration, D. P. Aguillard et al., *Detailed report on the measurement of the positive muon anomalous magnetic moment to 0.20 ppm*, *Phys. Rev. D* **110** (2024), no. 3 032009, [arXiv:2402.15410].

[146] F. Jegerlehner, *The Anomalous Magnetic Moment of the Muon*, vol. 274. Springer, Cham, 2017.

[147] **Muon g-2** Collaboration, J. Grange et al., *Muon (g-2) Technical Design Report*, arXiv:1501.06858.

[148] **Muon (g-2) Collaboration** Collaboration, G. W. Bennett et al., *Measurement of the negative muon anomalous magnetic moment to 0.7 ppm*, *Phys. Rev. Lett.* **92** (Apr, 2004) 161802.

[149] D. W. Hertzog, *Next Generation Muon $g - 2$ Experiments*, *EPJ Web Conf.* **118** (2016) 01015, [arXiv:1512.00928].

[150] N. Saito and J.-P. g 2/EDM Collaboration, *A novel precision measurement of muon g - 2 and EDM at J-PARC*, *AIP Conference Proceedings* **1467** (07, 2012) 45–56.

[151] H. Iinuma and (forJ-PARC New g-2/EDM experiment collaboration), *New approach to the muon g-2 and edm experiment at j-parc*, *Journal of Physics: Conference Series* **295** (may, 2011) 012032.

[152] T. Mibe, *Measurement of muon g-2 and edm with an ultra-cold muon beam at j-parc*, *Nuclear Physics B - Proceedings Supplements* **218** (2011), no. 1 242–246. Proceedings of the Eleventh International Workshop on Tau Lepton Physics.

[153] T. Aoyama et al., *The anomalous magnetic moment of the muon in the standard model*, *Physics Reports* **887** (Dec, 2020) 1–166.

[154] D. Bernecker and H. B. Meyer, *Vector Correlators in Lattice QCD: Methods and applications*, *Eur. Phys. J.* **A47** (2011) 148, [arXiv:1107.4388].

[155] S. Eidelman and F. Jegerlehner, *Hadronic contributions to g-2 of the leptons and to the effective fine structure constant alpha (M(z)**2)*, *Z. Phys. C* **67** (1995) 585–602, [hep-ph/9502298].

[156] F. Jegerlehner, *Hadronic contributions to the photon vacuum polarization and their role in precision physics*, *J. Phys. G* **29** (2003) 101–110, [hep-ph/0104304].

[157] F. Jegerlehner and A. Nyffeler, *The Muon g-2*, *Phys. Rept.* **477** (2009) 1–110, [arXiv:0902.3360].

[158] T. Blum, *Lattice calculation of the lowest order hadronic contribution to the muon anomalous magnetic moment*, *Phys. Rev. Lett.* **91** (2003) 052001, [hep-lat/0212018].

[159] T. Blum, N. Christ, M. Hayakawa, T. Izubuchi, L. Jin, C. Jung, and C. Lehner, *Hadronic Light-by-Light Scattering Contribution to the Muon Anomalous Magnetic Moment from Lattice QCD*, *Phys. Rev. Lett.* **124** (2020), no. 13 132002, [arXiv:1911.08123].

[160] B. Chakraborty, C. T. H. Davies, J. Koponen, G. P. Lepage, and R. S. Van de Water, *Higher-Order Hadronic-Vacuum-Polarization Contribution to the Muon G-2 from Lattice QCD*, *Phys. Rev. D* **98** (2018), no. 9 094503, [arXiv:1806.08190].

[161] **Particle Data Group** Collaboration, R. L. Workman et al., *Review of Particle Physics*, *PTEP* **2022** (2022) 083C01.

[162] V. V. Ezhela, S. B. Lugovsky, and O. V. Zenin, *Hadronic part of the muon g-2 estimated on the sigma**2003(tot)(e+ e- —> hadrons) evaluated data compilation*, hep-ph/0312114.

[163] **BaBar** Collaboration, B. Aubert et al., *Precise measurement of the e+ e- —> pi+ pi- (gamma) cross section with the Initial State Radiation method at BABAR*, *Phys. Rev. Lett.* **103** (2009) 231801, [arXiv:0908.3589].

[164] **BaBar** Collaboration, J. P. Lees et al., *Precise Measurement of the $e^+e^- \to \pi^+\pi^-(\gamma)$ Cross Section with the Initial-State Radiation Method at BABAR*, *Phys. Rev. D* **86** (2012) 032013, [arXiv:1205.2228].

[165] **KLOE** Collaboration, F. Ambrosino et al., *Measurement of $\sigma(e^+e^- \to \pi^+\pi^-\gamma(\gamma)$ and the dipion contribution to the muon anomaly with the KLOE detector*, *Phys. Lett. B* **670** (2009) 285–291, [arXiv:0809.3950].

[166] **KLOE** Collaboration, F. Ambrosino et al., *Measurement of $\sigma(e^+e^- \to \pi^+\pi^-)$ from threshold to 0.85 GeV^2 using Initial State Radiation with the KLOE detector*, *Phys. Lett. B* **700** (2011) 102–110, [arXiv:1006.5313].

[167] **KLOE** Collaboration, D. Babusci et al., *Precision measurement of $\sigma(e^+e^- \to \pi^+\pi^-\gamma)/\sigma(e^+e^- \to \mu^+\mu^-\gamma)$ and determination of the $\pi^+\pi^-$ contribution to the muon anomaly with the KLOE detector*, *Phys. Lett. B* **720** (2013) 336–343, [arXiv:1212.4524].

[168] **KLOE-2** Collaboration, A. Anastasi et al., *Combination of KLOE $\sigma\big(e^+e^- \to \pi^+\pi^-\gamma(\gamma)\big)$ measurements and determination of $a_\mu^{\pi^+\pi^-}$ in the energy range $0.10 < s < 0.95$ GeV^2*, *JHEP* **03** (2018) 173, [arXiv:1711.03085].

[169] **CMD-3** Collaboration, F. V. Ignatov et al., *Measurement of the e+e-→π+π- cross section from threshold to 1.2 GeV with the CMD-3 detector*, *Phys. Rev. D* **109** (2024), no. 11 112002, [arXiv:2302.08834].

[170] G. Colangelo, M. Hoferichter, and P. Stoffer, *Two-pion contribution to hadronic vacuum polarization*, *JHEP* **02** (2019) 006, [arXiv:1810.00007].

[171] P. Gambino, M. Jung, and S. Schacht, *The vcb puzzle: An update*, *Physics Letters B* **795** (2019) 386–390.

[172] A. Barone, *Inclusive semileptonic B(s)-meson decays from Lattice QCD*. PhD thesis, University of Southampton, Southampton U., Southampton U., 2024.

[173] **Extended Twisted Mass** Collaboration, A. Evangelista, R. Frezzotti, N. Tantalo, G. Gagliardi, F. Sanfilippo, S. Simula, and V. Lubicz, *Inclusive hadronic decay rate of the τ lepton from lattice QCD*, *Phys. Rev. D* **108** (2023), no. 7 074513, [arXiv:2308.03125].

[174] F. Karsch and H. W. Wyld, *Thermal Green's Functions and Transport Coefficients on the Lattice*, *Phys. Rev. D* **35** (1987) 2518.

[175] A. Hosoya, M.-a. Sakagami, and M. Takao, *Nonequilibrium Thermodynamics in Field Theory: Transport Coefficients*, *Annals Phys.* **154** (1984) 229.

[176] E.-k. Wang, U. W. Heinz, and X.-f. Zhang, *Spectral functions for composite fields and viscosity in hot scalar field theory*, *Phys. Rev. D* **53** (1996) 5978–5981, [hep-ph/9509331].

[177] J. I. Kapusta and C. Gale, *Finite-temperature field theory: Principles and applications*. Cambridge Monographs on Mathematical Physics. Cambridge University Press, 2011.

[178] M. Lüscher and P. Weisz, *Locality and exponential error reduction in numerical lattice gauge theory*, *JHEP* **09** (2001) 010, [hep-lat/0108014].

[179] M. Della Morte and L. Giusti, *Exploiting symmetries for exponential error reduction in path integral Monte Carlo*, *Comput. Phys. Commun.* **180** (2009) 813–818.

[180] M. Della Morte and L. Giusti, *A novel approach for computing glueball masses and matrix elements in Yang-Mills theories on the lattice*, *JHEP* **05** (2011) 056, [arXiv:1012.2562].

[181] M. Lüscher, *A New approach to the problem of dynamical quarks in numerical simulations of lattice QCD*, *Nucl. Phys.* **B418** (1994) 637–648, [hep-lat/9311007].

[182] A. Borici and P. de Forcrand, *Systematic errors of Lüscher's fermion method and its extensions*, *Nucl. Phys.* **B454** (1995) 645–662, [hep-lat/9505021].

[183] A. Borici and P. de Forcrand, *Variants of Lüscher's fermion algorithm*, *Nucl. Phys. Proc. Suppl.* **47** (1996) 800–803, [hep-lat/9509080].

[184] B. Jegerlehner, *Improvements of Lüscher's local bosonic fermion algorithm*, *Nucl. Phys.* **B465** (1996) 487–506, [hep-lat/9512001].

[185] A. Borrelli, P. de Forcrand, and A. Galli, *NonHermitian exact local bosonic algorithm for dynamical quarks*, *Nucl. Phys. B* **477** (1996) 809–834, [hep-lat/9602016].

[186] P. de Forcrand, *The Multiboson method*, *Parallel Comput.* **25** (1999) 1341, [hep-lat/9903035].

[187] H. A. Schwarz, "Gesammelte mathematische abhandlungen, vol. 2." Springer Verlag, Berlin, 1890.

[188] Y. Saad, *Iterative Methods for Sparse Linear Systems*. Society for Industrial and Applied Mathematics, Philadelphia, PA, USA, 2nd ed., 2003.

[189] M. Lüscher, *Lattice QCD and the Schwarz alternating procedure*, *JHEP* **05** (2003) 052, [hep-lat/0304007].

[190] M. Luscher, *Schwarz-preconditioned HMC algorithm for two-flavour lattice QCD*, *Comput. Phys. Commun.* **165** (2005) 199–220, [hep-lat/0409106].

[191] M. Lüscher, *Schwarz-preconditioned HMC algorithm for two-flavour lattice QCD*, *Comput. Phys. Commun.* **165** (2005) 199–220, [hep-lat/0409106].

[192] M. Dalla Brida, T. Korzec, S. Sint, and P. Vilaseca, *High precision renormalization of the flavour non-singlet Noether currents in lattice QCD with Wilson quarks*, *Eur. Phys. J.* **C79** (2019), no. 1 23, [arXiv:1808.09236].

[193] P. Fritzsch, F. Knechtli, B. Leder, M. Marinkovic, S. Schaefer, R. Sommer, and F. Virotta, *The strange quark mass and Lambda parameter of two flavor QCD*, *Nucl. Phys.* **B865** (2012) 397–429, [arXiv:1205.5380].

[194] M. Lüscher, *Solution of the Dirac equation in lattice QCD using a domain decomposition method*, *Comput. Phys. Commun.* **156** (2004) 209–220, [hep-lat/0310048].

[195] L. Giusti and M. Lüscher, *Topological susceptibility at $T > T_c$ from master-field simulations of the SU(3) gauge theory*, *Eur. Phys. J. C* **79** (2019), no. 3 207, [arXiv:1812.02062].

[196] M. Albergo, G. Kanwar, and P. Shanahan, *Flow-based generative models for markov chain monte carlo in lattice field theory*, *Physical Review D* **100** (aug, 2019).

[197] G. Kanwar, M. S. Albergo, D. Boyda, K. Cranmer, D. C. Hackett, S. Racanière, D. J. Rezende, and P. E. Shanahan, *Equivariant flow-based sampling for lattice gauge theory*, *Physical Review Letters* **125** (sep, 2020).

[198] R. Abbott, M. S. Albergo, D. Boyda, K. Cranmer, D. C. Hackett, G. Kanwar, S. Racanière, D. J. Rezende, F. Romero-López, P. E. Shanahan, B. Tian, and J. M. Urban, *Gauge-equivariant flow models for sampling in lattice field theories with pseudofermions*, 2022.

[199] G. Bailas, S. Hashimoto, and T. Ishikawa, *Reconstruction of smeared spectral function from Euclidean correlation functions*, *PTEP* **2020** (2020), no. 4 043B07, [arXiv:2001.11779].

[200] M. Asakawa, T. Hatsuda, and Y. Nakahara, *Maximum entropy analysis of the spectral functions in lattice QCD*, *Prog. Part. Nucl. Phys.* **46** (2001) 459–508, [hep-lat/0011040].

[201] Y. Burnier and A. Rothkopf, *Bayesian Approach to Spectral Function Reconstruction for Euclidean Quantum Field Theories*, *Phys. Rev. Lett.* **111** (2013) 182003, [arXiv:1307.6106].

[202] L. Kades et al., *Spectral Reconstruction with Deep Neural Networks*, *Phys. Rev. D* **102** (2020), no. 9 096001, [arXiv:1905.04305].

[203] J. Horak, J. M. Pawlowski, J. Rodríguez-Quintero, J. Turnwald, J. M. Urban, N. Wink, and S. Zafeiropoulos, *Reconstructing QCD spectral functions with Gaussian processes*, *Phys. Rev. D* **105** (2022), no. 3 036014, [arXiv:2107.13464].

[204] M. Buzzicotti, A. De Santis, and N. Tantalo, *Teaching to extract spectral densities from lattice correlators to a broad audience of learning-machines*, *Eur. Phys. J. C* **84** (2024), no. 1 32, [arXiv:2307.00808].

[205] L. Del Debbio, A. Lupo, M. Panero, and N. Tantalo, *Bayesian solution to the inverse problem and its relation to Backus-Gilbert methods*, arXiv:2409.04413.

[206] J. C. A. Barata and K. Fredenhagen, *Particle scattering in Euclidean lattice field theories*, *Commun. Math. Phys.* **138** (1991) 507–520.

[207] A. Patella and N. Tantalo, *Scattering Amplitudes from Euclidean Correlators: Haag-Ruelle theory and approximation formulae*, arXiv:2407.02069.

[208] L. Del Debbio, A. Lupo, M. Panero, and N. Tantalo, *Multi-representation dynamics of SU(4) composite Higgs models: chiral limit and spectral reconstructions*, *Eur. Phys. J. C* **83** (2023), no. 3 220, [arXiv:2211.09581].

[209] L. Del Debbio, A. Lupo, M. Panero, and N. Tantalo, *Approaches to the Inverse Problem*, in *EuroPLEx Final Conference*, 10, 2024. arXiv:2410.09944.

[210] L. Del Debbio, M. Naviglio, and F. Tarantelli, *Neural Networks Asymptotic Behaviours for the Resolution of Inverse Problems*, arXiv:2402.09338.

[211] A. Lupo, L. Del Debbio, M. Panero, and N. Tantalo, *Bayesian interpretation of Backus-Gilbert methods*, *PoS* **LATTICE2023** (2024) 004, [arXiv:2311.18125].

[212] P. Gambino, S. Hashimoto, S. Mächler, M. Panero, F. Sanfilippo, S. Simula, A. Smecca, and N. Tantalo, *Lattice QCD study of inclusive semileptonic decays of heavy mesons*, *JHEP* **07** (2022) 083, [arXiv:2203.11762].

[213] L. D. Debbio, A. Lupo, M. Panero, and N. Tantalo, *Fits of finite-volume smeared spectral densities*, arXiv:2212.08019.

[214] **Extended Twisted Mass Collaboration (ETMC)** Collaboration, C. Alexandrou et al., *Probing the Energy-Smeared R Ratio Using Lattice QCD*, *Phys. Rev. Lett.* **130** (2023), no. 24 241901, [arXiv:2212.08467].

[215] J. Bulava, *The spectral reconstruction of inclusive rates*, *PoS* **LATTICE2022** (2023) 231, [arXiv:2301.04072].

[216] M. Cè, T. Harris, A. Krasniqi, H. B. Meyer, and C. Török, *Photon emissivity of the quark-gluon plasma: A lattice QCD analysis of the transverse channel*, *Phys. Rev. D* **106** (2022), no. 5 054501, [arXiv:2205.02821].

[217] L. Del Debbio, T. Giani, and M. Wilson, *Bayesian approach to inverse problems: an application to NNPDF closure testing*, *Eur. Phys. J. C* **82** (2022), no. 4 330, [arXiv:2111.05787].

[218] E. Bennett et al., *Progress on the spectroscopy of lattice gauge theories using spectral densities*, in *41st International Symposium on Lattice Field Theory*, 10, 2024. arXiv:2410.11386.

[219] E. Bennett et al., *Meson spectroscopy from spectral densities in lattice gauge theories*, *Phys. Rev. D* **110** (2024), no. 7 074509, [arXiv:2405.01388].

[220] A. Candido, L. Del Debbio, T. Giani, and G. Petrillo, *Bayesian inference with Gaussian processes for the determination of parton distribution functions*, *Eur. Phys. J. C* **84** (2024), no. 7 716, [arXiv:2404.07573].

[221] A. Candido, L. Del Debbio, T. Giani, and G. Petrillo, *Inverse Problems in PDF determinations*, *PoS* **LATTICE2022** (2023) 098, [arXiv:2302.14731].

[222] R. E. Bellman and R. S. Roth, *The Laplace Transform*. World Scientific Press, Singapore, 1984.

[223] J. G. McWhirter and E. R. Pike, *On the numerical inversion of the laplace transform and similar fredholm integral equations of the first kind*, *Journal of Physics A: Mathematical and General* **11** (sep, 1978) 1729.

[224] C. L. Epstein and J. Schotland, *The bad truth about laplace's transform*, *SIAM Review* **50** (2008), no. 3 504–520, [https://doi.org/10.1137/060657273].

[225] T. Carleman, *Sur les équations intégrales singulières à noyau réel et symétrique*. Uppsala universitets årsskrift, Matematik och naturvetenskap. A.B. Lundequistska Bokhandeln, Uppsala, 1923.

[226] A. Tikhonov, *Solution of incorrectly formulated problems and the regularization method*, *Soviet Mathematics Doklady* **4** (1963) 1035–1038.

[227] A. N. Tikhonov and V. Y. Arsenin, *Solutions of ill-posed problems*. Scripta Series in Mathematics. V. H. Winston & Sons, 1977.

[228] M. Rosenblum, *On the hilbert matrix, i*, *Proceedings of the American Mathematical Society* **9** (1958), no. 1 137–140.

[229] A. Murli, S. Cuomo, L. D'Amore, and A. Galletti, *Numerical regularization of a real inversion formula based on the laplace transform's eigenfunction expansion of the inverse function*, *Inverse Problems* **23** (mar, 2007) 713.

[230] S. W. Indratno, A. G. Ramm, et al., *Inversion of the laplace transform from the real axis using an adaptive iterative method*, *International Journal of Mathematics and Mathematical Sciences* **2009** (2009) [arXiv:0910.3385].

[231] S. C. Power, *Hankel operators on hilbert space*, *Bulletin of the London Mathematical Society* **12** (1980), no. 6 422–442, [https://londmathsoc.onlinelibrary.wiley.com/doi/pdf/10.1112/blms/12.6.422].

[232] C. Groetsch, *The Theory of Tikhonov Regularization for Fredholm Equations of the First Kind*. Chapman & Hall/CRC research notes in mathematics series. Pitman Advanced Pub. Program, 1984.

[233] J. B. Conway, *A course in functional analysis*. Graduate Texts in Mathematics. Springer New York, 1990.

[234] M.-D. Choi, *Tricks or treats with the hilbert matrix*, *The American Mathematical Monthly* **90** (1983), no. 5 301–312.

[235] M. Fiedler, *Notes on hilbert and cauchy matrices*, *Linear Algebra and its Applications* **432** (2010), no. 1 351–356.

[236] S. Schechter, *On the inversion of certain matrices*, *Mathematical Tables and Other Aids to Computation* **13** (1959), no. 66 73–77.

[237] S. W. Indratno and A. G. Ramm, *Inversion of the laplace transform from the real axis using an adaptive iterative method*, *International Journal of Mathematics and Mathematical Sciences* **2009** (Jan, 2010) 898195.

[238] C. Clason, *Regularization of inverse problems*, 2021.

[239] G. Y. Shilov, *Mathematical analysis: a special course*. Pergamon Press, Oxford, 1965.

[240] J. S. Howland, *Spectral theory of operators of hankel type, i*, *Indiana University Mathematics Journal* **41** (1992), no. 2 409–426.

[241] J. S. Howland, *Spectral theory of operators of hankel type, ii*, *Indiana University Mathematics Journal* **41** (1992), no. 2 427–434.

[242] C. K. Hill, *On the Singly-Infinite Hilbert Matrix*, *Journal of the London Mathematical Society* **s1-35** (01, 1960) 17–29.

[243] R. Pike, J. Mcwhirter, M. Bertero, and C. Mol, *Generalized Information Theory for Inverse Problems in Signal Processing*, *Communications, Radar and Signal Processing, IEE Proceedings F* **131** (11, 1984) 660 – 667.

[244] R. Koekoek, P. Lesky, and R. Swarttouw, *Hypergeometric Orthogonal Polynomials and Their q-Analogues*. Springer Monographs in Mathematics. Springer Berlin Heidelberg, 01, 2010.

[245] E. Neuman, *On hahn polynomials and continuous dual hahn polynomials*, *Journal of Computational Analysis and Applications* **8** (07, 2006) 229–248.

[246] T. H. Koornwinder, *Group theoretic interpretations of askey's scheme of hypergeometric orthogonal polynomials*, in *Orthogonal Polynomials and their Applications* (M. Alfaro, J. S. Dehesa, F. J. Marcellan, J. L. Rubio de Francia, and J. Vinuesa, eds.), (Berlin, Heidelberg), pp. 46–72, Springer Berlin Heidelberg, 1988.

[247] A. Boumenir and A. Al-Shuaibi, *The inverse laplace transform and analytic pseudo-differential operators*, *Journal of Mathematical Analysis and Applications* **228** (1998), no. 1 16–36.

[248] R. Campagna, C. Conti, and S. Cuomo, *Smoothing exponential-polynomial splines for multiexponential decay data*, *Dolomites Research Notes on Approximation* **12** (04, 2020) 86–100.

[249] R. Campagna, C. Conti, and S. Cuomo, *Computational error bounds for laplace transform inversion based on smoothing splines*, *Applied Mathematics and Computation* **383** (2020) 125376.

[250] G. Backus and F. Gilbert, *The Resolving Power of Gross Earth Data*, *Geophys. J. Int.* **16** (1968), no. 2 169–205.

[251] G. Backus and F. Gilbert, *Uniqueness in the Inversion of Inaccurate Gross Earth Data*, *Philosophical Transactions of the Royal Society of London Series A* **266** (Mar., 1970) 123–192.

[252] **ALPHA** Collaboration, U. Wolff, *Monte Carlo errors with less errors*, *Comput. Phys. Commun.* **156** (2004) 143–153, [hep-lat/0306017]. [Erratum: Comput.Phys.Commun. 176, 383 (2007)].

[253] **ALPHA** Collaboration, S. Schaefer, R. Sommer, and F. Virotta, *Critical slowing down and error analysis in lattice QCD simulations*, *Nucl. Phys. B* **845** (2011) 93–119, [arXiv:1009.5228].

[254] M. Bruno and R. Sommer, *On fits to correlated and auto-correlated data*, *Comput. Phys. Commun.* **285** (2023) 108643, [arXiv:2209.14188].

[255] M. Bruno, "pyobs." https://doi.org/10.5281/zenodo.7546851, Jan., 2023.

[256] B. Blossier, M. Della Morte, G. von Hippel, T. Mendes, and R. Sommer, *On the generalized eigenvalue method for energies and matrix elements in lattice field theory*, *JHEP* **04** (2009) 094, [arXiv:0902.1265].

[257] F. S. A. Quarteroni, R. Sacco, *Numerical Mathematics*. Springer-Verlag, New York, 2000.

[258] T. Whyte, A. Stathopoulos, E. Romero, and K. Orginos, *Optimizing shift selection in multilevel Monte Carlo for disconnected diagrams in lattice QCD*, *Comput. Phys. Commun.* **294** (2024) 108928, [arXiv:2212.04430].